Technical University of Denmark

DTU

Accurate treatment of nanoelectronics through improved description of van der Waals Interactions

Kelkkanen, Kari André; Jacobsen, Karsten Wedel; Nørskov, Jens Kehlet

Publication date:
2011

Document Version
Publisher's PDF, also known as Version of record

[Link back to DTU Orbit](#)

DTU Library
Technical Information Center of Denmark

Implementation of van der Waals Forces in DFT for Nanoelectronics and Water Structure

André K. Kelkkanen

Technical University of Denmark
Center for Atomic-scale Materials Design
Department of Physics
DK-2800 Kongens Lyngby, Denmark

Abstract

This thesis emerges from a patented idea to utilize intentionally structured surfaces and differences in adsorption strengths to self-assemble some source material into nanoelectronic components, and ends up in the heated debate regarding structure of ambient water . It investigates the role and relevance of van der Waals (vdW) forces in molecular surface adsorption and water through density-functional theory (DFT), using the exchange-correlation functional vdW-DF [Dion et al., Phys. Rev. Lett. **92**, 246401 (2004)] and developments based on it.

Results are first computed for adsorption with vdW forces of, e.g., benzene on Au(111) and other coinage metals, phenol on nickel, and graphene on Co, Ni, Pd, Ag, Au, Cu and Pt surfaces. The vdW forces are ubiquitous but for transition metals and on structured surfaces, with defects, incl.

The vdW adsorbate attraction benefits from the two-dimensional extent of the surface and favors adsorption sites close to the surface, while the Pauli repulsion keeps the adsorbate away. Impurities, like an adatom or an adsorbed pyramid, pushes the adsorbate away from surface, giving a reduction of the attraction due to vdW forces. In this way the vdW force varies on an atomic scale, and in the weak-adsorption limit coordination rules for adsorption are affected. The thesis illustrates this force competition by varying adsorption site and substrate to find examples where the rule of under-coordination which holds according to DFT without vdW forces, does not when accounting for vdW.

An evaluation of the vdW-DF method is made by comparison with a detailed experimentally determined physisorption-potential for H_2 on Cu(111). The vdW-DF2 potential-energy curves appear to have an agreement at large with the

measured curve.

Competition between different kinds of forces rules also other systems. For instance, in water complexes hydrogen bonds compete with vdW force, just like chemisorptive forces due to d-electrons do on transition metals. Bond lengths are shorter than those for typical vdW bonds also here, making both adsorption and water call for improved exchange functionals. DFT calculations are performed for water dimer and hexamer, and for liquid water.

Calculations on four low-energetic isomers of the water hexamer show that the vdW-DF accurately determines the energetic trend on these small clusters. However, the dissociation-energy values with the vdW-DF functional are too small, as the exchange approximation used is too repulsive. With the vdW-DF and other functionals that account for vdW forces, the total isomer energies are minimized in molecular configurations, which are compact, and in which many hydrogen bonds (HBs) can be described as distorted, or even as broken.

The hexamer experience of the criteria and effects of vdW forces can be used in interpretation of results of molecular dynamics (MD) simulations of ambient water, where vdW forces qualitatively result in liquid water with fewer, more distorted HBs. This is interesting as there is currently a heated debate in the water community on the level of HB distortion in ambient water, and where MD simulations without first principles vdW forces have played an important role to suggest that liquid water is almost tetrahedral, with few distorted HBs. Simulations with improved vdW-DF functionals, called vdW-DF2 and optPBE-vdW, result in a structure similar to the HDL phase (high-density liquid) under proper conditions, and thus show that vdW forces may be vital in the two-liquid model suggested in http://www.sciencemag.org/content/304/5673/995.abstract.

Dansk resumé

Denne afhandling opstod fra en patenteret idé, nemlig det at udnytte forsætligt strukturerede overflader og forskelle i adsorption styrker til at selvstændige samle ("self-assemble ") nogle kildemateriale i nanoelektroniske komponenter og afhandlingen ender i den ophedede debat om strukturen af omgivende vand. Den undersøger van der Waals (vdw) kræfters rolle og relevans i molekylæroverfladeadsorption og vand gennem tæthedsfunktionalteori (DFT), ved hjælp af exchange-korrelation funktionalet vdW-DF [Dion et al. Phys. Rev Lett.**92**, 246.401 (2004)] og afledede funktionaler heraf.

Resultater er først beregnet for adsorption med vdw kræfter, f.eks benzen på Au(111) og andre møntmetaller, fenol på nikkel, og graphene på Co, Ni, Pd, Ag, Au, Cu og Pt overflader. vdw kræfterne er allestedsnærværende, men for overgangsmetaller og på struktureret overflader med defekter, inkl. overfladeatomer (adatoms), adsorberet pyramider, og kanter, er der konkurrence med kovalentekræfter. Dermed fremstår en interessant variation i adsorption. Specifikt er en detaljeret undersøgelse foretaget, som afslører, at dette har konsekvenser for svage adsorption og for adsorptionsregler typisk for teorier uden vdw beskrivelse.

Den vdw adsorberende attraktion drager fordel af den to-dimensionelle udstrækning af overfladen og fortrækker adsorptionpositioner tæt på overfladen, mens Pauli-frastødning holder adsorbaten væk. Urenheder, såsom et overfladeatom (adatom), eller en adsorberet pyramide, skubber adsorbaten væk fra overfladen, hvilket giver en reduceret vdw attraktion. På denne måde varierer vdw kraften på atomarskala og i den svage-adsorptionsgrænse, påvirkes koordineringsregler for adsorption og katalyse. Afhandlingen illustrerer disse konkurrerende kræfter ved at variere adsorption positionen og substrat for at finde eksempler, hvor reglen for underkoordination, der holder ifølge DFT uden

iv

vdw kræfter, ikke virker når man medregner vdw.

En evaluering af vdW-DF-metoden er lavet i forhold til detaljerede eksperimentelt bestemte physisorption-potentialer for H_2 på Cu (111). vdW-DF2 potentielenergikurverne ser ud til at stemmeoverens med den målte kurve.

Konkurrencen mellem forskellige former for kræfter bestemmer også andre systemer. F.eks. i vandkomplekser konkurrerer vdw kræfter med hydrogenbindinger, ligesom kemisorptionskræfter gør i overgangsmetaller pga. d-elektroner. Også her observeres at bindingslængder er kortere end for typiske vdw-bindinger, hvilket gør at både adsorption og vand kræver forbedret exchange-funktionaler. DFT beregninger er udført for vanddimer, -hexamer og flydende vand.

Beregninger på fire lavenergi isomerer af vandhexamerer viser, at vdW-DF præcist bestemmer tendensen af energierne på disse små vandklynger. Dog er dissociationsenergierne med vdW-DF funktionalet for små, da den anvendte tilnærmelse er for frastødende. Med vdW-DF og andre funktionaler, der beskriver vdw kræfter, er de samlede isomerenergi minimeret i molekylær konfigurationer, som er kompakte og hvor mange hydrogenbindinger (HBs) kan beskrives som fordrejet, endda som brudte med en fælles definition.

Erfaringerne fra hexamer kriteriet og virkningerne af vdw kræfter kan anvendes i fortolkningen af resultaterne af molekylær dynamik (MD) simuleringer af vand ved standard betingelser, hvor vdw kræfter kvalitativt resulterer i flydende vand med færre rene men mere forvrænget HBs. Dette er interessant, da der i øjeblikket er en ophedet debat i vandmiljøet på niveauet af HB forvrængning i vand ved standard betingelser og hvor MD simuleringer uden rent teoretisk beregnede vdw kræfter har spillet en vigtig rolle at forslå at flydende vand er næsten tetraedrisk med få forvrængede HBs. Simuleringer med forbedret vdW-DF funktionaler, de såkaldte vdw-DF2 og optPBE-vdW, resulterer i en struktur, der svarer til den HDL fase (høj-tæthedsvæske) under de rette forhold, og dermed illustrer, at vdw kræfter kan være afgørende i to-væske modellen foreslået i
http://www.sciencemag.org/content/304/5673/995.abstract.

Tillägnad Boije Rosenberg

För allt vi fick uppleva

Tack

Preface

Everything written in this thesis started with a lecture on "Innovation in Academia" in a course at Chalmers School of Entrepreneurship in 2007. The lecturer was talking about patents that had originated from Scientific research at Chalmers. The lecturer was my headmaster Mats Lundqvist who showed pictures of a proposed concept of making carbon nanotube transistors based on a patented process.

I though this was quite interesting and asked a lot of questions. After the lecture we talked some more and he explained that one of the inventors was Bengt Lundqvist, incidentally his father. Mats introduced us and we discussed the potential of the patented process. He suggested that this process could be evaluated as part of a Ph.D project that he could be supervising. If things went well it could potentially lead to an upstart company based on the technology, and if things went bad I still had a Ph.D degree in physics, whereafter I could always get a haircut and get myself a job. The Technical University of Denmark and CAMd was a very suitable place to work at since the same effects that we wished to study was already studied in the field of catalysis, where carbon poisoned the reaction sites of Ni steps and they wanted to get rid of this annoying effect, while we wanted it to build carbon nanotubes. Jens Nørskov was kind and accepted me as his Ph.D student.

It turned out that the small niche of Density Functional Theory calculations with account for van der Waals forces was not advanced enough to do calculations on the patented process. Self-consistency was out of the question as it was too expensive, as was periodic boundary conditions, and few had so far used the method for adsorption, especially on metals where the quality of the approximations was unknown. I had probably believed that I would apply a more or less mature method for most of my project. Instead the name of the

game has been method development. Luckily, many other groups were in the same position, and there has been a continuous technology race within the field where I more than a few times was amazed over what other groups had achieved in self-consistency, efficiency or accuracy, that I wouldn't have been able to keep up with without Jens-Jørgen Mortensen.

Interesting applications were unlocked as the technology front moved forward. In three years self-consistency has moved from impossible to standard, while accuracy improvements has unlocked system after system. In order to work with the patented process, it was crucial to have a method that accurately could balance weak vdW forces with other stronger forces. Most of the results in this thesis are in some way related to this needed balance. I can tell you already that there has been no time to develop the patented process, as some development is still needed on accuracy.

As I have been a part of a developing field I can safely say that I would have gotten nowhere without help from people close to me, as well as from people I never actually met. In addition to Jens, Bengt and Jens-Jørgen I want to thank Per Hyldgaard for accepting my visit at Chalmers. I want to thank Karsten Jacobsen for filling in as my supervisor. I want to thank my fianceé Sanna for moving to Denmark with me, and for staying with me when I wrote this thesis and didn't have time to shower, shave or cut my hair. Thanks to the CAMd soccer team for great games and thanks to Tao,Federico,David,Janosch,Kristian and Jess for the pleasure of sharing office and time with you. Thanks Andreas for soccer games, water discussions and for writing the Danish resume for me. Thanks Marco for exploring vdW adsorption with me, and for the free limo ride home that crazy night in Vegas.

Finally I want to thank Bengt Lundqvist one more time by borrowing a line from the rapper Jay-Z:

> You could have been anywhere in the world, but you're here with me
>
> I appreciate that
>
> Thank you

List of included publications

1. D. C. Langreth, B. I. Lundqvist, S. D. Chakarova-Käck, V. R. Cooper, M. Dion, P. Hyldgaard, A.K. Kelkkanen, J. Kleis, Lingzhu Kong, Shen Li, P. G. Moses, E. Murray, A. Puzder , H. Rydberg, E. Schröder and T. Thonhauser , **A density functional for sparse matter**, Journal of Physics: Condensed Matter **21** 084203 (2009)

2. A.K. Kelkkanen, B. I. Lundqvist, J.K. Nørskov, **Density functional for van der Waals forces accounts for hydrogen bond in benchmark set of water hexamers**, Journal of Chemical Physics **131** 046102 (2009)

3. J Wellendorff and A.K. Kelkkanen and J. J. Mortensen and B. I. Lundqvist and T. Bligaard, **RPBE-vdW Description of Benzene Adsorption on Au(111)**, Topics in Catalysis **53** 378 (2010)

4. M. Vanin, J. J. Mortensen, A. K. Kelkkanen, J. M. Garcia-Lastra, K. S. Thygesen and K. W. Jacobsen, **Graphene on metals: A van der Waals density functional study**, Physical Review B **81** 081408 (2010)

5. A.K. Kelkkanen, B. I. Lundqvist, and J. K. Nørskov, **van der Waals Effect in Weak Adsorption Affects Trends in Adsorption, Reactivity, and View of Substrate Nobility**, Physical Review B: Brief Report, in print

6. A. K. Kelkkanen, K. Berland, S. Andersson, K. Lee, D. C. Langreth, E. Schröder, B. I. Lundqvist and P. Hyldgaard, **Evaluation of New Density Functional with Account of van der Waals Forces by Use of Experimental H_2 Physisorption Data on Cu(111)**, manuscript

7. A. Møgelhøj, A. K. Kelkkanen, K. T. Wikfeldt, J. Schøtz, J. J. Mortensen, L. G. M. Pettersson, B. I. Lundqvist, K. W. Jacobsen, A. Nilsson and J.

Contents

CHAPTER 1

Introduction

1.1 Nanoelectronics

According to Moore's law, the number of transistors that can inexpensively be put on a chip doubles roughly every second year. This law is said to have become a self-fulfilling prophecy as it is now used for long-term planning in the industry. Although critics have often claimed that this law is bound to break, ingenious engineers, scientists and businessmen (yes, they too) have repeatedly been able to keep up, and our need for smaller and faster electronics has so far been met. At some point, however, the traditional silicon transistor needs to be replaced in order to maintain the law. Although some said already in 2004 that silicon transistors wouldn't get much smaller than 90 nanometers, the same voices say today that they will have problems building transistors smaller than 16 nm, and that transistors smaller than 10 nm will be impossible due to severe quantum effects [1].The term nanoelectronics suggests electronics on the scale of less than 100 nm. Typically the word implies that the nanocircuit must be understood in terms of Quantum Mechanics (QM), thus excluding conventional 16 nanometer silicon electronics. Instead it refers to electronics made of molecules, carbon nanotubes, graphene, or other materials that can be understood only by QM. The potential advantages of nanoelectronics over silicon technologies are ultra responsive atomic scale transistors with low heat generation. The disadvantage is that such a transistor is very sensitive to its environment, and that no process

A   B

C   D
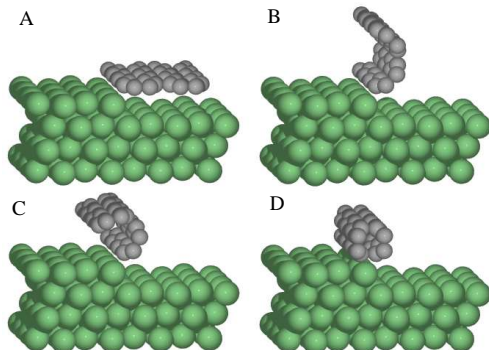
exists of how to enable scalable production.

Whether or not nanoelectronics will become the next disruptive technology that replaces silicon, or work in smaller niche markets, or never work in industrial applications remains to be seen. Although transistors from carbon nanotubes and graphene nanoribbons have been constructed [2], making one transistor in the lab is quite different from developing a method of making 10 million working transistors per mm^2.

1.1.1   Nano Integrated Circuit patent

In 2002, a patent application for a novel idea to design nano-integrated circuits was filed[1]. The idea of the patent is to utilize intentionally structured surfaces and differences in adsorption strengths of different surface structures to self-assemble some source material into nano-electric components.

One proposed way to do this is to grow a sheet of graphene [3] on a stepped metal surface. The graphene sheet is expected to physisorb weakly with van der Waals forces on the terraces but chemisorb on the steps, similarly to CO which has been observed to adsorb more strongly at under-coordinated sites [4, 5, 6, 7]. This anchors one edge of the graphene sheet to the surface, while the other still being adsorbed weakly through physisorption. If this system is excited, there is a chance that the weakly bonded edge could roll up to bond with the strongly anchored edge. In this case, the chirality of the formed carbon nano tube (CNT)

---

[1]P. Hyldgaard, D.C. Chakarov, and B.I. Lundqvist (inventors) Manufacturing method for nanostructure, by choosing substrate material, preparing template, forming film on template and causing film to restructure. fabricated nanostructures, , US patent <u>and</u> ESO patent application, US2009202787-A1, US7390527-B2, US-2005100736-A1. Patent held by Chalmers Intellectual Property Rights AB.
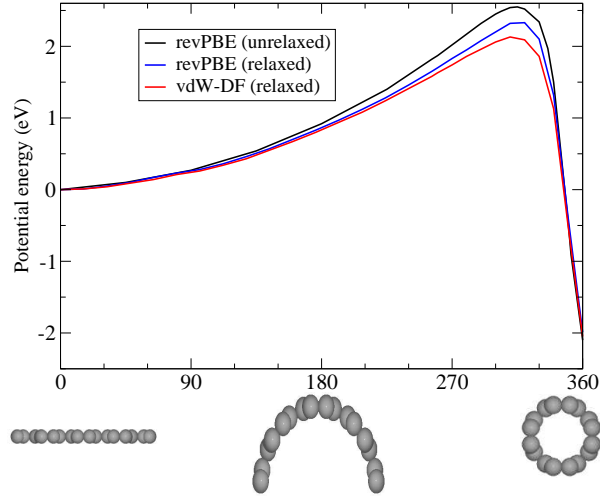
Figure 1.1: Potential energy of a gradually folding graphene sheet into a CNT in vacuum. The barrier is a consequence of built up strain energy during the formation of the CNT. Included are revPBE with (blue) and without (black) structural relaxations. The figure also includes vdW interactions through the vdW-DF (red) which slightly reduces the formation barrier.

is related to the surface step. As the chirality of the tube determines whether it is conducting or semi conducting [8], the alignment of the step potentially provides the necessary building blocks for a transistor. This is illustrated in Fig. 1.1.1

To test the plausibility of this process, the simplest test possible is to see whether the folding of the graphene sheet into a CNT is energetically stable in vacuum. This is illustrated in Fig. 1.1 where the graphene sheet of 16 carbon atoms, with periodic boundary conditions in the thought tube direction, is continuously folded into a tube. Density Functional Theory (DFT) calculations find the energy of the tube, E_{tube}, around 2 eV more stable than the energy of the sheet, E_{sheet}, with a barrier due to the built up strain energy in a tube over a sheet, $E_{barrier}$. The size of this barrier seems to be sensitive to the exchange-correlation (XC) approximation used, and inclusion of van der Waals (vdW) forces lowers the barrier marginally. The strain energy of the tube is proportional to R^{-2}, where R is the radius of the CNT [9, 10].

The condition that the tube has to be energetically more stable than the sheet is not enough. The energetic difference has to be large enough to break carbon bond to the surface, or a tube will not be formed from the sheet. This means

that the carbon bond to the step, E_{strong}, and the physisorption strength to the surface, E_{weak}, has to be known. Finally, the bond strength of E_{strong} has to be more stable than $E_{barrier} + K \cdot E_{weak}$ in order to excite the sheet enough to fold without letting it dissociate from the surface due to too weak anchor, where K is a constant less than unity, since $E_{barrier}$ represents a semi-folded structure where the bond to the surface is weaker. If E_{weak} originates from physisorption between surface and substrate, it can roughly be assumed to scale linearly with the number of carbon atoms[11]. This means that a tube that is too small may result in a too high $E_{barrier}$, while a too large a tube may result in a too high an E_{weak}.

$$E_{tube} - E_{sheet} < E_{strong} + E_{weak} \qquad (1.1)$$

$$E_{strong} < E_{barrier} + K \cdot E_{weak} \qquad (1.2)$$

Although these conditions are only crude guidelines they are still full of challenges. E_{weak} is typically the result of dispersion, like vdW forces. In DFT, dispersion forces are relatively newly implemented in XC functionals, and even more recently implemented self-consistently and cost-efficiently.

1.2 Outline

Every result in this thesis is somehow related to the challenges described above, although some results may have a more obvious connection than others. About half of the thesis will discuss the relevance of vdW forces in adsorption. Papers 1, 3 and 4 contain early adsorption calculations with the vdW-DF, which were made at an early stage when it was unknown if its approximations could be applied to metallic systems at all. Paper 5 studies if and how vdW forces compete with other forces, highly relevant to the problem above, and Paper 6 studies the accuracy of older and newer vdW-DF functionals compared with experimental results.

A few months into the project I learned that the balance between vdW and other forces are also relevant in water. As there existed high accuracy calculations on these systems we though it would be very good practice to test the vdW-DF functional to stronger bonds. For this reason I got involved with water, in which the force balance turned out so important and controversial that we expanded our calculations to liquid water. The structure of molecular and liquid

water is discussed in Papers 2 and 7. Paper 8 discusses the relevance of vdW forces for the hydrogen bond. In addition to the possible value of the results on water, the parallel work on water has been very important in testing and understanding functional development, and some of the functionals used here for both chemisorption and physisorption were originally developed by another group [12] with the main interest of its accuracy for water systems.

CHAPTER 2

Sparse Matter

When we experience materials, their hardness is an important property. To describe how hard a material is, one way is Mohs scale of mineral hardness. Here hardness can be characterized by its ability to scratch other materials [13]. If material A has a Mohs hardness of 3, while material B has one of 4, material C will will be placed in between the two if it is able to scratch material A, but not material B. Diamond has a hardness of 10, and is pretty much able to scratch any other material on earth. On the other hand, graphite, which is also a carbon material, has a hardness of 1.5 slightly softer than a finger nail. On the third hand, the carbon based buckyball is expected to be twice as hard as diamond when compressed [14]. The difference between the world's hardest material and one of the softest is all determined by its internal electronic bonds. Diamond is built by strong covalent carbon bonds, while graphite no doubt is built up by hard layers of strong covalent carbon bonds, but the scratching is typically determined by the fact that each layer is weakly bound by van der Waals (vdW) forces.

The term sparse matter is meant to include materials with regions of low electron density and thus of small electronic overlap [15]. With this definition, vdW forces are often relevant to understand such systems, as they are often long ranged compared to other forces, and thus attractive even with small or zero density overlap. This excludes ideal bulk metals from counting as sparse matter. The definition does certainly not exclude matter, however, in which other forces

than vdW are also relevant. It includes graphite, even though its covalent bonds in the layer are stronger than diamond. On the contrary, sparse matter does more often than not include both covalent and vdW forces, some examples being food, ski wax, plastics, DNA, and tape. Sparse matter is relevant for most things we do as the force composition strikes a healthy balance between inertness and reactivity.

There are also other properties to metals than their bulk properties. In heterogeneous catalysis, we are interested in the interactions between surface and adsorbate. For such systems there are certainly situations where some regions experience small electronic overlap, one such situation being physisorption. Therefore it is difficult to think of too many interesting systems that are not in any way sparse.

2.1   Forces in sparse matter

It is not obvious how to define vdW forces. One common definition[16] is to include permanent dipole - dipole interactions, permanent dipole - induced dipole interactions, and induced dipole - induced dipole interactions (dispersion)

In this thesis I choose to speak of vdW forces mainly as dispersion forces. This will be a practical notation since ordinary dipole-dipole interactions are typically well treated in DFT with standard GGA functionals, while dispersion forces are not [17]. Dispersion forces can instead be calculated by approximating the polarizability of the electronic density in the van der Waals density functional (vdW-DF)[18]. Other interesting methods are also available for the purpose, including the M06 functionals [19], DFT-D [20], TS-vdW[21], and the random phase approximation (RPA) [22] (including variations like EXX/RPA and RPA+). See Ref. [23] for an interesting comparison between RPA and vdW-DF theory. [1]

2.1.1   Van der Waals forces

As most phenomena, vdW forces can be understood with different models depending on required level of abstraction. In the simpler model, vdW forces

---

[1]The interest in the field is now growing almost exponentially, as indicated in the program of Sessions A31, B31, and D31 at the APS meeting in March, where many different methods and applications will be presented.
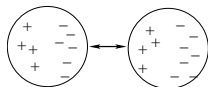
Figure 2.1: Simple illustration of fluctuating dipole. The small coupled and aligned fluctuating charge heterogeneities between two atoms result in net attraction.

are understood by temporary electronic heterogeneities inducing other electronic heterogeneities. These can be viewed as temporarily induced and coupled dipoles. One simple cartoon of this is illustrated in Fig. 2.1. In this example the electric field results in an attractive potential between dipole fragments. This model is sufficient for understanding why polarizability is a key concept of dispersion. There are some unclear concepts with this simplified model, however. In the Schrödinger Equation, the ground state of the hydrogen atom doesn't have any fluctuations, yet vdW forces still exists. On this level it is helpful to think of vdW forces as originating from the zero-point motion of electrons.

2.1.2   Hydrogen Bonds

The concept of hydrogen bonds (HBs) has been around for almost a hundred years [24]. HBs are directly responsible for life as they are a vital component in DNA where the base pairing of nucleotides are HBs, and also the reason why water boils at a relatively high temperature. They are typically weaker and more flexible than covalent bonds, while stronger and more directional than van der Waals bonds. They are strong enough to form a long and stable DNA double helix, yet weak enough for the helix to split during reproduction.

There are various definitions of the HB available in the literature. Typically these concern a geometrical definition, in some cases with restrictions on the nature of involved forces. One very broad definition states that a HB exists if: 1) there is evidence of a bond, and 2) there is evidence that this bond sterically involves a hydrogen atom already bonded to another atom [25]. This is a very intuitive definition that includes little geometrical constrains and none on physical nature. A way to specify what sterically means can be done by constraining the angle of $X - H \cdot \cdot A$ and distance of $H \cdot \cdot A$, where H is a hydrogen atom and where X and A are some electronegative atom or ion[2]. Although this geometric definition is bound to some subjectivity, it is relatively common, and some choices of parameter values get some support from experimental results [26].

---

[2]In this thesis X and A will both be Oxygens. The more exact and general properties of X and A are disclosed in greater detail in [24].
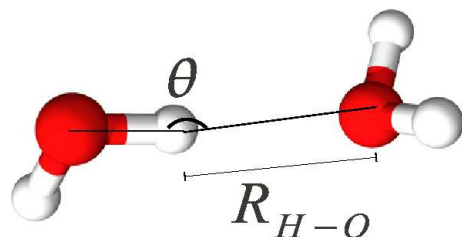
Figure 2.2: Schematic overview of the geometric definition of the HB in the case of water. θ marks the angular definition of $X - H \cdots A$ and R_{O-H} the separation $H \cdots A$. Common nomenclature is also to instead define $180°$-θ.

$X - H$ is often called proton donor while A is called proton acceptor, or just donor and acceptor. Water molecules with two hydrogens can be single donors (SDs), double donors (DDs) or no donors (NDs).

In general the HB consists of several forces of different nature, like electrostatic, polarization, charge transfer, and dispersion. While exchange repulsion is a force different in nature, it too affects the net HB strength [27]. The water HB involves considerable charge transfer, although its nature is believed to originate mainly from electrostatic interaction [24]. In this thesis the definition of the HB will only contain geometrical definitions, assuming that every force that affect the HB is part of the HB. With this definition I will then attempt to analyze the role of vdW forces in the HB. The reason for this is that the geometrical part of the HB mainly is used to understand the resulting structure of water, and that experiments made on liquid water can observe HBs, but not vdW forces per se.

2.2   Water

It has been claimed that "No one really understands water" [28]. Although some scientists may disagree about this, most would agree that water is a very complex substance with more anomalies than most substances. All in all, up to sixty-four anomalies have been reported on phase characteristics, density, and thermodynamics [29]. In order to understand these anomalies, an understanding of the molecular structure of water is needed, which is still a matter of much debate (see Paper 7).

2.2.1 Techniques to determine structure

The science of determining structure from experiments is beyond the scope of this thesis. However, since Paper 7 treats the role of vdW forces in liquid water, a short and non-exhaustive orientation about some common experimental techniques may be necessary just to be able to relate to different experiments.

Like for crystalline materials, the distance between atoms in liquid water can be determined by Bragg diffraction. Unlike crystalline materials, however, in which sharp crystal planes give sharp diffraction patterns, the average atomic separations in a liquid results in broad and smeared-out peaks. In X-ray diffraction the X-rays interact with electrons. The method is therefore sensitive mainly to the oxygen structure, as an O atom has more electrons than an H atom. Neutron diffraction, on the other hand, is sensitive to nuclei, and by using complementary experiments on water and deuterated water it is possible to obtain information of the hydrogen structure [30]. The relation between the measured structure factor S and the pair-correlation function (PCF) g in a monoatomic liquid can be written

$$S(q) = \rho \int r^2 (g(r) - 1) \frac{sin(qr)}{qr} dr \qquad (2.1)$$

where ρ is the electronic density, and where in water the PCF can be g_{OO}, g_{OH} or g_{HH}.

In order to obtain a PCF consistent with experimental data Reverse Monte Carlo (RMC) [31] and Empirical potential structure refinement (EPSR) [32] are two common methods. The RMC method iteratively moves the atoms to create a system that replicates the experimental data in combination with additional optional constraints. The EPSR method starts from an empirical potential that is optimized iteratively until the calculated system, based on the empirical potential, replicates experimental data. Although the methods are similar, the EPSR method typically samples a smaller but physically more realistic phase space, as its initial potential contains physical parameters.

Instead of measuring the g_{OO} indirectly through diffraction experiments, one can aim at measuring the mechanism that actually is responsible for the O-O correlation; the HB. With X-ray emission spectroscopy (XES) and X-ray adsorption spectroscopy (XAS) it is in principle possible to gain information on the electronic structure by interpretation of emission and adsorption spectra of water. One way is to compare a spectrum with unknown structure with a calculated spectrum with known structure, e.g, from DFT calculations or other theory. In water, XES and XAS spectra relevant for the HB are studied in
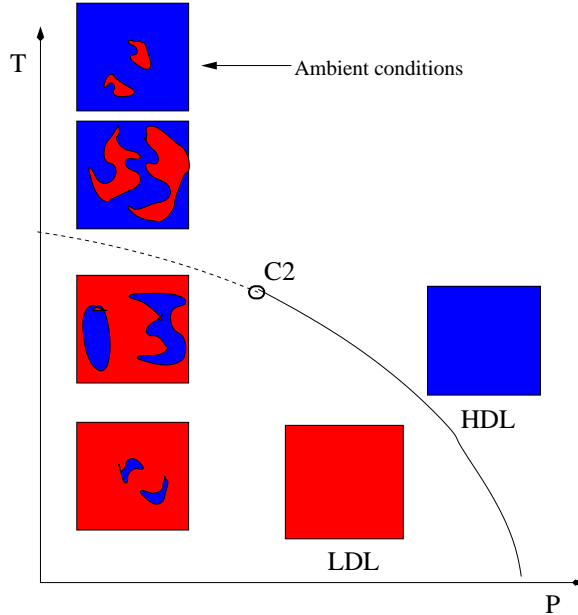
Figure 2.3: Cartoon of the phase space of water around the second critical point according to the critical point theory with complementary experimental results [39], where water at ambient conditions holds a large portion of HDL structure. The dotted line is a continuation of the coexistence line and is often called the Widom line [40]. Some thermal anomalies can be explained by their position on the Widom line [40], which is considered as an important argument for the LLCP hypothesis.

several papers [26, 33, 34, 35, 36, 37] with no clear consensus.

With small-angle X-ray scattering (SAXS) it is possible to probe structures for large scale heterogeneities, such as macromolecules on the nanometer scale [38].

2.2.2   On water models

In thermodynamics a critical point specifies under which conditions a phase boundary ceases to exist. In water, the vapor-liquid critical point shows the temperature and pressure for which both these phases cease to exist. The liquid-liquid critical point (LLCP) model is a theory which introduces a second critical point in the phase diagram of water. The phases that become distinct below the critical point are two forms of ice, called low density amorphous ice (LDA)

and high density amorphous ice (HDA) [41], both which have been discovered experimentally and and between which there are phase transitions [42].

Although this is interesting in itself, what makes the LLCP model important in this thesis is what it predicts "beyond "the critical point when both phases of amorphous ice cease to exist. According to the theory, these regions in phase space should support liquid versions of its corresponding amorphous ice, a high density liquid (HDL), and a low density liquid (LDL). This is schematically illustrated in Fig. 2.3.

Experimentally, this picture has gained some support. It has been found from XAS that ambient water contains more distorted HBs, characteristic for HDL, than previously thought [26]. Recently SAXS results was shown to demonstrate temperature dependence, something that was interpreted as temperature dependent density fluctuations on the nano meter scale, that was related to HDL and LDL by interpretation of X-ray emission spectroscopy and X-ray Raman scattering [43].

It is however important to note that this is still under much debate. The SAXS results have been criticized [44], and defended [45], and another SAXS study claims to see no need for temperature dependent structural heterogeneities [46]. The case for ambient water as a near-tetrahedral homogeneous HB structure has also been proposed and supported by diffraction experiments [47], by Raman spectroscopy [48] and by molecular dynamics (MD) simulations, using both empirical force fields and ab-initio methods [49].

Although there may nowadays be some consensus that ordinary diffraction experiments do not provide enough information on the fine structure of water [50], interpretation of XAS,XES, and SAXS data is still controversial. Paper 7 supports the theory of water heterogeneities. To avoid any impression of unintentional bias, the comprehensive review in Ref. [50] is therefore recommended.

2.2.3   Density Functional Theory and water

One could have hoped that MD simulations of water, where the structure is trivially extracted from a sufficient amount of iterations, would shed some light on these controversies. Unfortunately, the structure has been shown to depend much on calculational approximations. In DFT it has been shown that the qualitative properties of water vary much with choice of exchange-correlation approximation [51], and that the seemingly important strength of the dimer HB is a poor indicator [52] of quality for MD simulation results.
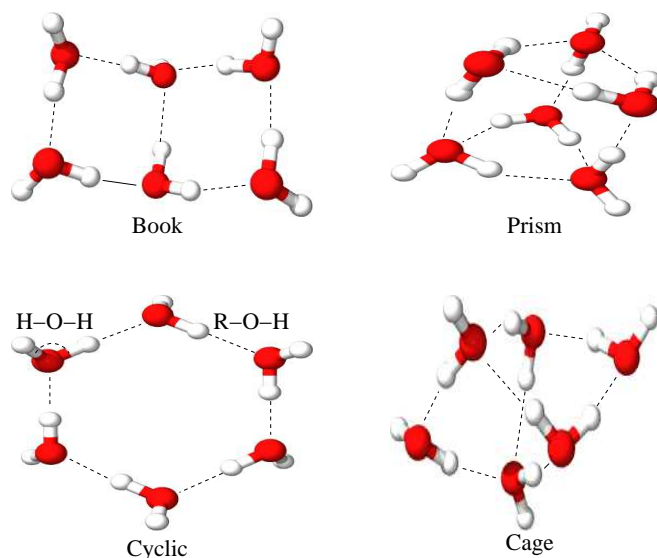
Figure 2.4: Four different possible geometries for the water hexamer. DFT benchmarking on these structures against more accurate wave-function methods enables testing on how well energy trends among different water geometries are reproduced. It has been shown that density functionals that do not account for vdW forces all get the energetic trend wrong, due to the importance of molecular compactness [58].

Overall, the water structures obtained in traditional DFT, *i.e.* with a GGA and LDA XC functional, are somewhat unconvincing, since most XC approximations do not match experimentally measured structures, while the few that do so may do it for the wrong reasons. RPBE [53] for example has been shown to produce good results for liquid water, despite its significant underestimation of the HB strength in the dimer [52]. PBE [54] on the other hand describes the HB well [55], but over-structures water significantly [52], resulting in too high melting temperatures. It has also been shown that inclusion of vdW forces significantly softens the water structure [56] and improves diffusivity [57].

2.2.3.1   Water hexamers

The accuracy of DFT results for water can be further tested by using the hexamers represented in Fig. 2.4 instead of dimer. By this it is possible to compare dissociation energies and stability trends to more accurate results from wave-function methods. Santra and co-workers [58] showed that no traditional
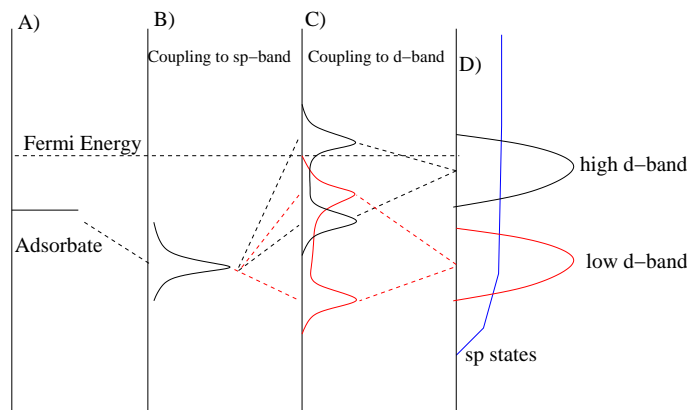
Figure 2.5: Schematic illustration of adsorbate interaction with metallic surface states. (A) The energy level of the adsorbate in gas phase. (B) adsorbate coupling with broad sp-band broadens the adsorbate state. (C) coupling with the narrow d-band results in a hybridization into a bonding orbital (lower) and an anti-bonding orbital (upper). (D) the energy of the d-band electrons determine if the anti-bonding orbital should be filled or not. A d-band close to the Fermi-level (black) will result in an unoccupied anti-bonding state and a strong bond. A low d-band (red) will result in a higher occupation of the anti-bonding state, and a weaker bond.

exchange-correlation approximation is able to reproduce the trend given by wave-function methods. They identified a lack of vdW forces as causing the wrong trend and showed that a vdW correction scheme alters the relative energies of the four isomers to the correct ordering. Simply, the mean intermolecular distances decrease upon going from cyclic to book to cage to prism and so the magnitude of the vdW correction decreases in the opposite order, ultimately giving the correct stability sequence [58].

2.3   Adsorption

Molecular adsorption on surfaces is an important process in heterogeneous catalysis. To create efficient catalysts with high conversion rates, the adsorption strength of the adsorbate needs to be tuned. When tuning adsorption strength on metals, it has been shown that d-electrons matters much. The role of d-electrons in surface adsorption can be explained by the Newns-Anderson model (NA) [59] and is the fundamental idea of the d-band model [60, 61].

The d-band model formulates how how adsorption strength can vary with the energetic center of the d-band, ϵ_d, with the coupling matrix element, V_{ad}, and the filling of the d-band, f [60, 61]. A higher d-band center typically increase adsorption strength, since the anti-bonding orbital of the adsorbate shifts upwards above the Fermi-level, resulting in less occupation and a stronger bond. Repulsion typically increase with an increased V_{ad}, which is a property dependent on the spatial extent of the d-electrons and density overlap related to the Pauli repulsion, while decreasing with a lower filling f of the d-band.

These parameters give a framework to choose between substrates when tuning adsorption strengths, and thus catalytic rates. For transition metals in a certain period (row in the periodic table), adsorption typically increase by moving to the left, due to a higher d-band and a lower filling. For the noble metals Cu, Ag, and Au, the d-band is filled, meaning that the dominating contribution comes from the repulsive V_{ad} which increase by moving down, making gold more inert to molecular adsorption than Ag and Cu [60].

Another example of how adsorption strengths can be tuned from this knowledge is by the use of defects. Under-coordinated surface atoms in defects like adatoms and steps generally have a higher d-band center. This makes such sites more reactive than sites with higher coordination [6], which has been verified by experiments[4, 5, 7]. Other ways to manipulate adsorption strength with the d-band parameter is by alloying or by straining the substrate.

CHAPTER 3

Theoretical tools

3.1 Density Functional Theory

In theory, the electronic structure is described by the Schrödinger equation (SE). In practice, however, the task of using this equation for interesting systems is often too complicated. P. M. Dirac supposedly once noted: "Chemistry had come to and end. Its content is entirely contained in that powerful equation (the SE). Too bad that in almost all cases, this equation is far too complex to allow solution " [62]. Perhaps the feeling Dirac had over this was similar to that of a pirate with a treasure map and no ship. Today, solving the SE directly is still a daunting task, even by computer, and several approximations are still made. High-accuracy wave-function methods are today able to treat around 100 electrons. For many applications, however, this is not good enough. One way to treat systems with more than 1000 electrons is by Density Functional Theory (DFT). The fundamentals of DFT are discussed in great detail in the literature [63], but since this thesis discuss some technical details of DFT, a small and non-exhaustive discussion of the DFT framework is needed.

DFT rests on two theorems from Hohenberg and Kohn [64]. It is valid for any system of interacting particles in an external potential $V_{ext}(\mathbf{r})$, where the Hamiltonian can be written

$$\widehat{H} = -\sum \frac{1}{2m_i}\nabla_i^2 + \sum V_{ext}(\mathbf{r}_i) + \frac{1}{2}\sum_{i\neq j}\frac{1}{\mathbf{r}-\mathbf{r}_j} \qquad (3.1)$$

The two Hohenberg-Kohn (HK) theorems show that the ground state density $n_0(\mathbf{r})$ uniquely determines the external potential V_{ext}, and that a universal density functional for the energy, $E[n]$, can be defined. The density $n(\mathbf{r})$ that minimizes $E[n]$ is the ground state $n_0(\mathbf{r})$. Although the theorem proves that the energy of a system is a density dependent functional, it doesn't provide any clues of what this functional may look like.

The problem of getting the energy functional can be approached by Kohn-Sham (KS) theory [65]. Instead of treating interacting real electrons, KS theory treats noninteracting electrons in an effective potential, V_{eff}. This potential is constructed to reproduce the real density from the noninteracting electrons. These two identical densities then have the same energy, according to the HK theorem, regardless of their different kind of electron-electron interactions. The KS energy can then be written as

$$E[n(\mathbf{r})] = T_s[n(\mathbf{r})] + V_H[n(\mathbf{r})] + E_{xc}[n(\mathbf{r})]) + V_{ext}[n(\mathbf{r})] \qquad (3.2)$$

, where $T_s[n(\mathbf{r})]$ is the kinetic energy of a noninteracting electron gas, and $V_H[n(\mathbf{r})]$ is the Hartree energy

$$V_H[n(\mathbf{r})] = \frac{1}{2}\iint \frac{n(\mathbf{r'})n(\mathbf{r})}{|\mathbf{r}-\mathbf{r'}|}d\mathbf{r'}d\mathbf{r} \qquad (3.3)$$

The exchange-correlation (XC) energy E_{xc} secures that the fictitious one-electron system actually behaves like a real many-body electron system. Without a good approximation of this term, KS electrons tell us nothing about how real electrons behave. Fortunately, there are ways to calculate this term for one important system, the homogeneous electron gas, which will be discussed soon. From here it is possible to find the ground state density and its corresponding potential by iterating the so called Kohn-Sham equations:

$$[-\frac{1}{2}\nabla^2 + V_{eff}]\phi_j(\mathbf{r}) = \epsilon\phi_j \qquad (3.4)$$

$$V_{eff}(\mathbf{r}) = V_{ext}(\mathbf{r}) + \int \frac{n(\mathbf{r'})}{|\mathbf{r}-\mathbf{r'}|}d\mathbf{r'} + V_{xc}(\mathbf{r}) \qquad (3.5)$$

$$V_{xc} = \frac{\delta E_{xc}}{\delta n(\mathbf{r})}$$

$$n(\mathbf{r}) = \sum_{occupied\ states} |\phi_j(\mathbf{r})|^2 \tag{3.6}$$

The KS equations give us an explicit formulation of the energy functional, to-
gether with a set of equations that can be solved to get the desired ground state
density. However, a good approximation of the XC functional is essential, and
finding a good approximation is a major field within DFT.

3.1.1   Exchange-Correlation Functionals

The simplest XC energy approximation can be expressed as the integral of the
XC energy per electron in each point $\mathbf{r}$, where the XC energy per electron is
some function of only the local density at point $\mathbf{r}$,

$$E_{XC}^{LDA}[n] = \int dr n(\mathbf{r}) \epsilon_{xc}^{hom}(n(\mathbf{r})) \tag{3.7}$$

This is the Local Density Approximation (LDA) and $\epsilon_{xc}^{hom}(n)$ is the XC energy
per electron of the homogeneous electron gas. For this system, exchange and
correlation can be treated separately, where the exchange energy per electron
can be calculated analytically, and where the correlation can be calculated nu-
merically by, *e.g.*, Monte Carlo methods [66] and tabulated. Although LDA has
been surprisingly successful, particularly in describing bond lengths and lattice
parameters, it typically overestimates the strength of bonds in molecules and
metals.

Generalized Gradient Approximations (GGAs) offer a way to fix LDA's system-
atic overestimate of bond energies and underestimate of bond lengths. GGAs
start off from the XC energy in the homogeneous electron gas but allows ϵ_{xc} to
depend on both local density and density gradients,

$$E_{XC}^{GGA}[n] = \int dr n(\mathbf{r}) \epsilon_{xc}^{hom}(n(\mathbf{r})) F_{xc}(s(n(\mathbf{r}), \nabla n(\mathbf{r}))) \tag{3.8}$$

$$s = \frac{|\nabla n|}{(2k_F)n} \tag{3.9}$$

Here s is a normalized gradient, large in regions of large gradients, but also in regions of very low density. The enhancement factor F_{xc} is a function of s with the role to enhance the XC energy per electron at points $\mathbf{r}$ where the density is not homogeneous. Differently from the homogeneous electron gas, where the relation between $\epsilon_{xc}^{hom}n(\mathbf{r})$ and the density is in principle known, there is no formally correct relation between $\epsilon_{xc}^{GGA}(n(\mathbf{r}), \nabla n(\mathbf{r}))$ and the gradient of the density. Therefore there are plenty of GGAs available, where some are developed to work as all-round functionals, and others for specific systems. There are hints of what $F_x(s)$ should look like under certain conditions, based on asymptotic gradient expansions for low s, restrictions due to physical sum rules, and interpretations from the XC hole originating from coupling constant integration, through the so-called adiabatic connection formula [67, 68, 69].

Electrons in metals are different from electrons in molecular orbitals, however. It cannot be guaranteed that one parametrization of the enhancement factor $F_{xc}(s)$ can treat both systems accurately. In fact, it has been argued that GGA functionals can either give accurate atomic exchange energies by violating the gradient expansion for a slowly varying density, or preserve the gradient expansion in order to accurately describe bulk and surface metals [70].

In the vdW-DF, the similarity of the exchange-functional approximation with Hartree-Fock (HF) functional is of great importance, the enhancement factor F_{xc} is an important tool when comparing different GGAs to each other when looking for an approximation similar to HF. It is therefore good to get a qualitative picture of the relation between the GGA enhancement factor and bond-strengths (cf.[71]).

3.1.2   Qualitative interpretation of $F_x(s)$

The exchange enhancement factor F_x is plotted for three different GGAs in Fig. 3.1. The PBE [54] and revPBE [72] functionals have similar functional forms, while the newer C09 functional is based on certain high and low s asymptotic behaviors [73]. To analyze the meaning of F_x in a pedagogical way I have plotted densities from two one-dimensional exponentially decaying orbitals in the upper panel of Fig. 3.2 and Fig. 3.3 . They are similar to the hydrogen-atom s orbital, and are drawn at two different separations, together with density from their sum as an approximation of the density of a dimer.
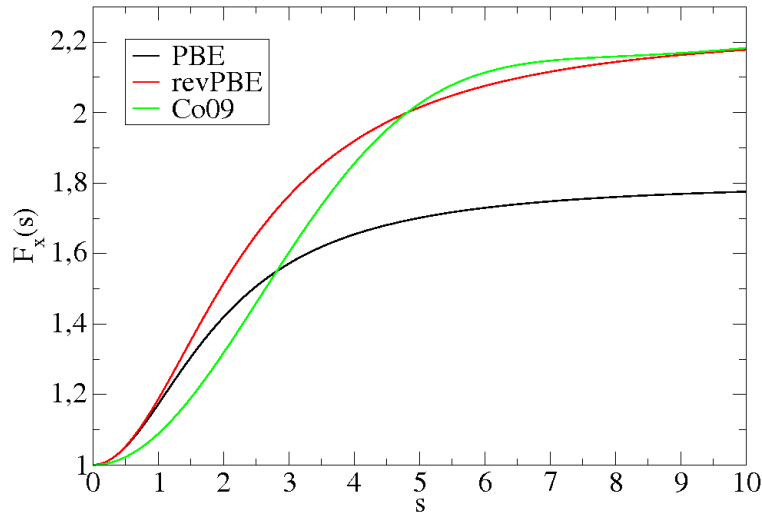
Figure 3.1: Exchange enhancement factor $F_x(s)$ for three common GGA exchange approximations that have been used in the vdW-DF.

The lower panel shows the corresponding s value for the dimer(black) and the two separate monomers (red and green). In the middle of the dimer the s value briefly goes to zero due to the vanishing gradient.

The binding energy of the artificial system is calculated as

$$E^{bond} = E^{dimer} - E^{monomer1} - E^{monomer2} \qquad (3.10)$$

In this case, we are only interested in the bond contribution coming from exchange functionals. Therefore we can write

$$E_x^{bond} = \int dr \ n_{dimer}\epsilon_x^{hom}(n_{dimer})F_x(s_{dimer}) -$$

$$- \int dr \ n_{monomer1}\epsilon_x^{hom}(n_{monomer1})F_x(s_{monomer1})$$

$$- \int dr \ n_{monomer2}\epsilon_x^{hom}(n_{monomer2})F_x(s_{monomer2})$$

Even though we don't know the value of ϵ_x^{hom}, it is always negative since exchange interaction can be interpreted as removing the interaction of one electron, called the exchange hole[63]. We also know that it does not vary with choice of GGA exchange functional. We therefore note that for a given density, since ϵ_x^{hom} is negative with no other negative factors in the integrals, E_x^{bond} gets more negative with increasing size of $F_x(s_{dimer})$ in the first term, resulting in a stronger
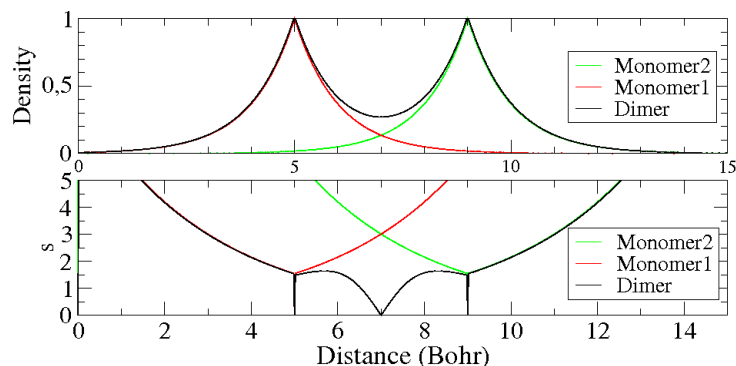
Figure 3.2: One-dimensional system with two exponentially decaying orbitals separated at 4 Bohr of separation. Upper panels show density distribution for sum of the two orbitals as well as for two orbitals in separate systems. Lower panel shows the corresponding s values

bond, while getting more positive with increasing size of $F_x(s_{monomer1})$ and $F_x(s_{monomer2})$ in the second and third term respectively, resulting in a weaker bond. Without ϵ_x^{hom} we cannot tell anything about absolute values, but we can talk about relative trends.

From looking at s values for the systems in Fig. 3.2, it becomes clear that s only differ between the dimer and the two monomers in the bond region. Although s rises rapidly in regions without density for both monomers, those regions are not important for the energy, as there is no density there. By comparing s for the dimer and monomers, it is clear that the monomer systems result in larger s values than the dimer, for which s goes to zero at the bond center. When looking at the enhancement curves for revPBE, PBE and C09 it is now possible to guess the relative bond energy trend. Since the s values are larger for the monomers than for the dimer in every point, and since $F(s)$ is a monotonically increasing function for each functional, the least attractive functional will be the one that increases fastest, thus increasing $F_x(s_{monomer1})$ and $F_x(s_{monomer2})$ the most. A slowly increasing enhancement curve is therefore more attractive than one that increases rapidly with s.

It is useful to compare s values in Fig. 3.2 and Fig. 3.3. Larger bond lengths are typically connected with larger s values, so the bond strength for long separations depend more on the enhancement of large s, while bond strength for short separations depend mainly on small s. Even though this is only a schematic illustration, it is handy to keep in mind. For example, it has been shown that revPBE is too repulsive at short separations but good at longer separations,
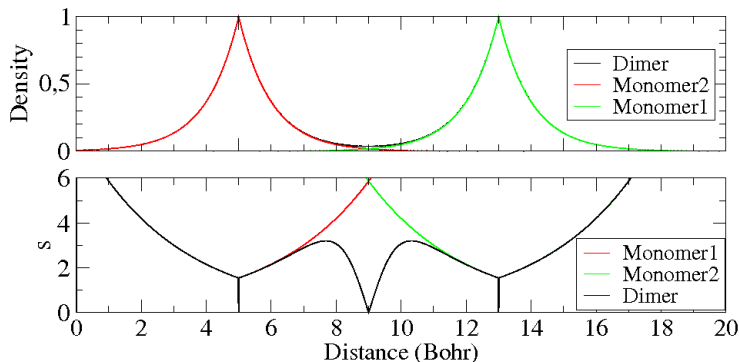
Figure 3.3: One-dimensional system with two exponentially decaying orbitals separated at 8 Bohr of separation.Upper panel show density distribution for sum of the two orbitals as well as for two orbitals in separate systems. Lower panel shows the corresponding s values

while PBE is a good candidate at shorter separations, while being too attractive at longer separations. A systematically improved candidate therefore needs to show less rapid increase for low s, while keeping revPBE enhancements for large s, like the C09 seems to do.

3.1.3   vdW-DF

The vdW-DF XC functional has the form

$$E_{xc}^{\,vdW-DF} = E_x^{\,revPBE} + E_c^{\,LDA} + E_c^{\,nl} \qquad (3.11)$$

For the vdW-DF, approximate exchange functionals are designed to be close to the HF approximation. This is an appealing argument, as it allows for systematic design and comparisons towards the exact formulation. There is no obvious criterion for the comparison of approximate exchange functionals with the HF approximation. As the vdW-DF [18] is developed for pure vdW interactions, a suitable and natural criterion used to compare magnitudes of the exchange energies for the Ar dimer, a system with an atomic separation typical for vdW interactions (4 - 5 Å), where the revPBE functional is closer to HF than PBE. The PBE even gives a small net attraction by exchange only for large separations like these, which for a vdW bonded system like the Ar dimer is physically wrong, as it indicates a spurious vdW attraction coming from the exchange [18].

However, several studies show that the vdW-DF gives slightly (10 - 20 per cent) too long separations [74, 18, 75, 15, 76, 77]. Further, it underestimates the

strength of the HB [78]. The common interpretation is that this problem is caused by the revPBE exchange approximation, being too repulsive compared to Hartree-Fock exchange for separations shorter than the 4 - 5 Å region that it was designed for. For such systems, other functionals, like the PBE gives closer agreement with the HF energy and less repulsion, which often results in better values for binding energies and bond lengths. In order to get a functional that correctly treats both chemisorption and physisorption, this needs to be addressed.

It is not obvious that the conceptual framework behind the functional in the form of Eq.3.11 provides means for systematic improvement and development. But the exchange part can be compared with HF to determine accuracy, and this has been used as a guide for exchange development. A general starting point for correlation functionals is the adiabatic connection formula [68, 67, 69], applied to get the vdW-DF [18] and vdW-DF2 [79] functionals, and more recent functionals, including the RPA [22, 23]. In the former the correlation approximation is designed to use one term to treat local correlation by the LDA approximation, while treating all non-local interactions by the other term. This design is meant to eliminate double counting of correlation effects, as a semi-local correlation functional in theory could pick up non-local (or semi-local) correlation effects also treated by the non-local term [18]. The documented tendency of LDA correlations to underestimate correlation in non-homogeneous systems, like molecules [80], is certainly a wanted feature, as it means there is systematic room for additional non-local correlation effects. At the end of the day however, the accuracy of the correlation term, and hence the accuracy of the whole functional, is best verified by comparing with higher order wave function methods or experiments.

3.2   Available exchange functionals

This chapter briefly treats the most used exchange approximations used to improve the vdW-DF and how they are performing according to literature. It should be pointed out that the differences between functionals like PBE, revPBE, and RPBE are significant already at the GGA level, revPBE being better on atomization energies and covalent bonds [72], RPBE on adsorption systems [53] and PBE on lattice parameters and hydrogen bonds [81, 55]. The system-specific strengths and weaknesses of each exchange functional is likely to be inherited by the vdW-DF variants. This means that the quest for the best exchange functional in the vdW-DF is no more trivial than the quest for the best GGA functional.

RevPBE: As mentioned, the revPBE exchange functional is the originally chosen exchange functional in the vdW-DF: the general tendency is a slight overestimation of bond lengths, usually combined with a small underestimation of bond energies. This has been documented for noble-gas dimers [18], benzene dimers [74], benzene adsorption on noble metals [82], CO_2 dimer [75], water on benzene [75], and graphene sheets [76], with more examples in Ref. [15]. The general underestimation of bond energies has also been shown for 17 of the 22 molecules in the S22 data set [78], as compared with high accuracy wave function methods [83, 84, 85], and that the underestimation is worst for HB bonded systems [78], where bond lengths tend to be shorter than for dispersion bonded systems. This original exchange approximation was very successful in a study of hydrocarbons on graphene, where it agreed with experiments better than any other method [86].

PBE: The PBE exchange has been shown to treat hydrogen bonded systems accurately, while slightly overestimating binding energies for dispersion bonded systems [78].

Hartree-Fock: Although this is by definition the best choice of exchange, using HF in the vdW-DF often gives too strong bonds [74, 87]. This has been used as an argument for an altered correlation treatment, more consistent with HF exchange and with some more empiricism [88], with an updated version that also dealt with logarithmic divergence [89]. The latter version has be criticized for, among other things, not being charge conserving [90].

OptPBE-vdW: The optPBE-vdW functional [12], and relatives, is developed by fitting the exchange enhancement parameters of PBE to the energies of the S22 data set when included in the vdW-DF framework. This is a very interesting perspective and the optPBE-vdW has been shown to deliver chemical accuracy for the S22 data set, as well as very good energy trends for the water hexamer [12]. The optPBE-vdW is thus further tested in this thesis to investigate its performance for adsorption systems and liquid water.

PW86: The issue of spurious vdW binding originating from exchange has been studied by Harris [91]. He noted that if the density overlap between two He atoms is M, then the exchange energy for that system should be proportional to M^2, as is the case in HF. The same proportionality applies for the kinetic energy. For the LDA approximation however, the exchange energy is instead proportional to $M^{4/3}$, the kinetic energy still being proportional to M^2. For small density overlaps, M, then

$$dE = C_T M^2 - C_E M^{4/3}, \tag{3.12}$$

where the second term is the dominant one for small M, resulting in spurious exchange binding. In Ref. [92], it is pointed out that the enhancement factors for high s values, usually dominating in low density regions, may offset this systematic error. It is also pointed out that the key is the slope of the enhancement curve, rather than the enhancement value itself. The authors therefore test exchange functionals like B86 [93], B88 [94], and PW86 [95], which all have relatively high slopes for high s values. It is then shown that the PW86, with an enhancement slope of $s^{2/5}$ for high s, cancels the spurious exchange binding even at very large separations. From a functional development perspective, this is most interesting. These results show the origin of spurious exchange binding, present in PBE, and marginally in revPBE, as well as a method to solve the problem. This makes PW86 a very interesting exchange functional, even though it is still too repulsive for small separations.

C09: The C09 functional [73] is developed to reduce the short range exchange repulsion by letting the new functional approach the Gradient Expansion Approximation (GEA) for a slowly varying density, putting the following constraint on the enhancement factor

$$F_{GEA} = 1 + \mu s^2, s \to 0, \tag{3.13}$$

while forcing the enhancement to approach the revPBE limit for large s values. This is shown to improve bond lengths for the benzene dimer, compared with CCSD(T) data [96]. This is very interesting as the author here shows how constraints for small s values reduces repulsion. Very recently it has been proven able to treat graphene adsorption on metals, where it accurately treats chemisorption (graphene-Nickel) and physisorption (graphene-platinum) [97]. This is most interesting as it is an indication that the C09 is a strong candidate for an exchange approximation that can be used to treat both chemisorption and physisorption in a balanced fashion. Further, the C09 functional give good lattice parameters for for V_2O_5 [98].

3.3   Molecular Dynamics Simulations

Empirical force fields have been and are still being largely applied in the study of water. In this method the contributing forces to the bond are parametrized and split up, *e.g.* like

$$E_{tot} = E_{bond} + E_{angle} + E_{rotational} + E_{electrostatic} + E_{vdW}, \tag{3.14}$$
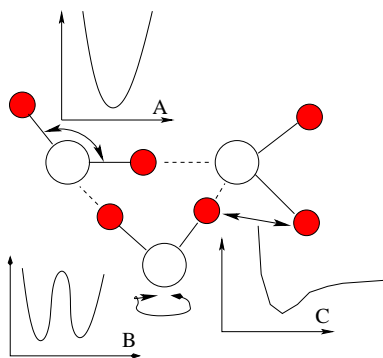

Figure 3.4: A cartoon example of three of the potential energy curves illustrated for the water trimer.

in which the potential energy in all terms are models derived from experimental works and quantum mechanical calculations. The potential energy depend on parameters like bond length, atomic mass, vdW radius, bond angle and partial charge. A cartoon example of three of the potential energy curves (Fig 3.4) illustrates this for the water trimer. Together with the trimer is (A) the angular potential energy term, dependent on the H-O-H angle and perhaps approximated by a harmonic oscillator, (B) the rotational potential energy term, dependent on how the third monomer is positioned towards the dimer, and (C) the vdW term, parametrized by the Lennard-Jones potential and dependent on H-H and other separations.

While the force fields are often parametrized against experimental data and accurate calculations, the transferability between systems may be questioned. These deficiencies do not occur for Car-Parrinello [99] (CP) and Born-Oppenheimer (BO) molecular dynamics (MD), collectively known as *ab initio* (AI) MD. In AIMD the forces are calculated using a first principle electronic structure method, typically density functional theory (DFT). BOMD, used in the study of liquid water, minimizes the Kohn-Sham energy functional at each timestep keeping all other parameters fixed, assuming that slowly moving atoms do not affect the electronic wave functions. In MD the molecules are situated together and trajectories are calculated using Newton's second law of motion. Phase space is then sampled by taking snapshots of the coordinates at different times. From the obtained configurations, structural properties, such as radial distribution functions (RDFs), can can easily be extracted.

For the simulation on water in this thesis, the number of molecules, the volume, and the energy are kept fixed. This is called an NVE ensemble. When starting this type of simulation, one can first minimize the potential energy of the struc-

ture and then assign a kinetic energy to the water molecules corresponding to two times the desired temperature of the system. One system half of the kinetic energy will then slowly transfer into potential energy according to the Virial theorem.

3.4   Calculational details

All calculations in this thesis are done with the grid-based projector-augmented wave method (GPAW) [100] software. The benefit of representing the density n a real space grid is mainly scalability, since subspace domains can be efficiently parallelized over, as well as the possibility of systematic numerical convergence through the grid spacing. Since GPAW is a projector-augmented waves (PAW) method it works by use pseudo potentials outside atom centered augmentation spheres, while still including core-electrons inside the spheres by using a linear transformation to switch from pseudo wave functions to all electron wave functions. The core-electrons are approximated by the so called frozen core approximation, and the core-density and information necessary for the linear transformation between pseudo wave function and all-electron wave function is generated for each atom by so called atomic setups. These setups have to be tested to correct atomic properties, as well as to secure transferability to various solids and molecules. Computational parameters are specified in the papers, except when default parameters are used.

For molecular dynamics, visualization, structure optimization and user interface the Atomic Simulation Environment (ASE) [101] is used, with default parameters except when stated otherwise in the articles.

CHAPTER 4

Results, including brief review of publications

Most of the results of this thesis are presented in the publications. This chapter is meant to give a brief review of the publications, to tie them together, and to set the results into the perspective of the thesis.

4.1 Water

This section is meant to contribute to the interpretation of the effects of vdW forces in water (Papers 2, 7 and 8). A growing general expectation that they are important is supported by calculations and simulations. It is shown that vdW-DF functionals give reasonable results for the water dimer, predict the energetic trend of the low-lying isomers of the water hexamer correctly, that dissociation energies of dimer and hexamer are underestimated with the vdW-DF functional but given chemical accuracy with vdW-DF2. It will then be shown that vdW forces are of key importance for the understanding the HB and that they strech, bend, and breaks HBs to create an energetically stable water hexamer. Finally it will be shown that that these properties translate to liquid water and connects explicitly to the current debate on the structure of liquid water in ambient conditions.
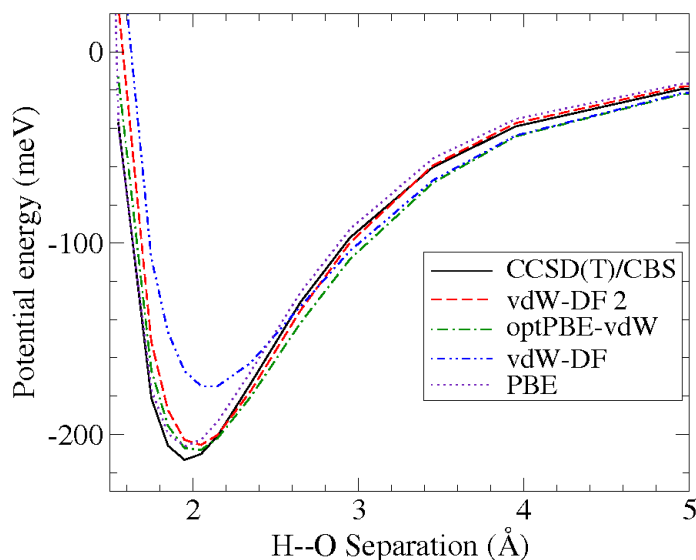
Figure 4.1: Dimer potential energy curve for the water dimer. The DFT results LDA, PBE, vdW-DF, optPBE-vdW and vdW-DF2 are compared with those of an accurate wave-function method CCSD(T)/CBS [85]
.

4.1.1   Dimer

It has been shown that PBE describes the bond in the water dimer down to chemical accuracy, an accuracy better than than 1 kcal/mol [55]. As the vdW forces might contribute to the water dimer bond, DFT with accounts for vdW forces has been used through the vdW-DF and its relatives. As can be seen from Fig. 4.1, the vdW-DF underbinds the dimer with too long an equilibrium bond length. The reason for this [74] can be seen in a plot of the variation of the potential energy with correlation energy removed with separation R_{O-H} for the same system, seen in Fig. 4.2. Removing correlation enables comparisons with Exact Exchange (EXX) [102], which is DFT approximation very close to Hartree-Fock (HF) exchange. Dimer results for several XC functionals are compared with those for EXX, showing that revPBE exchange is too repulsive to describe the HB. It also shows that at small separations the PBE is a better approximation for EXX for the HB, consistent with the findings of Ref. [78]. Newer functionals like the vdW-DF2 [79] and the optPBE-vdW [12] are for this system somewhere between PBE and revPBE. Fig. 4.2 also illustrates the tendency of LDA to overestimate exchange for this system.
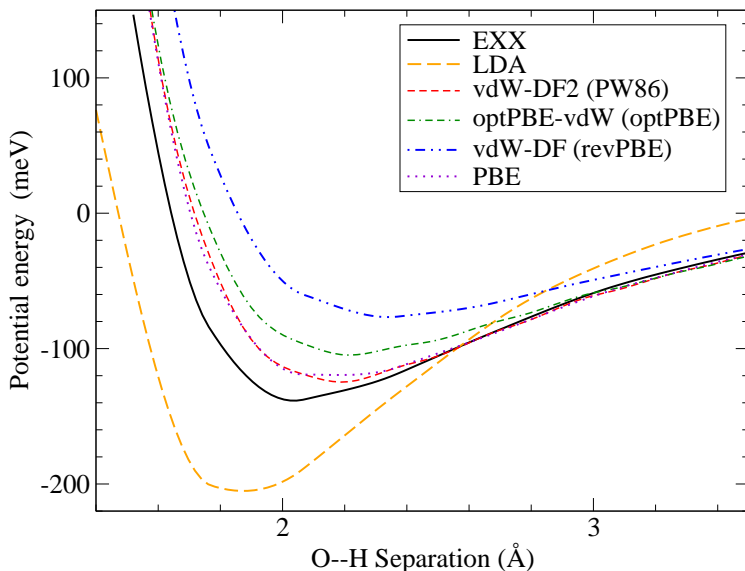
Figure 4.2: Potential energy with no correlation approximation makes it possible to compare functionals with EXX, a DFT version of HF which contains no correlation effects. revPBE is too repulsive compared with EXX, while LDA is too attractive. PW86, the XC approximation in the vdW-DF2, is similar to PBE, while optPBE is placed between PBE and revPBE. Note that although the PW86 exchange is slightly more attractive than the optPBE, the optPBE-vdW is still slightly more attractive in Fig 4.1 due to a more attractive non-local approximation.

Both optPBE-vdW and vdW-DF2 restore chemical accuracy for the HB, for slightly different reasons. The optPBE-vdW is based on the same non-local correlation approximation as the vdW-DF, while the vdW-DF2 is based on the newer, slightly softer and less attractive, approximation [79]. The difference can be seen for larger separations as the vdW-DF2 follows the shape of CCSD(T)/CBS calculations [85], while both the vdW-DF and the optPBE-vdW slightly overestimates the attraction from the non-local interaction. This is compensated for in the exchange approximation where the optPBE is less attractive than PW86, as seen in Fig. 4.2. Since both functionals eventually agree very well on the dissociation energy for the dimer this difference may seem irrelevant, but it will serve later as an example of how such small force perturbation echoes in a small but noticeable difference in the structure of liquid water, which will indicate the qualitative nature of vdW forces in the HBs of liquid water.
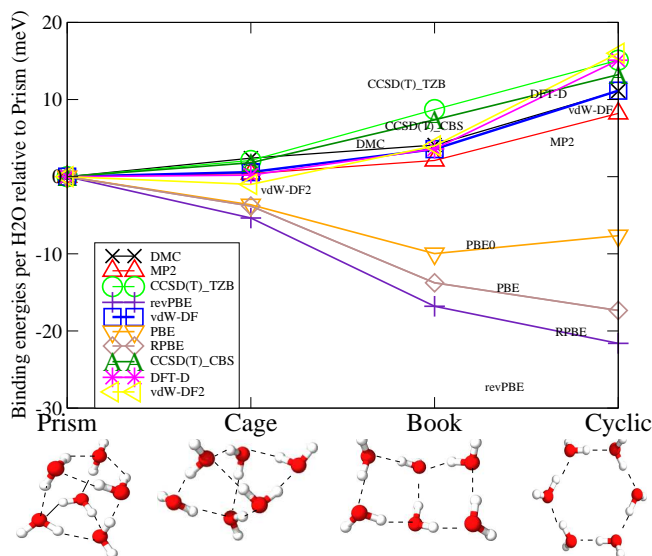
4.1.2 Hexamer

Figure 4.3: Dissociation energy per H$_2$O molecule of the water hexamer in the energetically low-lying isomer structures shown below, calculated with wave-function methods (MP2$_{augccpVTZ}$ [58], DQMC [58], and a recent CCSD(T)$_{CBS}$ calculation [103]), and DFT methods (with XC functionals in the PBE0 [104],DFT-D[58],PBE, RPBE and revPBE flavors of GGA and in vdW-DF and vdW-DF2), relative energy of the prism isomer.

In agreement with other vdW approximations [58] the vdW-DF accurately predicts the right energetic trend of the water hexamers, as can be seen from Fig. 4.3. Consistent with the results for the water dimer, however, Table 4.1 (in the end of the chapter) shows that the dissociation energies are underestimated with the vdW-DF functional. This underestimation is remedied both by optPBE-vdW[12], and by vdW-DF2.

The reason for the reversal in stability trends lies in the van der Waals forces and their non-local dependencies on separations [58]. While semi-local GGA:s cannot account for the energy trend for the low-energy isomers, the stabilizing effect of the non-local correlation is represented either by average atomic distances [20], or by the density and distance dependent interaction kernel Φ [18]. Furthermore, the consequences of vdW forces are shown in Fig 4.4. At first glance, vdW forces seem to stabilize hexamer structures with more available HBs, as prism, cage, book and cyclic has 9, 8, 7, and 6 HB candidates respectively (dashed lines connecting atoms in Fig 4.4). However, this clearly depends
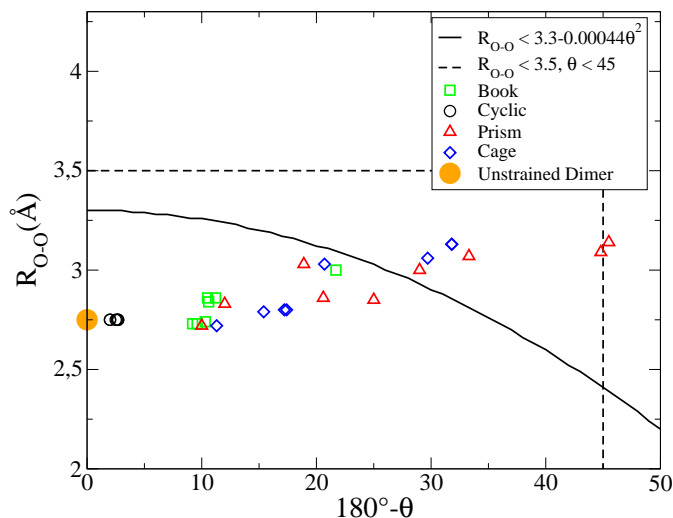
Figure 4.4: Hydrogen bond distortion for the six hexamers. The figure illustrates O-O separation and angular distortion from linearity, $180° − \theta$ in Fig. 2.2. The two hexamers that are stabilized by vdW forces are the ones with most distorted HBs. With the cone-criterion [26] nearly one half of the HBs are outside the cone curve, and thus by definition broken in the prism configuration.

on the definition of the HB, as is seen in Fig 4.4. One common definition is that the angle $O − H − O$ is allowed to deviate up to 45 degrees from linearity, while the O-O separation at maximum can be 3.5 Å. By this definition, only one HB is broken, and the prism and cage configurations both end up with 8 HBs per hexamer, while the book and cyclic structure get 7 and 6 HBs respectively. A tighter definition, argued for in connection with analysis of HB XAS spectra [26], suggests that the $R_{O−O}$ can be at most 3.3 Å, with a penalty proportional to the square deviation from linearity. With this definition, many HBs are broken on the two denser hexamers, resulting in 5 HBs for prism and cage, compared with 7 for the book and 6 for the cyclic. Although the geometrical definition of a HB is bound to include some subjectivity, it is clear that the structures stabilized by vdW forces are the ones with strained and bent HBs, some of which count as broken depending which definition used.

Another way to compare the structures is by measuring the mutual distances between the O atoms. All in all this results in 15 distances that are plotted in a histogram in Fig.4.5. This histogram illustrates nicely that the cyclic structure, favored by GGA, has a large amount of close distance neighbors, as well as a large amount of long distance neighbors. The cage configuration on the other hand, favored by vdW together with prism, has most of its neighbors at
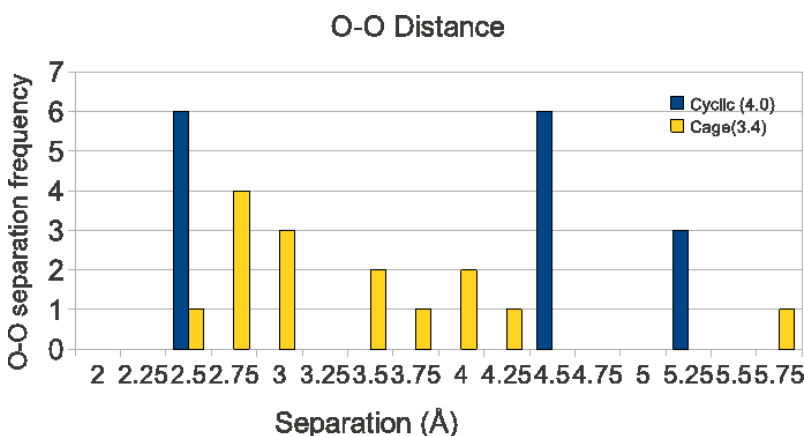
O-O Distance

Figure 4.5: Oxygen-Oxygen separations according to total-energy calculations for the cyclic and cage water hexamers. The histogram shows how frequent each O-O separation is. The density of histogram bars illustrate that the isomers get more compact from cyclic to cage, as do the average O-O separation values that are shown in the legend. The cage configuration has the shortest average separation and also the highest stability together with prism, when vdW forces are accounted for. While cyclic has three distinct separations, cage has a continuous region of 2 to 4 Åwhere all but one $O - O$ separations lie.

intermediate separations. The average O-O separation is smallest for prism and cage structures (3.4 Å), and longest for the cyclic configuration (4.0 Å). This shows that vdW prefers compact isomer configurations, shown earlier by Santra *et.al.* [58].

The mechanism of the underlying trend in isomer energies is that vdW forces prefer more compact isomer structures. The vdW forces then also have the consequence to strain the internal HBs. The more restrictive cone-criterion definition of the HB tells us that stabilization by vdW forces occurs by straining, bending, and often breaking HBs. The concept of broken HBs is also easier to observe in experiments of liquid water with XAS spectroscopy [26] than general compactness.

4.1.3 Liquid water

The structure of liquid water, represented by its O-O pair correlation function (PCF), changes vividly with inclusion of vdW forces. Figure 4.6 shows that the second solvation shell, a geometric consequence of tetrahedrality, is almost
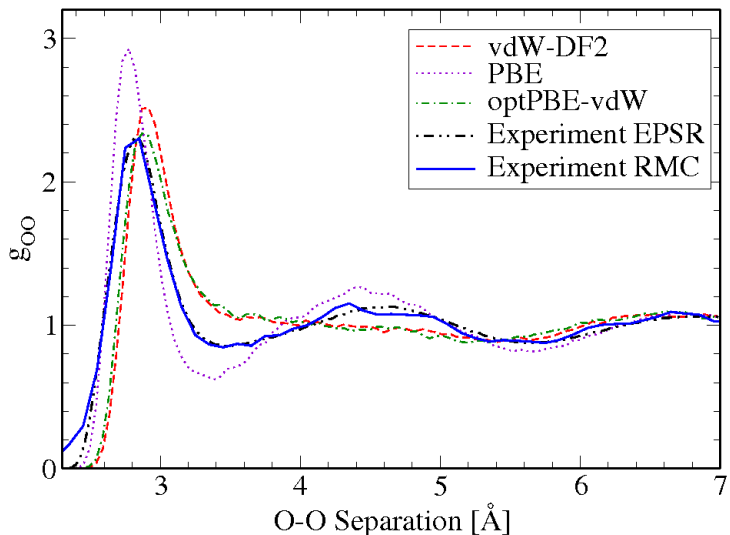
Figure 4.6: Oxygen-oxygen (g_{OO}) PCFs obtained from experimental data using EPSR [105] and RMC [106], in comparison with PCFs from PBE, optPBE-vdW and vdW-DF2.

washed out due to vdW forces. This is a clear indication that vdW forces in DFT simulations disrupts the tetrahedral network predicted by PBE and by other MD simulations. The internal difference between optPBE-vdW and vdW-DF2 is small however, so the washed out structure is unlikely to come from the overestimated non-local force reported for the dimer in Fig. 4.1. Another significant change is the size of the first PCF peak that gets closer to experimental results by accounting for vdW forces, with a peculiar shift closer to 3 Å.

What does the new water structure tell about its HBs? The most direct way to analyze how vdW forces affect HBs is to count the HBs. From Table 4.2 and Table 4.3 (found in the end of this chapter) it becomes clear that the number of unbroken HBs decrease with vdW forces accounted for. The tables illustrate the average number of HBs per water molecule by using the cone criterion HB definition in Table 4.2, and the other, looser, HB definition in Table 4.3 . With the PBE approximation, void of vdW forces, the vast majority of water molecules have four HBs connected to each molecule, consistent with the traditional tetrahedral picture of water. With vdW accounted for, the picture becomes somewhat dependent on the definition of the hydrogen bond, similar to the situation for the hexamers in Fig. 4.4. With the looser definition presented in Table 4.3, the majority of water molecules still have four neighbors. With the stricter cone criterion in Table 4.2 , this pictures changes drastically, making two
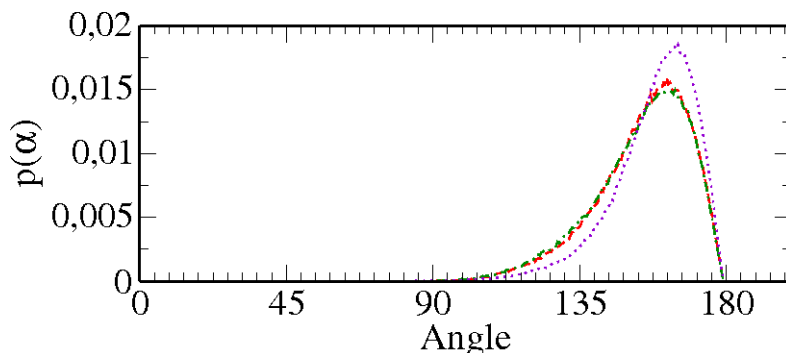
Figure 4.7: The angular distribution functions of the O-H$\cdots$O angle in liquid water at ambient conditions according to MD simulations. The angle corresponds to θ in Fig. 2.2

HBs per molecule more common than four, consistent with experimental XAS results [26]. Regardless of definition, however it is apparent that HBs becomes both longer (seen from the first peak in Fig. 4.6 being shifted outwards), and angularly more distorted (seen from the peak shift in Fig.4.7). The HBs in liquid water are perturbed similarly to those in the most stable hexamer configurations. The small difference in non-local approximation between optPBE-vdW and vdW-DF2 can also be seen, where optPBE-vdW with stronger vdW interaction has a slightly lower first peak in the PCF, as well as fewer molecules with 4 neighbors. Apparently, the subtle difference in force balance results in a small but noticeable difference in liquid structure.

4.1.4   Discussion

Even though the concept of a weakened HB is supported by XAS results [26], the PCF's obtained by optPBE-vdW and vdW-DF2 differ significantly from the PCFs extracted from experiments with RMC [106] and EPSR [105]. Why do two functionals that perform so well for dimer and hexamer seem to fail to describe the structure of liquid water?

One reason could be the size of the simulation cell. It is certainly possible that the suggested picture with two competing structures, LDL and HDL, cannot be reproduced in a cell where every fifth water molecule is identical in every direction (with 4x4x4 molecules in the cell). The reported nano-sized density fluctuations [43] may be larger than the simulation cell, which is a cube with a side of 1.24 nm. Another possibility is the time scale: the simulation time of
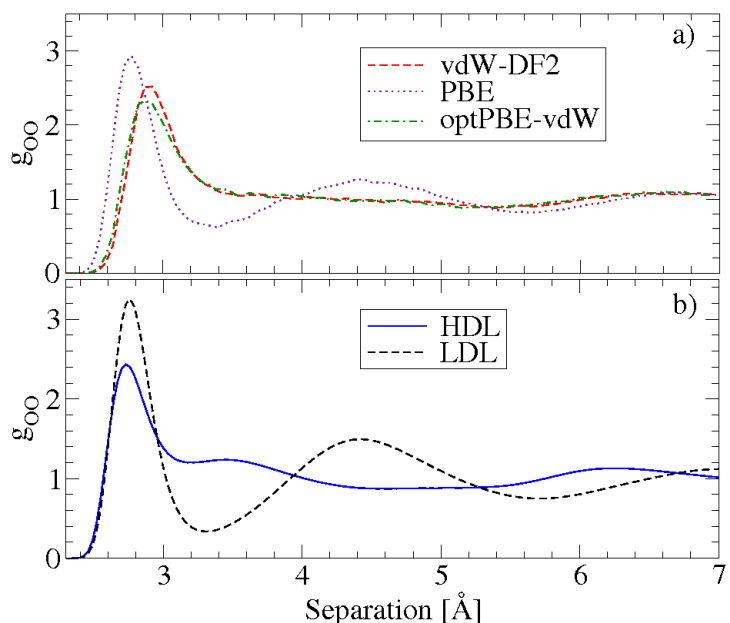
Figure 4.8: a) Oxygen-oxygen PCF's (g_{OO}) obtained from PBE, optPBE-vdW, and vdW-DF2 functionals. b) Experimental PCFs for high (HDL) and low density water (LDL). [107]

10 ps may be significantly shorter than the average fluctuation time. Although these technicalities can certainly be improved, it is possible to extrapolate the simulated results with some assumptions, which will be discussed in this chapter. It should also be noted that the simulations are run in the NVE ensemble with density fixed to correspond to ambient conditions. Under the assumption that ambient water is dominated by HDL [39], this may favor an HDL-like structure over an LDL-like, if energetically allowed, as seems to be the case with vdW interactions included.

The PCF's of high- and low density water can be obtained for pressurized water below the freezing point, and are shown in Fig. 4.8 b. The comparison between the PBE, optPBE-vdW, and vdW-DF2 results in Fig. 4.8 a suggests that the vdW PCFs are similar to the HDL PCF, while the PBE PCF is more similar to LDL. By assuming that the PCF of the vdW-DF2 and optPBE-vdW give HDL structures and that water consists of a mixture of LDL and HDL, a simple linear combination of the experimental LDL PCF from Ref. [107] and the vdW-DF2 PCF should approximately resemble the experimental PCF. The simple
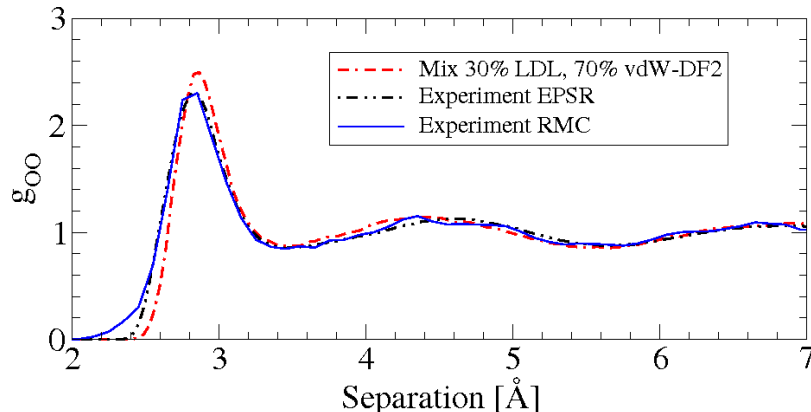
Figure 4.9: Mixing of experimental LDL and vdW-DF2 oxygen-oxygen PCFs compared with PCFs from RMC [106] and EPSR [105]. A mixture of 70/30 agree well with experimental results.

expression can be written like

$$PCF(r) = \alpha \cdot PCF(r)_{vdW-DF2} + (1 - \alpha) \cdot PCF(r)_{LDL} \qquad (4.1)$$

The best fit compared with experiments is obtained by a HDL/LDL mix of 70/30, shown in Fig. 4.9 . This ratio is most interesting since it is very close to the original estimate of Wernet *et al.* [26] and the estimation based on X-ray emission spectroscopy [108, 39]. The argument for the two structures in water is that LDL is driven my minimizing enthalpy, while HDL is driven by maximizing entropy. The pretty much isotropic vdW forces would therefore team up with entropy, which would stabilize the HDL structure, while PBE which only gains energy from directional HBs would favor LDL. It has been pointed out that when combining two separate PCFs, one must also consider whether the combination introduces additional cross-terms between the two strucutres, *i.e.* one LDL-LDL term, one HDL-HDL term, and one cross-term with LDL-HDL strucutre [50], which would not be included in our linear combination. This would be expected from a combination of two highly structured PCFs with well-defined peaks occurring at different interparticle separations in the two distributions. However, considering that both the LDL and HDL local structures give a peak in the region of 2.7 - 3Å and beyond that the HDL-like PCF is basically without structure it seems likely that in this particular case no extra features should be expected from cross contributions to a combined PCF.

The resemblance between the hexamer results and those of liquid water regarding the straining and breaking of HBs is interesting. In the hexamer case the cause for this is increased compactness, equivalent to higher electronic density,

resulting in stronger dispersion interactions. Could this also be the driving force why vdW forces favor the high density liquid? When comparing the $O-O$ histogram of the cage structure in Fig 4.5 with the vdW-DF2 PCF in Fig 4.6 they do have some features in common. Both have its first peak shifted outwards compared with the cyclic histogram and the PBE PCF. After the first peak at around 3Å both distributions gradually decline, without a clear minimum or void that cyclic and the PBE PCF share. The structural heterogeneities in water is reported to be on the 1 nm scale [39], just slightly larger than the cross section of the prism and cage structures which measure 0.5-0.7 nm. If the reported fluctuations exists, perhaps they share similarities with the prism and cage structure, rather than with the cyclic structure?

A fit of a linearly composed PCF to the experimental one does certainly not prove the existence of two competing structures in liquid water. Earlier the PCF has been described as too crude a descriptor for the structure of liquid water[109]. So although this is interesting, it doesn't prove density heterogeneities in water under ambient conditions, and larger and longer simulations are needed, preferably with an NPT ensemble.

4.1.5   Outlook

The results for the linear combination of two structures are very interesting. However, the necessary approximations in the MD simulations, like simulation time, constant volume, and cell size call for future work with a longer simulation, a larger cell, and with an NVT ensemble in order to remove any potential bias for a particular structure. Another interesting way would be to study NVE ensembles with different cell sizes. For an NVE ensemble this would be equivalent to changing the simulation pressure. In Fig. 4.10 preliminary results from simulations with PBE and vdW-DF2 with a 15 per cent larger cell are shown, representing a water density of 0.8 g/cm^3. With PBE and a simulation time of 8 ps, the resulting PCF is merely a shifted version of the PCF from the original simulation. With vdW-DF2, the simulation result show some qualitative differences from the original PCF. The new PCF marginally restores the second peak in the PCF, indicating more tetrahedrality than in the denser simulation. It would be very interesting to follow this trend over a larger span of densities and simulation time to see if the vdW-DF2 simulation can give a structure that by time develops into one that is similar to an LDL structure.
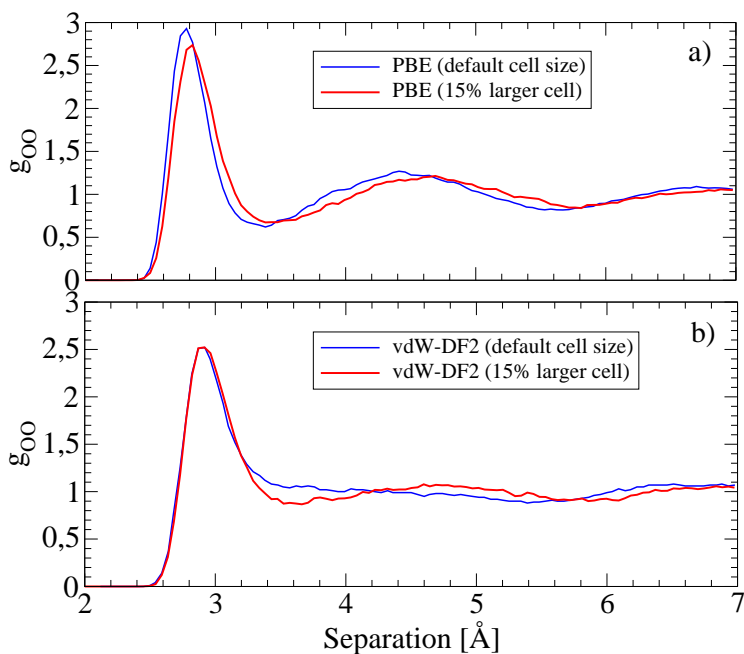
Figure 4.10: Preliminary results on the effects of the size of simulation cell, equivalent to the effects of altered pressure. With reduced pressure the vdW-DF2 PCF seem to restore its second peak, indicative for tetrahedrality. With this sort of simulation it may be possible to sample the effect of pressure.

	Prism	Cage	Book	Cyclic
E_{Diss}^{MP2}	-332	-332	-330	-324
E_{Diss}^{vdW-DF}	-280	-279	-277	-269
$E_{Diss}^{optPBE-vdW}$	-335	-334	-332	-323
$E_{Diss}^{vdW-DF2}$	-333	-335	-329	-317
$R_{O-O}^{average}$ [Å]	3.4	3.4	3.7	4

Table 4.1: Calculated dissociation energy values for the low-lying isomers of the water hexamer, calculated with the vdW-DF and vdW-DF2, compared with MP2 results from Ref. [58] and with optPBE-vdW results from Ref. [12]. Although all three DFT functionals reproduce the MP2 energy trend, vdW-DF significantly underestimates the absolute dissociation energy, while both vdW-DF2 and optPBE-vdW essentially give the same dissociation energies as MP2. $R_{O-O}^{average}$ indicates the average oxygen-oxygen separation in each molecule, where shorter average separations correlate with energetic stability, consistent with findings from Ref. [58].

No. HBs \ Method	PB	optPBE-vdW	vdW-DF2
1	2	10	8
2	12	29	27
3	31	37	38
4	52	22	25
5	3	1	1

Table 4.2: Percentage distribution of unbroken HBs per water molecule calculated with with the cone criterion from Ref. [26]. PBE results are shown to favor more HBs compared to either vdW functional, which both allows for a larger number of molecules to break the tetrahedral structure with four bonds.

No. HBs \ Method	PBE	optPBE-vdW	vdW-DF2
1	0.2	0.4	0.5
2	3	5	6
3	17	29	26
4	64	51	54
5	15	17	13

Table 4.3: Percentage distribution of hydrogen bonds per water molecule calculated using the criterion $r_{OO} < 3.5$ Å and OH$\cdots$O angle $> 135°$ as HB definition. PBE results are shown to favor more unbroken HBs compared to either vdW functional, which both allow for a larger number of molecules to break the tetrahedral structure with four bonds, although with this definition the majority still have four HBs.
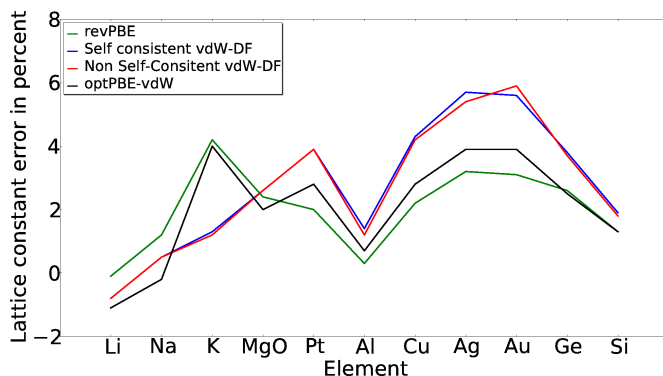
Figure 4.11: Calculated lattice constants with vdW-DF, optPBE-vdW and revPBE. vdW-DF tends to increase the overestimation of lattice parameters inherent from revPBE. while optPBE-vdW gives roughly the same values as revPBE.

4.2   Adsorption

This section concerns the use of DFTs with account of vdW forces in adsorption calculations, *i.e.* the interaction between atoms or molecules and surfaces, when the interaction includes vdW forces. It has four main themes: (i) adsorption-energy values of typical vdW systems, like benzene (Papers 3 and 5) and phenol (Paper 1), and graphene sheets on coinage metals (Papers 4), (ii) study of the vdW field, as expressed by the non-local correlation functional of the vdW-DF density functional, which is shown to have significant atomic-scale variations (Paper 5), implying reconsideration of GGA rules, incl. the coordination rules for adsorption sites, and of mechanism of stronger adsorption on steps than on terraces, (iii) competition between vdW and other forces in adsorption (Paper 5), and (iv) analysis of the accuracy of functionals, in particular the vdW-DF2 functional, by comparing the calculated PEC to physisorption potentials derived from accurate experiments (Paper 6).

Before actual adsorption results are discussed the effects of the vdW-DF on metallic bulk quantities, like lattice parameters will be shown. Figure 4.11 illustrates how the lattice parameters of various metals change with the vdW-DF framework. While revPBE is known to slightly overestimate lattice parameters, the vdW-DF increase this overestimation for transition and noble metals, while somewhat surprisingly decreasing overestimation on alkali metals. This is not an issue of self-consistency as self-consistent vdW-DF calculations give similar values. optPBE-vdW improves lattice parameters over vdw-DF, making lattice parameters only slightly longer than revPBE. Overestimation of the lattice pa-
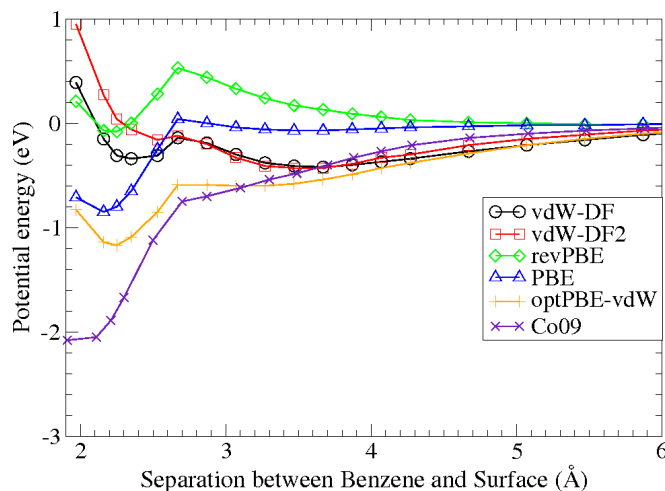
Figure 4.12: PECs for benzene on Ni(111) for the most common vdW-DFs, as well as for PBE and revPBE. The nature of the surface bond varies with XC functional. With vdW-DF2 and vdW-DF the PECs indicate physisorption around 3.7 Å. C09 and optPBE-vdW on the other hand, indicate strong chemisorption. The difference between the dunctionals is almost 2 eV, worse than the difference between PBE and revPBE.

rameters with up to 6 per cent with the vdW-DF could potentially affect the accuracy of chemisorption energies. A metal with expanded lattice parameters will have a higher d-band center[61], which may artificially increase adsorption. But if this is dealt with consistently, adsorption trends will probably not be affected. Unless otherwise stated, all adsorption calculations are made with revPBE lattice parameters.

4.2.1   Adsorption energies

Figure 4.12 plots the PEC for benzene on a Ni(111) surface with six different density functionals. The revPBE functional gives just a weak chemisorption minimum, while the vdW-DF gives the benzene molecule two minima, one inner due to chemisorption, and one outer due to physisorption, where the physisorption minimum is the deepest. With the vdW-DF2 functional there is certainly a physisorption minimum, but a weak and unstable chemisorption state is barely indicated. The optPBE-vdW gives only a chemisorption minimum, deeper than than the experimental adsorption well. Finally, C09 also suggests a chemisorption minimum, significantly deeper than than the experimental adsorption well.
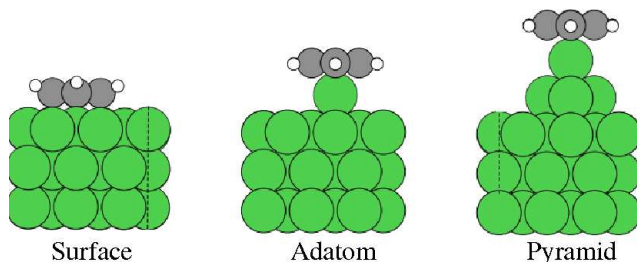
Figure 4.13: Studied substrate structures for adsorption of benzene molecule on planar Ni(111) surface, adatom, and pyramid Ni clusters adsorbed on Ni(111) surface. The adsorption sites are not equivalent, since benzene binds to several Ni-metal atoms in planar case to only top atom on, *e.g.*, the pyramid and adatom. The deformation of the adsorbed benzene molecule on the planar surface is indicated.

This sensitivity to choice of exchange functional affects the electronic structure of the system in its equilibrium configuration. It makes calculations in weak adsorption,*e.g.*, on adsorption systems of interest for *e.g.* molecular electronics problematic. According to available experimental results, estimated adsorption separations suggests that the chemisorption minimum is the correct site, with a a bond energy around 0.75 eV [110].

An additional example of the role of exchange functional in adsorption can be seen from graphene adsorption on Ni(111). In Paper 4 a study on graphene adsorption on metals is conducted. The adsorbate-substrate hybridization of the graphene density of states (DOS) can be obtained experimentally and may be used as an indicator of weak or strong adsorption. Experiments have estimated the graphene separation to the surface to be 2.1 Å [111]. The vdW-DF estimates the separation to 3.5 Å (Paper 4), as do optPBE-vdW results. Recently however it was found that a modified version of C09, where the softer approximation of E_c^{nl} taken from the vdW-DF2 was used, gives a graphene separation of 2.1 Å to the Ni(111) surface and thus get very good agreement with experiments. Thus it looks promising that the C09 enhancement factor for small s values, where it behaves like GEA, may be an appropriate approximation for graphene on Ni(111). On the other hand the C09 overbinds benzene on Ni(111) severely, as seen in Fig. 4.12.
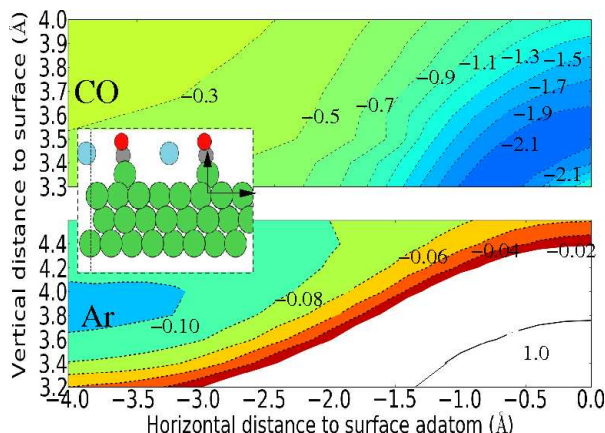
Figure 4.14: Spatial difference in interaction energy between strong and weak adsorption shown by potential-energy surfaces (PES's) for CO (top) and Ar (bottom) adsorbed on Ni(111) surface with Ni adatom (inset), calculated with the vdW-DF method [18]. The CO molecule prefers to be close to adatom, while the Ar atom prefers terrace, as indicated by coordinate system in inset. Units are eV and Å.

4.2.2   Non-local correlation fields in adsorption

The site preferences of adsorbates bound by vdW forces differ radically from those of adsorbates bonded by chemisorption. This is illustrated in Fig 4.14, where a CO molecule prefers to adsorb on the lower coordinated Ni adatom instead of the extended Ni terrace, in agreement with known chemisorption rules [6, 59]. Argon, on the other hand, has nothing to gain energetically from the higher d-band of the Ni. Rather, Pauli repulsion between surface and adsorbate electrons keeps the adsorbate away (Paper 5). As the vdW forces benefit from the large two-dimensional extent of the surface, the net result is that the Ar atom physisorbs weakly on the extended surface, with preference for terraces (Paper 5).

This particular example illustrates the competing site-preference between benefiting in vdW strength from the extended surface and and in chemisorptive covalent strength enhanced by under-coordination. It is clear that for systems like CO on Ni vdW interactions might be at a disadvantage, with a typical magnitude on the adsorption of less than 0.1 eV, compared to the covalent values typically in the eV range. Even in a weak-adsorption case, as CO adsorption on Au(111), Au(211), and Au(310), the balance is such that coordination numbers determine trends in both experimental and vdW-DF calculated
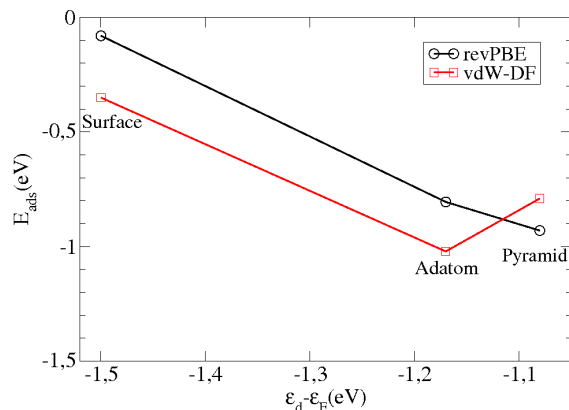
Figure 4.15: Interaction energy variation with d-band center. revPBE results indicate a linear scaling with the d-band center, as it does for many smaller adsorbates on many metals [6, 112]. The vdW-DF interaction breaks this linear relationship, favoring the adatom structure over the surface due to the d-band center, but also the adatom structure over the pyramid structure due to closeness to the extended surface.

adsorption-energy values (Paper 5). There is a preference for steps and their low coordinations. It is therefore interesting to test a larger adsorbate, as vdW forces are known to increase with molecular size [11]. The next section analyzes the adsorption trends of benzene on various substrates to show when this force competition for site-preference becomes relevant.

4.2.3   vdW and competing forces

To test the influence of vdW forces adsorption energies for benzene has been calculated on the structures shown in Fig 4.13. Ni,Cu and Au have been used as substrate in order to test substrate trends. In Fig. 4.15 the correlation between adsorption energy and the d-band center is plotted for Ni, which is the only metal of the three, on which benzene is expected to chemisorb. With revPBE the correlation is surprisingly linear, considering the dissimilarities between the adsorption-site structures, and that the adsorbates buckles slightly on the surface, while remaining flat on the other two structures. Without vdW forces, adsorption trends for benzene on Ni is determined by the d-electrons. By including vdW forces through the vdW-DF this trend becomes less clear. Although the adatom structure is still more stable than surface, the pyramid structure is less stable despite a higher d-band center (Fig 4.15).
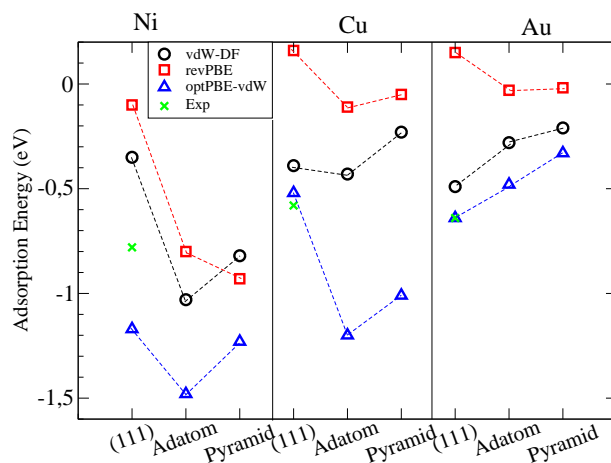
Figure 4.16: Interaction-energy values, calculated with vdW-DF and revPBE, respectively, for benzene on Ni, Cu, and Au, for the planar (111), adatom, and pyramid configurations illustrated in Fig4.13. Adsorption trends illustrate the competition between preference for low coordination, called for by covalency, and that for proximity to the extended surface, called for by vdW forces. Like in Fig. 4.17 the top panels show that the GGA revPBE (no vdW) prefers the low-coordinated adatom and pyramid sites over the planar (111) surface, for all the metals, and that the vdW-DF prefers the planar (111) surface over both adatom and pyramid, for the coinage metals. Other patterns appear, when several driving forces have comparable strengths, as illustrated by the vdW-DF case for Ni (left), where under-coordination favors the adatom over planar (111) surface and over the pyramid (due to a closer proximity to the extended surface). Experimental results for Ni [110], Cu [113, 114], Ag [115, 116], and Au [117] are indicated by crosses). Bond lengths are measured from the carbon ring to the closest metal atom, in Å, and listed to signal chemi- (short) and physisorption (long).

A likely explanation is that both high d-band and closeness to the extended surface are desirable for adsorption, and that on Ni a favorable d-band is worth the price of increased surface separation for the adatom site (compared to planar surface) but not for the pyramid (compared to adatom). The energetically favorable d-band hybridization is worth the price of increased surface separation for the adatom structure, but not for the pyramid. For gold, on which benzene physisorbs on the planar surface, the adsorption trend is reversed and surface seeking vdW forces dominate. In between Ni and Au, there lies Cu, where the surface and adatom sites give similar adsorption energies, thus giving an example of where vdW forces roughly balance covalent forces, dependent on the exchange functional used (Fig. 4.16).
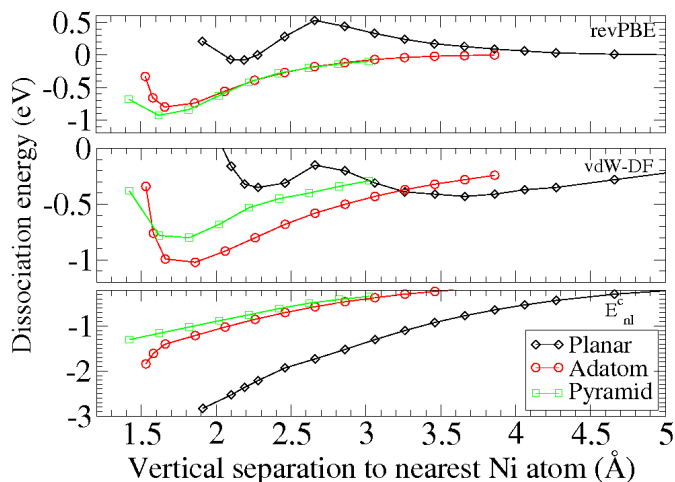
Figure 4.17: PECs for benzene adsorption on planar, adatom, and pyramid structures (see Fig. 4.13) of Ni, in the revPBE (top; for comparison) and the vdW-DF (middle) approximations, the coordinate d being the separation between the adsorbate point of gravity and the closest metal atom (Energy scales differ). The bottom figure shows a key contribution to the total vdW-DF energy, the non-local correlation E_c^{nl}, which is seen to be strongest for the planar surface, where the average separation between adsorbate and the Ni atoms is shortest, and weakest for the pyramid structure, where the average separation is longest.

This explanation is supported in Fig 4.17. The energy contribution of E_c^{nl} to the PEC, *i.e* the term containing vdW interactions in the vdW-DF, is plotted in the bottom figure for the three structures. Here the non-local term is plotted as a function of the vertical separation of the benzene molecule and its closest Ni atom. At 2 Å the non-local interaction energy for the surface structure is more than twice as strong as for the adatom and pyramid structures, and the non-local contribution favors the adatom structure over pyramid structure with 0.25 eV, altering the revPBE trend seen in Fig 4.15. When adding everything up, the extra 0.25 eV gained by relative proximity to the surface reverses the energetic trend given by GGAs.

A few more things are worth pointing out. Despite the big energy stabilization that benzene gets from E_c^{nl} close to the surface (almost 3 eV at 2 Å) both adatom and pyramid result in a stronger bond than the planar surface. The reason for this is the increased Pauli-repulsion (approximated by revPBE) close to the surface, which actually buckles the hydrogen atoms of the benzene molecule upwards away from the surface, illustrated in Fig 4.13, an probably is the reason

for the bump in the PEC at 2.5 Å . In a less repulsive approximation like with optPBE exchange, the surface structure becomes significantly more stable, making the surface almost as attractive as the pyramid for the benzene, seen by the blue trend line in Fig 4.16. Another point can be made about the conceptual structure of the vdW-DF. The vdW-DF and the revPBE are formulated as

$$E_{xc}^{vdW-DF} = E_x^{revPBE} + E_c^{LDA} + E_c^{nl} \qquad (4.2)$$

$$E_{xc}^{revPBE} - DF = E_x^{revPBE} + E_c^{PBE} \qquad (4.3)$$

It is possible to argue that the LDA correlation is a poor approximation, which significantly and systematically underestimates real correlation [80]. With this argument, one could be tempted to instead just use a better correlation like the PBE correlation approximation in the vdW-DF. Changing LDA to PBE correlation is thus equivalent to adding the non-local interaction to a revPBE calculation, which could be done by adding the results from the top and bottom graph in Fig4.17. Doing so would result in an adsorption energy of around 2.5 eV for benzene on the Ni surface, almost four times as much as predicted by experiments. The reason for this very strong overestimation should mean that there is an overlap between PBE correlation and E_c^{nl}, and that LDA correlation is more appropriate than PBE correlation in the vdW-DF.

4.2.4 V_{ad} and vdW forces

For chemisorption on transition metals the d-band model is a valuable tool.In addition to d-band width and energy center, the coupling matrix element V_{ad} plays a key role in chemisorption. For instance, it explains why metals become less reactive when moving down in columns in the periodic table and the geometric extent of the d-electrons increase. [60, 61]. In particular, it explains why Oxygen binds harder to Cu and Ag than to Au, making it noble, that is, inert to atmospheric gases. For physisorption, this trend does not apply. Figure 4.16 shows that benzene physisorbs slightly stronger to the Au surface than on the Cu surface. This is discussed in more detail in paper 5.

4.2.5   Physisorption potentials

This section compares the results of the vdW-DF and the vdW-DF2 to results from traditional physisorption theory based on experiments [118]. Physisorption energy, potential energy shape, and physisorption trends are tested. The energy terms will also be compared separately to learn more about the accuracy of the vdW-DF approximation. It is discussed in greater detail in Paper 6
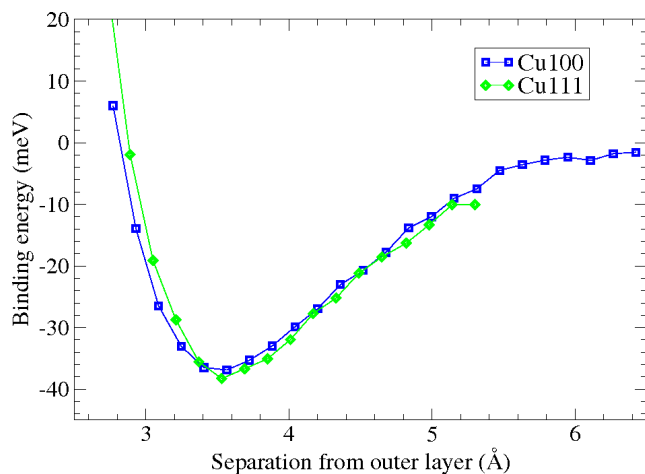
Figure 4.18: PEC calculated with vdW-DF2 for H_2 physisorbed on Cu(111) and Cu(100) surfaces averaged over bridge, hollow and top site.

H_2 physisorption on Cu(111) and Cu(100) has been calculated with the vdW-DF2. The PECs averaged over top, hollow, and bridge sites are plotted in Fig. 4.18. The physisorption energy on both surfaces are around 38 meV, slightly favoring the (111) surface. This is slightly different to experimental results of around 30 meV, slighly favoring the (100) surface [118]. The structure of a vdW-DF functional is that of an approximate exchange functional, a local correlation approximation, and a non-local correlation functional, where vdW or dispersion forces reside. Each contribution has its background and its limitations, so to validate the functional versatile tools are valuable. One way is to test against experiments. Accurate experimental surface-physics results offer possibilities to analyze the accuracy of functionals that account for the vdW forces. In traditional physisorption theory, the potential energy expression is assumed to be two-parted $V_0 = V_R + V_{vdW}$, where one term, V_R, is due to Pauli repulsion, and the other , V_{vdW}, due to vdW forces. The parameters of these terms have been extracted from experimental results [118] and can be compared with the vdW-DF2, where $E_x^{GGA} + E_c^{LDA}$ is compared with V_R, and E_c^{nl} with V_{vdW} (Fig. 4.19)

In Fig 4.20 vdW-DF and vdW-DF2 PECs are compared with experimental results interpreted by a traditional theoretical picture. It becomes clear that the vdW-DF2 significantly improves both physisorption energies and bond lengths over vdW-DF. The vdW-DF2 slightly overbinds the H_2 dimer with about 10 meV. The origin of this slight overestimation originates from E_c^{nl}, as is shown in Figure 4.19. Here it is shown that the repulsive part of the vdW-DF2 (DFT
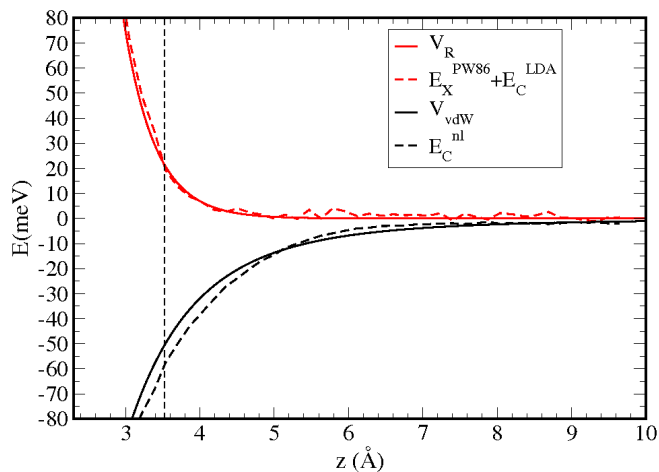
Figure 4.19: vdW-DF2 components compared with physisorption theory. The repulsive part V_R matches vdW-DF less E_c^{nl} well ($E_x^{PW86} + E_c^{LDA}$),apart from some unwanted numerical oscillations. The match between E_c^{nl} and V_{vdW} is not perfect: for short separations E_c^{nl} is too attractive, while not being attractive enough for longer separations.For equilibrium separations to the surface (dotted vertical lin), the small overestimation in bond energy comes from E_c^{nl}.

energies minus E_c^{nl}) matches experimental Pauli repulsion well at equilibrium bond lengths (indicated with vertical line). The vdW approximation on the other hand is slightly too attractive at small separations, while being slightly too repulsive at long separations. Fig 4.19 also shows that the numerical noise of the DFT calculation seems to increase slightly with longer separation (seen by the oscillating repulsive part of the vdW-DF2). This noise may be due to the very high s values (reduced gradient,Eq. 3.9) in low density regions.

4.2.6   Discussion

Although the vdw-DF is relatively often compared with accurate calculations, comparisons of its different constituents with real experiments are relatively uncommon. The experiments for H_2 on Cu surfaces offer a nice opportunity to anchor the validity of the vdW-DF for physisorption reality. The energy discrepancy between calculations and experiments of around 8 meV for the physisorption potential well depth is quite acceptable and within the margin of error in the DFT calculation. It is worth noting the relatively big difference between the vdW-DF and the vdW-DF2, where the latter with the more weakly
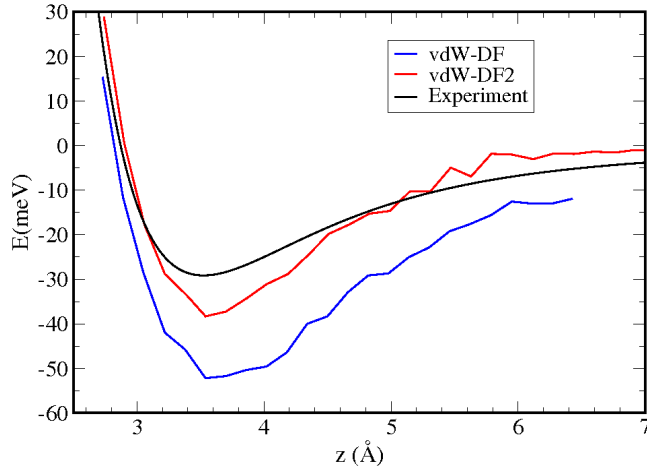
Figure 4.20: PEC for H2 adsorption on Cu(111) as calculated with vdW-DF and vdW-DF2, compared with experimental results[118].

attractive vdW approximation of E_c^{nl} seems to be closer to traditional theory than the former, illustrated in Fig. 4.20.

The repulsive part of the vdW-DF2 agrees very well with traditional theory, although the numerical noise of about 3 meV in the local part is worth noting. The shape of E_c^{nl} is not perfectly agreeable with traditional theory, being slightly too strong in some regions, and too small in other. Although this may seem like a very small problem, it makes estimation and comparison of C_6 coefficients difficult. Due to the very small energy scale (2-3 meV) it is possible that this could be within the accuracy of the numerical implementation of the vdW-DF. It is also possible that density far out in the tails in DFT are slightly too small.

CHAPTER 5

Conclusions and Outlook

This thesis shows the importance of vdW forces in different types of systems through DFT calculations and the vdW-DF and newer versions of it. It is shown in Papers 1,3 and 6 that the vdW-DF is very accurate for adsorption under conditions of physisorption, with energies better than MP2 for benzene on Au(111) (Paper 3), and with differences to experiments of only 8 meV for H_2 on Cu(111) (Paper 6). These are very encouraging results as the approximations in the vdW-DF are not designed to treat metals but mainly molecules interacting by pure van der Waals forces. Comparisons with experimental physisorption results indicate that the newer and softer approximation of of the non-local correlation-energy functional, E_c^{nl}, used in the vdW-DF2 is more accurate than the older approximation used in vdW-DF and optPBE-vdW.

The vdW-DF functional has been successfully applied to vdW-bound systems and has there shown a promising accuracy. When it is applied to systems, where other forces in addition to vdW forces are relevant, the accuracy of the functional is challenged. For instance, although the vdW-DF functional is able to give results for water hexamer energy trends that agree with those of accurate wave function methods, dissociation energies come out too low. The too low energies are consistent with previous findings [74, 78] and it has been shown that it relates to the too repulsive exchange functional (revPBE) in the original vdW-DF method, as compared to the exact exchange expressed in the Hartree-Fock and EXX approximations. Similarly for adsorption, when vdW

forces compete with chemisorption, e.g., for benzene or graphene on Ni(111) surfaces, bond energies are too low compared with experiments, with too long equilibrium bond lengths (Papers 1 and 4). Newer and updated versions of the vdW-DF method have been designed by other groups to resolve this problem, with systematic improvement for most molecular systems. For chemisorption systems these improvements are not as systematic, as it has been shown in the thesis that some newer and less repulsive exchange functionals instead tend to overestimate bond energies for some systems. As an example no exchange approximation tested has been able to treat graphene and benzene adsorption on a Ni(111) surface properly.

Under certain conditions vdW forces affect conventional adsorption trends like the coordination-rule, which states that adsorption increase with lower coordination of the substrate atoms at the adsorption site. Under conditions of weak chemisorption the separation to the extended surface (affecting vdW bond) becomes energetically as important as a higher d-band center (affecting covalent bonds). The increased separation decreases the relative vdW adsorption strength on defects like adatoms over that of extended surfaces. Although adsorption trends are on a small scale, this may be relevant when designing molecular contacts in molecular electronics, as potential molecular transistors need to adsorb weakly to contacs in order to preserve electronic band structure. If defects are used as contacts, weaker adsorption on defects than on terraces could make self-assembly difficult.

Effects of vdW forces on the HB is also discussed where it is suggested that vdW forces stabilize strained, bent and broken HB's in the water hexamer and in liquid water. This effect is believed to be very relevant within the field of water structuring, as the nature of liquid water is highly contested, where experiments have showed that there are many more broken HB's in liquid water than previously thought [26]. The very different PCF results from vdW-DF2 and the optPBE-vdW indicate that vdW forces favor HDL-similar strucure, whereas a PBE calculation favors an LDL-similar structure, which is explained by the isotropic nature of vdW forces. Based on experimentally suggested proportions [108, 39] of HDL:LDL, a linear combination of the vdW PCF and an LDL PCF from experiments reproduces experimentally derived PCF's. Although this does not prove that liquid water is bimodal, it certainly is encouraging and calls for deeper and expanded studies.

5.1   Outlook

Looking back, it becomes clear that the discoveries made by the vdW-DF and its relatives progressed as numerical code implementations and computer power let it. In 2008 a non-selfconsistent calculations on two graphene sheets took five minutes, and the only way to calculate periodic systems was to expand the size of the cell and create periodic images. As implementations improved, so did the possibility to do calculations on interesting systems. Although very efficient implementations are now available [119], improvements may still be necessary to progress. GPAW has been shown to scale well up to 20,000 CPU:s [120]. The most interesting DFT calculation I can think of at the moment would be a MD simulation 100 times larger than the one in this paper, run for ten times as long a time. This could potentially prove heterogeneity in liquid water. At the moment, however, such a calculation requires many thousands of CPU:s, and while the ordinary components of GPAW may handle this, the vdW-DF implementation does certainly not. Better computer implementations are thus needed. Both optPBE-vdW and C09 are promising functionals for balancing physisorption and chemisorption, although neither is accurate enough in every detail for full scale calculations on the patented process described in the introduction. Exchange approximations fitted to experiments may be one way to improve.

Bibliography

[1] Mike Magee. Moore's law lives but silicon cmos is doomed. *TechEyer.net, Online: http://www.techeye.net/chips/moores-law-lives-but-silicon-cmos-is-doomed*, 2010.

[2] SJ Tans, A. R. M. Verschueren, and C Dekker. *Nature*, 393(6680):49–52, 1998.

[3] A. K. Geim and K. S. Novoselov. *Nature Materials*, 6(3):183–191, 2007.

[4] M. Boudart. *Advances in Catalysis*, 20(C):153–166, 1969.

[5] Jr. John T. Yates. volume 13, pages 1359–1367. AVS, 1995.

[6] B. Hammer, O.H. Nielsen, and J.K. Nørskov. *Catalysis Letters*, 46:31–35, 1997.

[7] N.P Lebedeva, M.T.M Koper, E Herrero, J.M Feliu, and R.A van Santen. *Journal of Electroanalytical Chemistry*, 487(1):37 – 44, 2000.

[8] Ray H. Baughman, Anvar A. Zakhidov, and Walt A. de Heer. 297(5582):787–792, 2002.

[9] GH Gao, T Cagin, and WA Goddard. *Nanotechnology*, 9(3):184–191, 1998.

[10] RS Ruoff, D Qian, and WK Liu. *Comptes Rendus Physique*, 4(9):993–1008, 2003.

[11] Poul Georg Moses, Jens J. Mortensen, Bengt I. Lundqvist, and Jens K. Norskov. *Journal of Chemical Physics*, 130(10):104709, 2009.

[12] J. Klimes, D.R. Bowler, and A. Michaelides. *J. Phys.Conden. Matter*, 22:022201, 2010.

[13] D Tabor. *Proceedings of the Physical Society. Section B*, 67(3):249, 1954.

[14] R F Curl and R E Smalley. *Scientific American*, 265(4):54–&, 1991.

[15] D C Langreth, B I Lundqvist, S D Chakarova-Käck, V R Cooper, M Dion, P Hyldgaard, A Kelkkanen, J Kleis, Lingzhu Kong, Shen Li, P G Moses, E Murray, A Puzder, H Rydberg, E Schröder, and T Thonhauser. *Journal of Physics: Condensed Matter*, 21(8):084203, 2009.

[16] A. D. McNaught and A. Wilkinson. van der waals forces. *IUPAC. Compendium of Chemical Terminology, 2nd ed. (the Gold Book).*, 1997.

[17] B.I. Lundqvist, Y Andersson, H Shao, S Chan, and D.C. Langreth. *International Journal of Quantum Chemistry*, 56(4):247–255, 1995.

[18] M. Dion, H. Rydberg, E. Schroder, D.C. Langreth, and B.I. Lundqvist. *Phys. Rev. Lett.*, 92:246401, 2004.

[19] Yan Zhao and Donald Truhlar. *Theoretical Chemistry Accounts: Theory, Computation, and Modeling (Theoretica Chimica Acta)*, 120:215–241, 2008.

[20] S. Grimme. *J. Comput. Chem.*, 25:1463, 2004.

[21] Alexandre Tkatchenko and Matthias Scheffler. *Phys. Rev. Lett.*, 102(7):073005, 2009.

[22] John F. Dobson and Jun Wang. *Phys. Rev. Lett.*, 82(10):2123–2126, 1999.

[23] Deyu Lu, Huy-Viet Nguyen, and Giulia Galli. *The Journal of Chemical Physics*, 133(15):154110, 2010.

[24] T Steiner. *Angewandte Chemi-International Edition*, 41(1):48–76, 2002.

[25] A. L. McClellan G. C. Pimentel. The Hydrogen Bond. *San Francisco*, 1960.

[26] Ph. Wernet, D. Nordlund, U. Bergmann, and et al. *Science*, 304:995, 2004.

[27] Keiji Morokuma. *Accounts of Chemical Research*, 10(8):294–300, 1977.

[28] Philip Ball. *Nature*, 452(7185):291–292, 2008.

[29] M Chaplin. http://www.lsbu.ac.uk/water/anmlies.html, and references therein.

[30] K Fucke and J. W. Steed. *Water*, 2(3):333–350, 2010.

[31] R. L. McGreevy. *Nuclear Instruments and Methods in Physics Research Section A: Accelerators, Spectrometers, Detectors and Associated Equipment*, 354(1):1–16, 1995.

[32] A. K. Soper. *Chemical Physics*, 202(2-3):295–306, 1996.

[33] John S. Tse, Dawn M. Shaw, Dennis D. Klug, Serguei Patchkovskii, György Vankó, Giulio Monaco, and Michael Krisch. *Phys. Rev. Lett.*, 100(9):095502, 2008.

[34] Lars-Åke Näslund, David C. Edwards, Philippe Wernet, Uwe Bergmann, Hirohito Ogasawara, Lars G. M. Pettersson, Satish Myneni, and Anders Nilsson. *The Journal of Physical Chemistry A*, 109(27):5995–6002, 2005.

[35] M. Cavalleri, H. Ogasawara, L. G. M. Pettersson, and A. Nilsson. *Chemical Physics Letters*, 364(3-4):363–370, 2002.

[36] Jared D. Smith, Christopher D. Cappa, Benjamin M. Messer, Walter S. Drisdell, Ronald C. Cohen, and Richard J. Saykally. *The Journal of Physical Chemistry B*, 110(40):20038–20045, 2006.

[37] Teresa Head-Gordon and Margaret E. Johnson. *Proceedings of the National Academy of Sciences*, 103(44):16614–16615, 2006.

[38] Kratky O Glatter O. Academic Press., 1982.

[39] C. Huang, K. T. Wikfeldt, T. Tokushima, D. Nordlund, Y. Harada, U. Bergmann, M. Niebuhr, T.M. Weiss, Y. Horikawa, M. Leetmaa, M.P. Ljungberg, O. Takahashi, A. Lenz, L. Ojamae, A.P. Lyubartsev, S. Shin, L.G.M. Pettersson, and A. Nilsson. *Proc. Natl. Acad. Sci. USA*, 106:15214, 2009.

[40] H E Stanley, S V Buldyrev, G Franzese, P Kumar, F Mallamace, M G Mazza, K Stokely, and L Xu. *Journal of Physics: Condensed Matter*, 22(28):284101, 2010.

[41] P.H. Poole, F. Sciortino, U. Essmann, and H.E. Stanley. *Nature*, 360:324–328, 1992.

[42] O Mishima, LD Calvert, and E Whalley. *Nature*, 314(6006):76–78, 1985.

[43] C. Huang, K. T. Wikfeldt, T. Tokushima, D. Nordlund, Y. Harada, U. Bergmann, M. Niebuhr, T. M. Weiss, Y. Horikawa, M. Leetmaa, et al. *Proceedings of the National Academy of Sciences (USA)*, 106(36):15214, 2009.

[44] AK Soper, J. Teixeira, and T. Head-Gordon. *Proceedings of the National Academy of Sciences*, 107(12):E44, 2010.

[45] C. Huang, K. T. Wikfeldt, T. Tokushima, D. Nordlund, Y. Harada, U. Bergmann, M. Niebuhr, T. M. Weiss, Y. Horikawa, M. Leetmaa, M. P. Ljungberg, O. Takahashi, A. Lenz, L. Ojamäe, A. P. Lyubartsev, S. Shin, L. G. M. Pettersson, and A. Nilsson. *Proceedings of the National Academy of Sciences*, 107(12):E45, 2010.

[46] Gary N. I. Clark, Greg L. Hura, Jose Teixeira, Alan K. Soper, and Teresa Head-Gordon. *Proceedings of the National Academy of Sciences*, 107(32):14003–14007, 2010.

[47] T. Head-Gordon and G. Hura. *Chem. Rev.*, 102:2651, 2002.

[48] Jared D. Smith, Christopher D. Cappa, Kevin R. Wilson, Ronald C. Cohen, Phillip L. Geissler, and Richard J. Saykally. 102(40):14171–14174, 2005.

[49] Robert Bukowski, Krzysztof Szalewicz, Gerrit C. Groenenboom, and Ad van der Avoird. *Science*, 315(5816):1249–1252, 2007.

[50] A. K. Soper. *Pure Appl. Chem.*, 82(10):1855–1867, 2010.

[51] J. VandeVondele, F. Mohamed, M. Krack, J. Hutter, M. Sprik, and M. Parrinello. *J. Chem. Phys.*, 122:014515, 2005.

[52] Ann E. Mattsson and Thomas R. Mattsson. *Journal of Chemical Theory and Computation*, 5(4):887–894, 2009.

[53] B. Hammer, L.B. Hansen, and J.K. Nørskov. *Phys. Rev. B*, 59:7413, 1999.

[54] J.P. Perdew, K. Burke, and M. Ernzerhof. *Phys. Rev. Lett.*, 77:3865, 1996.

[55] J. Ireta, J. Neugebauer, and M. Scheffler. *J. Phys. Chem. A*, 108:5692, 2004.

[56] I.C. Lin, A.P. Seitsonen, M.D., Tavernelli I. Coutinho-Neto, and U. Rothlisberger. *J. Phys. Chem. B*, 113:1127, 2009.

[57] J. Wang, G. Roman-Perez, J. M. Soler, E. Artacho, and M. V. Fernandez-Serra. arXiv:1005.2680v1, 2010.

[58] Biswajit Santra, Angelos Michaelides, Martin Fuchs, Alexandre Tkatchenko, Claudia Filippi, and Matthias Scheffler. *J. Chem. Phys.*, 129:194111, 2008.

[59] D. M Newns. *Phys. Rev.*, 178(1123), 1969.

[60] B Hammer and JK Nørskov. *Surface Science*, 343(3):211–220, 1995.

[61] B Hammer and J K Nørskov. *Adv. in Cat.*, 45:71–129, 2000.

[62] W. Kohn. *Rev. Mod. Phys.*, 71(5):1253–1266, 1999.

[63] R. M. Martin. *Electronic Structure: Basic Theory and Practical Methods (Cambridge University Press, Cambridge, UK*, 2004.

[64] P Hohenberg and W Kohn. *Phys. Rev. B*, 136(3B):B864–&, 1964.

[65] W. Kohn and L. J. Sham. *Phys. Rev.*, 140(4A):A1133–A1138, 1965.

[66] D. M. Ceperley and B. J. Alder. *Phys. Rev. Lett.*, 45(7):566–569, 1980.

[67] D. C. Langreth and John P. Perdew. *Phys. Rev. B*, 15(6):2884–2901, 1977.

[68] O. Gunnarsson and B. I. Lundqvist. *Phys. Rev. B*, 13(10):4274–4298, 1976.

[69] D. C. Langreth and J. P. Perdew. *Solid State Communications*, 17(11):1425 – 1429, 1975.

[70] John P. Perdew, Adrienn Ruzsinszky, Gábor I. Csonka, Oleg A. Vydrov, Gustavo E. Scuseria, Lucian A. Constantin, Xiaolan Zhou, and Kieron Burke. *Phys. Rev. Lett.*, 100(13):136406, Apr 2008.

[71] Ales Zupan, Kieron Burke, Matthias Ernzerhof, and John P. Perdew. *The Journal of Chemical Physics*, 106(24):10184–10193, 1997.

[72] Y.K. Zhang and W.T. Yang. *Phys. Rev. Lett.*, 80:890, 1998.

[73] V.R. Cooper. *Phys. Rev. B*, 81:161104, 2010.

[74] A. Puzder, M. Dion, and D.C. Langreth. *J. Chem. Phys.*, 124, 2006.

[75] T. Thonhauser, Valentino R. Cooper, Shen Li, Aaron Puzder, P Hyldgaard, and D. C. Langreth. *Phys. Rev. B*, 76(12):125112, Sep 2007.

[76] S. D. Chakarova-Käck, E. Schröder, B. I. Lundqvist, and D. C. Langreth. *Phys. Rev. Lett.*, 96(14):146107, 2006.

[77] L Romaner, D Nabok, P Puschnig, E Zojer, and C Ambrosch-Draxl. *New Journal of Physics*, 11(5):053010, 2009.

[78] A. Gulans, M.J. Puska, and R.M. Nieminen. *Phys. Rev. B*, 79(20):201105, 2009.

[79] K. Lee, E.D. Murray, L. Kong, B.I. Lundqvist, and D.C. Langreth. *Phys. Rev. B*, 82:081101, 2010.

[80] S Kurth, JP Perdew, and P Blaha. *International Journal OF Quantum Chemistry*, 75(4-5):889–909, 1999.

[81] J. P. Perdew, K. Burke, and M. Ernzerhof. *Phys. Rev. Lett.*, 80(4):891, 1998.

[82] Kenji Toyoda, Yosuke Nakano, Ikutaro Hamada, Kyuho Lee, Susumu Yanagisawa, and Yoshitada Morikawa. *Surface Science*, 603(18):2912–2922, 2009.

[83] P. Jurecka, J. Sponer, J. Cerny, and P. Hobza. *Phys. Chem. Chem. Phys.*, 8:1985, 2006.

[84] Tait Takatani, Edward G. Hohenstein, Massimo Malagoli, Michael S. Marshall, and C. David Sherrill. *The Journal of Chemical Physics*, 132(14):144104, 2010.

[85] L.F. Molnar, X. He, B. Wang, and K.M. Merz. *J. Chem. Phys.*, 131:065102, 2009.

[86] Jonas Bjork, Felix Hanke, Carlos-Andres Palma, Paolo Samori, Marco Cecchini, and Mats Persson. *The Journal of Physical Chemistry Letters*, 1(23):3407–3412, 2010.

[87] Oleg A. Vydrov and Qin Wu and Troy Van Voorhis. *J. Chem. Phys.*, 129(1), 2008.

[88] Oleg A. Vydrov and Troy Van Voorhis. *J. Chem. Phys*, 130(10), 2009.

[89] Oleg A. Vydrov and Troy Van Voorhis. *Phys. Rev. Lett.*, 103(6), 2009.

[90] David C. Langreth and Bengt I. Lundqvist. *Phys. Rev. Lett.*, 104(9), 2010.

[91] J. Harris. *Phys. Rev. B*, 31(4):1770–1779, 1985.

[92] E.D. Murray, K. Lee, and D.C. Langreth. *J. Chem. Theory Compt.*, 5:2754, 2009.

[93] A. D. Becke. *The Journal of Chemical Physics*, 85(12):7184–7187, 1986.

[94] A.D. Becke. *Phys. Rev. A*, 38:3098, 1988.

[95] J.P. Perdew and W. Yue. *Phys. Rev. B*, 33:8800, 1986.

[96] C. David Sherrill, Tait Takatani, and Edward G. Hohenstein. *The Journal of Physical Chemistry A*, 113(38):10146–10159, 2009.

[97] Ikutaro Hamada and Minoru Otani. *Phys. Rev. B*, 82(15):153412, 2010.

[98] E. Londero and E. Schröder. *Phys. Rev. B*, 82(5):054116, 2010.

[99] R. Car and M. Parrinello. *Phys. Rev. Lett.*, 55:2471, 1985.

[100] J.J. Mortensen, L.B. Hansen, and K.W. Jacobsen. *Phys. Rev. B*, 71:035109, 2005.

[101] S. R. Bahn and K. W. Jacobsen. *Computing In Science & Engineering*, 4(3):56–66, 2002.

[102] M. Städele, M. Moukara, J. A. Majewski, P. Vogl, and A. Görling. *Phys. Rev. B*, 59(15):10031–10043, 1999.

[103] D.M Bates and G.S Tschumper. *J. Phys. Chem. A*, 113:3555, 2009.

[104] C Adamo and V Barone. *J. Chem. Phys.*, 110(13):6158–6170, 1999.

[105] A.K. Soper. *J. Phys. Condens. Matter*, 19:335206, 2007.

[106] K.T. Wikfeldt, M. Leetmaa, M.P. Ljungberg, A. Nilsson, and L.G.M. Pettersson. *J. Phys. Chem. B*, 113:6246, 2009.

[107] A.K. Soper. *Chem. Phys.*, 258:121, 2000.

[108] T. Tokushima, Y. Harada, O. Takahashi, Y. Senba, H. Ohashi, L. G. M. Pettersson, A. Nilsson, and S. Shin. *Chemical Physics Letters*, 460(4-6):387–400, 2008.

[109] M. Leetmaa, K. T. Wikfeldt, M. P. Ljungberg, M. Odelius, J. Swenson, A. Nilsson, and L. G. M. Pettersson. *The Journal of Chemical Physics*, 129:084502, 2008.

[110] AK Myers, GR Schoofs, and JB Benziger. *J. Phys. Chem.*, 91(9):2230–2232, 1987.

[111] Y Gamo, A Nagashima, M Wakabayashi, M Terai, and C Oshima. *Surface Science*, 374(1-3):61–64, 1997.

[112] T. Jiang, D. J. Mowbray, S. Dobrin, H. Falsig, B. Hvolbæk, T. Bligaard, and J. K. Nørskov. *The Journal of Physical Chemistry C*, 113(24):10548–10553, 2009.

[113] H Koschel, G Held, and HP Steinruck. *Surf. Rev. Lett.*, 6(5):893–901, 1999.

[114] PS Bagus, K Hermann, and C Woll. *J. Chem. Phys.*, 123(18), 2005.

[115] XL Zhou, ME Castro, and JM White. *Surface Science*, 238(1-3):215–225, 1990.

[116] Riccarda Caputo, Brian P. Prascher, Volker Staemmler, Paul S. Bagus, and Christof Woell. *J. Phys. Chem. A*, 111(49):12778–12784, 2007.

[117] D Syomin, J Kim, BE Koel, and GB Ellison. *J. Phys. Chem. B*, 105(35):8387–8394, 2001.

[118] S Andersson and M Persson. *Phys. Rev. B*, 48(8):5685–5688, 1993.

[119] G. Roman-Perez and J.M. Soler. *Phys. Rev. Lett.*, 103:096102, 2009.

[120] J Enkovaara, C Rostgaard, J J Mortensen, J Chen, M Dułak, L Ferrighi, J Gavnholt, C Glinsvad, V Haikola, H A Hansen, H H Kristoffersen, M Kuisma, A H Larsen, L Lehtovaara, M Ljungberg, O Lopez-Acevedo, P G Moses, J Ojanen, T Olsen, V Petzold, N A Romero, J Stausholm-Møller, M Strange, G A Tritsaris, M Vanin, M Walter, B Hammer, H Häkkinen, G K H Madsen, R M Nieminen, J K Nørskov, M Puska, T T Rantala, J Schiøtz, K S Thygesen, and K W Jacobsen. *Journal of Physics: Condensed Matter*, 22(25):253202, 2010.

Paper 1

D. C. Langreth, B. I. Lundqvist, S. D. Chakarova-Käck, V. R. Cooper, M. Dion,
P. Hyldgaard, A.K. Kelkkanen, J. Kleis, Lingzhu Kong, Shen Li, P. G. Moses, E.
Murray, A. Puzder , H. Rydberg, E. Schröder and T. Thonhauser ,

A density functional for sparse matter,

A density functional for sparse matter

A density functional for sparse matter

D C Langreth[1]**, B I Lundqvist**[2,3]**, S D Chakarova-Käck**[2]**,**
V R Cooper[1]**, M Dion**[1]**, P Hyldgaard**[4]**, A Kelkkanen**[3]**, J Kleis**[2,3]**,**
Lingzhu Kong[1]**, Shen Li**[1]**, P G Moses**[3]**, E Murray**[1]**, A Puzder**[1]**,**
H Rydberg[2]**, E Schröder**[2] **and T Thonhauser**[1]

[1] Center for Materials Theory, Department of Physics and Astronomy, Rutgers University,
Piscataway, NJ 08854-8019, USA
[2] Department of Applied Physics, Chalmers University of Technology, SE-41296 Göteborg,
Sweden
[3] Center for Atomic-scale Materials Design, Department of Physics, Technical University of
Denmark, DK-2800 Kongens Lyngby, Denmark
[4] Department of Microtechnology and Nanoscience, Chalmers University of Technology,
SE-41296 Göteborg, Sweden

Abstract

Sparse matter is abundant and has both strong local bonds and weak nonbonding forces, in
particular nonlocal van der Waals (vdW) forces between atoms separated by empty space. It
encompasses a broad spectrum of systems, like soft matter, adsorption systems and
biostructures. Density-functional theory (DFT), long since proven successful for dense matter,
seems now to have come to a point, where useful extensions to sparse matter are available. In
particular, a functional form, vdW-DF (Dion *et al* 2004 *Phys. Rev. Lett.* **92** 246401; Thonhauser
et al 2007 *Phys. Rev.* B **76** 125112), has been proposed for the nonlocal correlations between
electrons and applied to various relevant molecules and materials, including to those layered
systems like graphite, boron nitride and molybdenum sulfide, to dimers of benzene, polycyclic
aromatic hydrocarbons (PAHs), doped benzene, cytosine and DNA base pairs, to nonbonding
forces in molecules, to adsorbed molecules, like benzene, naphthalene, phenol and adenine on
graphite, alumina and metals, to polymer and carbon nanotube (CNT) crystals, and hydrogen
storage in graphite and metal–organic frameworks (MOFs), and to the structure of DNA and of
DNA with intercalators. Comparison with results from wavefunction calculations for the
smaller systems and with experimental data for the extended ones show the vdW-DF path to be
promising. This could have great ramifications.

(Some figures in this article are in colour only in the electronic version)

1. Introduction

By sparse matter we mean systems with important regions
having very low electron density. It is exemplified by soft
matter (figure 1), biological matter, nanostructures, corrosion
and catalyst layers. Both strong local bonds and weak
nonbonding forces are important. In particular, the nonlocal
correlations behind the van der Waals (vdW) forces between
atoms separated by empty space is a ubiquitous and often
important phenomenon. Examples of such matter are found
in vdW molecules, soft matter, molecule adsorption systems
and biostructures.

For dense matter, density-functional theory (DFT) has
well proven its usefulness to account for structure, cohesion

and other static properties. Today the standard DFT
approach involves the general-gradient approximation (GGA),
particularly successful for describing valence bonds. To extend
DFT's usefulness to the large classes of matter with *both*
high-density chunks and low-density regions, a general density
functional that includes vdW interactions is very desirable.

Soft matter is abundant in nature. It encompasses
solids, like graphite, molecular crystals, and polymers,
liquids and macromolecular systems, interacting systems,
like in adsorption, water overlayers and hydrogen storage,
biostructures, like DNA, protein structure and protein folding,
and numerous other sparse systems surrounding us in our daily
lives, like bread, butter, cheese, grease, tissues, tape, paint,
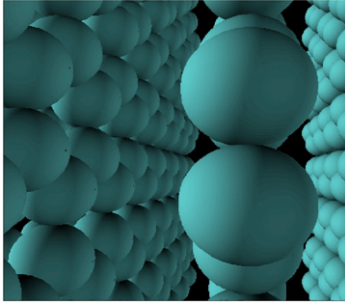dust, rust, cloth, plastics, snowflakes, ski wax, leaves and

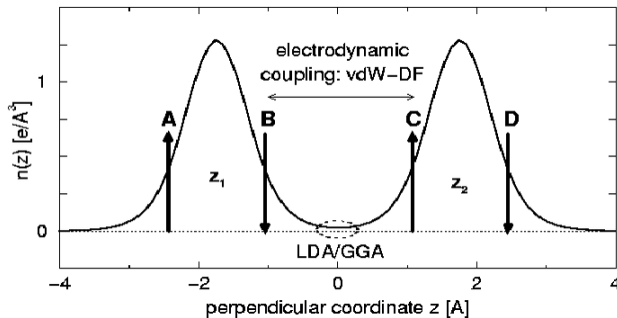**Figure 1.** Sparse matter: model of graphite [1].

Figure 2. Schematic account of vdW forces in sparse, layered matter (two graphene sheets at equilibrium separation) [2]. Towards a background of laterally averaged electron density, the vertical arrows mark typical locations of charge fluctuations, the horizontal arrow the region of correlation between them and the dotted ellipse the very different region of relevance for GGA (and LDA).

flowers. With perspectives of condensed-matter theorists and surface and materials theoreticians, after crucial development and the work of many [1], we have proposed such a functional (vdW-DF) [2, 3].

In this paper the background and basis for vdW-DF are briefly reviewed, as are the growing number of applications of it. The outcome of these applications is assessed, and the anticipations for the future are expressed.

2. van der Waals forces

van der Waals (vdW) interactions, also known as London dispersion interactions, constitute a quantum-mechanical phenomenon with charge fluctuations in one part of an atomic system that are electrodynamically correlated with charge fluctuations in another. The system experiences this as an attractive vdW force (figure 2). The vdW force at one point thus depends on charge events at another region and is a truly nonlocal correlation effect.

3. van der Waals interactions in DFT

The exact density functional [4, 5] contains the vdW forces [6]. Unfortunately, we do not have access to the exact DFT. Approximate versions are abundant, however. Commonly, the local-density approximation (LDA) [5, 7–11] and the general-gradient approximation (GGA) [12–18] are used. They depend on the density in local and semilocal ways, respectively, however, and give no account of the nonlocal vdW interaction (figure 2).

There are empirical and semi-empirical accounts for the vdW or London dispersion forces that rely on the asymptotical form $-1/d^4$ for insulating sheets of boron nitride (for example) and $-1/r^6$ for atoms and molecules. The correct values of these forces at important distances like vdW bond lengths are substantially different from those predicted by the asymptotic forms.

Today there are proposals for how the vdW *can* be treated in DFT, in particular at large separations [19–21]. We have proposed functionals for all separations, one for layered systems [1] and one for general geometries [2, 3]. They are both developed in the same spirit but differ in detail. The earlier functional [1] relied on lateral averaging to render the charge-density truly planar and is considered only of historical importance as it gave guidance to the construction of the general-geometry functional [2, 3], which after all can be used on layered systems as well.

In DFT, the electron density $n(r)$ is the key quantity, and the energy functional can be expressed as [5]

$$E[n] = T_s[n] + V_{ee}[n] + V_{ion}[n] + E_{xc}[n], \quad (1)$$

where the first three terms are the functionals for the kinetic energy of noninteracting electrons, the Coulomb energy of the electrons and the interaction energy between electrons and ions, respectively. The remaining term, $E_{xc}[n]$, the exchange–correlation energy functional, contains all the interactions for which there is no exact functional.

However, there is a so-called adiabatic-connection formula that provides a formal basis for $E_{xc}[n]$, a recipe for how approximate exchange–correlation energy functionals can be generated [22, 23, 10]. The 'standard' DFT calculations today typically use the local LDA or the semilocal GGA for $E_{xc}[n]$, with quite some success for dense matter, including hard materials and covalently bound molecules.

4. Density functional in vdW-DF

The vdW-DF procedure is in short

$$E_{xc}[n] = E_x^{GGA}[n] + E_c^{new}[n], \quad (2)$$

that is (i) to take an appropriately selected GGA exchange functional, (ii) to develop a properly constructed *nonlocal* correlation functional that includes an account of vdW forces and (iii) to perform calculations with some efficient and accurate electron-structure scheme, for instance, with plane-wave and real-space codes. The computer resources required for vdW-DF [2] are comparable to ordinary DFT (e.g. GGA). By using the functional derivative of $E_c^{new}[n]$ with respect to the density $n(r)$ as a component of the Kohn–Sham electron potential [5], the calculations are made fully self-consistent [3].
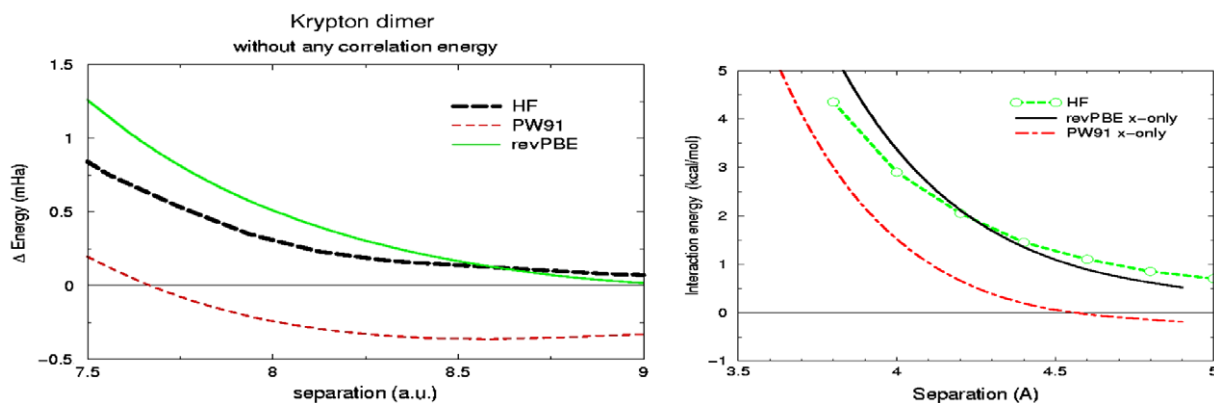
Figure 3. Variation of exchange functionals and exact Hartree–Fock (HF) with separation for the krypton (left) [26] and benzene dimers (right) [27].
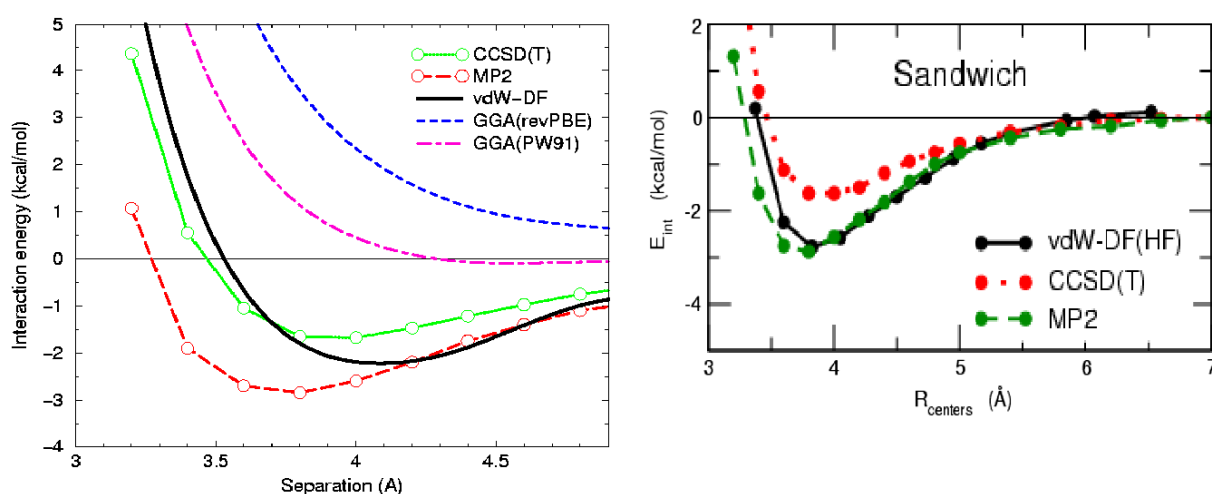

Figure 4. Binding-energy calculations for the benzene dimer in various approximations [2, 27].

4.1. Exchange

Among approximation schemes for the *exchange* energy, many standard GGA flavors give substantial 'vdW' binding from *exchange* alone [24]! Exact exchange calculations in some test cases, like those in figure 3, show this behavior to be incorrect. From such comparisons (figure 3), we find that the revPBE flavor of GGA exchange [25] has less of this problem and was closer to Hartree–Fock (figure 3). Therefore, we chose revPBE exchange. The successes of LDA and GGA stem from their accounts of exchange and correlation in high-density regions, important for the covalent bond. Less attention has been given to the low-density regions in the tails of the electron distribution. This might be a reason for the spread between different flavors of GGAs in the tails. One should note that PW91 [16] exchange is an extreme case, and the more recent PBE [18] functional gives curves closer to HF, but still with an attractive part.

The ultimate exchange functional, the exact Hartree–Fock (HF) exchange, is possible to use, in particular for small systems. It has been explored for dimers of benzene [27], where it gives improved values for the equilibrium separation values but larger values for the binding energy [27]. Similar

results have recently been presented in [28]. Values of the vdW bond lengths that are a couple of per cent too large seem to be the rule in the vdW-DF results reviewed below. It is good to know the cause of this and to know a possible remedy for it that can be used, at least in principle. Still, it is important to realize that there is a cancellation of errors between exchange and correlation in DFT, and that it is normally important to have a match between the exchange and correlation functionals used. This means that comparison of the exchange functional with HF is not necessarily the most effective test.

For the benzene dimer (figure 4), an HF calculation is a realistic option, as one can test the use of HF exchange instead of revPBE exchange in a vdW-DF calculation. For the sandwich configuration, the resulting potential-energy curve (PEC) is similar, but the bond length is much better, the sandwich structure is a saddle point in the energy landscape and the binding is stronger, even stronger than the 'best' wavefunction-method result (CCSD(T)) [27].

Needless to say, these short-range interactions should be worried about, including the urgent problem of improving the exchange functional, but this would involve testing on a great number of non-vdW systems. As this paper illustrates, the large number of interesting vdW systems around us has

made us give priority to *applications* of the proposed vdW-DF, knowing well the limitations in the revPBE [25] account of the exact exchange. Results similar to those for the benzene dimer apply for other test systems. The revPBE exchange is chosen because it best eliminates the spurious bonding from exchange alone, but the fact that it is not perfect is reflected in the slightly longer bonds obtained with it. Nevertheless it has proved a good match for the vdW-DF correlation functional in giving better equilibrium energies than when HF exchange is used. The search for an improved exchange functional has high priority.

4.2. Correlation

The correlation energy is split into shorter- and longer-ranged parts:

$$E_c[n] = E_c^o[n] + E_c^{nl}[n]. \tag{3}$$

The short-ranged term, $E_c^o[n]$, is evaluated in LDA, which implicitly uses the exact dielectric function. The longer-ranged part, E_c^{nl}, depends nonlocally on the density and contains the principal vdW terms. It is also much smaller in magnitude and in positional sensitivity, so it can be evaluated with a lower accuracy. In particular, in the vdW-DF it is evaluated with a simple model dielectric function.

As a matter of fact, in the vdW-DF [2], the key ingredients of this long-range (nonlocal) part of the correlation functional are (i) the adiabatic-connection formula [22, 23, 10] as the starting point, (ii) an approximate coupling-constant integration, (iii) which as in the planar case [1] is exact for the asymptotic long-range vdW term, (iv) the use of an approximate dielectric function ε in a single-pole form, (v) which is fully nonlocal and satisfies known limits, sum rules and invariances, (vi) whose pole position is scaled to give the exact electron-gas ground-state energy locally, including the appropriate gradient correction (the pole strength is determined by a sum rule) and (vii) the lack of empirical or fitted parameters.

The coupling-constant (λ) integration in the nonlocal correlation term $E_c^{nl}[n]$ in equation (3) is performed by making the simplest of approximations:

$$(\varepsilon - 1)_\lambda = \left[\frac{(\varepsilon - 1)}{\lambda} \right]_{\lambda=1} \lambda \tag{4}$$

as this can be shown to give the longest-range van der Waals terms exactly, if long-range 'spectator' interactions are also left out of the dielectric function (as they implicitly are in our simple model) [2]. A thorough discussion of this issue has been given by Dion [29]. This secures the proper asymptotic dependence. For intermediate separations its accuracy is tested in a large number of applications and comparisons with accurate results of wavefunction methods and/or experimental results, whenever such results are available. While singular in the well-known asymptotic form at large separations, the vdW interaction given by vdW-DF at small separations gives a saturation of the interaction. This is guaranteed by the form of the kernel (figure 5).
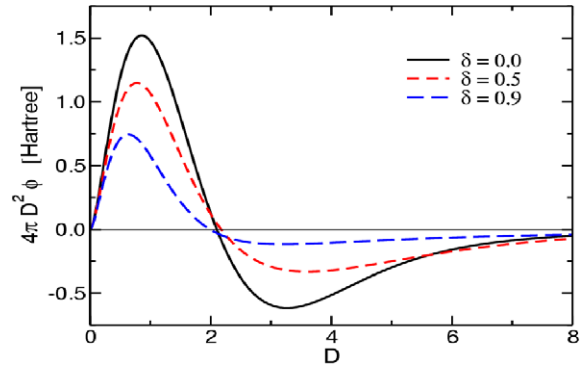

Figure 5. The kernel in equation (5) as a function of the dimensionless separation parameter D for several values of the asymmetry parameter δ, both parameters defined in the text.

The form of the general-geometry functional for $E_c^{nl}[n]$ derived in [2] is

$$E_c^{nl} = \frac{1}{2} \int d^3r \int d^3r' \, n(r) \Phi(r, r') n(r') \tag{5}$$

where $\Phi(r, r') = \Phi(q(r), q(r'))$. The interaction kernel depends on the density and its gradient, $q(r) = q(n(r), \nabla n(r))$, and can be given a scalable form via

$$D = \frac{q + q'}{2} |r - r'|, \qquad \delta = \frac{1}{2} \frac{q - q'}{q + q'},$$
$$q = q(r), \qquad q' = q(r').$$

The kernel Φ (figure 5) is attractive at large and intermediate effective distances D. At very large D values, it takes its proper asymptotic form, and it has an oscillation at short distances D. Its repulsive part is such that the area under the solid black curve vanishes, which is the key to seamlessness and the lack of double counting [2, 26]. Double counting is avoided, as the short-range part is treated in LDA (no nonlocal component), while the long-range part has no local component, by construction, as made evident by the vanishing of the integral mentioned above.

In the self-consistent version of vdW-DF [3], there are oscillatory nonlocalities also in the exchange–correlation potential in the Kohn–Sham equations [5]:

$$V_c^{nl}(r) = \delta E_c^{nl}[n]/\delta n(r). \tag{6}$$

Obviously, the self-consistent version [3] is the more complete and proper one. However, the extensive computations that it calls for do not always have to be performed. Comparison of results of the self-consistent vdW-DF scheme [3] with those of the 'older' post-GGA perturbation of vdW-DF [2] typically show negligible differences. This is illustrated by the vdW binding energies of the displaced CO_2 dimer [3] and of H_2O on benzene [3, 30], with about the same results near equilibrium separations and only small differences at smaller separations (figure 6). However, there are situations, where the self-consistent version is needed very much, for instance, for Hellmann–Feynman forces in molecular-dynamics simulations [3] and for incipient charge transfer
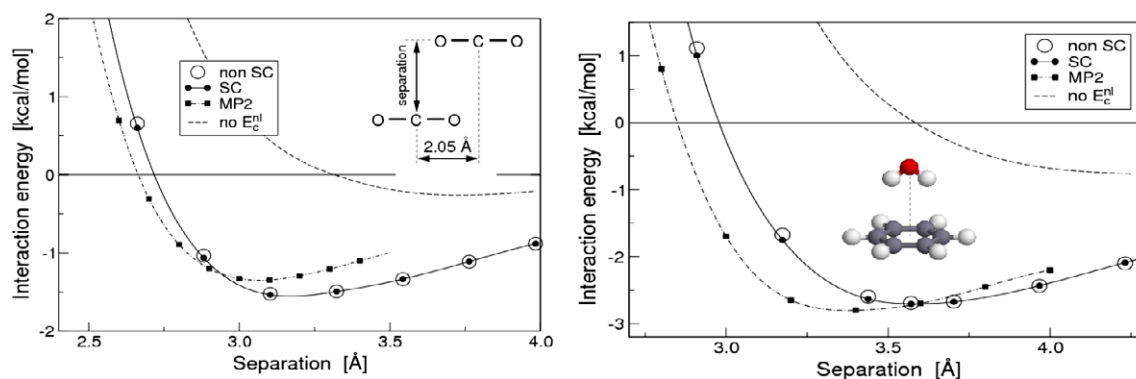
Figure 6. Self-consistent (dots) [3] and post-GGA perturbative (circles) [2] vdW-DF results for PECs of dimers of displaced parallel CO_2 molecules (left) and H_2O on top of the midpoint of a benzene molecule (right) [3]. Wavefunction-calculation (MP2) and GGA-calculation results are shown for comparison.
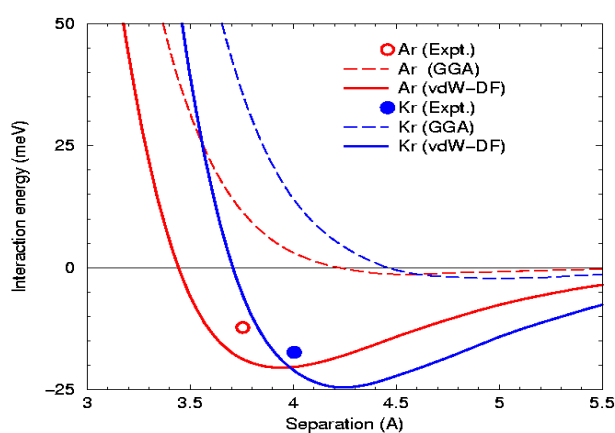

Figure 7. PECs calculated with the vdW-DF [2] (solid lines) compared with the generalized gradient approximation (GGA) (dashed lines), for the Ar (red curves starting at the left) and Kr (blue curves starting at the right) dimers. Experimental equilibrium data [40] are shown for comparison.

affected by vdW forces, as relevant for, e.g., self-assembled molecular-electronic systems.

5. Applications of vdW-DF

5.1. Atoms and molecules

The vdW-DF has been applied to dimers of atoms [2]. Results for argon and krypton dimers can be compared to experimental data (figure 7) to show the virtues and vices of the method on such localized systems. There should be better methods to obtain accurate vdW descriptions of such localized systems.

However, as vdW-DF is based on electron-gas (homogeneous and almost homogeneous) many-body results [1–3, 26], its main targets are systems with extended electron states. Among molecular systems, there are presently applications to dimers of benzene [2, 27, 31] and benzene-like molecules [32], pairs of other small molecules [3, 27, 30, 31], dimers of PAHs [41, 31], polymer interactions [43] and dimers of cytosine [3] and other DNA and RNA base-pair molecules [47].

They have typically a size that allows wavefunction calculations to be performed and thus comparisons to be made, and it is gratifying that there is a generally fair agreement between the results of the two types of methods, when comparisons are possible.

The benzene molecule has extended valence-electron states and a small energy gap. It is not jellium but closer to it than, for example, He. Further, it is generally used as a model system for vdW interaction and a prototypical system for π-electron (figure 8) interactions. The benzene dimer, this smallest aromatic system, appears in sandwich, slip parallel and T-shape configurations (figure 8), and the question, which of these configurations is stable, is still debated.

Polycyclic aromatic hydrocarbon (PAH) dimers have even more extended electron states, which make them apt for application of vdW-DF. vdW-DF calculations on PAH dimers give increased dimer binding and separation with increasing numbers of benzene rings [41, 31] (figure 9). Comparisons with equilibrium binding energy and (vertical) separation values from CCSD(T) calculations [42] are favorable, e.g. 0.247 eV/dimer and 3.5 Å for naphthalene in AB stacking, compared to 0.29 eV and 3.7 Å in the vdW-DF calculation [41, 31].

Water on aromatic molecules constitutes a small system with several types of interactions. A system with an H_2O molecule interacting with a benzene molecule involves both vdW and electrostatic forces, and could be important for understanding the hydrogen bond and adsorbed water layers. vdW-DF calculations on it [3, 30] show that the stable configuration is with the water molecule standing above or below with the H atom as shown in the right panel of figure 6. Here the water makes a hydrogen bond with the π cloud of the benzene (enhanced by London dispersion), with a vdW-DF predicted strength of 2.9 kcal mol^{-1}. This is confirmed to be the minimum energy configuration by the best MP2/CCSD(T) calculations [33–35], which give a binding energy of about 3.3 kcal mol^{-1}. The authors [30] trace out the interaction energy between water and benzene in a variety of configurations. One of the sequences considered is shown in figure 10.

This type of study can be extended to the noncovalent forces in C–H/π interactions [36]. On complexes like
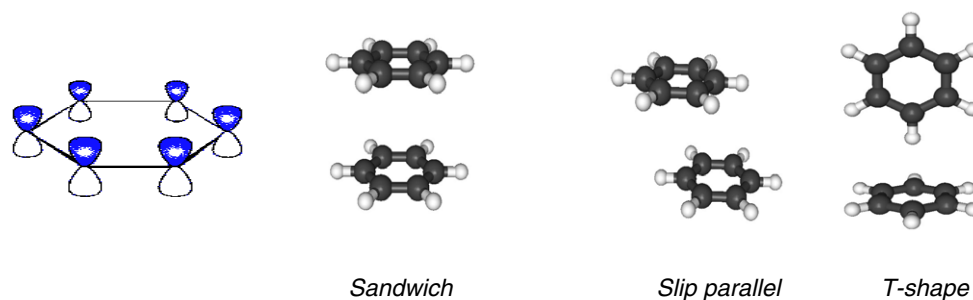
Figure 8. Schematics of the π-electron system of the benzene molecule, and some relevant structures of benzene dimers.
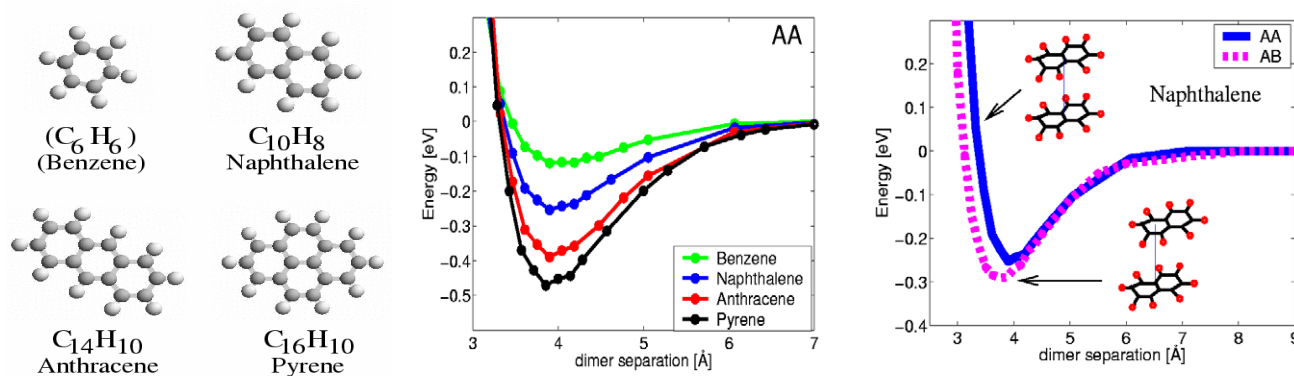

Figure 9. Polycyclic aromatic hydrocarbons (PAH) (left) and PECs of PAH dimers calculated with vdW-DF in the AA (middle) and AB (right) stackings [41, 31].
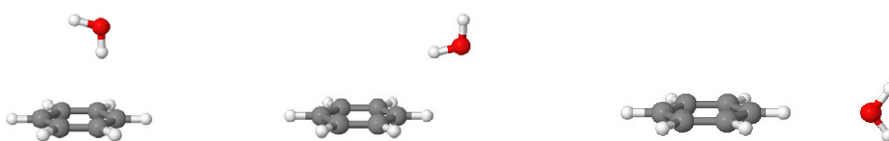

Figure 10. The optimized orientation and height of the water molecule as the horizontal coordinate of the oxygen is moved from the global minimum energy configuration (left) to a saddle point configuration (right) [30]. If instead the horizontal oxygen coordinate is moved to the left, one reaches another saddle point configuration, with the oxygen over the center of the benzene and the H atoms equidistant from the benzene plane. This latter saddle point is the lowest-energy configuration of the geometry shown in figure 6.

Table 1. Bonding results for systems with an aromatic π and an aliphatic C–H group calculated with different methods [36]. The separations R are in Å, while interaction energies E_{int} are in kcal mol^{-1}.

	C_6H_6–CH_4		C_6H_6–CHF_3		C_6H_6–$CHCl_3$		C_8H_7N–CH_4	
	R	E_{int}	R	E_{int}	R	E_{int}	R	E_{int}
vdW-DF	4.1	−1.57	3.6	−3.73	3.6	−5.11	4.0	−1.81
PBE	4.2	−0.40	3.7	−2.04	3.7	−2.07	4.2	−0.41
CCSD(T)	3.8	−1.45	3.4	−4.20	3.2	−5.60	3.8	−1.57
MP2	3.8	−1.79	3.4	−4.60	3.2	−7.20	3.7	−1.96

Figure 11. Benzene dimers with the substituents CH$_3$ and OH, which are electron donors. Comparison via vdW-DF with the substituents F and CN, which are electron acceptors, has allowed the effects of electronegativity to be studied [32].

methane–benzene (C$_6$H$_6$–CH$_4$), trifluoromethane (C$_6$H$_6$–CHF$_3$), trichloromethane (C$_6$H$_6$–CHCl$_3$) and methane–indole (C$_6$H$_3$N–CH$_4$), the vdW-DF predicts noncovalent interactions that are characterized by a weak bond between an aromatic π system and an aliphatic C–H group. The results (table 1) show significant improvement over traditional DFT and compare favorably with CCSD(T) and MP2 results [36].

With substituents like CH$_3$ and OH (figure 11), the variation of binding properties of benzene-like dimers with electronegativity can be studied in a systematic way [32], as OH is a strong electron donor, CH$_3$ an electron donor, F an electron acceptor and CN a strong electron acceptor. Doing this in sandwich (figure 12), T-shape 1 and T-shape 2 configurations gives a large database to study the effect [32, 44].
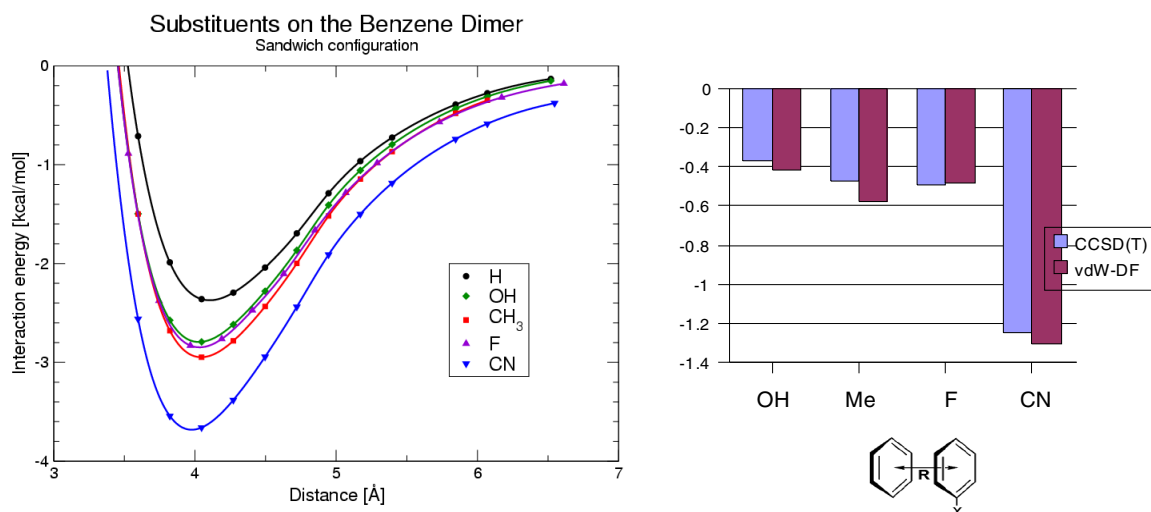
Figure 12. PECs for 'doped' benzene dimers, in sandwich configuration, calculated with vdW-DF [32] (left) and binding energy shifts from calculations in vdW-DF [32] and CCSD(T) [44] (right).
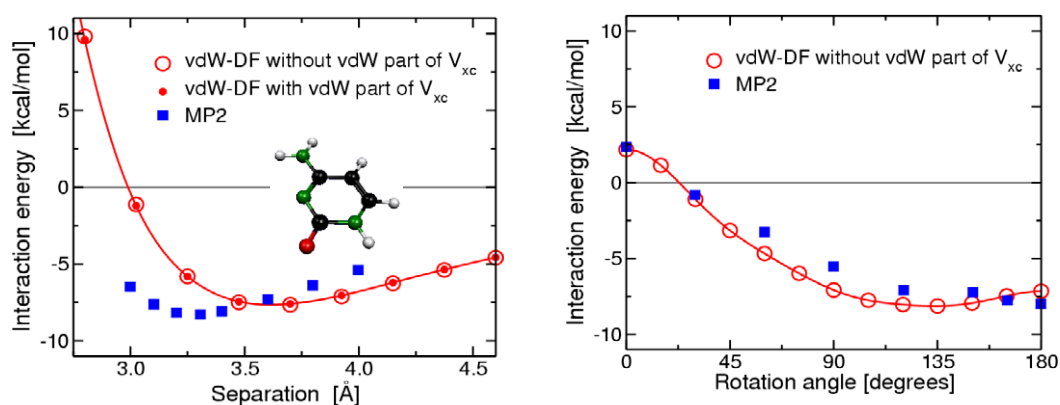

Figure 13. The PEC for the cytosine dimer composed of two parallel cytosine molecules ($C_4H_5N_3O$, shown as an inset in the left panel). The left panel gives the PEC as a function of separation at zero rotation angle, while the right panel shows the PEC as a function of rotation angle at a fixed separation of 3.4 Å. In each case the vdW-DF results [3, 47] are compared with those of wavefunction methods [46]. The left panel also shows that it is not necessary to consider the change in density that occurs when the vdW interaction is turned on, as results of self-consistent calculations (black dots [3]) and by post-GGA perturbation of vdW-DF [2] show negligible differences.

Before 2004 there was a common wisdom, based on arguments of electrostatics and exchange repulsion: 'donors increase $\pi-\pi$ repulsion and acceptors decrease it. *Therefore acceptors increase binding energy and donors decrease it.*' However, in 2004 a wavefunction calculation [44] disproved this claim. Interaction-energy differences for the sandwich structure, i.e. doped benzene value minus benzene value (kcal/mol) are all negative! For the T-shape 1 and T-shape 2 configurations, there are also strong deviations from the old rules. Calculations with the vdW-DF give interaction-energy difference values for the twelve systems, obtained with four substitutions and three structures, the same sign and size as the CCSD(T) wavefunction calculation (figure 13 shows results in the sandwich structure; similar results are for other structures, with only F substitution in T-shape 2 differing in size) [32].

Multiple substituents in benzene in cytosine (figure 13) do not only provide a careful step further on the substitution road but point at subsequent applications on DNA and RNA. Although a many-atom system, for the cytosine dimer there

are also valuable wavefunction calculations to compare with (figure 13) [3].

An attempt for a more general assessment of the accuracy of the vdW-DF versus wavefunction methods is made in table 2 [47], where binding-energy results from recent quantum-chemical (QC) calculations for the Hobza group's set S22 [35] and from the semi-empirical DFT-D method [48, 49] are given for comparison.

The comparisons in table 2 and the other favorable comparisons with wavefunction calculations for molecular systems show promise and make us believe that the vdW-DF method can be fruitfully applied to more extended systems, where wavefunction calculations are lacking.

5.2. Crystalline solids

Graphite is the textbook example of a vdW-bonded solid. Within the layers, sp^2-hybridized covalent bonds give a strength missing its parallel. This strength together with
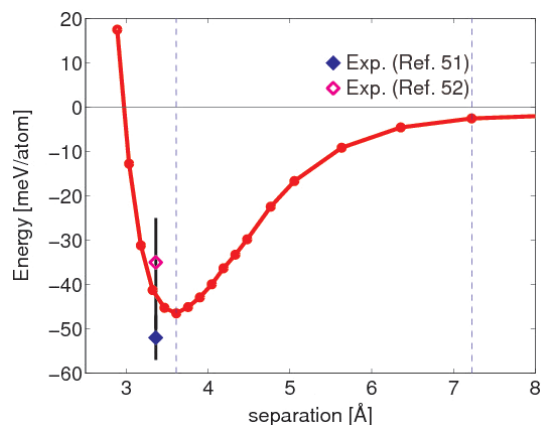
Figure 14. The PEC of a graphene dimer according to vdW-DF [45]. The interlayer binding of graphite is given by the sum of the PEC values at the two vertical dashed lines (first and second layer positions). The experimental points are derived from extrapolation of carbon nanotube (CNT) unfolding [51] and of desorption data [52].

Table 2. Binding-energy results (kcal mol^{-1}) for characteristic noncovalently bound molecules (the Hobza group's set S22 [35]) calculated with the vdW-DF method (compiled In [47]), with quantum-chemical methods (QC) [35], and from the semi-empirical DFT-D method with BLYP-D (04) [48] and BLYP-D (07) [49].

	vdW-DF	QC	BLYP-D (04)	BLYP-D (07)
AT (WC)	−15.20	−16.37	−15.01	−17.19
Benzene-CH$_4$ (C$_3$)	−1.57	−1.50	−0.90	−1.37
Benzene-H$_2$O (C$_s$)	−2.86	−3.28		−4.16
Benzene dimer (C$_{2v}$)	−2.28	−2.74	−2.03	−2.76
Benzene dimer (C$_{2h}$)	−2.80	−2.73	−2.00	−2.35
AT (stack)	−9.55 [a]	−12.23	−10.47	−12.85

[a] Not geometrically optimized.

the vdW bonds between the layers make graphite the stable carbon solid, leaving diamond as a metastable structure. The vdW-DF calculations are typically performed for two parallel graphene sheets. Thanks to the rapid decay of vdW forces with separation the binding energy between these sheets are almost equal to the interlayer binding energy. Figure 14 gives the PEC from a vdW-DF calculation [45]. While it is known that the semi-metallic nature of graphite leads to a small weakening of that asymptotic vdW interaction for these systems [50], the extent to which this may influence the interaction near the equilibrium position is unknown, and no attempt to include it was made in the calculations shown below.

For comparison with experimental results, x-ray data have long been available for the interlayer separation, which is a few per cent shorter than the calculated value. For the binding energy, actually that between two graphene sheets, the two experimental numbers that we have found are both indirect, one from extrapolation of carbon nanotube (CNT) unfolding [51] and one from extrapolation of desorption data [52].

To answer questions about the effects on hard materials, vdW-DF calculations have been performed on an Si crystal

in the diamond structure, showing that the good agreement between GGA results and experiment is not hurt [3].

Potassium intercalation in graphite has been studied by vdW-DF [55], as an account of the intercalation formation energy from pure K atoms and graphite requires a description of the graphite interlayer binding energy and thus of the vdW forces. The vdW-DF calculation indicates that the vdW interaction supplements the ionic bond in the final intercalation compound C$_8$K, with key contributions to the binding separation, layer binding energy, formation energy and bulk modulus (vdW forces strengthen the interlayer binding energy of the C$_8$K by more than 50%, from 511 meV in GGA to 793 meV per formula unit) [55]. The vdW-DF results for structure and elastic response are in fair agreement with experiment. However, the intercalation process is predicted to leave the bulk modulus unchanged, while experiments indicate a moderate hardening [55].

The vdW-DF is of particular interest for molecular crystals. Applications have been made to crystalline polyethylene (figure 15) [53], with results close to experiment, about as close as with an empirical force-field method, and to a semiconducting CNT crystal (figure 16) [43], where vdW-DF predicts (i) an intertube bonding with a strength consistent with recent observations for the interlayer binding in graphitics (30 versus 50 meV/atom) and (ii) a CNT wall-to-wall separation (*D* approx. 3.45 Å) in very good agreement with experiment (*D* = 3.4 Å) [43].
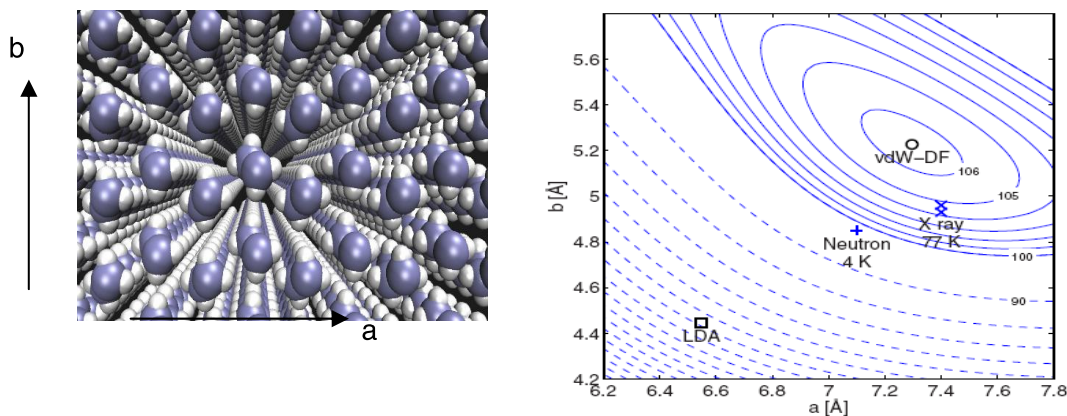

Figure 15. The polyethylene crystal and its energy landscape according to vdW-DF [53].
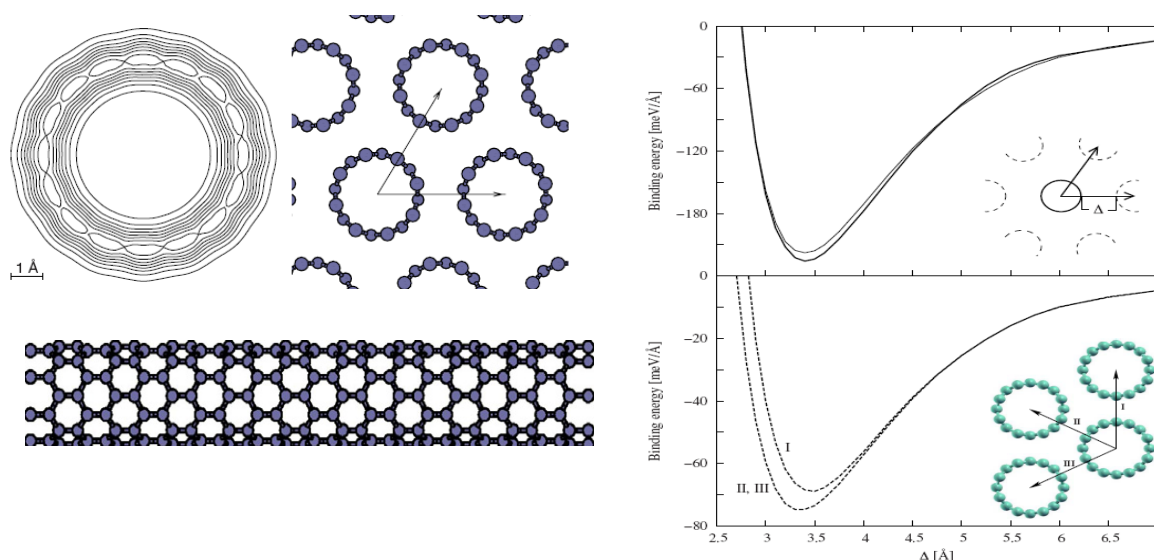
Figure 16. The semiconducting CNT crystal and its energy landscape according to vdW-DF [43].
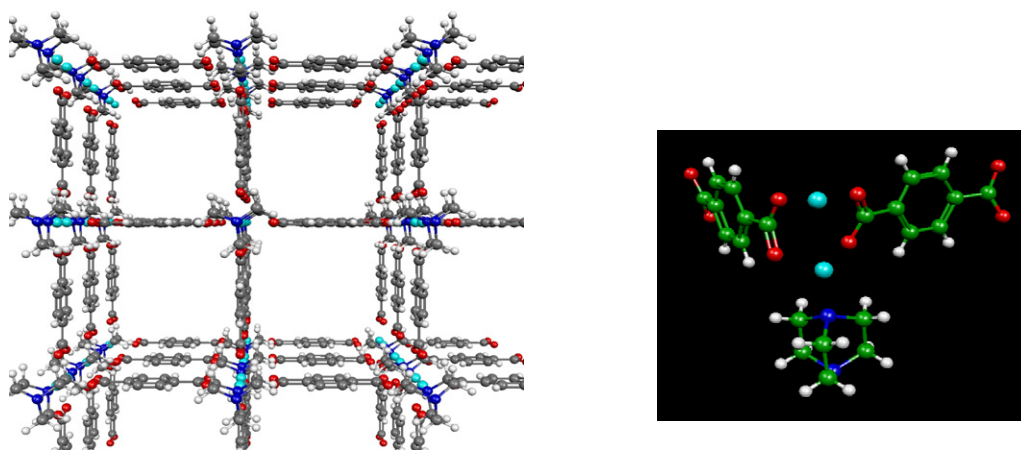

Figure 17. Example of a simple MOF structure (left) and its components, two linkers and a pillar, joined by two metal atoms (in this case Zn) (right) [56]. The H_2 is bound in several channels which are difficult to guess, but which have been calculated using vdW-DF [56].

Recent developments with the vdW-DF on molecular crystals can be exemplified by complications in connection with H_2 monolayer calculations in the mentioned problem of hydrogen storage in graphite [37, 38]. Calculational methods have to be improved to account for the many orientations of the H_2 molecule [54].

Application [56] to hydrogen storage in metal–organic frameworks (MOFs) [57, 58] clearly demonstrates the advantages of using a DFT-like vdW-DF. The components of simple MOF are metal atoms connected by organic molecule pillars and linkers (figure 17). It allows the study of the binding of H_2 to an individual linker, where the vdW-DF results for the H_2–linker interaction energy [56] can be compared with quantum-chemical results [59]. It also allows a modeling of the entire MOF, which shows differences in H_2 binding energy and binding sites between the MOF and the fragment [56]. Shifts in H_2 stretching frequency have been calculated, providing a valuable possibility of validation of the modeling [56]. Ultimately the relation of binding sites to structure will be fed

back to experts [57, 58] in MOF fabrication, in the hopes of creating improved hydrogen-storage materials.

5.3. Adsorption

Molecular adsorption offers interesting possibilities to test vdW-DF results against experiment. The binding energy, or rather the adsorption or desorption energy, is directly measurable in, for example, desorption experiments. The systems studied so far include adsorbates like benzene and aromatic molecules, and a number of different planar substrates.

The vdW-DF calculation of the desorption energy for benzene from graphite [45] has constituted an important milestone for the development of the functional in the general-geometry form. A thermal-desorption experiment had been performed on this vdW model system and PAHs on graphite, largely for the purpose of providing benchmarks for possible relevant theories, with estimates of the experimental error [52].
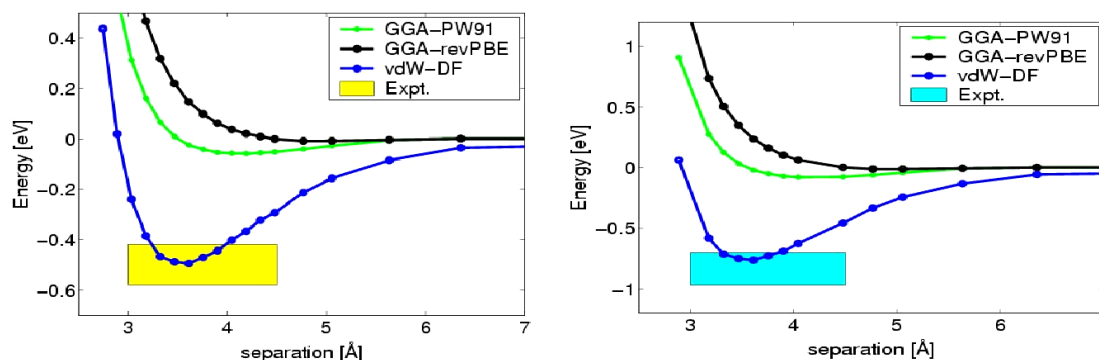
Figure 18. Benzene–graphene (left) and naphthalene–graphene (right) PECs [45], compared to experimental values for the desorption energy (heights of boxes accounting for error bars) [52].
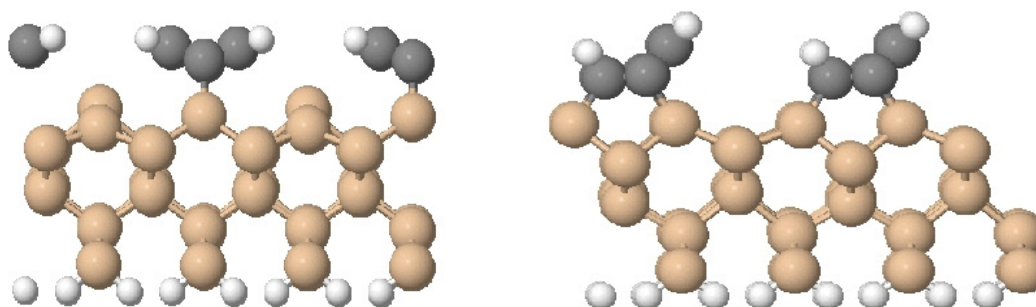

Figure 19. Butterfly (BF; left) and tight-bridge (TB; right) structures of C_6H_6 on Si(001)-(2 × 1), viewed along [$\bar{1}$10] [60].

The fact that the calculated PEC minima for both benzene and naphthalene on graphite (figure 18) fall within these error bars is promising for the vdW-DF method.

Adsorption of benzene has also been studied with vdW-DF on the Si(001)-(2 × 1) surface [60], where extensive studies with a variety of experimental tools have given conflicting results [60]. There is agreement on the two most stable structures, the butterfly (BF) and tight-bridge (TB) structures (figure 19), but to date none such on which is the stable one. Inclusion of vdW forces is found to make a *qualitative* difference to the results. Standard DFT with PBE or revPBE functionals finds that the TB structure is always stable, whereas vdW-DF calculations imply that, for some coverages, vdW forces stabilize the BF structure [60]. The results have significant implications for many DFT studies, as vdW forces are generally considered to have a negligible effect on covalently bonded systems and are usually ignored [60].

Adsorption of adenine on graphite has been studied with the vdW-DF as a response to a recent letter [61], where a semi-empirical approach is used. A semi-empirical vdW potential, a dipolar formula with damping functions caused by a cutoff on the dipolar singularity, has been proposed early on [62], and is now in extensive use [63, 24, 48, 61]. However, the 'procedure cannot be rigorously justified, although it is certainly more reasonable than the use of the [asymptotic] vdW potential where it is divergent' [62]. With no fitted parameters, the vdW-DF gives [39] (i) an adsorption energy of 0.7 eV (like experiment [61]), (ii) an equilibrium separation of 3.5 Å and (iii) a longitudinal optical phonon frequency in the *c* direction in graphite of 13 meV (experiment: 15.6 meV).

Phenol is a benzene molecule with one H atom replaced by an OH radical (figure 20). The adsorption of phenol (figure 20) [64] demonstrates a covalent bond to dominate on Al_2O_3, a vdW bond dominating on graphite and a metallic bond on nickel [65]. The vdW bond is ubiquitous but absent in the Ni PBE calculation of [65]. Preliminary results with the vdW-DF point at a weaker adsorption (0.41 eV) and even a different adsorption site [66].

Molybdenum sulfide (MoS_2) is a layered compound. Adsorption of aromatic and conjugated compounds on the basal plane of MoS_2 has been calculated with the vdW-DF [67] and shown to be well described in comparisons with available desorption data [68]. The benzene PEC (figure 21) looks very much like that for benzene on graphite (figure 18).

Morikawa *et al* [69] have used vdW-DF to study benzene adsorption on the (111) surfaces of Al, Cu, Ag and Au. While the binding energy for these systems is small within GGA (~0.02 eV), it is found that the vdW contribution causes an order of magnitude increase. The adsorption geometry undergoes no change for the noble metal surfaces, although for Al the metal–molecule distance decreases by ~15% when the vdW interaction is included. Comparison of calculated workfunction change vs. experimental values suggests that the metal–molecule distances are overestimated by both GGA and vdW-DF.

Applications of the vdW-DF [70] have been made to the adsorption of butane (C_4H_{10}) on metals, in particular n-butane on the (111) surfaces (figure 22) of Cu, Au and Pt [70], with GGA results from [71] and with experimental data
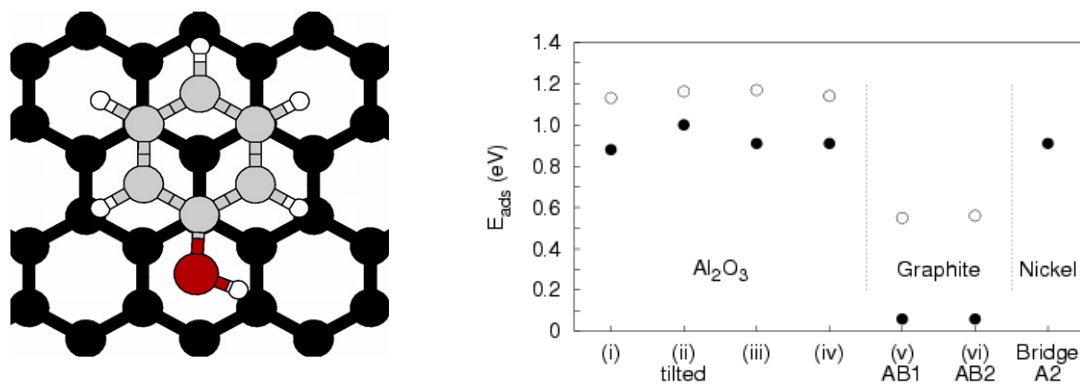
Figure 20. A phenol molecule symmetrically placed on a graphite surface (left). Phenol adsorption-energy values calculated with the vdW-DF method [2] for adsorption on Al_2O_3 and graphite, where covalent (GGA; filled circle) and covalent plus vdW (vdW-DF; empty circle) energy contributions are indicated [64] and with PBE for adsorption on Ni [65] are shown on the right.
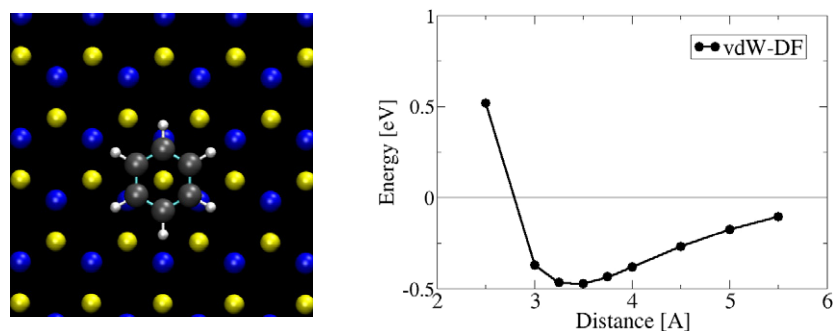
Figure 21. Benzene adsorption on the basal plane of MoS_2: geometry (left) and potential-energy curve (right) [67].
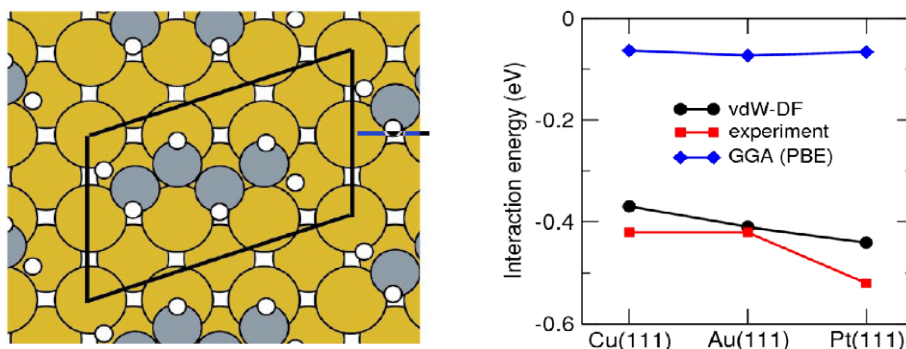
Figure 22. Adsorption structure and energy values for n-butane on Cu(111), Au(111) and Pt(111) [70]. GGA values [71] and experimental numbers [72–74] are shown for comparison. Left panel reprinted with permission from [71]. Copyright 2004 by the American Physical Society.

from [72–74]. The calculated and measured adsorption-energy values show good agreement in figure 22 [70].

Adsorption of thiophene on Cu(110) has recently been addressed in [75]. In this prototype case, relevant for organic field-emitter transistors (OFETs), the interface between metal and a π-conjugated molecule is of interest. In their vdW-DF calculation, the authors use RPBE, which they find to give results close to revPBE. The calculated adsorption energy is 0.26 eV. The variation of the inner potential is calculated with vdW-DF [75] and the workfunction with a thiophene overlayer is found to be 3.63 eV, as compared to the experimental value 3.65 eV, a substantial lowering of the clean Cu(110) surface value of 4.45 eV (figure 23).

The adsorption calculations have a favorable direct link to experimental adsorption-energy values, typically measured in desorption experiments. At large, comparisons with experiments indicate that the vdW-DF has a useful accuracy. An even more detailed assessment of vdW-DF can be made when experimental results for adsorption geometries and vibrational properties are available. The adsorption-induced change of the workfunction is another calculable quantity of key interest.

5.4. Interfaces

Alq3 (tris-(8-hydroxyquinoline)) is one of the most widely used materials in OLEDs. The barrier for injection is
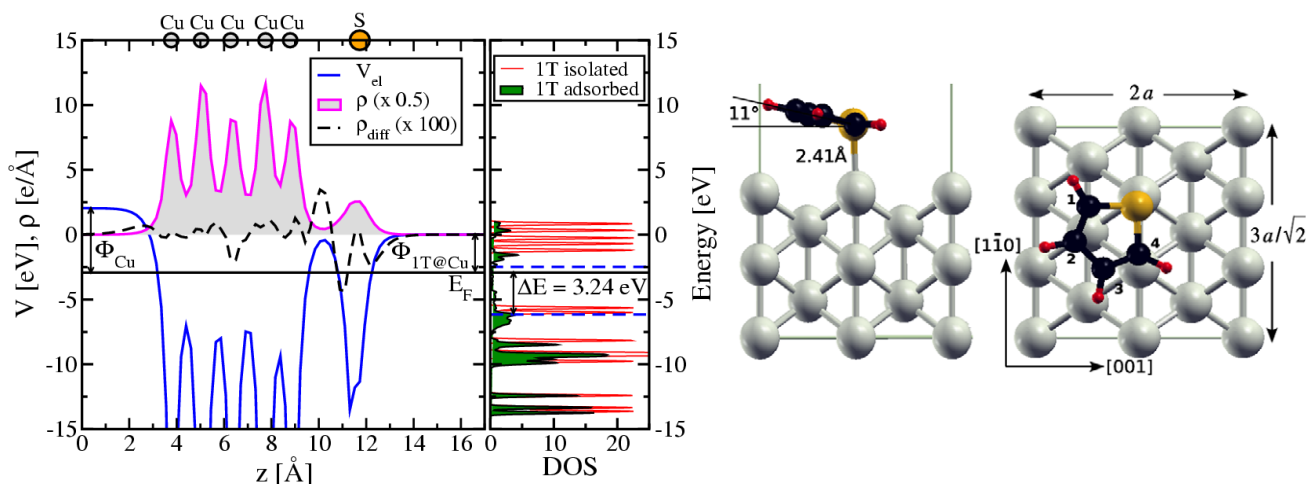
Figure 23. The calculated inner potential, charge-density profile and adsorbate-induced Kohn–Sham spectrum [75] (left). The adsorption structure (right) [75]. Reprinted with permission from [75]. Copyright 2008 by the American Physical Society.

Figure 24. Adenine–adenine interactions in vdW-DF [78] compared with wavefunction calculations. vdW-DF calculations between all other combinations [78] show comparable or better agreement with the MP2 calculation than what is shown in the comparison above.

Table 3. vdW-DF results for twist and rise in DNA [78].

	vdW-DF predictions	Nucleic acid database
Twist	$34° \pm 10°$	$36° \pm 7°$
Rise	3.5 ± 0.1 Å	3.3 ± 0.2 Å

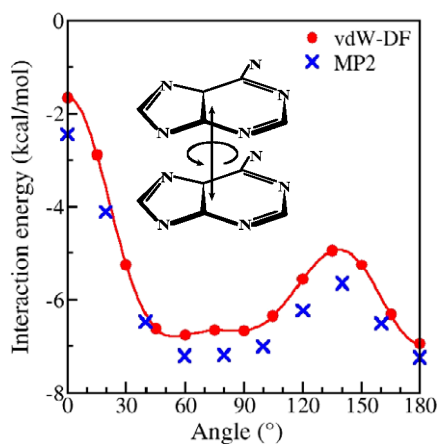phosphate backbone, with specific pairing of nucleic acids. vdW-DF has been used to show that the stacking interactions between the neighboring base pairs, caused to a large degree by the vdW or London dispersion interactions, play an important role in defining the twist and rise from one base pair to the next, even in the absence of the sugar phosphate backbone.

For the stacking interactions of individual bases, the results are in good agreement between vdW-DF and MP2 calculations [77, 78, 46]. This applies to adenine–adenine (figure 24), cytosine–cytosine, guanine–guanine. uracil–uracil, adenine–cytosine, adenine–guanine, adenine–uracil, cytosine–guanine, cytosine–uracil and guanine–uracil pairs. Thymine–thymine, thymine–adenine, thymine–cytosine, thymine–guanine and thymine–uracil pairs form a special group.

In applications to stacked DNA base-pair duplexes (figure 25), the vdW-DF does as well on the hydrogen bond as PBE [77] and compares well with high-level calculations. Stacked base pairs are beyond the limits of standard quantum-chemical methods, except by partitioning the system into smaller units. The stacking energy versus twist of the several base-pair duplexes shown below is not practical to obtain by any other method.

The vdW-DF calculated values of the twist and rise [78] have a good overlap with the experimental ones [82] (table 3). The $\pm$ signs do not represent errors, but are rather the standard deviations caused by different sequence dependences.

In comparison with the best quantum-chemical calculations the vdW-DF results come out well (figure 26). Note that the vdW-DF calculations appear more accurate than the force field with many fitted parameters.

significantly altered by the Alq3/Al interfacial dipole layer, for which quite a number of origins have been proposed. This interfacial dipole when Alq3 is adsorbed on Al has been studied using vdW-DF [76]. Although binding energies obtained by ordinary functionals give a poor description, the bonding configurations are found to have correct binding energies when the vdW-DF is included, and one obtains interface dipoles that agree reasonably well with experimental results, including a decreased surface workfunction [76].

5.5. DNA

To understand the structures and forces behind the genetic code is a true challenge. In the nucleic acids the base-pair stacking is of key importance, and in cancer treatment DNA intercalation has a central role.

A briefing on DNA certainly includes the double helix of nucleic acids, which happens to be right handed in B-DNA, and also mentions RNA. DNA and RNA are connected by a sugar

Figure 25. Typical vdW-DF stacking energy curves [78] for several base-pair duplexes of DNA are shown in the left panel. A couple are irregular, one of which is shown in the middle panel and illustrated in the right panel. The downward bump in the solid blue curve is caused by what appears to be an incipient hydrogen bond between the hydrogen of the methyl groups of thymine (T) with an unsaturated nitrogen on the adenines (A). In uracil (U), found in RNA instead of thymine, the methyl terminations are replaced by hydrogen ones, thus causing, as revealed by the dashed red curve, less binding and a partial rotational instability. The weakened binding in the RNA version is suggested by experiment [79–81].
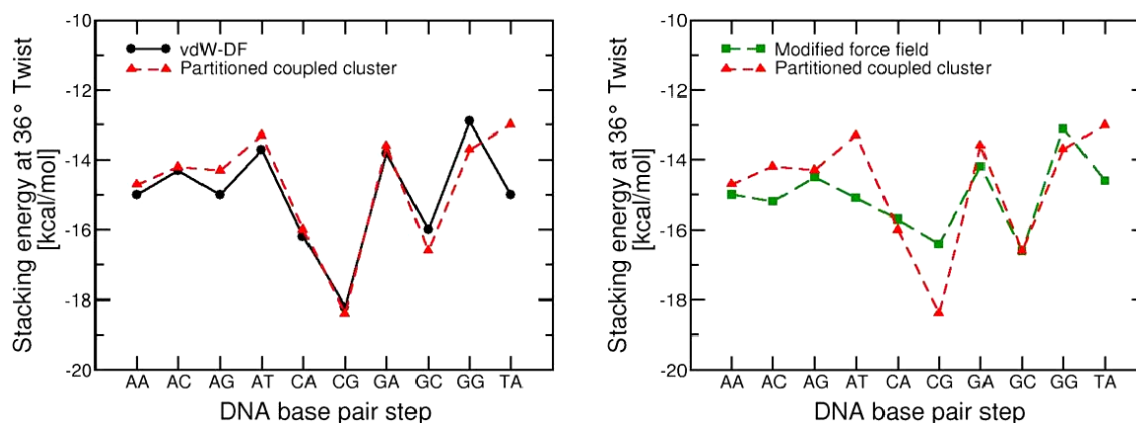
Figure 26. Comparison of vdW-DF results [78] with partitioned coupled cluster [83] (left) and Amber force field (modified [83] for better fit) with partitioned coupled cluster (right).

The DNA applications can be summed up as (i) vdW-DF gives good comparison with MP2 for stacked nucleic acids, (ii) it does not disturb the GGA's accurate description of the H-bond, (iii) it is able to easily model stacking interactions of base pairs and (iv) it is able to reveal insights related to the stabilizing effect of thymine within DNA. vdW-DF is thus an adequate and powerful method for modeling DNA.

5.6. DNA intercalators

DNA intercalators are molecules that find their way between the stacked base pairs in DNA. They are mostly flat and aromatic. Their usefulness lies in drug design and drug action, e.g. chemotherapy drugs against cancer. They also have roles as antibacterial agents and DNA dyes. An example of a DNA intercalator is proflavine (figure 27). The most stable form is charged.

The interaction of proflavine and GC and AT pairs has been studied with vdW-DF [84], and the interesting
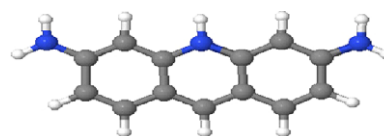
Figure 27. Proflavine, a DNA intercalator and an antibacterial agent. The intercalating form of proflavine has a single positive charge, which is spread out rather uniformly through the aromatic rings, rather than concentrated on the central nitrogen as might be suggested by simple bond counting [84].

results, like much smaller twist with proflavin present, might have biological consequences. This preference is observed experimentally in intercalators [85–88], specifically in proflavine [89], and it likely provides some impetus for the DNA to unwind enough to allow intercalation. It also has a stronger interaction with a neighboring base pair than they have with each other, perhaps a necessary condition for intercalation. The conclusion, that most binding comes from

dispersion, but that charge is necessary, e.g. for G:C to prefer proflavine over another G:C or C:G, is also interesting [84]. Qualitatively similar results were found for the three other combinations [84]. They all point at the vdW-DF method also being promising in this context.

6. Summary, conclusions and outlook

We have made an approximate DFT that includes van der Waals interactions (now also self-consistently). Correlation energy is divided into two pieces. The LDA is used to approximate the local-density piece. A simple dielectric function is used in the small nonlocal piece. A growing number of calculations on molecules and materials show that this vdW-DF has a useful accuracy.

The vdW-DF study is only in its beginnings. There are many more applications to do. The exchange functional, $E_x[n]$, calls for further studies. As the vdW interaction is out in the tails of orbitals, these need further study. The correlation functional, $E_c^{nl}[n]$, needs further study. Applications in molecular dynamics should be done.

The vdW-DF method shows promise to extend the broad successes of density-functional theory to new classes of matter. This is shown in several applications that cannot be done by any other nonempirical method.

Acknowledgments

References

[1] Rydberg H, Dion M, Jacobson N, Schröder E, Hyldgaard P, Simak S I, Langreth D C and Lundqvist B I 2003 *Phys. Rev. Lett.* **91** 126402
  Rydberg H, Jacobson N, Hyldgaard P, Simak S I, Lundqvist B I and Langreth D C 2003 *Surf. Sci.* **532** 606
[2] Dion M, Rydberg H, Schröder E, Langreth D C and Lundqvist B I 2004 *Phys. Rev. Lett.* **92** 246401
  Dion M, Rydberg H, Schröder E, Langreth D C and Lundqvist B I 2005 *Phys. Rev. Lett.* **95** 109902
[3] Thonhauser T, Cooper V R, Shen Li, Puzder A, Hyldgaard P and Langreth D C 2007 *Phys. Rev. B* **76** 125112
[4] Hohenberg P and Kohn W 1964 *Phys. Rev.* **136** B864
[5] Kohn W and Sham L J 1965 *Phys. Rev.* **140** A1133
[6] Lundqvist B I, Andersson Y, Shao H, Chan S and Langreth D C 1995 *Int. J. Quantum Chem.* **56** 247
[7] Gell-Mann M and Brueckner K A 1957 *Phys. Rev.* **106** 364
[8] Hedin L and Lundqvist B I 1971 *J. Phys. C: Solid State Phys.* **4** 2064
[9] von Barth U and Hedin L 1972 *J. Phys. C: Solid State Phys.* **5** 1629
[10] Gunnarsson O and Lundqvist B I 1976 *Phys. Rev. B* **13** 4274
[11] Ceperley D A and Alder B J 1980 *Phys. Rev. Lett.* **45** 566
[12] Ma S-K and Brueckner K A 1968 *Phys. Rev.* **165** 18
[13] Langreth D C and Mehl M J 1981 *Phys. Rev. Lett.* **47** 446
[14] Becke A D 1988 *Phys. Rev.* A **38** 3098
[15] Lee C, Yang Y and Parr R G 1988 *Phys. Rev. B* **37** 785
[16] Perdew J P, Chevary J A, Vosko S H, Jackson K A, Pederson M A, Singh D J and Fiolhais C 1992 *Phys. Rev. B* **46** 6671
[17] Becke A D 1993 *J. Chem. Phys.* **98** 5648
[18] Perdew J P, Burke K and Ernzerhof M 1996 *Phys. Rev. Lett.* **77** 3865
[19] Andersson Y, Langreth D C and Lundqvist B I 1996 *Phys. Rev. Lett.* **76** 1780
[20] Kohn W, Meir Y and Makarov D E 1998 *Phys. Rev. Lett.* **80** 4153
[21] Dobson J F and Wang J 1999 *Phys. Rev. Lett.* **82** 2123
[22] Langreth D C and Perdew J P 1975 *Solid State Commun.* **17** 1425
[23] Langreth D C and Perdew J P 1977 *Phys. Rev. B* **15** 2884
[24] Wu X, Vargas M C, Nayak S, Lotrich V and Scoles G 2001 *J. Chem. Phys.* **115** 8748
[25] Zhang Y and Yang W 1998 *Phys. Rev. Lett.* **80** 890
[26] Langreth D C, Dion M, Rydberg H, Schröder E, Hyldgaard P and Lundqvist B I 2005 *Int. J. Quantum Chem.* **101** 599
[27] Puzder A, Dion M and Langreth D C 2006 *J. Chem. Phys.* **126** 164105
[28] Vydrov O A, Wu Q and Van Voorhis T 2008 *J. Chem. Phys.* **129** 012106
[29] Dion M 2004 van der Waals forces in density functional theory *PhD Thesis* Rutgers University
[30] Li S, Cooper V R, Thonhauser T, Puzder A and Langreth D C 2008 *J. Phys. Chem.* A at press
[31] Chakarova-Käck S D, Kleis J and Schröder E 2008 private communication
[32] Thonhauser T, Puzder A and Langreth D C 2006 *J. Chem. Phys.* **126** 164106
[33] Feller D 1999 *J. Phys. Chem.* A **103** 7558
[34] Zhao Y, Tishchenko O and Truhlar D G 2005 *J. Phys. Chem.* B **109** 19046
[35] Jurecka P, Sponer J and Hobza P 2006 *Phys. Chem. Chem. Phys.* **8** 1985
[36] Hooper J, Cooper V C, Thonhauser T, Romero N A, Zerilli F and Langreth D C 2008 *ChemPhysChem* **9** 891
[37] Jacobson N, Tegner B, Schröder E, Hyldgaard P and Lundqvist B I 2002 *Comput. Mater. Sci.* **24** 373
[38] Hyldgaard P *et al* 2008 private communication
[39] Chakarova-Käck S D, Schröder E, Lundqvist B I, Cooper V R and Langreth D C 2008 private communication
[40] Ogilvie J and Wang F 1992 *J. Mol Struct.* **273** 277
[41] Chakarova-Käck S D 2006 Towards first-principles understanding of biomolecular adsorption *PhD Thesis* Chalmers University of Technology, Sweden
[42] Tsuzuki S, Honda K, Uchimaru T and Mikami M 2004 *J. Chem. Phys.* **120** 647
[43] Kleis J, Schröder E and Hyldgaard P 2008 *Phys. Rev.* B **77** 205422
[44] Sinnokrot M O and Sherrill C D 2004 *J. Am. Chem. Soc.* **126** 7690
[45] Chakarova-Käck S D, Schröder E, Lundqvist B I and Langreth D C 2006 *Phys. Rev. Lett.* **96** 146107
[46] Elstner M, Hobza P, Frauenheim T, Suhai S and Kaxiras E 2001 *J. Chem. Phys.* **114** 5149
[47] Cooper V C, Thonhauser T and Langreth D C 2008 *J. Chem. Phys.* **128** 204102
[48] Grimme S 2004 *J. Comput. Chem.* **25** 1463
[49] Grimme S, Anthony J, Schwabe T and Mück-Lichtenfeld C 2007 *Org. Biomol. Chem.* **5** 741
[50] Dobson J F, White A and Rubio A 2006 *Phys. Rev. Lett.* **96** 073201

[51] Benedict L X, Chopra N G, Cohen M L, Zettl A, Louie S G and Crespi V H 1998 *Chem. Phys. Lett.* **286** 490

[52] Zacharia R, Ulbricht H and Hertel T 2004 *Phys. Rev. B* **69** 155406

[53] Kleis J, Lundqvist B I, Langreth D C and Schröder E 2007 *Phys. Rev. B* **76** 100201

[54] Hyldgaard P *et al* 2008 private communication

[55] Ziambaras E, Kleis J, Schröder E and Hyldgaard P 2007 *Phys. Rev. B* **76** 155425

[56] Li J, Chabal Y and Langreth D C 2008 private communication

[57] Pan L, Sander M B, Huang X Y, Li J, Smith M, Bittner E, Bockrath B and Johnson J K 2004 *J. Am. Chem. Soc.* **126** 1308

[58] Lee J Y, Pan L, Kelly S R, Jagiello J, Emge T J and Li J 2005 *Adv. Mater.* **17** 2703

[59] Sagara T, Ortony J and Ganz E 2005 *J. Chem. Phys.* **123** 214707

[60] Johnston K, Kleis J, Lundqvist B I and Nieminen R M 2008 *Phys. Rev. B* **77** 121404

[61] Ortmann F, Schmidt W G and Bechstedt F 2005 *Phys. Rev. Lett.* **95** 186101

[62] Brooks F C 1952 *Phys. Rev.* **46** 92

[63] Halgren T A 1992 *J. Am. Chem. Soc.* **114** 7827
Elstner M, Hobza P, Frauenheim T, Suhai S and Kaxiras E 2001 *J. Chem. Phys.* **114** 5149
Wu Q and Yang W 2002 *J. Chem. Phys.* **116** 515
Hasegawa M and Nishidate K 2004 *Phys. Rev. B* **70** 205431
Zimmerli U, Parrinello M and Koumoutsakos P 2004 *J. Chem. Phys.* **120** 2693

[64] Chakarova-Käck S D, Borck Ø, Schröder E and Lundqvist B I 2006 *Phys. Rev. B* **74** 155402

[65] Delle Site L, Alavi A and Abrams A F 2003 *Phys. Rev. B* **67** 193406

[66] Kelkkanen A *et al* 2008 private communication

[67] Moses P G, Mortensen J J, Lundqvist B I and Nørskov J K 2008 private communication

[68] Salmeron M, Somorjai G A, Wold A, Chianelli R and Liang K S 1982 *Chem. Phys. Lett.* **90** 105

[69] Morikawa Y *et al* 2008 private communication

[70] Lee K 2008 private communication

[71] Morikawa Y, Ishii H and Seki K 2004 *Phys. Rev. B* **69** 041403

[72] Taplyakov A V, Gurevich A B, Yang M X, Bent B E and Chen J G 1998 *Surf. Sci.* **396** 340

[73] Wetterer S M, Lavrich D J, Cummings T, Bernasek S L and Scoles G 1998 *J. Phys. Chem. B* **102** 9266

[74] Weaver J F, Ikai M, Carlsson A and Madix R J 2001 *Surf. Sci.* **470** 226

[75] Sony P, Pusching P, Nabok D and Ambrosch-Draxl C 2008 *Phys. Rev. Lett.* **99** 176401

[76] Yanagisawa S, Lee K and Morikawa Y 2008 *J. Chem. Phys.* **128** 244704

[77] Cooper V R, Thonhauser T and Langreth D C 2008 *J. Chem. Phys.* **128** 204102

[78] Cooper V R, Thonhauser T, Puzder A, Schröder E, Lundqvist B I and Langreth D C 2008 *J. Am. Chem. Soc.* **130** 1304

[79] Ross P D and Howard F B 2003 *Biopolymers* **68** 210

[80] Howard F B 2005 *Biopolymers* **78** 221

[81] Soto A M, Rentzeperis D, Shikiya R, Alonso M and Marky L A 2006 *Biochemistry* **45** 3051

[82] Olson W K, Bansal M, Burley S K, Dickerson R E, Gerstein M, Harvey S C, Heinemann U, Lu X-J, Neidle S, Shakked Z, Sklenar H, Suzuki M, Tung C-S, Westhof E, Wolberger C and Berman H M 2001 *J. Mol. Biol.* **313** 229

[83] Šponer J, Jureka P, Marchan I, Luque F J, Orozco M and Hobza P 2006 *Chem. Eur. J.* **12** 2854

[84] Li S *et al* 2008 private communication

[85] Lerman L S 1961 *J. Mol. Biol.* **3** 18

[86] Bond P J, Landridge R, Jennette K W and Lippard S J 1975 *Proc. Natl Acad. Sci. USA* **72** 4825

[87] Shieh H-S, Berman H, Dabrow M and Neidle S 1980 *Nucleic Acids Res.* **8** 85

[88] Canals A, Purciolas M, Aymami J and Coll M 2005 *Acta Crystallogr.* D **61** 1009

[89] Schneider B, Ginell S L and Berman H 1992 *Biophys. J.* **63** 1572

Paper 2

A.K. Kelkkanen, B. I. Lundqvist, J.K. Nørskov,
Density functional for van der Waals forces accounts for hydrogen bond in benchmark set of water hexamers,

Density functional for van der Waals forces accounts for hydrogen bond in benchmark set of water hexamers

André K. Kelkkanen,[1] Bengt I. Lundqvist,[1,2,a)] and Jens K. Nørskov[1]

[1]*Department of Physics, Center for Atomic-Scale Materials Design, Technical University of Denmark, DK-2800 Kgs. Lyngby, Denmark*
[2]*Department of Applied Physics, Chalmers University of Technology, SE-41296 Göteborg, Sweden*

A recent extensive study[1] investigates how various exchange-correlation (XC) functionals treat hydrogen bonds (HBs) in water hexamers, a critical HB benchmark set. Accurate wave-function studies including perturbative (MP2),[1] quantum-Monte Carlo (DQMC),[1] and coupled-cluster [CCSD(T)] (Ref. 2) calculations agree on the relative energetics of the low-lying isomers:[1] The prism has lowest energy followed by (in order) cage, book, and cyclic isomers (Fig. 1). The study[1] shows that traditional generalized gradient approximation (GGA) and hybrid functionals used in density-functional theory (DFT) give the wrong dissociation-energy trend of the four isomers (Fig. 1) and that van der Waals (vdW) dispersion forces give key contributions to the dissociation energy and asks whether functionals that incorporate vdW forces implicitly into the XC functional predict the correct trend and yield accurate total dissociation-energy values.[1] Here an affirmative answer is given for the vdW-DF functional.[3]

Typically, a HB is an intermolecular bond between an intramolecular bond of an H atom on a donor molecule and an acceptor molecule. The directionality is the angle between these bonds. Studies on various HB-ed dimers suggest that vdW forces can have a significant effect on the strength of the HB, including an indicated directionality effect.[4] The DFT-local-density approximation (LDA) and DFT-GGAs also fail to describe highly bent HBs, another effect blamed on their lack of vdW account.[5]

For calculation of electronic structure and total energy, DFT offers an alternative to wave-function methods that is particularly powerful for extended systems, a well-proven excellent tool for strongly bound systems. For also abundant sparse systems that are bound by weak nonbonding forces, including HBs, nonlocal correlation functionals have been proposed recently. One such, the vdW-DF (Ref. 3) includes vdW forces in a seamless fashion with a derived XC functional,

$$E_{\text{vdW-DF}} = E_X^{\text{revPBE}} + E_C^{\text{LDA}} + E_C^{\text{nl}},\tag{1}$$

where

$$E_C^{\text{nl}} = \frac{1}{2}\int d^3r\,d^3r'\,n(\vec{r})\phi(\vec{r},\vec{r}')n(\vec{r}')\tag{2}$$

depends nonlocally on the density $n(\vec{r})$ with a general kernel ϕ derived from first principles.[3] Already used successfully for a wide spectrum of systems,[6] its virtues, e.g., biological molecules, are highlighted by its account of stacking and HB interactions between nucleobases[7] and DNA intercalation.[8] The vdW-DF describes vdW effects approximately[3,9] but differs significantly from another method doing so, DFT-D,[10] being derived from first principles and thus nonempirical and informing about the electron structure.

All calculations are made with the GPAW software.[11] The vdW-DF (Ref. 3) implementation is the same real-space method as in Ref. 14, which adds vdW forces perturbatively[3] to a self-consistent revPBE[15] calculation. The latter uses a well converged grid spacing of 0.13 Å and Eq. (2) is evaluated on a grid twice as dense (a grid spacing of 0.15 Å results in binding-energy differences smaller than 1%). The hexamer is in a cubic cell with side 18 Å and 35 electronic bands are used. The dissociation energy is calculated as in Ref. 1 but with the vdW-DF.

Figure 1 shows trends in dissociation-energy values of the water-hexamer isomers relative to the prism configuration. Even within the narrow energy scale, the trends in the results from wave-function methods [MP2 (Ref. 1), DQMC (Ref. 1), and CCSD(T) (Ref. 2)] are very distinct and close to each other and to earlier CCSD(T) results.[16] These trends cannot be accounted for by DFT with traditional GGA [PBE (Ref. 17), RPBE (Ref. 18), and revPBE (Ref. 15)] and hybrid [PBE0 (Ref. 13)] XC functionals.[1] Clearly, the vdW-DF and DFT-D methods give both the right stable configuration and the proper energetic order of the lowest isomers.

To follow a trend is not a sufficient criterion for a good XC functional. For instance, LDA gives trend but is ignored due to lack of basic nonlocal interactions and its known overestimate of dissociation of water clusters by more than 50%.[1,19] The vdW-DF dissociation-energy values of the low-lying isomers show an underbinding of about 50 meV/H_2O (Table I). At typical vdW separations (about 3–5 Å) the accuracy of vdW-DF might be about 0.01 eV,[14] but it is expected to be worse at the short separations of HBs (O–H separations being 1.9 Å in the water dimer[20] and, e.g., 1.7–2.0 Å in the water hexamer cage,[1] with vdW-DF and MP2 numbers given in Table I). The revPBE exchange functional[15] used in vdW-DF lies close to exact exchange [Hartree–Fock (HF)] results for, e.g., argon, krypton,[3] and benzene dimers[21] but gets repulsive at shorter separations,
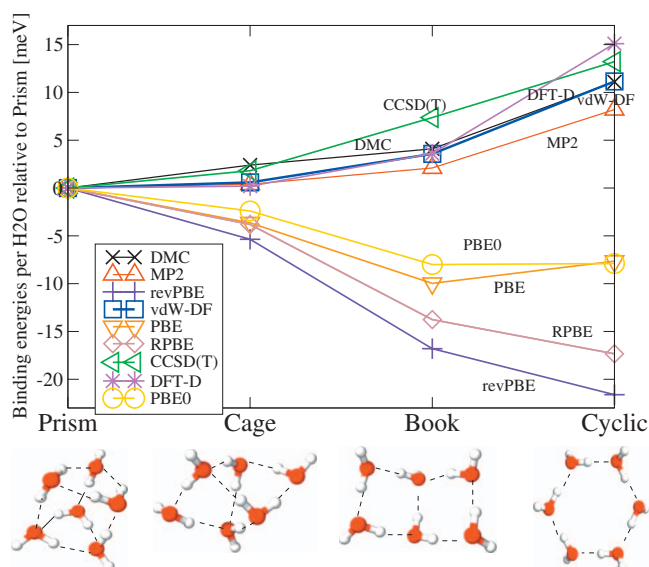
FIG. 1. Dissociation energy per H_2O molecule of the water hexamer in low-lying isomers shown below calculated with wave-function [MP2 (Ref. 1), DQMC (Ref. 1), and CCSD(T) (Ref. 2)] and DFT methods [with XC functionals in the PBE, RPBE, and revPBE flavors of GGA and in PBE0 (Ref. 1), DFT-D (Ref. 1), and vdW-DF] relative to the prism isomer.

FIG. 2. Exchange part of the dissociation energy for the water dimer at varying separations (defined by inset) with exact exchange (HF) calculated by the EXX(X) method (Ref. 12) and with DFT using PBE, RPBE, revPBE, and LDA XC functionals, each calculated self-consistently and then subtracting the correlation energy. LDA exchange is showed to illustrate its tendency to overbind. The nonself-consistent (PBE densities) exchange part of PBE0 is also included by mixing of PBE and EXX exchange as in Ref. 13.

where other flavors of GGA might be closer as for the water dimer (Fig. 2). The relatively small underbinding by use of other less repulsive exchange functionals such as PBE,[17] HF, and a hopefully soon developed systematically improved exchange functional. The latter should be accurate in regions where the HB applies and where vdW and covalent bonds have comparable strengths. Figure 2 shows that there is room for further stabilization for the hexamer. We believe that the relative error found for the water hexamer will translate to other more complex water clusters and that the vdW-DF could be expected to predict structure and phase diagrams of liquid water.

TABLE I. Calculated dissociation-energy values in meV/H_2O and shortest separations between hydrogen and oxygen atoms (R–O–H) of the low-lying water-hexamer isomers. Absolute-energy values E_{diss} calculated with the vdW-DF (Ref. 3) allows comparison with MP2 result (Ref. 1) (numbers in parentheses), and relative energy values $E_{reldiss}$ with results from a recent CCSD(T) calculation (Ref. 2) (numbers in square brackets).

	Prism	Cage	Book	Cyclic
E_{diss}	−280(−332)	−279(−332)	−277(−330)	−269(−324)
$E_{reldiss}$	0[0]	1[2]	4[7]	11[13]
R–O–H (Å)	1.8(1.7)	1.9(1.9)	1.8(1.8)	1.8(1.7)

a)Electronic mail: bengt.lundqvist@chalmers.se.

[1] B. Santra, A. Michaelides, M. Fuchs, A. Tkatchenko, C. Filippi, and M. Scheffler, J. Chem. Phys. **129**, 194111 (2008).

[2] D. Bates and G. Tschumper, J. Phys. Chem. A **113**, 3555 (2009).

[3] M. Dion, H. Rydberg, E. Schröder, D. C. Langreth, and B. I. Lundqvist, Phys. Rev. Lett. **92**, 246401 (2004).

[4] T. Steiner and G. R. Desiraju, Chem. Commun. (Cambridge) **8**, 891 (1998).

[5] J. N. Ireta and M. Scheffler, J. Phys. Chem. A **108**, 5692 (2004).

[6] D. C. Langreth, B. I. Lundqvist, S. D. Chakarova-Kack, V. R. Cooper, M. Dion, P. Hyldgaard, A. Kelkkanen, J. Kleis, L. Kong, S. Li, P. G. Moses, E. Murray, A. Puzder, H. Rydberg, E. Schröder, and T. Thonhauser, J. Phys.: Condens. Matter **21**, 084203 (2009).

[7] V. R. Cooper, T. Thonhauser, A. Puzder, E. Schröder, B. I. Lundqvist, and D. C. Langreth, J. Am. Chem. Soc. **130**, 1304 (2008); V. R. Cooper, T. Thonhauser, and D. C. Langreth, J. Chem. Phys. **128**, 204102 (2008).

[8] S. Li, V. R. Cooper, T. Thonhauser, B. I. Lundqvist, and D. C. Langreth, "Stacking interactions and DNA intercalation," J. Phys. Chem. B (in press).

[9] T. Thonhauser, V. R. Cooper, S. Li, A. Puzder, P. Hyldgaard, and D. C. Langreth, Phys. Rev. B **76**, 125112 (2007).

[10] S. Grimme, J. Comput. Chem. **25**, 1463 (2004).

[11] J. J. Mortensen, L. B. Hansen, and K. W. Jacobsen, Phys. Rev. B **71**, 035109 (2005).

[12] M. Stadele, M. Moukara, J. Majewski, P. Vogl, and A. Görling, Phys. Rev. B **59**, 10031 (1999).

[13] C. Adamo and V. Barone, J. Chem. Phys. **110**, 6158 (1999).

[14] P. G. Moses, J. J. Mortensen, B. I. Lundqvist, and J. K. Nørskov, J. Chem. Phys. **130**, 104709 (2009).

[15] Y. Zhang and W. Yang, Phys. Rev. Lett. **80**, 890 (1998).

[16] R. M. Olson, J. L. Bentz, R. A. Kendall, M. W. Schmidt, and M. S. Gordon, J. Chem. Theory Comput. **3**, 1312 (2007).

[17] J. P. Perdew, K. Burke, and M. Ernzerhof, Phys. Rev. Lett. **77**, 3865 (1996).

[18] B. Hammer, L. B. Hansen, and J. K. Nørskov, Phys. Rev. B **59**, 7413 (1999).

[19] C. Lee, H. Chen, and G. Fitzgerald, J. Chem. Phys. **101**, 4472 (1994).

[20] T. Taketsugu and D. J. Wales, Mol. Phys. **100**, 2793 (2002).

[21] A. Puzder, M. Dion, and D. C. Langreth, J. Chem. Phys. **124**, 164105 (2006).

Paper 3

ORIGINAL PAPER

RPBE-vdW Description of Benzene Adsorption on Au(111)

Jess Wellendorff · André Kelkkanen ·
Jens Jørgen Mortensen · Bengt I. Lundqvist ·
Thomas Bligaard

Abstract Density functional theory has become a popular methodology for the analysis of molecular adsorption on surfaces. Despite this popularity, there exist adsorption systems for which commonly used exchange–correlation functionals fail miserably. Particularly those systems where binding is due to van der Waals interactions. The adsorption of benzene on Au(111) is an often mentioned such system where standard density functionals predict a very weak adsorption or even a repulsion, whereas a significant adsorption is observed experimentally. We show that a considerable improvement in the description of the adsorption of benzene on Au(111) is obtained when using the so-called RPBE-vdW functional.

Keywords Benzene · Au(111) · Van der Waals · RPBE-vdW · Density functional theory

1 Introduction

The adsorption of aromatic molecules on transition metal surfaces is a topic of great interest in surface science. Understanding the interactions of an aromatic adsorbate with a metallic surface also has important industrial applications. Catalytic conversion of aromatic compounds

J. Wellendorff · A. Kelkkanen · J. J. Mortensen ·
B. I. Lundqvist · T. Bligaard (✉)
Department of Physics, Center for Atomic-Scale Materials
Design (CAMD), Technical University of Denmark,
Building 307, 2800 Kgs. Lyngby, Denmark
e-mail: bligaard@fysik.dtu.dk

J. Wellendorff · T. Bligaard
Materials Sciences Division, Lawrence Berkeley National
Laboratory, Berkeley, CA 94720, USA

is a key reaction in many petrochemical processes [1, 2] and has been studied experimentally for decades [3].

Benzene is the smallest aromatic molecule, and the close-packed (111) surface of gold is among the least reactive surfaces known. For coverages up to one mono-layer (ML) of benzene on Au(111) there appears to be a general consensus that benzene adsorbs with its molecular plane parallel to the surface in a physisorbed state from which it can desorb reversibly [4, 5]. The physisorption is believed to be mediated by dispersive van der Waals (vdW) interactions. Contrary to the case of adsorption of benzene on the much more reactive Pt(111) surface, Wöll and co-workers [4, 6] observed no non-planar benzene distortion (bending of C–H bonds) in near edge X-ray absorption fine structure (NEXAFS) studies of benzene monolayers physisorbed on Au(111). From temperature programmed desorption (TPD) experiments, Koel and co-workers [5] used a desorption peak temperature of 239 K to estimate the desorption energy of physisorbed benzene on Au(111) to 0.64 eV (14.7 kcal/mol) at a sub-monolayer coverage.

Theoretical first principles calculations have also been applied to the benzene/Au(111) interaction. Indeed, density functional theory (DFT) using exchange and correlation (xc) functionals within the generalized gradient approximation (GGA) has well proven its usefulness for describing many strongly interacting systems [7] also with respect to adsorption on transition and noble metal surfaces [8, 9] where in particular the RPBE xc-functional [10] has proven useful. However, when the adsorbate-substrate interaction is dominated by van der Waals interactions, the GGA-level of theory proves insufficient for calculating adsorption energies [11, 12]. This is clearly exemplified in a recent DFT study [13] of benzene adsorbed on (111) surfaces of Cu, Ag, and Au. At all three surfaces the binding energy was dramatically underestimated and often fell below the

anticipated accuracy of the methodology itself. Even though other qualitative features of experimental results were reproduced by the calculations, the largest calculated adsorption energy of benzene on Au(111) was −0.08 eV (−1.92 kcal/mol). Insufficient description of the correlation effects responsible for vdW interactions was the reason for this. Similar conclusions were drawn from another recent GGA-DFT study of benzene/Au(111) interactions [14]. These authors furthermore concluded that GGA-DFT is well-suited for describing the ground state electronic structure of closed-shell molecules such as benzene on metallic surfaces, but that the adsorption structure (e.g., equilibrium adsorbate-metal distance) not necessarily is correctly captured due to the absence of van der Waals interactions in the calculations.

Ab initio MP2 calculations have been applied with some success to describe the vdW-interactions between benzene and Au(111). In recent MP2 calculations benzene adsorption on the (111) surfaces of Cu, Ag, and Au was considered [15]. The calculated adsorption energy for the Au(111) surface of −0.31 eV at an equilibrium benzene–metal distance of 3.6 Å was somewhat weaker than the experimental value of −0.6 eV reported in the same study.

A density functional that includes the nonlocal correlation effects responsible for van der Waals interactions has recently been developed [16]. This van der Waals density functional (vdW-DF) describes the exchange and correlation energy as a sum of GGA exchange and a correlation term consisting of both local correlation (evaluated in the local density approximation) and nonlocal correlation (depending nonlocally on the electron density) [17]:

$$E_{xc}[n] = E_x^{GGA}[n] + E_c^0[n] + E_c^{nl}[n] \qquad (1)$$

The nonlocal correlation term is expressed as

$$E_c^{nl}[n] = \frac{1}{2} \int d\vec{r}_1 d\vec{r}_2 n(\vec{r}_1) \phi(q_1, q_2, r_{12}) n(\vec{r}_2) \qquad (2)$$

where ϕ is the vdW-DF kernel, $r_{12} = |\vec{r}_1 - \vec{r}_2|$ and q_1 and q_2 are the values of a universal function $q_0\left(n(\vec{r}), \left|\vec{\nabla} n(\vec{r})\right|\right)$ evaluated at the two points $\vec{r}_1$ and $\vec{r}_2$. The vdW-DF has recently been used to treat a number of diverse systems such as, e.g., layered structures, dimers, adsorbed molecules, carbon nanotubes, metal organic frameworks, and DNA with promising results [17]. In this study we use RPBE [10] exchange for the GGA exchange term in the vdW-DF. This approximation was called RPBE-vdW in Ref. [18], where it was also shown to give adsorption-energy values that deviate only about 0.04 eV from the vdW-DF values for a number of different cyclic molecules adsorbed on the basal plane of MoS_2.

In the present study we use first principles DFT calculations with the RPBE-vdW functional to calculate the adsorption energy of benzene on the Au(111) surface.

2 Computational Methods

We used the grid-based real-space code GPAW [19] for all the reported calculations. It is an implementation of the projector augmented wave (PAW) method of Blöchl [20], which is an all-electron full-potential method within the frozen core approximation. The Atomic Simulation Environment (ASE) [21] provided an interface to GPAW. Wave functions, electron densities and potentials are represented on grids in real space and a grid spacing of 0.20 Å was used in all directions of the supercell. Brillouin-zone integrations were performed using a $4 \times 4 \times 1$ Monkhorst–Pack grid [22] and a Fermi smearing of 0.1 eV, and Pulay density mixing [23] was used.

All RPBE-vdW calculations were done non self-consistently; the RPBE xc-functional was used to obtain self-consistent GGA electron densities where after the vdW-DF scheme of Eq. 1 was applied to those densities as a post-GGA correction using RPBE exchange. The inclusion of vdW interactions in DFT calculations in other studies have shown to modify the total energy significantly without appreciably affecting the self-consistent electronic structure itself [13, 14, 24, 25]. Therefore, we assume that performing geometry optimizations within RPBE and *a posteriori* applying the RPBE-vdW to the density to be a reasonably reliable procedure for obtaining total energies. Evaluation of $E_c^{nl}[n]$ (Eq. 2) by direct summation in real space has an operation count that scales as N^2 for system size N, which turned out to require computation times of about 50% of those required for self-consistent RPBE calculations. Instead, we have implemented the fast Fourier transformation (FFT) evaluation technique introduced by Román-Pérez and Soler [26] where the scaling is $N \log N$. We have used 20 interpolation points, q_α, distributed between zero and $q_c = 5.0$ according to the formula $(q_{\alpha+1} - q_\alpha) = \lambda(q_\alpha - q_{\alpha-1})$ with $\lambda = 1.2$. The logarithmic divergence of the vdW-DF kernel ϕ is cut off smoothly at $r_{12}\left(q_1^2 + q_2^2\right)^{1/2} < 1.0$ with $\phi(q_1, q_2, 0)$ set to 0.5. For more details, see Ref. [26]. With the non self-consistent FFT evaluation of the vdW-DF parallelized over the 20 interpolation points, we typically find that the required computational time amounts to 0.5% of that required for a self-consistent RPBE calculation, thus becoming insignificant.

The three model systems treated in this study are (1) benzene adsorbed on the Au(111) surface [C_6H_6/Au(111)], (2) the Au(111) surface before adsorption [Au(111)] and (3) gas phase benzene [C_6H_6]. The extended Au(111) surface was modeled by an orthorhombic supercell with 16 atoms per metal layer. The surface lattice cell was repeated periodically in the surface plane to create an infinite slab, while non-periodic boundary conditions were employed in the direction perpendicular to the slab. The benzene molecule was added parallel to the surface with the center of
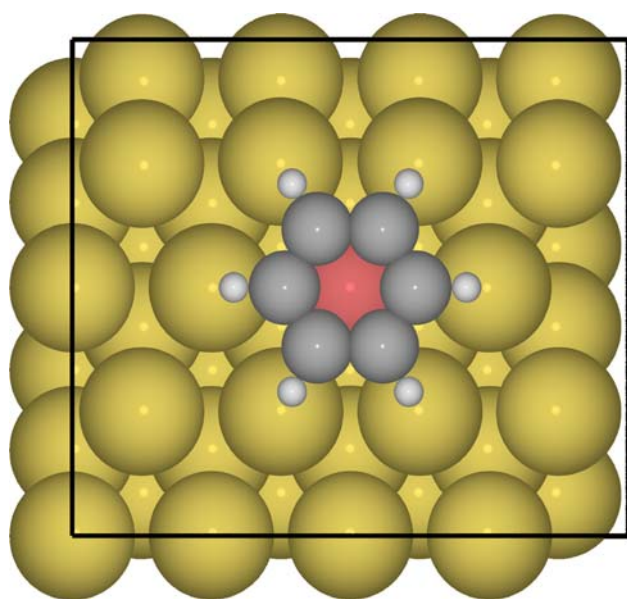
Fig. 1 Top-view of benzene adsorption over a central gold atom (in red) in the 16-metal atom rectangular surface cell

the C_6 ring at an on-top site directly above a central Au atom. A schematic top-view of this adsorption geometry is depicted in Fig. 1.

All geometry relaxation was done by minimizing the Hellmann–Feynman forces using the RPBE xc-functional. The two top layers of the Au(111) slab were allowed to relax freely while the bottom layers further from the surface were fixed at the bulk Au lattice constant of 4.21 Å, likewise determined within RPBE. With the parallel-oriented benzene placed 3.65 Å above the (111) surface the adsorption system was relaxed while constraining the benzene atoms to only relax in the plane parallel to the surface. Experimental [4, 6] and theoretical [14] studies have shown that the non-planar distortions of the benzene molecule upon adsorption on Au(111) are negligible. The van der Waals interaction responsible for physisorption is not expected to depend significantly on the adsorption geometry and theoretical studies of benzene adsorption on coinage metals often consider this completely planar benzene geometry in the on-top adsorption site [15, 27, 28]. Defining the benzene–Au(111) separation as the distance between the center of the aromatic ring and the top-layer Au atom residing exactly beneath the center of the C_6 ring unambiguously defines the molecule-surface distance. Gas phase benzene was fully relaxed in a non-repeated cell with more than 6 Å vacuum to the cell boundaries. This determined the equilibrium geometry of gas phase benzene to be completely planar with bond lengths of 1.404 Å and 1.092 Å for C–C and C–H bonds, respectively.

The finite grid spacing in real-space DFT calculations leads to the so-called egg-box effect where the total energy

of a system depends on the positions of all atoms in the system relative to the grid points [29]. The effect can be reduced by reducing the grid spacing. However, since each atom in the system may introduce an egg-box error upon translation of all atoms in the supercell, the sum of egg-box errors may be significant when large systems are considered. Care was taken to avoid sources of numerical errors from egg-box effects in all calculations. As adsorption energies are calculated from comparison of the total energies of the C_6H_6/Au(111), Au(111) and C_6H_6 model systems, egg-box effects were minimized within each adsorption energy by, as far as possible, positioning the atoms in corresponding model systems in identical positions relative to the 3D real-space mesh.

3 Results and Discussion

In order to enable high accuracy and reliability in calculating the benzene adsorption energy on Au(111) care was taken to ensure the reliability of the employed model systems.

In DFT slab calculations with non-periodic boundary conditions perpendicular to the surface plane the electronic structure is forced to extinction at the supercell boundaries above and below the slab. It is therefore important to use vacuum layers thick enough to eliminate the risk of artificial quenching of the self-consistent electron density in both directions. The benzene adsorption energy, E_{ads}, we define as

$$E_{ads} = E_{tot}^{C_6H_6/Au(111)} - E_{tot}^{Au(111)} - E_{tot}^{C_6H_6} \qquad (3)$$

such that $E_{ads} < 0$ corresponds to bonding. In Fig. 2 is shown the convergence of the calculated adsorption energy of benzene on Au(111) as the vacuum layer above and below the adsorption and the slab system is increased. The computations were done by first relaxing the C_6H_6/Au(111) model system with benzene initially placed in the on-top site 3.65 Å above the Au(111) surface. Vacuum layers of 6.33 Å were used above the C_6H_6 adsorbate and below the Au slab. Minor geometry changes were observed for the two top metal layers while the benzene did not relax its bond lengths at all. The central gold atom (colored red in Fig. 1) moved 0.04 Å towards the surface upon relaxation, causing the equilibrium benzene–metal distance to be 3.69 Å. The equilibrium geometry of the Au(111) surface before adsorption was determined by removing the benzene molecule from the supercell of the relaxed C_6H_6/Au(111) system and relaxing the bare surface. Self-consistent RPBE adsorption energies for these geometries were then obtained using different vacuum layer thicknesses and the corresponding RPBE-vdW adsorption energies were
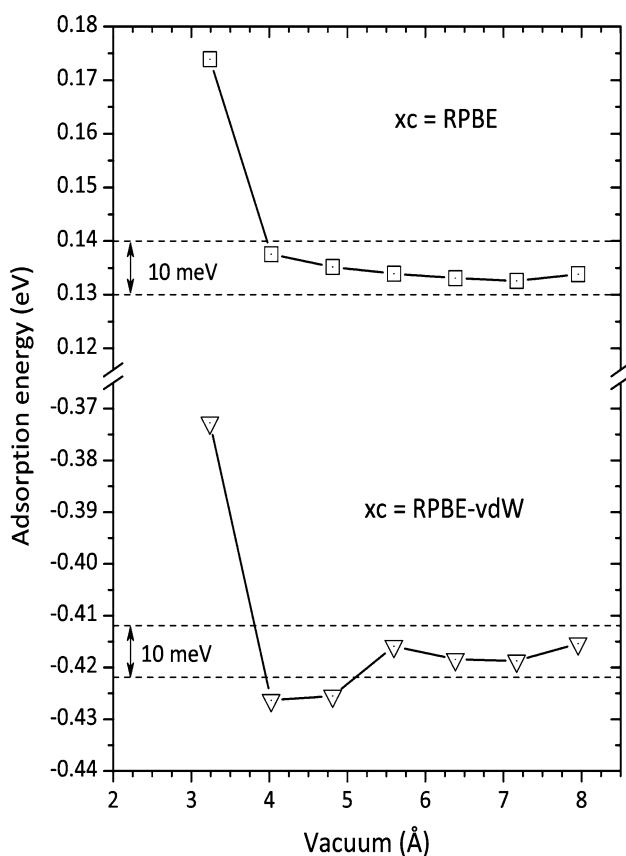
Fig. 2 Convergence of the RPBE and RPBE-vdW adsorption energy of benzene in the on-top site of Au(111) as the vacuum layers employed in the supercell are enlarged. For any vacuum layer >6 Å above and below the adsorption system the adsorption energy is converged to within 10 meV

computed. We see from Fig. 2 that both the RPBE and the RPBE-vdW adsorption energy are converged to within 10 meV for vacuum layers exceeding 6 Å above and below the system. RPBE repulsion of 0.13 eV was derived for the three-layer Au(111) slab while E_{ads} turned out exothermic by -0.42 eV within the RPBE-vdW.

To investigate the dependence of E_{ads} on the number of metal layers in the Au(111) slab we calculated the benzene adsorption energy for slabs containing up to ten Au layers (160 Au atoms in total). The geometries of the top-two metal layers in the C_6H_6/Au(111) and Au(111) model systems were taken from those previously found for three metal layers while the remaining layers were kept in their bulk geometry. The vacuum layers above and below the systems were at least 6.33 Å (with small variations introduced by the constant grid spacing).

The results are shown in Fig. 3 where the calculated benzene adsorption energies on Au(111) are plotted against the number of metal layers in the slab. Over the range of 3–10 metal layers both the RPBE and the RPBE-vdW adsorption energy fall within a 20 meV energy window.
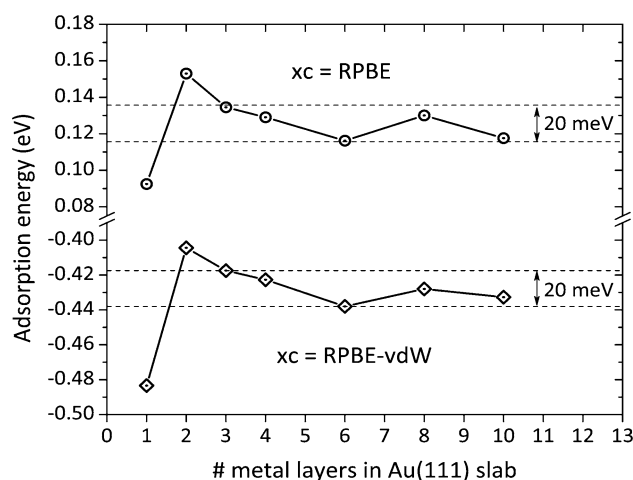
Fig. 3 Convergence of the RPBE and RPBE-vdW adsorption energy of benzene as the number of metal layers in the slab is increased from one through ten. For slabs comprised of three or more Au layers the calculated adsorption energies fall within a 20 meV energy window

Calculations using the three-layer Au(111) slab therefore capture the RPBE-vdW benzene/Au(111) interactions well.

Having established that closed-boundary DFT calculations with vacuum layers exceeding 6 Å above and below the three-metal-layer benzene/Au(111) adsorption system yields converged adsorption energies we calculated the benzene adsorption energy on the (111) surface plane of Au for a range of benzene–metal distances. Adsorption distances, d, in the range 0.75–6.05 Å were considered for the three-layer Au(111) substrate. While only varying the benzene–metal distance we kept the model system and supercell geometries fixed for calculation of E_{ads} for each d. To ensure computational accuracy over this range of separations a slightly enlarged supercell in the direction perpendicular to the surface plane was used. This implies that the vacuum layers above and below the adsorption system exceeded 6 Å for the case of the largest benzene–metal separation, $d = 6.05$ Å. With this enlarged supercell the previously determined equilibrium geometry of the C_6H_6/Au(111) model system with $d = 3.69$ Å yielded no relaxation. The geometries of the Au(111) and C_6H_6 reference model systems were determined by relaxation after removing the adsorbate and substrate from the enlarged supercell, respectively, as described above. This led to no relaxation of the bond lengths in gas phase benzene. The only atoms moving in the supercell when changing d were those of the C_6H_6 adsorbate.

The calculated RPBE-vdW adsorption energies are plotted against the benzene–Au(111) distance in Fig. 4. The bottom of a van der Waals type potential energy curve is mapped out. The minimum of the binding energy curve is found at $d = 3.7$ Å, making this the calculated equilibrium adsorption distance of benzene on the Au(111) surface when van der Waals interactions are taken into
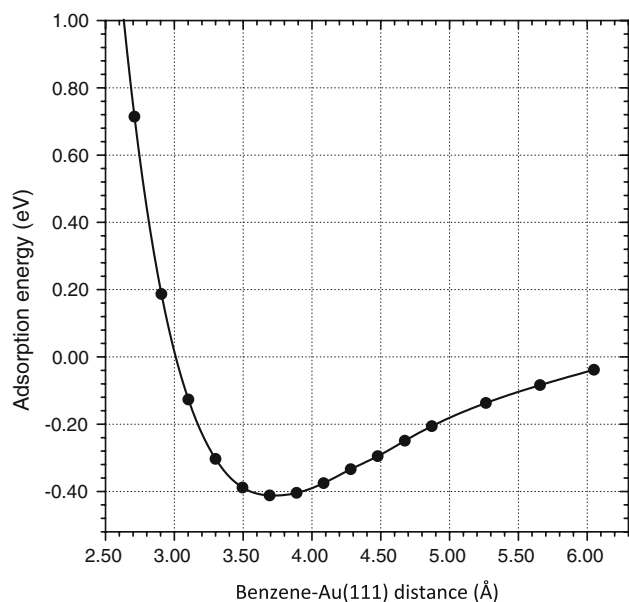
Fig. 4 RPBE-vdW binding energy curve for benzene adsorption on Au(111). The largest adsorption energy of -0.42 eV is obtained at the equilibrium benzene–Au(111) distance of 3.7 Å

account. The corresponding adsorption energy for the parallel-oriented C_6H_6 on Au(111) is -0.42 eV. To our knowledge, this is the first electronic structure study of benzene on Au(111) reporting an adsorption energy this close to the experimental data available, appearing to agree on C_6H_6/Au(111) adsorption energies of ~ 0.6 eV. Also, the equilibrium binding energy obtained in the present study of benzene adsorption in the on-top site on Au(111) is an order of magnitude larger than that obtained for the same adsorption site in a recent GGA-DFT study of C_6H_6/Au(111) interface interactions [13]. The inclusion of dispersive interactions by using the RPBE-vdW is clearly seen from Figs. 2 and 3 to be the reason for this significant improvement; with RPBE-vdW corrections the adsorption energies are shifted down into the region of bonding. Furthermore, the van der Waals type binding energy curve in Fig. 4 shows that dispersive interactions are indeed important in benzene adsorption on Au(111). The calculated adsorption distance of 3.7 Å is similar to those found in MP2 calculations for benzene on the (111) surfaces of Au, Ag and Cu [15] and to DFT calculations using the vdW-DF of benzene adsorption on graphene [24] and on the basal plane of MoS_2 [18].

4 Conclusions

The experimentally observed temperature programmed desorption spectra for benzene on Au(111), combined with Redhead analysis, indicate a desorption energy of 0.64 eV

for benzene on Au(111) [5]. Such TPD/Redhead experiments have some inherent uncertainty. It is certain from these experiments and standard density functional calculations, however, that GGA density functional theory significantly underestimates the adsorption energy of benzene on Au(111). Our fast implementation of the vdW-DF nonlocal correlation functional enables us to obtain a significantly improved adsorption energy for the purely van der Waals bonded benzene on Au(111) system. The improvement is comparable to the improvements observed using the computationally more expensive correlated electron method MP2, but is achievable at essentially no additional cost. It can also be applied to much larger systems than MP2, which we illustrate by applying the method to systems with up to 160 gold atoms.

References

1. Somorjai GA (1981) Chemistry in two dimensions: surfaces. Cornell University Press, Ithaca, NY
2. Stanislaus A, Cooper BH (1994) Catal Rev Sci Eng 36:75
3. Somorjai GA (1994) Introduction to surface chemistry and catalysis. Wiley–Interscience, New York
4. Wöll C (2001) J Synchrotron Radiat 8:129
5. Syomin D, Kim J, Ellison G, Koel E (2001) J Phys Chem B 105:8387
6. Weiss K, Gebert S, Wün M, Wadepohl H, Wöll C (1998) J Vac Sci Technol A 16:1017
7. Kohn W, Becke AD, Parr RG (1996) J Phys Chem 100:12974
8. Neurock M (2003) J Catal 216:73
9. Nørskov JK, Bligaard T, Rossmeisl J, Christensen CH (2009) Nature Chem 1:37
10. Hammer B, Hansen LB, Nørskov JK (1999) Phys Rev B 59:7413
11. Kristyán S, Pulay P (1994) Chem Phys Lett 229:175
12. Wu X, Vargas MC, Nayak S, Lotrich V, Scoles G (2001) J Chem Phys 115:8748
13. Bilić A, Reimers JR, Hush NS, Hoft RC, Ford MJ (2006) J Chem Theory Comput 2:1093
14. Schuster C, Schwingenschlögl U (2009) Chem Phys Lett 468:75
15. Caputo R, Prascher BP, Staemmler V, Bagus PS, Wöll C (2007) J Phys Chem A 111:12778
16. Dion M, Rydberg H, Schröder E, Langreth DC, Lundqvist BI (2004) Phys Rev Lett 92:246401
17. Langreth DC, Lundqvist BI, Chakarova-Käck SD, Cooper VR, Dion M, Hyldegaard P, Kelkkanen A, Kleis J, Kong L, Li S, Moses PG, Murray E, Puzder A, Rydberg H, Schröder E, Thonhauser T (2009) J Phys: Condens Matter 21:084203
18. Moses PG, Mortensen JJ, Lundqvist BI, Nørskov JK (2009) J Chem Phys 130:104709
19. Mortensen JJ, Hansen LB, Jacobsen KW (2005) Phys Rev B 71:035109

20. Blöchl PE (1994) Phys Rev B 50:17953
21. Bahn S, Jacobsen KW (2002) Comput Sci Eng 4:56
22. Monkhorst HJ, Pack JD (1976) Phys Rev B 13:5188
23. Pulay P (1980) Chem Phys Lett 73:393
24. Chakarova-Käck SD, Schröder E, Lundqvist BI, Langreth DC (2006) Phys Rev Lett 96:146107
25. Johnston K, Kleis J, Lundqvist BI, Nieminen RM (2008) Phys. Rev B 77:121404(R)
26. Román-Pérez G, Soler JM (2009) Phys Rev Lett 103:096102
27. Witte G, Lukas S, Bagus PS, Wöll C (2005) Appl Phys Lett 87:263502
28. Bagus PS, Hermann L, Wöll C (2005) J Chem Phys 123:184109
29. Nogueira F, Castro A, Marques MAL (2003) In: Fiolhais C, Nogueira F, Marques MAL (eds) A primer in density functional theory. Springer, Heidelberg

Paper 4

M. Vanin, J. J. Mortensen, A. K. Kelkkanen, J. M. Garcia-Lastra, K. S. Thygesen
and K. W. Jacobsen,
Graphene on metals: A van der Waals density functional study,

Graphene on metals: A van der Waals density functional study

M. Vanin, J. J. Mortensen, A. K. Kelkkanen, J. M. Garcia-Lastra, K. S. Thygesen, and K. W. Jacobsen

Center for Atomic-Scale Materials Design, Department of Physics, Technical University of Denmark,

DK-2800 Kongens Lyngby, Denmark

We use density functional theory (DFT) with a recently developed van der Waals density functional (vdW-DF) to study the adsorption of graphene on Co, Ni, Pd, Ag, Au, Cu, Pt, and Al(111) surfaces. In contrast to the local-density approximation (LDA) which predicts relatively strong binding for Ni,Co, and Pd, the vdW-DF predicts weak binding for all metals and metal-graphene distances in the range 3.40–3.72 Å. At these distances the graphene band structure as calculated with DFT and the many-body G_0W_0 method is basically unaffected by the substrate, in particular there is no opening of a band gap at the K point.

The recently reported synthesis of graphene,[1] a single layer of graphite, on top of a SiO_2 substrate has renewed the interest for this unique material. The uniqueness of this two-dimensional (2D) crystal is mainly due to its very peculiar band structure, with the π and π^* bands showing linear dispersion around the Fermi level where they touch in a single point. The great variety of physics and chemistry which derives from this electronic structure makes graphene very attractive for a range of applications. In particular, its high stability and good conductivity under ambient conditions makes it an interesting candidate for future nanoscale electronics.[2] In this perspective, the interaction of graphene with metallic contacts plays a fundamental role. Moreover, catalytic growth of graphene on transition metal surfaces from carbon containing gases has become a standard way to obtain high quality graphene samples.[3–6] Nevertheless the nature of the metal-graphene chemical bond is still not well understood.[3]

The widely used density functional theory (DFT) with local and semilocal functionals for exchange and correlation usually provides an accurate description of covalent and ionic chemical bonds. On the other hand it fails to reproduce nonlocal dispersive forces, in particular van der Waals forces, which are important in weakly bonded materials such as graphite, molecular crystals, and many organic compounds.[7–9] It is also well known that the local-density approximation (LDA) tends to overbind systems where van der Waals interactions are important, while the generalized gradient approximations (GGAs) usually tend to underestimate the binding in these systems. In the case of graphene on metals many GGAs, contrary to experiments, predict no binding at all, and therefore most theoretical work on graphene-metal interfaces has relied on the LDA. In view of the fact that LDA in general cannot be considered a reliable approximation in nonhomogeneous systems such as surfaces and molecules, the graphene-metal interface clearly calls for new and improved functionals.

The interaction of graphene with the (111) surfaces of Co, Ni, Pd, Ag, Au, Cu, Pt, and Al was studied in Ref. 10 using the LDA approximation. The LDA results divide the metals into two classes: Co, Ni, and Pd which bind graphene strongly and Ag, Au, Cu, Pt, and Al which bind graphene weakly. In contrast the Perdew-Burke-Ernzerhof (PBE) approximation (Ref. 11) gives no binding of graphene at room

temperature.[12] This remarkable disagreement between the two most commonly used approximations of DFT might be related to the incorrect description of dispersion interactions in both of the functionals.

In this Rapid Communication we use the recently developed van der Waals density functional (vdW-DF) (Refs. 13 and 14) to investigate the nature of the bonding at the metal-graphene interface. The functional is explicitly constructed to include nonlocal dispersion interactions and has proved successful in several cases where standard functionals fail, such as rare gases,[13] benzene dimers,[15,16] graphite,[17] polymers,[18] DNA,[19] and organic molecules on surfaces.[20–22] Within the vdW-DF approximation, the exchange-correlation energy is

$$E_{xc}^{\text{vdW-DF}} = E_x^{\text{revPBE}} + E_c^{\text{LDA}} + E_c^{\text{nl}}, \qquad (1)$$

where E_x^{revPBE} is the revPBE (Ref. 23) exchange energy, E_c^{LDA} is the LDA correlation energy, and E_c^{nl} is the nonlocal correction given by

$$E_c^{\text{nl}} = \frac{1}{2} \int \int n(\mathbf{r}_1) n(\mathbf{r}_2) \phi(q_1, q_2, r_{12}) d\mathbf{r}_1 d\mathbf{r}_2, \qquad (2)$$

where $r_{12} = |\mathbf{r}_1 - \mathbf{r}_2|$ and q_1 and q_2 are values of a universal function $q_0(n(\mathbf{r}), |\nabla n(\mathbf{r})|)$. Equation (2) is efficiently evaluated by factorizing the integration kernel ϕ and by using fast Fourier transform to compute the self-consistent potential as proposed in Ref. 24 and implemented in the real-space projector augmented wave GPAW code.[25]

In this Rapid Communication we consider graphene on Co, Ni, Pd, Ag, Au, Cu, Pt, and Al metal (111) surfaces. We fix the atoms in the metal slabs at their experimental lattice parameters and relax the graphene sheet using the vdW-DF Hellmann-Feynman forces. We observe that the vdW-DF results do not change significantly if we fix the graphene lattice parameter to its optimized value and adjust the metals correspondingly. We use a (6,6,1) and (4,4,1) Monkhorst Pack k-point sampling, respectively, for the smaller (Co, Ni, and Cu) and the larger (Pd, Ag, Au, Pt, and Al) orthorhombic unit cells. The two different unit cells are needed in order to obtain commensurate structures without significant strain, as discussed in Ref. 10. The metal slabs are modeled with four atomic layers and a vacuum of 14 Å in the direction normal to the surface; the grid spacing is 0.16 Å. The calculations

TABLE I. Binding energies (E_b) per carbon atom and binding distances (d) of graphene on metal (111) surfaces. Fermi level shift ΔE_F and charge transfer δQ at the vdW-DF equilibrium separation. Negative (positive) ΔE_F indicates n (p)-type doping. Negative (positive) δQ indicates electron transfer to (from) the graphene layer. The charge transfer has been evaluated using the Bader scheme (Ref. [26]). The revPBE functional yields no binding for all metals.

		Co	Ni	Pd	Ag	Au	Cu	Pt	Al
vdW-DF	d (Å)	3.40	3.50	3.50	3.55	3.57	3.58	3.67	3.72
	E_b (meV)	30	37	39	33	38	38	43	35
	ΔE_F (eV)	−0.20	0.13	0.65	−0.40	0.21	−0.43	0.66	−0.51
	$\delta Q (10^{-3}e)$	−5.0	−3.0	+5.0	−5.0	+0.4	−4.0	+5.0	−8.0
LDA	d (Å)	2.08	2.08	2.33	3.32	3.35	3.21	3.25	3.46
	E_b (meV)	175	123	79	45	31	35	33	25
Expt.	d (Å)	1.5–2.2[a]	2.1[b]			5[c]		3.3[d]	
	Hybridization	strong [a]	strong [e]	strong [f]	weak [g]	weak [c]	weak [g]	weak [d]	

[a]Ref. 27
[b]Ref. 28
[c]Ref. 29
[d]Ref. 30
[e]Ref. 31
[f]Ref. 32
[g]Ref. 33

for Ni and Co surfaces are spin polarized: notice however that the nonlocal correlation [last term in Eq. (1)] is independent of spin. The calculated binding energies and distances for the relaxed structures are listed in Table I. The vdW-DF results show that the metal-graphene interaction is relatively similar across the different metals. This is in contrast with the LDA prediction of two separate classes of metal-graphene interfaces, as found in very good agreement with Ref. 10. Note that in the LDA calculations the graphene lattice parameter was fixed to its optimized LDA value. We also repeated the same calculations using the revPBE functional, and we obtained no binding for all the metals. Interestingly, for the systems that LDA finds to be weakly bonded (Ag, Au, Cu, Pt, and Al), the binding energies obtained with the vdW-DF are very similar to the LDA ones. Nevertheless the binding distances are systematically slightly larger in the vdW-DF case. In fact it has been reported that the vdW-DF functional usually produces equilibrium distances somewhat larger than experiments.[20] In the case of Co, Ni, and Pd, on the other hand, the relatively strong binding predicted by LDA is not found by the vdW-DF functional.

In order to analyze these results, we now focus on the interaction between graphene and Ni(111). Figure 1 shows the binding curves for graphene on the Ni(111) surface calculated with the LDA, revPBE, and vdW-DF functionals. The revPBE curve is positive at all distances, while the LDA curve shows a relatively deep minimum at ~ 2 Å consistent with previous LDA calculations. The vdW-DF result lies in between, following the revPBE curve at small separations and the LDA curve at larger separations, and it predicts a shallow minimum at 3.5 Å. Note that a metastable plateau is found by the revPBE functional around 2.5 Å.

In Fig. 2 we show the calculated band structure of graphene on Ni(111). The size of the dots indicate the weight of the corresponding Bloch eigenstate on the carbon p_z orbitals with darker meaning larger weight. In free graphene, the carbon p_z orbitals placed at A sites (p_z^A) are decoupled from the p_z orbitals at B sites (p_z^B) at the Dirac point, thus

producing two degenerate states (see inset in Fig. 1 for the structure). Since the A sites are located directly on top of Ni atoms at a close distance in the LDA calculation (2.08 Å), a strong hybridization between p_z^A orbitals and Ni_{3z-r} is observed, which gives rise to an unoccupied antibonding state σ^* and two occupied bonding states σ_1 and σ_2. The LDA gaps for $\sigma^* - \sigma_1$ and $\sigma^* - \sigma_2$ are 2 and 4 eV, respectively. On the other hand, the p_z^B orbitals (occupied in the spin-up channel and unoccupied in the spin-down one) hardly interact with Ni d states and therefore remain unmodified. The vdW-DF band structures (evaluated at the vdW-DF relaxed distance of 3.50 Å), on the other hand, resemble the free graphene, preserving the Dirac point and only shifting it up by 0.13 eV. A very similar behavior is found for Co and Pd. For the remaining interfaces both the LDA and vdW-DF band structures resemble that of free-standing graphene with the Dirac point shifted with respect to the metal Fermi level. The Fermi level shifts and calculated charge transfer between the metal and graphene are summarized in Table I.
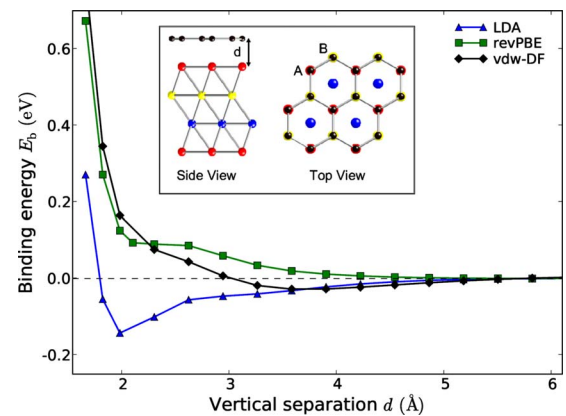

FIG. 1. (Color online) Binding energy (E_b) per carbon atom of graphene on the Ni(111) surface calculated with LDA, revPBE, and vdW-DF functionals. The graphene is adsorbed in the top-fcc configuration (see inset).
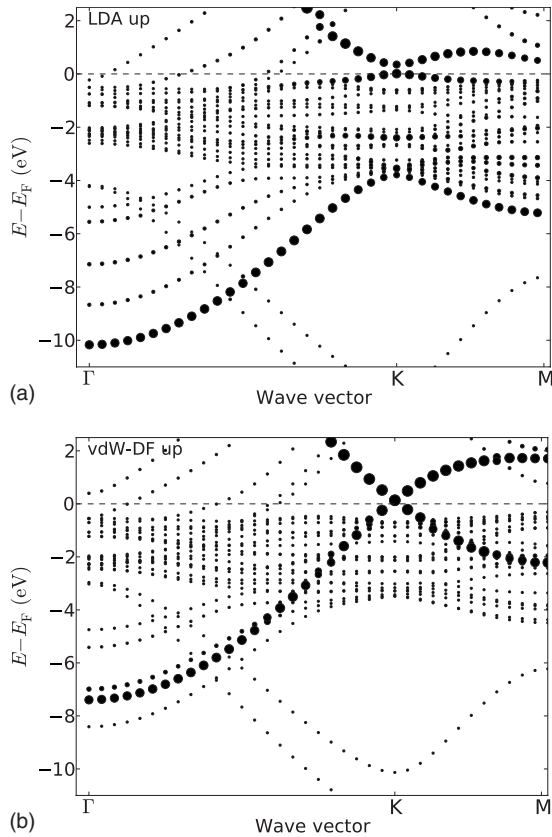
FIG. 2. LDA (top) and vdW-DF (bottom) band structures for graphene on Ni(111) in the top-fcc configuration. Larger dots represent larger weight of the carbon p_z orbitals. Only one spin channel is shown, the other being almost identical.

the graphene K point thus suggesting some hybridization between the graphene and Ni orbitals.[31,35] Earlier low-energy electron diffraction (LEED) measurements found a Ni-graphene bond distance of 2.1 Å.[28] We note that both of these results are in line with the LDA calculations. On the other hand LDA is not expected to work well for highly inhomogeneous systems such as the interface structures investigated here. Similar experimental conclusions[27] are found for the Co/graphene interface, using scanning tunneling spectroscopy (STS) techniques. These results might indicate a difficulty for the present vdW-DF in describing systems with mixed bonding character, in line with the conclusions of Ref. 22. Moreover, results involving the application of the vdW-DF functional to metallic systems should be taken with care due to the choice of the response function employed in the construction of the vdW-DF.[36] It should also be noted that the present calculations are restricted to two specific interface configurations and hence do not take into account the variety of Moiré superstructures observed in experiments. Recent ARPES and LEED data is also available for the Pt/graphene interface[30] which provides clear evidence of weak interaction between graphene and the substrate, with an estimated separation of 3.3 Å, in fair agreement with both LDA and our vdW-DF results. STS measurements for graphene on Pd (Ref. 32) show a band-gap opening of ~0.3 eV, in contrast with both LDA and vdW-DF predictions. STS experiments on the Au/graphene interface,[29] particularly relevant since most electronic contacts employ gold, demonstrate a weak interaction between Au and graphene, and a p-type doping in good agreement with both LDA and our vdW-DF results. We have summarized the available recent experimental data in the last two rows of Table I.

Since LDA is known to underestimate band gaps significantly we have also performed G_0W_0 calculations for the graphene-Ni structures corresponding to the LDA and vdW-DF distances.[34] In both cases we find no noteworthy difference between the G_0W_0 and DFT Kohn-Sham band structures close to the K point.

Recent experimental work on the Ni/graphene interface is based on angle-resolved photoemission spectroscopy (ARPES). The ARPES band structures reveal a band gap at

Figure 3 shows the total (full lines) and the exchange-only (dashed lines) binding energy curves for revPBE, PBE, and LDA in the case of graphene on Cu(111) (left panel) and on Ni(111) (right panel). The exchange-only energies are calculated without including the correlation energy term in the exchange-correlation functional and have been evaluated non-self-consistently. Clearly, the bonding for the physisorbed graphene on Ag, Au, Cu, Pt, and Al originates partially from the exchange term in the LDA xc-functional, as
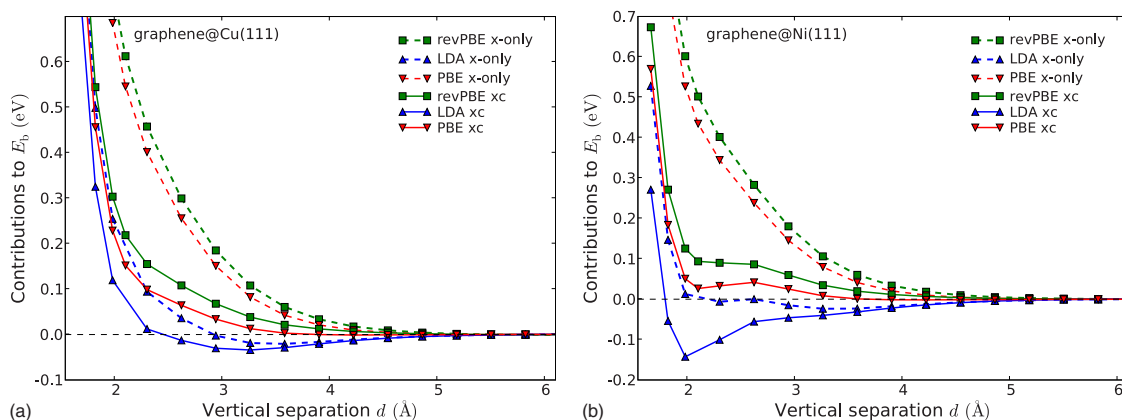

FIG. 3. (Color online) Decomposition of the binding energy E_b into exchange-only contributions (dashed lines—only the correlation term is removed) and total binding energy (full lines) for different functionals.

shown for Cu as an example in the left panel of Fig. 3. This is in principle incorrect since the van der Waals interaction is a purely nonlocal correlation effect. The weak bonding predicted by the vdW-DF functional, similar in magnitude to the LDA results, is produced by the correlation term instead, which is physically correct. Interestingly, this applies to the Ni/graphene system as well, as shown in the right panel of Fig. 3. The LDA exchange-only curve shows a broad and weak attractive contribution between 2 and 5 Å with two local minima. We note that in a genuine covalent bond the exchange contribution to the binding energy is generally significantly larger than in this case. The revPBE and PBE exchange-only curves are repulsive at all separations for both systems. This is the typical behavior which is observed in van der Waals bonded dimers or organic molecules on surfaces.[13,21]

In conclusion we have performed DFT calculations of graphene adsorbed on different metal surfaces using the recently developed vdW-DF functional which explicitly includes nonlocal correlations. For Ag, Au, Cu, Pt, and Al both LDA and vdW-DF consistently predicts a weak binding. Similar weak binding is found for Ni, Co and Pd with the vdW-DF where LDA on the other hand predicts stronger binding and significant hybridization between graphene and metal d states. At the vdW-DF binding distances graphene's band structure was shown to be essentially unaffected by the substrate. This appears to be in conflict with LEED and ARPES measurements for graphene on Ni, Co, and Pd indicating that more work is needed in order to reconcile experiments and theory for the graphene-metal interface.

---

[1] K. S. Novoselov *et al.*, Science **306**, 666 (2004).

[2] A. K. Geim and K. S. Novoselov, Nature Mater. **6**, 183 (2007).

[3] J. Wintterlin and M.-L. Bocquet, Surf. Sci. **603**, 1841 (2009).

[4] K. S. Kim *et al.*, Nature **457**, 706 (2009).

[5] J. Coraux *et al.*, New J. Phys. **11**, 039801 (2009).

[6] P. W. Sutter *et al.*, Nature Mater. **7**, 406 (2008).

[7] P. Hobza *et al.*, J. Comput. Chem. **16**, 1315 (1995).

[8] S. Kristyán and P. Pulay, Chem. Phys. Lett. **229**, 175 (1994).

[9] E. Ruiz *et al.*, J. Am. Chem. Soc. **117**, 1141 (1995).

[10] G. Giovannetti, P. A. Khomyakov, G. Brocks, V. M. Karpan, J. van den Brink, and P. J. Kelly, Phys. Rev. Lett. **101**, 026803 (2008).

[11] J. P. Perdew, K. Burke, and M. Ernzerhof, Phys. Rev. Lett. **77**, 3865 (1996).

[12] M. Fuentes-Cabrera, M. I. Baskes, A. V. Melechko, and M. L. Simpson, Phys. Rev. B **77**, 035405 (2008).

[13] M. Dion, H. Rydberg, E. Schröder, D. C. Langreth, and B. I. Lundqvist, Phys. Rev. Lett. **92**, 246401 (2004).

[14] M. Dion, H. Rydberg, E. Schröder, D. C. Langreth, and B. I. Lundqvist, Phys. Rev. Lett. **95**, 109902 (2005).

[15] A. Puzder, M. Dion, and D. C. Langreth, J. Chem. Phys. **124**, 164105 (2006).

[16] T. Thonhauser, A. Puzder, and D. C. Langreth, J. Chem. Phys. **124**, 164106 (2006).

[17] E. Ziambaras, J. Kleis, E. Schröder, and P. Hyldgaard, Phys. Rev. B **76**, 155425 (2007).

[18] J. Kleis, B. I. Lundqvist, D. C. Langreth, and E. Schröder, Phys. Rev. B **76**, 100201 (2007).

[19] V. R. Cooper, T. Thonhauser, A. Puzder, E. Schröder, B. I. Lundqvist, and D. C. Langreth, J. Am. Chem. Soc. **130**, 1304 (2008).

[20] D. C. Langreth, B. I. Lundqvist, S. D. Chakarova-Káck, V. R. Cooper, M. Dion, P. Hyldgaard, A. Kelkkanen, J. Kleis, L. Kong, S. Li, P. G. Moses, E. Murray, A. Puzder, H. Rydberg, E. Schröder, and T. Thonhauser, J. Phys.: Condens. Matter **21**, 084203 (2009).

[21] P. G. Moses, J. J. Mortensen, B. I. Lundqvist, and J. K. Nørskov, J. Chem. Phys. **130**, 104709 (2009).

[22] L. Romaner, D. Nabok, P. Puschnig, E. Zojer, and C. Ambrosch-Draxl, New J. Phys. **11**, 053010 (2009).

[23] Y. K. Zhang and W. T. Yang, Phys. Rev. Lett. **80**, 890 (1998).

[24] G. Román-Pérez and J. M. Soler, Phys. Rev. Lett. **103**, 096102 (2009).

[25] J. J. Mortensen, L. B. Hansen, and K. W. Jacobsen, Phys. Rev. B **71**, 035109 (2005).

[26] W. Tang, E. Sanville, and G. Henkelman, J. Phys.: Condens. Matter **21**, 084204 (2009).

[27] D. Eom, D. Prezzi, K. T. Rim, H. Zhou, M. Lefenfeld, S. Xiao, C. Nuckolls, M. S. Hybertsen, T. F. Heinz, and G. W. Flynn, Nano Lett. **9**, 2844 (2009).

[28] Y. Gamo, A. Nagashima, M. Wakabayashi, M. Terai, and C. Oshima, Surf. Sci. **374**, 61 (1997).

[29] Z. Klusek, P. Dabrowski, P. Kowalczyk, W. Kozlowski, W. Olejniczak, P. Blake, M. Szybowicz, and T. Runka, Appl. Phys. Lett. **95**, 113114 (2009).

[30] P. Sutter, J. T. Sadowski, and E. Sutter, Phys. Rev. B **80**, 245411 (2009).

[31] A. Varykhalov, J. Sanchez-Barriga, A. M. Shikin, C. Biswas, E. Vescovo, A. Rybkin, D. Marchenko, and O. Rader, Phys. Rev. Lett. **101**, 157601 (2008).

[32] S.-Y. Kwon, C. V. Ciobanu, V. Petrova, V. B. Shenoy, J. Bareo, V. Gambin, I. Petrov, S. Kodambaka, Nano Lett. **9**, 3985 (2009).

[33] A. M. Shikin, V. K. Adamchuka, and K. H. Rieder, Phys. Solid State **51**, 2390 (2009).

[34] The $G_0 W_0$ calculations were performed with the YAMBO code.[37] We included 100 empty bands (corresponding to 40 eV above the Fermi level), a 12×12 k point for the simple rhombohedral unit cell, and a plasmon frequency of 1 Hartree.

[35] A. Grüneis and D. V. Vyalikh, Phys. Rev. B **77**, 193401 (2008).

[36] T. Thonhauser, V. R. Cooper, S. Li, A. Puzder, P. Hyldgaard, and D. C. Langreth, Phys. Rev. B **76**, 125112 (2007).

[37] A. Marini, C. Hogan, M. Grüning, and D. Varsano, Comput. Phys. Commun. **180**, 1392 (2009).

Paper 5

A.K. Kelkkanen, B. I. Lundqvist, and J. K. Nørskov,
van der Waals Effect in Weak Adsorption Affects Trends in Adsorption, Reactivity, and View of Substrate Nobility,

van der Waals Effect in Weak Adsorption Affects Trends in Adsorption, Reactivity, and View of Substrate Nobility.

André K Kelkkanen[1], Bengt I Lundqvist[1,2], and Jens K Nørskov[1]

Center for Atomic-scale Materials Design, Department of Physics
Technical University of Denmark, DK - 2800 Kongens Lyngby, Denmark[1] and
Department of Applied Physics, Chalmers University of Technology , SE-41296 Göteborg, Sweden[2]
(Dated: January 10, 2011)

The ubiquitous van der Waals (vdW) force, particularly discernible in weak adsorption, is studied on noble and transition metals. In calculations with the vdW-DF density functional (M. Dion *et al.*, Phys. Rev. Lett. **92**, 246401 (2004)), the atomic structure near the adsorption site is systematically varied, incl. dense fcc(111) surface, adatom, pyramid, and step defects. In weak adsorption the vdW force (i) is shown necessary to account for, (ii) is sizable, (iii) has a strong spatial variation, relevant for adsorption on surface defects, (iv) changes reaction rules, and (v) changes adsorption trends in agreement with experimental data. Traditional physisorption theory is also given support and interpretation.

When molecules and materials meet, as a molecule hitting a surface in catalysis or a contact between two pieces of materials, the tails of each chunk of electrons guide the further fate of the systems. Often stronger processes take over and the effect gets lost, but not so for an important class of phenomena, here called weak adsorption, incl. physisorption and hydrogen bonding.

Well-prepared crystallographically ordered surfaces provide the basis for the accurate comparisons between experiment and theory that stand behind the impressive accomplishments of surface science. The even more general property of a surface, its two-dimensional extent, is profitable for phenomena that gain strength by a surface source, like the ubiquitous van der Waals (vdW) force. In this letter the vdW-force landscapes are calculated for some representative atomic configurations, showing that the extent of surfaces matters, and that they upset some adsorption experiences and reaction rules.

Weak adsorption, with adsorption-energy values less than about 1 eV, is abundant, often significant, and encompasses several kinds of forces. Some of them derive from electrostatics and quantum statistics and can be accounted for at the level of the general-gradient approximation (GGA) of density-functional theory (DFT), others derive from quantum-mechanical correlations, like vdW forces, and surface properties, like lateral forces.

Many catalytic reactions are structure sensitive, rates and binding energies depending on the detailed geometric structure of the surface atoms of the catalysts [1, 2]. At defects, like steps, kinks, edges, and adparticles, atoms and molecules are generally more reactive than on flat surfaces, a fact attributed to an under-coordination of the reacting particle [1–4]. This can be tied to the altered electron structure at such sites, since the local d band narrows and shifts upward in energy close to the Fermi level, giving stronger bonds for many atoms on such sites than on flat surfaces, as described in the d-band model [5, 6], calculated in GGA [2, 7–9] , and measured for, *e.g.*, CO, O, O_2, NO, N, and N_2 [10].

Electron structure is designed to get better catalysts both by alloying, surface structuring, growth, deposition of ultra-fine particles [11–16] and by direct atom manipulation in STM and AFM [17, 18]. Noble metals illustrate the delicate difference between inertness and reactivity, the noble solid being inert to atmospheric attack while used as a catalyst in reactive nano-particle form [19].
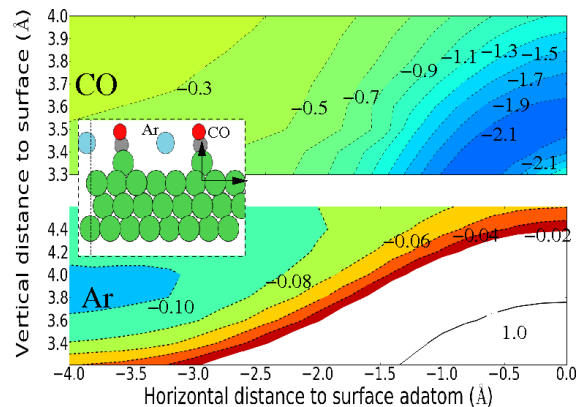
FIG. 1. Spatial difference in interaction energy between strong and weak adsorption shown by potential-energy surfaces (PES's) for CO (top) and Ar (bottom) adsorbed on Ni(111) surface with Ni adatom (inset), calculated with the vdW-DF method [23]. CO molecule prefers to be close to adatom, while the Ar atom prefers terrace, as indicated by coordinate system in inset. Units are eV and Å.

Strong and weak adsorption differ also in spatial behavior, illustrated (Fig. 1) by the almost reversed (left-right) potential-energy surfaces (PES's) for Ar and CO adsorbed on a dense Ni surface with an adatom of Ni. The CO molecule adsorbs more strongly on transition metals than on noble metals, with an overall preference for low-coordination sites, as is well known from GGA calculations [2, 8, 9, 20–22]. The vdW-DF method [23], used for Fig. 1 also favors CO adsorption on Ni adatom ($E_{ads} = 2.2$ eV) over terrace (interaction energies down
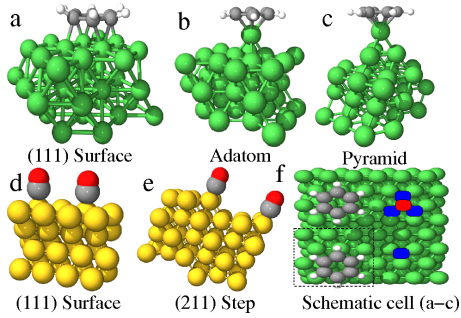
FIG. 2. Studied substrate structures for adsorption of benzene molecule on (a) planar Ni(111) surface, (b) adatom and (c) pyramid Ni clusters adsorbed on Ni(111) surface, and of CO molecule on (d) planar Au(111) and (e) stepped Au(211) surfaces. The adsorption sites are not equivalent, since benzene binds to several Ni-metal atoms in planar case to only top atom on, *e.g.*, the pyramid and adatom. The deformation of the adsorbed benzene molecule on the planar surface is indicated. The cell used for benzene (dashed square) is illustrated in (f), where circles represent the adatom defect in the lower right, and the pyramid defect in the upper right (also a common model structure for an STM tip).

FIG. 3. Potential-energy curves (PEC's) for benzene adsorption on planar, adatom, and pyramid structures (see Fig. 2) of Ni, in the revPBE (top; for comparison) and the vdW-DF (middle) approximations, the coordinate d being the separation between the adsorbate point of gravity and the closest metal atom (Energy scales differ). The bottom figure shows a key contribution to the total vdW-DF energy, the nonlocal correlation E_c^{nl} (Eq. (1)), which is seen to be strongest for the planar surface, where the average separation between adsorbate and the Ni atoms is shortest, and weakest for the pyramid structure, where the average separation is longest.

to 1.8 eV). For Ar, the weak adsorption is determined by vdW forces, favoring proximity to extended surface at terrace ($E_{ads} = 0.10$ eV), but avoiding unnecessary Pauli repulsion, as on top of Ni adatom (interaction energies down to 0.06 eV).

What we call novel is an atomic-scale spatial variation of the vdW-force field, which we derive with the vdW-DF method, but which we claim is a true physical phenomenon, present also in more recent DFT's with account of vdW forces. The vdW-DF functional [23] is used perturbatively from revPBE [24] densities for all calculated interaction energies, unless otherwise stated. It expresses the exchange-correlation energy as $E_{xc}^{vdW-DF} = E_x^{revPBE} + E_c^{LDA} + E_c^{nl}$, *i.e.* with exchange accounted for by E_x^{revPBE}, local correlation by E_c^{LDA}, and nonlocal correlation, and thus vdW interactions, by

$$E_c^{nl} = \frac{1}{2} \int d^3r \, d^3r' \, n(\vec{r})\phi(\vec{r},\vec{r}')n(\vec{r}'). \qquad (1)$$

Equation (1) depends nonlocally on the electron density $n(\vec{r})$, the scalable interaction kernel $\phi(\vec{r},\vec{r}')$ being attractive at medium-to-large separations and repulsive at small ones [23]. It expresses the electron-response nature of the vdW interaction [23].

The integration in Eq. (1) is sped up by factorization and fast Fourier transforms [25].

All calculations are made with the GPAW software [26], which also has a self-consistent version of the vdW-DF [25, 27] available. The slab calculations are performed with orthogonal unit cells and a slab of three layers (4 x 3), when benzene is the adsorbate, and four layers (2 x 2) for CO. Default GPAW parameters are used, apart from a grid spacing of 0.18 Å. We use 4x4

k-points. Every point on the PEC allows benzene relaxation in plane parallel to surface. The vdW-DF parameters are as in Ref. [25]. During relaxation of slabs, the bottom layer of the slab is fixed. The height of the cell is 23 Å. In Fig. 1, a linear combination of atomic orbitals basis set with double zeta polarized precision is used for reasons of electronic spin convergence of the O atom.Elsewhere, the more accurate default grid mode in GPAW is used for the density.

The vdW effects are illustrated by calculated vdW-DF energy landscapes for representative molecules on a variety of substrate configurations (Fig 2). PEC results for benzene adsorbed on planar Ni(111) surface, and Ni(111) surface with Ni adatom and pyramid, respectively, show (i) GGA (revPBE) results to follow the low-coordination rule [1–4], (ii) noticable differences between revPBE and vdW-DF results, and (iii) significant structure-dependent differences in nonlocal correlations, E_c^{nl} (lower panel), most attractive for planar surface (several eV's), and significantly smaller for adatom and pyramid structures of the nonlocal character of the vdW interaction [23] and easily understood from Eq. (1) and the form of the kernel $\phi(\vec{r},\vec{r}')$, being attractive in key regions [23]. The average separation between electrons on adsorbate and Ni atoms in substrate, respectively, is shortest on the planar surface, giving the strongest vdW effect, but longest for the pyramid structure, making the vdW attraction weakest here, a clear effect of the extended surface.

In weak adsorption, the outcome of the delicate competition between covalent, vdW, and Pauli-repulsion forces
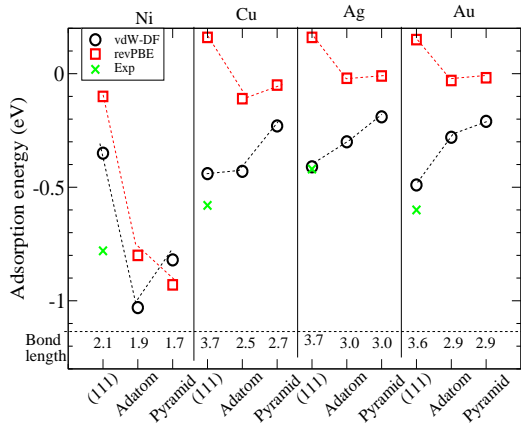
FIG. 4. Interaction-energy values, calculated with vdW-DF and revPBE, respectively, for benzene on Ni, Cu, Ag, and Au, for the planar (111), adatom, and pyramid configurations (described as a, b, and c in Fig. 2). Adsorption trends illustrate the competition between preference for low coordination, called for by covalency, and that for proximity to the extended surface, called for by vdW forces. Like in Fig. 3 the top panels show that the GGA revPBE (no vdW) prefers the low-coordinated adatom and pyramid sites over the planar (111) surface, for all the metals, and that the vdW-DF prefers the planar (111) surface over both adatom and pyramid, for the coinage metals. Other patterns appear, when several driving forces have comparable strengths, as illustrated by the vdW-DF case for Ni (left), where under-coordination favors the adatom over planar (111) surface and over the pyramid (due to a closer proximity to it). The force balance can be delicate, as the Ni case also illustrates in Fig. 3: The vdW-DF suggests two minima, the inner for chemisorption, the outer for physisorption. This feature is however functional dependent, a less repulsive exchange approximation, like the optPBE-vdW [47], slightly overestimates the adsorption and result in only one (inner) minimum at 1.1 eV (Cf. recent findings for graphene adsorption [48]). Experimental results for Ni [28], Cu [29, 30], Ag [31, 32], and Au [33] are indicated by crosses). Bond lengths are measured from the carbon ring to the closest metal atom, in Å, and listed to signal chemi- (short) and physisorption (long).

also depends on the nature of the substrate atoms. Benzene interaction-energy values for the three indicated structures illustrate this (Figs. 3 and 4). For Ag(111) and Au(111), and marginally for Cu(111), vdW attraction and Pauli repulsion (lower on the surface than on the adatom and pyramid) overcome any d-electron-benzene hybridization, to make benzene most stable on the planar surface. This is at variance with the revPBE trend, which gives no significant binding to any structure in the Au and Ag cases, while having a small preference for the adatom site in the Cu case, and which trends on Ni supports the low-coordination rule [5, 6], with stronger bonds on structures with lower coordination (higher d-band). The vdW-DF results imply that the rule does not apply for weak adsorption in presence of vdW forces. This can be seen from that the vdW-DF alters the low-
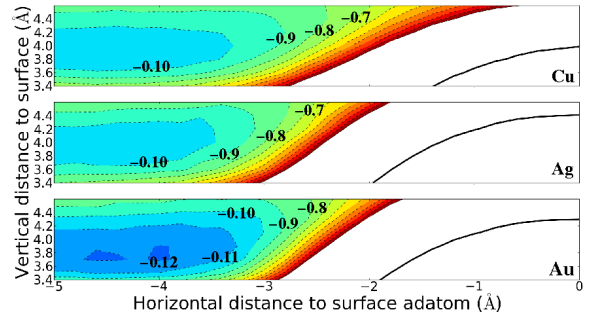
FIG. 5. PES's for an Ar atom physisorbed on Cu, Ag, and Au(111) surfaces with an adatom of the same kind in the origin. The adsorption energy varies weakly between metals, Ar adsorption being slightly stronger on Au than on Ag, consistent with the lower polarizability of Ag [34, 35]. The PES's also show the Ar preference for terrace away from the adatom. Black equipotential curve in white area, representing a 1 eV repulsion, calculated with revPBE, illustrates the strong repulsion at small separations and the approximate correlation of these curves with the coupling matrix element V_{ad} [6]. So, polarizability determines strength of physisorptive attraction around the phsisorption minima, while V_{ad} gives trend for the Pauli repulsion near the substrate.

coordination trend on Ni predicted by revPBE, favoring the adatom structure over the pyramid. Secondly on the flat surfaces, the adsorption of benzene is slightly weaker on Ag(111) than on Cu(111) and, in particular, Au(111) (Fig. 4) . This physisorption trend radically differs from that in strong adsorption, given by GGA for , *e.g.*, the O atom, whose bond is weakest on Au and then grows with size of the coupling matrix element V_{ad} [6].

Traditional physisorption studies [34, 35] involve PEC's as sums of a vdW attraction and a Pauli repulsion. The former is expressed in terms of dielectric properties of the substrate, thus relating to excitation energies of each surface. Ag has its d band more than 4 eV below the Fermi level (2 eV for Cu and Au), which makes [34, 35] Ag less polarizable and less vdW attractive (Figs. 4 and 5). The latter relates to the electronic density profile at the surface and is traditionally given with an empirical input.

The variation of the vdW attraction in space is a general phenomenon [36] PES's for a single Ar adatom on Ni, Cu, Ag, and Au(111) surfaces, each with a single adatom of the same kind (Figs. 1 and 5) show the typical broad range of attraction, the PES forming a shallow, semiinfinite and not so substrate-sensitive trough high over the surface, and steep repulsive potential, growing in strength and range (indicated by black curve in white area) in order Ni, Cu, Ag, and Au, roughly consistent with known correlation between coupling matrix element V_{ad} and repulsion [6]. This first-principles calculation thus both supports the qualitative picture of the traditional physisorption theories [34, 35] and accounts for the repulsion. For the strength and range of the latter,

[eV]	111	211		310
Site	Atop (9)	Step (7)	Terrace (9)	Step (6)
vdW-DF	0.10	0.24	0.14	0.35
Exp	<0.26 [39]	0.28−0.52 [40]	0.28−0.39 [41]	0.48 [42]
revPBE	N.B.	0.36	N.B.	0.55

TABLE I. CO adsorption-energy values (in eV) on various Au surface and site structures, and comparison with experiments and revPBE. Coordination number n is indicated as (n).

empirical input can be replaced by a well-founded [6, 38] and tabulated [12] quantity, V_{ad}, which characterizes each atom.

For weak adsorption of CO on stepped Au surfaces, experimental data [39–42] can be compared with calculated vdW-DF adsorption-energy values (Table I). Trends are right, including the preference for steps, and values are comparable. The slight underbinding can be remedied by a more favorable [43] exchange functional [44–46], like the optPBE-vdW [47].

This Letter exemplifies that in weak adsorption vdW forces can give significant changes, in particular spatial ones, by presenting results from the vdW-DF method [23] for systems with carefully chosen adsorbate, substrate, and configuration. vdW effects (i) are radically more pronounced in weak adsorption than in strong, with adsorption sites and strengths that change from those for mere covalency, (ii) depend strongly on the local substrate configuration, giving strongest adsorption for proximity to extended surfaces, (iii) changes adsorption trend on, *e.g.*, noble metals, the coupling V_{ad} still being relevant, but only after vdW and polarization properties have been considered, (iv) create a variety of behaviors, when varying kind of substrate atom and local adsorption-site structure, (v) accounts for experimental data for weak adsorption of CO on stepped Au surfaces by giving reasonably sized adsorption-energy values and right trends, including that steps are preferred, and (vi) give a first-principles support to and deeper understanding of the traditional physisorption-potential models.

[1] M. Boudart, Adv. Catal. **20**, 153 (1969).
[2] B. Hammer, O. H. Nielsen, and J. K. Norskov, Catal. Lett. **46**, 31 (1997), and references given there.
[3] J. T. Yates, J. Vac. Sci. Technol. A **13** 3 (1995).
[4] N. P. Lebedeva, M. T. M. Koper, J. M. Feliu, and R. A. van Santen, J. Electroanal. Chem. **487**, 37-44 (2000).
[5] B. Hammer and J. K. Norskov, Surf. Sci, **343**, 211 (1995).
[6] B. Hammer and J. K. Norskov, Adv. in Catal. **45**, 71 (2000).
[7] Z.-P. Liu, P. Hu, and A. Alavi, J Am. Chem. Soc. **124**, 14770 (2002).
[8] T. Jiang, D. J. Mowbray, S. Dobrin, H. Falsig, B. Hvolbaek, T. Bligaard and J. K. Norskov, J. Phys. Chem. C **113**, 10548 (2009).
[9] L.M Molina and B. Hammer, Appl. Catal., A **291**, 21 (2005).
[10] N. P. Lebedeva, M. T. M. Koper, J. M. Feliu, and R. A. van Santen, J. Phys. Chem. B **106**, 12937 (2002), and references therein.
[11] M. Haruta, CATTECH **6**, 102 (2002).
[12] A. Ruban, B. Hammer, P. Stoltze, H. Skriver, and J. Norskov, J. Mol. Catal. **115**, 421 (1997).
[13] F. Studt, F. Abild-Pedersen, T. Bligaard, R. Z. Sorensen, C. H. Christensen, and J. K. Norskov, Science **320**, 1320 (2008).
[14] J. Greeley, I. E. L. Stephens, A. S. Bondarenko, T. P. Johansson, H. A. Hansen, T. F. Jaramillo, J. Rossmeisl, I. Chorkendorff, and J. K. Norskov, Nature Chem. **1**, 552 (2009).
[15] J. K. Norskov, T. Bligaard, J. Rossmeisl, and C. H. Christensen, Nature Chem. **1**, 37 (2009).
[16] M. Haruta, Catal. Today **36**, 153 (1997).
[17] F. E. Olsson, S. Paavilainen, M. Persson, J. Repp, and G. Meyer, Phys. Rev. Lett. **98**, 176803 (2007).
[18] L. Gross, F. Mohn, P. Liljeroth, J. Repp, F. J. Giessibl, and G. Meyer, Science **324**, 1428 (2009).
[19] F. Marino, C. Descorme, and D. Duprez, Appl. Cat B -Env. **54**, 59 (2004) gives an example.
[20] N. Lopez and J. K. Norskov, J Am. Chem. Soc. **124**, 11262 (2002).
[21] M. Mavrikakis, P. Stoltze, and J. K. Norskov, Catal. Lett. **64**, 101 (2000)
[22] L.M Molina and B. Hammer, Phys. Rev. B **69**, 155424 (2004).
[23] M. Dion, H. Rydberg, E. Schroder, D.C. Langreth, and B.I. Lundqvist, Phys. Rev. Lett. **95**, 109902(E) (2005).
[24] Y. Zhang and W Yang, Phys. Rev. Lett. **80**, 890 (1998).
[25] G. Román-Pérez and J. M. Soler, Phys. Rev. Lett. **103**, 096102 (2009).
[26] J. J. Mortensen, L. B. Hansen, and K. W. Jacobsen, Phys. Rev. B **71**, 035109 (2005).
[27] T. Thonhauser, V. R. Cooper, S. Li, A. Puzder, P. Hyldgaard, and D. C. Langreth, Phys. Rev. B **76**, 125112 (2007).
[28] A. Myers, G. Schoofs, and J. Benziger, J. Phys. Chem. **91**, 2230 (1987).
[29] H. Koschel, G. Held, and H. Steinruck, Surf. Rev. Lett. **6**, 893 (1999).
[30] P. Bagus, K. Hermann, and C. Woll, J. Chem. Phys. **123** 184109 (2005).
[31] X. Zhou, M. Castro, and J. White, Surf. Sci. **238**, 215 (1990).
[32] R. Caputo, B. P. Prascher, V. Staemmler, P. S. Bagus, and C. Woell, J. Phys. Chem. A **111**, 12778 (2007).
[33] D. Syomin, J. Kim, B. Koel, and G. Ellison, J. Phys. Chem. B **105**, 8387 (2001).
[34] E. Zaremba and W. Kohn, Phys. Rev. B **15**, 1769 (1977).
[35] P. Apell and C. Holmberg, Solid State Commun. **49**, 693 (1984).
[36] In a particular case, adsorption of CO on Pt(111), the vdW-DF functional has been shown to destabilize the hollow site on the Pt(111) surface by variation of the

nonlocal correlation functional (Eq. (2)) between different adsorption sites, which reduces the site-preference discrepancies in GGA [37]

[37] P. Lazic, M. Alaei, N. Atodiresei, V. Caciuc, R. Brako,and S. Blugel, Phys. Rev. B **81**, 045401 (2010).

[38] D. M. Newns, Phys. Rev. **178**, 1123 (1969).

[39] M. Lazaga, D. Wickham, D. Parker, G. Kastanas, and B. Koel, ACS Symp. Ser. **523**, 90 (1993).

[40] E. Samano, J. Kim, and B. E. Koel, Catal. Lett. **128**, 263 (2009).

[41] J. Kim, E. Samano, and B. E. Koel, J. Phys. Chem. B **110**, 17512 (2006).

[42] C. J. Weststrate, E. Lundgren, J. N. Andersen, E. D. L. Rienks, A. C. Gluhoi, J. W. Bakker, I. M. N. Groot, and B. E. Nieuwenhuys, Surf. Sci. **603**, 2152 (2009).

[43] A. Puzder, M. Dion, and D. C. Langreth, J. Chem. Phys. **124**, 164105 (2006).

[44] A. Gulans, M. J. Puska, and R. M. Nieminen, Phys. Rev. B **79**, 201105 (2009).

[45] E. D. Murray, K. Lee, and D. C. Langreth, J. Chem. Theor. Comput. **5**, 2754 (2009).

[46] A. K. Kelkkanen, B. I. Lundqvist, and J. K. Norskov, J. Chem. Phys. **131**, 046102 (2009).

[47] J. Klimes, D. R. Bowler, and A. Michaelides, J. Phys. Condens. Matter **22**, 022201 (2010).

[48] I. Hamada and M. Otani, Phys. Rev. B **82**, 153412 (2010).

Paper 6

A. K. Kelkkanen, K. Berland, S. Andersson, K. Lee, D. C. Langreth, E. Schröder,
B. I. Lundqvist and P. Hyldgaard,
Evaluation of New Density Functional with Account of van der Waals Forces by Use of Experimental H2 Physisorption Data on Cu(111),

Evaluation of New Density Functional with Account of van der Waals Forces by Use of Experimental H₂ Physisorption Data on Cu(111)

André Kelkkanen,[1] Kristian Berland,[2] Stig Andersson,[3] Kyuho Lee,[4]

David C. Langreth,[4] Elsebeth Schröder,[2] Bengt I. Lundqvist,[1, 2, 5] and Per Hyldgaard[2]

[1]*Center for Atomic-scale Materials Design, Department of Physics,*
Technical University of Denmark, DK-2800 Kongens Lyngby, Denmark
[2]*Department of Microtechnology and Nanoscience, MC2, Chalmers University of Technology, SE-41296 Göteborg, Sweden*
[3]*Department of Physics, Göteborg University, SE-41296 Göteborg, Sweden*
[4]*Department of Physics and Astronomy, Rutgers University, Piscataway, NJ 08854-8019, USA*
[5]*Department of Applied Physics, Chalmers University of Technology, SE-41296 Göteborg, Sweden*
(Dated: January 31, 2011)

For almost two decades, detailed experimental data for physisorption potential-energy surfaces of H₂ on low-indexed faces of Cu have challenged theory, with results for potential well depth, strength of lateral corrugation, energy transfer, and couplings between translation, vibration, and rotation of the particle. Recent development of density-functional theory, with functionals like vdW-DF and vdW-DF2 that account for nonlocal correlation effects, including van der Waals (vdW) forces, reveals a promising comparison and a useful evaluation. The vdW-DF2 functional appears to give a potential-energy curve promisingly close to the experiment-derived physisorption-energy curve in the bond region, but the comparison also gives indications for further improvements of the functionals.

Density-functional theory (DFT) gives in principle an exact description of electron systems, but in practice, approximations have to be made to describe exchange and correlation (XC) of the electrons [1, 2]. One way to evaluate such an XC functional is to compare results from it with those from other supposedly accurate electron-structure theories. Another way is to compare with relevant experiments, which typically provides test numbers for only one or two experimental quantities, however. This paper illustrates the advantages of a third approach, which builds the experiment-theory calibration and benchmarking on access to a full potential-energy curve (PEC) obtained from surface-physics investigations.

Accurate (adsorbate) PECs can be extracted from a multitude of experimentally determined numbers and features, for example, as investigated here, obtained for physisorption of H₂ and D₂ on Cu surfaces [3–6]. We propose to benchmark the performance of a nonempirical theory for an extended system by comparison against the resulting observation-based PEC. Density functionals that aspire to account for nonlocal electron-correlation effects, including van der Waals (vdW) forces, can then be assessed. In particular, we study the vdW-DF method [7–10] and show that calculations with versions of it provide a promising description of the physisorption potential for H₂ on the Cu(111) surface and that the most recent one, vdW-DF2 [10], is more accurate than the first one [7, 9] and other tested functionals.

Sparse matter is abundant. Since long, dense matter rests on a pillar of DFT for its description. The recent extensions of DFT functionals to regions of low electron density, where the ubiquitous vdW forces are particularly relevant, cover also sparse matter. The vdW-DF functional accounts for vdW interactions with a truly nonlocal correlation functional of the density $n(\mathbf{r})$ [7, 9]. Its key ingredients are (i) its origin in the Adiabatic Connection Formula [11–13], (ii) an approximate coupling-constant integration, (iii) the use of an approximate dielectric function in a single-pole form, (iv) which is fully nonlocal and satisfies known limits, sum rules, and invariances, and (v) whose pole strength is determined by a sum rule and whose pole position is scaled to give the approximate gradient-corrected electron-gas ground-state energy locally. There are no empirical or fitted parameters, just references to general theoretical criteria.

Like composite molecules, adsorption systems have electrons in separate molecule-like regions, with exponentially decaying tails in between. Then the slowly varying electron gas, used in the original vdW-DF method [7], might not be the most appropriate reference system for the gradient correction [14]. For the recent vdW-DF2 functional, the gradient coefficient of the B88 exchange functional [15] is used for the determination of the pole position [10]. This is based on application of the large-N asymptote [16, 17] on appropriate molecular systems. First-principles DFT calculations using the large-N asymptote show the B88 exchange functional [15] to perform best here [18]. The B88 exchange parameter β gives the pole position [10]. For exchange, the PW86 exchange functional [19] gives the most consistent agreement with Hartree-Fock results in the appropriate range of separations, without spurious exchange binding [20], thus chosen in vdW-DF2 [10].

Evaluation of XC functionals by comparing to other theoretical results is often done in a systematic way. A common benchmark is provided by the S22 datasets [21–25], which contain twenty-two prototypical small molecular duplexes for noncovalent interactions (hydrogen-bonded, dispersion-dominated, and mixed) in biological molecules and provides PEC's at a very accurate level of wave-function methods, in particular the CCSD(T) method. However, by necessity, the electron systems in such benchmark sets are finite in size. Benchmarking on

the S22 dataset [21, 23, 24] shows the original vdW-DF to perform well, except for hydrogen-bonded duplexes (underbinding by about 15% [10, 26]). The vdW-DF2 functional reduces the mean absolute deviations of binding energy and equilibrium separation significantly [10]. Shapes of PEC's away from the equilibrium separation are greatly improved. The long-range part of the vdW interaction, particularly crucial for extended systems, has a weaker attraction with vdW-DF2, thus reducing the error to 8 meV at separations 1 Å away from equilibrium [10].

The important step taken by the present work is to benchmark a full PEC in an extended system. For extended systems, experimental information provides the ultimate basis for assessing functionals. The vdW-DF functional has been successfully applied to a variety of systems [26], but primarily vdW bonded ones, typically tested on binding-energy and bond-length values, that happen to be available. The vdW-DF2 functional has also been benchmarked on such extended systems, like graphite [10], metal-organic-frameworks systems [27] and surface physisorption systems [28]. However, those studies often focused on comparison against just a few accessible observations. Fortunately, since almost two decades, accurate experimental values for the eigenenergies of H_2 and D_2 molecules bound to the Cu(111) surface [3, 4] lie waiting for theoretical account and assessment. The data bank here is rich, containing data for adsorption energy and equilibrium separation, and the whole shape of the physisorption potential, in addition to possible couplings to other phenomena!

Chemically inert atoms and molecules adsorb physically on cold metal surfaces [5], with characteristic low desorption temperatures ranging from a few (He) to tens of K (say Ar and CH_4). Adsorption energies, which take values from a few meV to around 100 meV, may be determined from thermal-desorption or isosteric-heat-of-adsorption measurements. For light adsorbates, like He and H_2, gas-surface-scattering experiments, with resonance structure of the elastic backscattering, provide a more direct and elegant method, with accurate and detailed measurements of bound-level sequences in the potential well. The availability of isotopes with widely different masses (^{3}He, ^{4}He, H_2, D_2) permits a unique assignment of the levels and a determination of the well depth and ultimately a qualified test of model potentials [6]. The availability of several isotopes, both H_2 and D_2 in this case, gives an abundance of experimental data, as illustrated by Table I.

The angular dependence for H_2, a finer detail of the interaction, can be determined from rotational (j, m) sublevel splittings, using molecular beams composed of para-H_2 or normal-H_2. In fact, molecular-beam-scattering (MBS) experiments have established a very detailed and challenging picture of the physisorption interaction between H_2 (D_2) and the low-index (111), (100), and (110) surfaces of Cu. The lateral variation of the interaction is relatively weak, in particular on the (111) surface, as

TABLE I: Sequences of bound-level energies in H_2 and D_2 potential. The experimental numbers are from Ref. [3, 4], and the DFT ones are calculated with the vdW-DF2 potential of Fig. 3.

n	ϵ_n [meV]			
	H_2		D_2	
	DFT	Exper.	DFT	Exper.
0	-30.8	-23.9	-32.7	
1	-19.1	-15.6	-23.9	-19.0
2	-10.2	-8.8	-16.4	-12.9
3	-3.5	-5.0	-10.8	-8.9
4			-5.5	-5.6
5			-1.6	-3.3

shown by the small measured corrugation [3]. The basic interaction is essentially one-dimensional, resulting in a potential-well depth of around 30 meV for the three copper faces.

The MBS data have been analyzed within the traditional theoretical picture of the interaction between inert adsorbates and metal surfaces. This picture approximates the PES as a superposition of a long-range vdW attraction, V_{vdW}, and a short-range Pauli repulsion, V_R, reflecting overlap between tails of metal Bloch electrons and the adparticle's closed-shell electrons [5, 29]. Calculations of H_2 physisorption on simple and noble metals have been made with a jellium model of the metal substrate, resulting in a laterally and angularly averaged potential $V_o(z) = V_R(z) + V_{vdW}(z)$, where

$$V_R(z) = V_{R0} \exp{(-\alpha z)} \qquad (1)$$

and

$$V_{vdW}(z) = -\frac{C_{vdW}}{(z - z_{vdW})^3} f\left(2k_c(z - z_{vdW})\right). \qquad (2)$$

Here z is the normal distance of the H_2 bond center from the jellium edge. V_{R0} and α determine the strength and range of the repulsive potential and are sensitive to the metal work function and the electron density at the selvage [5]. The vdW constant, C_{vdW}, and reference-plane position, z_{vdW}, depend on the dielectric properties of metal substrate and adsorbate. The function $f(x)$ introduces a saturation of the attraction at atomic-scale separations. However, $f(x)$ lacks a rigorous prescription, which results in a level of arbitrariness to Eqs. (1) and (2). Tuning to experimental data provides a possible empirical solution to this dilemma. It should be stressed that we only use the cut off function f in Eq. (2) to contruct the physisorption potential from detailed experimental data, and not in the vdW-DF calculations.

For H_2 and D_2 on low-index surfaces of Cu, spectra of bound levels have been deduced from resonance-scattering measurements with monochromatic, well-collimated molecular beams. The particle may be diffracted in selective adsorption, where it is trapped
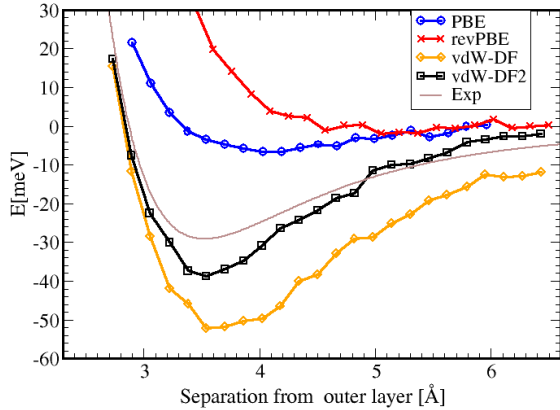
FIG. 1: Experimentally determined effective physisorption potential for H_2 on Cu(111) (solid curve) [3], compared with potential-energy curves for H_2 on Cu(111), calculated for the atop site in GGA-revPBE (red crosses), GGA-PBE (blue circles), vdW-DF2 (black squares), and vdW-DF (yellow diamonds).

FIG. 2: Interaction potential for H_2 on Cu(111), calculated with the vdW-DF2 functional in the bridge, hollow and atop sites. The inset shows the interaction potential for H_2 on Cu(111) in the top site, calculated with the vdW-DF2 functional [10] self-consistently (SC) [9] and non-self-consistently (NSC), *i.e.* perturbatively, like in Ref. 7.

into bound states of the potential well with enhanced kinetic energy along the surface plane. For the bound-level sequences for H_2 and D_2 on the Cu(111) surface, as observed using nozzle beams of para-H_2 and normal-D_2 at suitable nozzle temperatures, the beams are predominantly composed of $j = 0$ molecules. This implies that measured bound-level energies, ϵ_n (listed in Table I for H_2 and D_2 on Cu(111)), refer to an isotropic distribution of the molecular orientation. For this particular ordering, all ϵ_n values fall accurately on a common curve, when plotted versus the mass-reduced level number $\eta = (n + 1/2)/\sqrt{m}$. This implies a level assignment that is compatible with a single gas-surface potential for the two hydrogen isotopes [4]. A third-order polynomial fit to the data yields for $\eta = 0$ a potential-well depth $D = 29.5$ meV. The bound-level sequences in Table I can be accurately reproduced (< 0.3 meV) by a physisorption potential given by Eqs. (1) and (2), having a well depth of 29.5 meV and a potential minimum located 3.50 Å outside the topmost layer of copper ion cores. From the measured intensities of the first-order diffraction beams, a very small lateral variation of the H_2-Cu(111) system can be deduced (less than 0.5 meV between minimum and maximum at minimum of potential well).

Thus, identification of resonances in diffractive selective adsorption scattering of atoms and molecules, like He, Ne, Ar, and H_2, at Cu surfaces provides an accurate data bank of experimental information that challenges any proposal for a relevant PES and for an approximate density functional. Here the vdW-DF [7, 9] and vdW-DF2 [10] functionals are benchmarked.

The original vdW-DF version is derived with electron-gas assumptions apt for extended systems [7–9, 30], us-
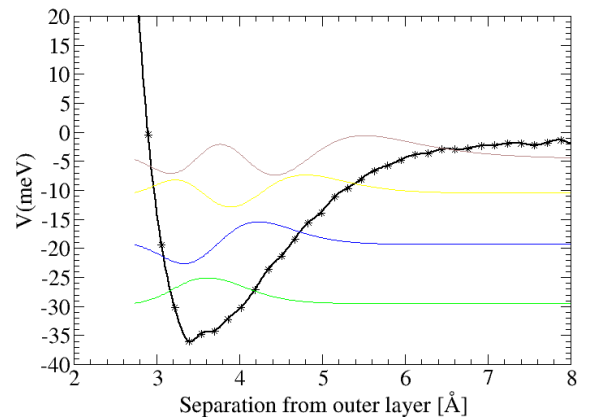
FIG. 3: Interaction potential for H_2 on Cu(111) in the atop site, calculated with the vdW-DF2 functional [10]. Calculated wavefunctions in this potential, drawn at energy levels given in Table I.

ing revPBE [31] exchange, good at separations in typical vdW complexes [7, 9]. The latter choice can be improved on [20, 32–34]. The vdW-DF2 functional [10] employs the PW86 exchange functional [19] and a molecule-type non-local correlation functional. Here promising results on the S22 benchmark set [10] are supplemented with vdW-DF2 results that compare well with experimental data for an extended system.

Figure 1 compares the experimental physisorption potential with PES's for H_2 in flat orientation above an atop site on the Cu(111) surface, calculated with the vdW-

DF with the GPAW code [35]. The PES's of Fig. 1 are calculated in the original perturbative vdW-DF way [7]. GGA gives an inadequate PES, revPBE providing a GGA exchange functional with almost no "fake" attraction [7, 32], and PBE exchange giving a weak attraction for wrong reasons. The description of vdW forces requires an account of nonlocal correlations. The calculated well depth in vdW-DF, 53 meV (65 meV with dacapo [36, 37]), should be compared with the measured one (Fig. 1), 29.5 meV, and that calculated with Eqs. (1) and (2), suitably parametrized, 28.5 meV [3].

Figure 1 also indicates that the vdW-DF2 PEC lies close to the experimental physisorption potential, both at the equilibrium position and at separations further away from the surface. Calculated PEC's of H_2 above bridge, atop, and center sites on the Cu(111) surface are shown in Fig. 2, their closeness illustrating the lack of corrugation on this surface, as in experimental findings [3, 4]. Similar results for bridge, atop, and center sites on Cu(100) show the PES's on the two surfaces to be very close to each other, just like for the experimental result [3, 4]. The vdW-DF equilibrium separation is about 3.5 Å, a value close to the value 3.4 Å that can be deduced from the experimental data, using Eqs. (1) and (2) and reasonable physical assumptions about the parameters [3, 4].

A further refined comparison with experimental data is provided by the bound energy levels in the selective adsorption of H_2 that are deduced from the resonant-backscattering intensities (experimental numbers in Table I) [3, 4]. Calculated eigenvalues and eigenfunctions for the point-of-gravity motion of H_2 in the vdW-DF2 potential are shown in Table I comparing calculated eigenvalues with the measured ones. The analysis [6] above with the traditional physisorption potential (Eqs. (1) and (2)) gives a well depth $D = 29.5$ meV and bound-level sequences accurately reproduced (< 0.3 meV) by empirical tuning of potential parameters. This depth should be compared with that of the vdW-DF2 potential in Fig. 1, $D = 37$ meV. Coming from a first-principles method, where characteristic electron energies are typically in the eV range, this is promising. So is the relative closeness of experimental and calculated eigenenergy values (Table I).

However, the discrepancies between the eigenvalues signals that the vdW-DF2 PEC might not have the right shape (in contrast to the S22 results of Ref. 10). A second look at Fig. 1 reveals that at intermediate z values the vdW-DF2 PEC lies slightly above the physisorption potential. For a well established conclusion, higher accuracies are called for, both in the analysis of experimental

data and in the numerical procedures, however. On the theory side, there is an uncertainty of 3 meV or more in the numerical procedure. Also, the set of default choices used in the GPAW calculations are not designed to deliver an account of the interaction tails and minima which ensures accuracy on the meV level [38], and this creates, for instance, the noise in the PEC curves of Figs. 1 and 3. A revPBE calculation shows this noise to be present already at the GGA level and leaves smooth E_c^{nl} curve. Further, in the vdW-DF2 functional, the exchange part has not yet settled down on an optimal approximative functional. On the experimental side, in the constructions of the PEC from direct measurements, it would be valuable to perform the LeRoy analysis [6], without the restrictive assumptions of Eqs. (1) and (2) and with consideration of the surface configuration from the start.

In summary, accurate and extensive experimental data for the physisorption PEC of H_2 on Cu(111) are used to evaluate vdW-DF functionals and their adequacy for metal surfaces. Several qualitative similarities are found for both vdW-DF and vdW-DF2 functionals. The vdW-DF2 functional gives PEC's in quantitative agreement with the experimental PEC, with respect to well depth, equilibrium separation, and main shape of PEC, which is very promising for applications of this nonlocal correlation functional at short, intermediate and other separations relevant for the adsorption. However, the accuracy of data is high enough to stimulate an improved analysis of both experiment and theory on a higher level, which should be valuable for the further XC-functional development. The Cu(111) is chosen here, as its flatness implies clarity in the analysis and eliminates several side-issues that could have made interpretations fuzzier. Frequent comparisons with results for the Cu(100) give support for the generality of our conclusions. As the experimental results informs on about many properties, incl. steepness of the potential wall, strength of lateral corrugation, energy transfer, possible quasi-bound states, and couplings between translation, vibration, and rotation of the particle, the method has important ramifications.

[1] P. Hohenberg and W. Kohn Phys. Rev. **136**, B864 (1964).
[2] W. Kohn and L.J. Sham, Phys. Rev. **140**, A1133 (1965).
[3] S. Andersson and M. Persson, Phys. Rev. Lett. **70**, 202 (1993).
[4] S. Andersson and M. Persson, Phys. Rev. B **48**, 5685 (1993).
[5] See, *e.g.*, M. Persson and S. Andersson, Chapter 4, "Physisorption Dynamics at Metal Surfaces", in Handbook of Surface Science, Vol. 3 (Eds. E. Hasselbrink and B.I. Lundqvist), Elsevier, Amsterdam (2008), p. 95.
[6] R. J. Le Roy, Surf. Sci. **59**, 541 (1976).
[7] M. Dion, H. Rydberg, E. Schröder, D.C. Langreth, and

B.I. Lundqvist, Phys. Rev. Lett. **92**, 246401 (2004) and **95**, 109902 (2005).

[8] D.C. Langreth, M. Dion, H. Rydberg, E. Schröder, P. Hyldgaard, and B.I. Lundqvist, Int. J. Quant. Chem. **101**, 599 (2005).

[9] T. Thonhauser, V.R. Cooper, S. Li, A. Puzder, P. Hyldgaard, and D.C. Langreth, Phys. Rev. B **76**, 125112 (2007).

[10] K. Lee, É.D. Murray, L. Kong, B.I. Lundqvist, and D.C. Langreth, Phys. Rev. B (RC) **82**, 081101 (2010).

[11] D.C. Langreth and J.P. Perdew, Solid State Commun. **17**, 1425 (1975).

[12] O. Gunnarsson and B.I. Lundqvist, Phys. Rev. B **13**, 4274 (1976).

[13] D.C. Langreth and J.P. Perdew, Phys. Rev. B **15**, 2884 (1977).

[14] D.C. Langreth and S.H. Vosko, in "Density Functional Theory of Many-Fermion Systems", ed. S.B. Trickey, Academic Press, Orlando, 1990.

[15] A.D. Becke, Phys. Rev. A **38**, 3098 (1988).

[16] J. Schwinger, Phys. Rev. A **22**, 1827 (1980).

[17] J. Schwinger, Phys. Rev. A **24**, 2353 (1981).

[18] P. Elliott and K. Burke, Can. J. Chem. **87**, 1485 (2009).

[19] J.P. Perdew and Y. Wang, Phys. Rev. B **33**, 8800(R) (1986).

[20] É.D. Murray, K. Lee, and D.C. Langreth, Jour. Chem. Theor. Comput. **5**, 2754 (2009).

[21] P. Jurečka, J. Šponer, J. Černý, P. Hobza, Phys. Chem. Chem. Phys. **8**, 1985 (2006).

[22] D. Sherrill, T. Takatani, and E. G. Hohenstein, J. Phys. Chem. A **113**, 10146 (2009).

[23] L. F. Molnar, X. He, B. Wang, and K. M. Merz, J. Chem. Phys. **131**, 065102 (2009).

[24] T. Takatani et al., J. Chem. Phys. **132**, 144104 (2010).

[25] R. Podeszwa, K. Patkowski, and K. Szalewicz, Phys. Chem. Chem. Phys. **12**, 5974 (2010).

[26] D.C. Langreth, B.I. Lundqvist, S.D. Chakarova-Käck, V.R. Cooper, M. Dion, P. Hyldgaard, A. Kelkkanen, J. Kleis, L. Kong, S. Li, P.G. Moses, E. Murray, A. Puzder, H. Rydberg, E. Schröder, and T. Thonhauser, J. Phys.: Cond. Mat. **21**, 084203 (2009).

[27] L. Z. Kong, G. Roman-Perez, J. M. Sole, and D. C. Langreth, Phys. Rev. Lett. **103**, 096103 (2009).

[28] K. Lee et al., Phys. Rev. B **82**, 155461 (2010).

[29] E. Zaremba and W. Kohn, Phys. Rev. B **15**, 4 1769 (1977).

[30] H. Rydberg, B.I. Lundqvist, D.C. Langreth, and M. Dion, Phys. Rev. B **62**, 6997 (2000).

[31] Y. Zhang and W. Yang, Phys. Rev. Lett. **80**, 890 (1998).

[32] A. Puzder, M. Dion, and D.C. Langreth, J. Chem. Phys. **126**, 164105 (2006).

[33] J. Klimeš, D.R. Bowler, and A. Michaelides, J. Phys.: Condens. Matter **22**, 022201 (2010).

[34] V.R. Cooper, Phys. Rev. B **81**, 161104(R) (2010).

[35] J.J. Mortensen, L.B. Hansen, K.W. Jacobsen, Phys. Rev. B **71**, 035109 (2005).

[36] Open-source plane-wave DFT computer code DACAPO, http://wiki.fysik.dtu.dk/dacapo.

[37] S.R. Bahn and K.W. Jacobsen, Comput. Sci. Eng. **4**, 56 (2002).

[38] E. Londero and E. Schröder, Computer Physics Communications, in press (2011).

Paper 7

A. Møgelhøj, A. K. Kelkkanen, K. T. Wikfeldt, J. Schøtz, J. J. Mortensen, L. G.
M. Pettersson, B. I. Lundqvist, K. W. Jacobsen, A. Nilsson and J. K. Nørskov,
**Ab initio van der Waals interactions in simulations of water alter
structure from mainly tetrahedral to high-density-like**,
submitted to Journal of Chemical Physics

Ab initio van der Waals interactions in simulations of water alter structure from mainly tetrahedral to high-density-like

Andreas Møgelhøj[a,d], André Kelkkanen[a,b], K. Thor Wikfeldt[c], Jakob Schiøtz[a], Jens Jørgen Mortensen[a], Lars G.M. Pettersson[c], Bengt I. Lundqvist[a,b], Karsten W. Jacobsen[a], Anders Nilsson[d] and Jens K. Nørskov[a,e,f]

[a]*Center for Atomic-scale Materials Design (CAMD),*
Department of Physics, Building 307, Nano DTU,
Technical University of Denmark, DK-2800 Kgs. Lyngby, Denmark
[b]*Department of Applied Physics, Chalmers University of Technology SE-412 96 Göteborg, Sweden*
[c]*Department of Physics, Stockholm University, SE-106 91 Stockholm, Sweden*
[d]*Stanford Synchrotron Radiation Lightsource, 2575 Sand Hill Road, Menlo Park, California 94025, USA*
[e]*SLAC National Accelerator Laboratory, 2575 Sand Hill Road, Menlo Park, California 94025, USA and*
[f]*Department of Chemical Engineering, Stanford University, Stanford, CA 94305, USA*
(Dated: January 28, 2011)

The structure of liquid water at ambient conditions is studied in *ab initio* molecular dynamics simulations using van der Waals (vdW) density-functional theory, *i.e.* using the new exchange-correlation functionals optPBE-vdW and vdW-DF2. Inclusion of the more isotropic vdW interactions counteracts highly directional hydrogen-bonds, which are enhanced by standard functionals. This brings about a softening of the microscopic structure of water, as seen from the broadening of angular distribution functions and, in particular, from the much lower and broader first peak in the oxygen-oxygen pair-correlation function (PCF), indicating loss of structure in the outer solvation shells. In combination with softer non-local correlation terms, as in the new parameterization of vdW-DF, inclusion of vdW interactions is shown to shift the balance of resulting structures from open tetrahedral to more close-packed. The resulting O-O PCF shows some resemblance with experiment for high-density water (A. K. Soper and M. A. Ricci, Phys. Rev. Lett., 84:2881, 2000), but not directly with experiment for ambient water. However, an O-O PCF consisting of a linear combination of 70% from vdW-DF2 and 30% from experiment on low-density liquid water reproduces near-quantitatively the experimental O-O PCF for ambient water, indicating consistency with a two-liquid model with fluctuations between high- and low-density regions.

I. INTRODUCTION

Liquid water plays a crucial role in all biological and numerous chemical processes which has been the incentive for many detailed experimental and theoretical studies probing both structural and dynamical properties of the fluid. However, the microscopic structure of ambient liquid water is still a matter of recent debate.[1–23] In particular two classes of models are currently being considered, where the traditional model of water is based on a continuous distribution of distorted tetrahedral structures. This is typical of what most molecular dynamics simulations currently give. However, most of these simulations give over-structured O-O and O-H pair-correlation functions (PCFs) and show discrepancies in comparison to x-ray and neutron scattering experimental data.[10,14] It is, however, possible to generate a more distorted tetrahedral structure model that is consistent with the diffraction data, but equivalent agreement is seen also for alternative asymmetrical and mixture models illustrating that diffraction data do not discriminate between differently hydrogen-bonded structure models.[10,14,24] Based on recent findings correlating x-ray emission spectroscopy (XES) with x-ray Raman scattering (XRS) and small angle x-ray scattering (SAXS) data,[15] a model has been suggested where a division into contributions from two classes of local instantaneous hydrogen-bonded structures is driven by incommensu-

rate requirements for minimizing enthalpy and maximizing entropy; in particular the XES data shows two well-separated peaks, which interconvert with changes in temperature.[12,15,19] In the proposed picture the dominating class consists of a continuum of structures with some resemblance to high-pressure water,[15] but with a further expanded first shell (more distorted H-bonds) and more disorder in the 2nd shell; this was based on the temperature dependent shift of the dominating peak in the XES spectra indicating more thermal distortion and disorder with increasing temperature. The second class corresponds to fluctuations where regions of strongly tetrahedral structures (similar to low-density water) appear in different sizes and shapes with a mean size interpreted from the SAXS data as ~1nm,[15] but naturally many sizes and shapes would appear. It should be emphasized that since these are fluctuations no strict boundaries between the two classes should be expected. The attosecond (XRS, SAXS) to femtosecond (XES) time scales of the experimental probes are too fast for molecular motion to be followed and the experimental data thus correspond to a statistical sampling of instantaneous, frozen local structures in the liquid; no experimental information on the time-scale of such fluctuations is thus currently available.[15] Besides being consistent with both neutron and x-ray scattering,[14] this picture was recently also shown to bring a consistency between x-ray scattering and extended x-ray absorption fine structure (EXAFS) data, requiring both a fraction of straight, strong hydrogen-

bonds and disordered structures.[25] However, other opinions exist regarding the interpretation of SAXS, XES and XRS.[2,8,11,17,18,20–23]

Most simple rare gas solids and liquids have a nearest-neighbor coordination of 12 whereas hexagonal ice, due to the directional H-bonds has a coordination of only 4. The latter leads to large open spaces in the ice lattice and low density. The dispersion, or vdW force, in condensed rare gases leads to non-directional, isotropic interactions. Similarly the inclusion of vdW interactions in *ab initio* simulations of water may counteract the directional interactions and lead to better agreement with, *e.g*, experimental PCFs where it should be understood that, while this could be regarded as a minimum requirement of a water model, it is by no means sufficient for a complete description. Interestingly, it has been argued on thermodynamic grounds that over a large range of the liquid-vapor coexistence line the averaged water interaction potential should resemble that of liquid Argon.[26]

Water shows many anomalies in its thermodynamic properties, such as compressibility, density variation and heat capacity.[27,28] In attempts to explain this, directional H-bonds and more isotropic vdW forces are key concepts. While vdW forces are well defined as results of non-local electronic correlations, there is no unique way to characterize H-bonds in terms of topology or interaction strength. And yet "the H-bond governs the overall structure and the dynamics of water".[29] One of the models to explain the enhanced anomalies in supercooled water is the liquid-liquid critical-point (LLCP) hypothesis,[30–32] with the most substantial role played by cooperative H-bond interactions among the water molecules.[33] The LLCP model explains the significant increase in density fluctuations upon supercooling water, which is evidenced by the anomalously increasing isothermal compressibility,[34] as resulting from the local formation of open tetrahedrally coordinated H-bond regions. It furthermore connects the deeply supercooled liquid state of water to the polyamorphism seen in ices, *i.e.* the distinct low-density and high-density amorphous ice phases (LDA/HDA). A high-density liquid (HDL) phase transforms to an ordered low-density phase (LDL) in the deeply supercooled region, through a first-order phase transition at high pressures above the LLCP and through a continuous smooth transition upon crossing the Widom line at ambient pressure.[32,35–38] There are differences in their respective local structures; in pure HDL the local tetrahedrally coordinated H-bond structure is perturbed by a partially collapsed second coordination shell, while in the LDL a more open and locally "bulk-ice-like" H-bond network is realized.[16,35]

The combined XES, XAS and SAXS results described above,[15] which indicated nanoscale density and structural fluctuations, can be easily interpreted as reflections of this "competition" between the two local forms, HDL (maximizing entropy) and LDL (minimizing enthalpy) and thus viewed as extending an established picture of supercooled water into the ambient regime. Whether HDL and LDL can exist as pure phases, accompanied by a liquid-liquid phase transition and a critical point, is still unresolved and alternative models, *e.g.*, singularity-free (SF),[31,39] the critical-point-free (CPF)[40] and stability limit (SL) conjecture[41] scenarios have been proposed, however still building on structural HDL/LDL fluctuations.

In the quantitative characterization of water, computer simulations play a vital role. Empirical force fields are frequently applied but with a questionable transferability since force fields are parameterized against experimental data or against a limited set of quantum chemically computed structures. Furthermore, many-body interactions beyond pair-interactions are frequently not taken into account. These deficiencies are eliminated in Car-Parrinello[42] (CP) and Born-Oppenheimer (BO) molecular dynamics (MD), collectively known as *ab initio* (AI) MD. In AIMD, the forces are calculated using a first-principles electronic structure method, typically based on density functional theory (DFT). BOMD, used in the present study, minimizes the Kohn-Sham energy functional at each time step, keeping the nuclear positions frozen. In nearly all force field and *ab initio* molecular dynamics (MD) simulations of water at ambient conditions there seems to be a strong driving force to form highly directional hydrogen bonds (H-bond) leading to tetrahedral structures that are in general over-structured in terms of the derived PCFs. One exception is the coarse-grained mW water model[43] which has two terms in the interaction potential corresponding to anisotropic tetrahedral interactions and isotropic van der Waals (vdW) interactions, respectively, and which gives a maximum peak height of 2.3 in the O-O PCF at room temperature, in close agreement with recent analyses of experimental diffraction results.[10,14,44–46] This model was shown to feature fluctuations between tetrahedral and disordered species resulting in a liquid-liquid transition in the supercooled region.[47] Empirical force-field models which have over-structured PCFs in agreement with older determinations[48,49] have however also been shown to exhibit liquid-liquid phase transitions in the supercooled regime, *e.g.*, Refs. 32,50 and 51, indicating that the PCFs are not decisive for general trends in the thermodynamic behavior in water simulations.

Until recently, AIMD simulations of water have almost exclusively been performed with the BLYP[52] and PBE[53] exchange-correlation (XC) functionals. However, these functionals are shown to significantly over-structure liquid water,[54] as seen from the maximum value and sharpness of the first peak in the oxygen-oxygen PCF.[10,14,44–46,55,56] AIMD simulations of water have furthermore been shown to depend on which functional is applied and to give different predictions for different XC functionals.[57] MD simulations performed using generalized gradient approximations (GGA) tend to over-structure liquid water and lead to diffusion constants two to three times too small compared to experiment; using hybrid functionals only marginally improves the

results.[58] In addition, it has been shown that PBE-based AIMD simulations lead to a melting point of ice at 417 K and therefore simulations at ambient conditions with this functional will describe a deeply supercooled state which is over-structured with respect to real liquid water at ambient conditions.[59] As we will show in the following, inclusion of the more isotropic vdW interaction balances the directional forces allowing a partial break-down of the H-bond network and a much less structured liquid.

II. METHODS

A. Role of van der Waals forces

Small water clusters have been studied using the PBE and BLYP XC functionals, which do not explicitly include van der Waals (vdW) interactions, and the results compared to high accuracy methods such as coupled cluster (CCSD(T)) and Møller-Plesset (MP2). Near chemical accuracy for the strength of the H-bond for the water dimer is obtained using PBE[60] while BLYP consistently underbinds small water clusters.[61] However, discrepancies arise and increase with the size of the water cluster for both PBE and BLYP which has been ascribed to the lack of a description of vdW forces.[61] One could thus argue that obtaining the correct result for the water dimer is no guarantee for a correct description since not all physical interactions relevant for larger clusters are sampled by the dimer.

While it is well established that H-bonds give the major contributing factor to the dynamics and structure of water, vdW interactions have also been suggested to be important[62,63] and, in line with this, thermodynamic considerations have led to the suggestion that the averaged water interaction potential should resemble that of liquid Argon.[26] The angular dependence of the H-bond is anticipated to have a big impact on the PCF and self-diffusion coefficient.[64] If, for example, it is too difficult to bend a DFT H-bond, the diffusion coefficient should come out too small, which it does. Many other suggestions to explain the too small diffusion coefficient exist however[64] but balancing the directional H-bond interactions with more isotropic vdW forces would intuitively contribute to softening the H-bond network and allow more efficient diffusion. Traditional local and semi-local DFT do not, however, contain non-local vdW interactions, e.g., BLYP being especially incapable of describing dispersion.[65] Influences of vdW interactions have been investigated using MD based on empirical potentials,[62,66] e.g., performed with a dispersion-corrected BLYP XC functional,[67] or using empirically damped C_6R^{-6} corrections[68–70] to describe the vdW interactions.

A way to introduce vdW forces in DFT from first principles is provided by the van der Waals density functional vdW-DF,[71] recently used for the first time in AIMD on liquid water.[72] The inclusion of vdW forces using the vdW-DF was shown to greatly improve water's equilib-

rium density and diffusivity. However the vdW-DF MD also produces a collapsed second coordination shell giving rise to new structural problems that have been suggested to depend partially on the choice of exchange used in the vdW functional.[72]

The vdW-DF method proposed by Dion et al.[71] accounts for exchange by an exchange functional that gives Hartree-Fock-like repulsion at relevant separations and that includes non-local correlation, and thus vdW forces, by calculating the dielectric response in a plasmon-pole approximation. It gives the correct stability trend for low-lying water hexamers[73] but returns a significant underbinding for most H-bonds.[73–75] The underbinding can be remedied by using an exchange functional that gives more binding[76] at typical H-bond separations,[73,74,77] like the PW86,[78] optPBE,[79] and C09[80] exchange functionals. Recently Klimes et al.[79] proposed a new vdW density functional, optPBE-vdW, based on the original vdW-DF functional.[71] This scheme shows promise in the description of dispersion and H-bond systems, as it reduces the underbinding given by the vdW-DF down to chemical accuracy while preserving the correct hexamer trends. However, this improved behavior is obtained at the cost of poorer performance on the binding energy of small molecules.[81] Very recently a second version of the vdW-DF, called vdW-DF2, was suggested,[82] using a new non-local correlation functional along with PW86 as an appropriate exchange functional. Both optPBE-vdW and vdW-DF2 give chemical accuracy on the water dimer, albeit with slightly different non-local-correlation and exchange functionals. In the present study we therefore wish to investigate the microscopic structure of liquid water by performing AIMD using both the new optPBE-vdW and vdW-DF2 XC functionals to also investigate the importance of the balance between correlation and exchange in liquid water AIMD simulations.

B. The optPBE-vdW and vdW-DF2 exchange-correlation functionals

In general a vdW-DF functional takes the form

$$E_{xc} = E_x^{\text{GGA}} + E_c^{\text{LDA}} + E_c^{\text{nl}}, \qquad (1)$$

where E_x^{GGA} is an exchange functional using the generalized gradient approximation (GGA), E_c^{LDA} accounts for the local correlation energy by using the local density approximation (LDA). LDA is chosen to avoid double counting of correlation. The non-local correlation energy describing the vdW interaction is given by the six-dimensional integral[71]

$$E_c^{\text{nl}} = \frac{1}{2} \int \int n(\mathbf{r})\phi(\mathbf{r}, \mathbf{r}')n(\mathbf{r}')\mathrm{d}\mathbf{r}\mathrm{d}\mathbf{r}', \qquad (2)$$

where $\phi(\mathbf{r}, \mathbf{r}')$ is the interaction kernel and depends on the density and its gradient. The non-local term is calculated as suggested in Ref. 83. In the original vdW-DF from

Dion *et al.* the exchange functional from revPBE[84] is utilized.

The optPBE-vdW functional is constructed like vdW-DF[71] but uses an alternative exchange functional. The latter takes the same form as both the PBE and RPBE exchange, but the parameters of the exchange enhancement factor are optimized against the S22 database. [79] The S22 database[85] is a set of 22 weakly interacting dimers, mostly of biological importance, including the water dimer.

The vdW-DF2[82] has the form of Eq. (1) and uses the PW86 exchange,[86] which is argued in Ref. 77 to give the most consistent agreement with Hartree-Fock (HF) exact exchange, and with no spurious exchange binding. Furthermore, a new approximation for E_c^{nl} is used to calculate the value of the interaction kernel in Eq. (2).[82] This new functional has been shown to give very accurate results for the water dimer as compared to benchmark CCSD(T) calculations[82,87] and to compare closely to the present S22 benchmark. [88]

C. Computational protocol

Ab initio molecular dynamics simulations are performed in the NVE ensemble with optPBE-vdW, vdW-DF2, and PBE, using the grid-based real-space projector augmented wave code, GPAW.[89,90] A wave function grid spacing of 0.18 Å and Fermi smearing with a width of 0.01 eV have been used. The grid spacing has been determined by comparing DFT calculations of water hexamers with CCSD(T) results. In the electronic structure calculations a strict energy convergence criterion of 10^{-7} eV per electron is used in order to determine the forces adequately.

All internal bond lengths are kept fixed at 0.9572 Å (an MP2 optimized gas phase geometry obtained from the G2-database)[91] but angles are allowed to vary (*i.e.* bending vibrations are included); eliminating the high-frequency OH-stretch allows longer time steps in the simulations. In the initial configuration 64 water molecules are placed in a simple cubic lattice with random orientations in a cubic periodic box with side lengths 12.42 Å, to reproduce a water density of 1 g/cm^3. The geometry is then optimized to obtain a configuration at zero Kelvin (using PBE), from which the MD is started giving the atoms random velocities according to a Maxwell-Boltzmann velocity distribution corresponding to two times 300K, keeping the center of mass of the box stationary. Approximately half of the kinetic energy converts to potential energy thus giving an average temperature around 300K. An initial equilibration of 10 ps using the PBE XC functional is performed followed by 2.5 ps vdW equilibration of the simulations using optPBE-vdW and vdW-DF2. For all methods equilibration was followed by production runs for 10 ps which is the minimum time reported necessary due to the slow diffusion of water.[92] Using 64 water molecules has been shown to be adequate

to remove the most significant problems concerning finite size effects[93] and is feasible within the current computational capabilities. The Verlet algorithm is employed using a time step of 2 fs in the NVE ensemble. Using this type of ensemble the temperature is allowed to fluctuate and the average temperature of the PBE, vdW-DF2 and optPBE-vdW simulations were 299K, 283K and 276K, respectively.

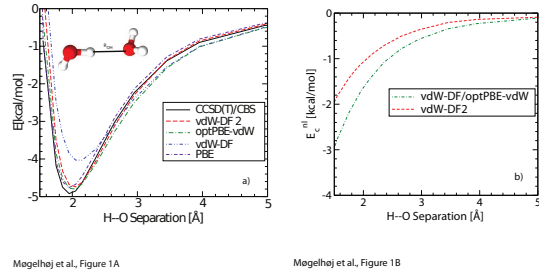Møgelhøj et al., Figure 1A   Møgelhøj et al., Figure 1B

FIG. 1: a) The water dimer potential energy curves calculated with DFT using the XC functionals PBE, vdW-DF, vdW-DF2 and optPBE-vdW, respectively, are compared to CCSD(T)/CBS wave function results.[87] b) The distance dependence of the non-local contribution (Eq. (2)) to the interaction energy of the water dimer for the XC functionals vdW-DF2 and optPBE-vdW, shows that, when they give similar potential energies (Fig. 1a)) they do so for different reasons; the optPBE-vdW gets more binding from a stronger vdW attraction but vdW-DF2 gets more net attraction from a less repulsive exchange.

III. RESULTS

A. Water dimer

Before discussing the MD results we compare the functionals for a simpler but still relevant system: the water dimer. Fig. 1 a) illustrates the potential energy curve for the water dimer calculated using PBE, vdW-DF, vdW-DF2 and optPBE-vdW in comparison with the benchmark CCSD(T) curve from Ref. 87. Fig. 1 a) shows that the vdW functionals are capable of describing this basic constituent of liquid water extremely accurately, however for different reasons. The non-local contribution (E_c^{nl}) to the dimer binding from the two functionals is plotted in Fig. 1 b). The non-local part of the optPBE-vdW functional, which is based on the older approximation, is more attractive as mentioned in Ref. 82. Since less attraction stems from the non-local interaction in the vdW-DF2, while the total energy for the dimer is almost identical to that of optPBE-vdW, the remaining part of the interaction energy must give a larger contribution for the vdW-DF2 than for optPBE-vdW. The remaining part of the interaction energy includes electrostatic interaction, electronic correlation, and more or less repulsive exchange. Since electrostatic interactions only depend

4

on separation, and local correlation is treated identically with the LDA correlation in both cases, this difference has to come from the different choices for the exchange. The PW86 exchange in vdW-DF2 is hence less repulsive than the optPBE exchange in optPBE-vdW; a possible cause of the reported collapsed second-shell structure was in Ref. 72 suggested to be that the non-local parameterization of exchange used in vdW-DF and optPBE-vdW may be too attractive when used in MD. This is, however, not the case, as seen from the pair-correlation functions (PCFs), to be discussed next.

B. Pair-correlation functions

Fig. 2 a) illustrates that AIMD simulations of liquid water using vdW-DF2 and optPBE-vdW give very similar O-O PCFs which are, however, very different from the O-O PCF from PBE and furthermore from those derived from experiment using either Empirical Potential Structure Refinement (EPSR)[44] or Reverse Monte Carlo (RMC) [94] to fit the structure factor.[10,14] In the simulations both functionals result in the same characteristics as reported in Ref. 72, including a lower first peak shifted to larger O-O separation than for normal GGAs as well as for experiment on ambient water. The second coordination shell at 4.5 Å is also completely smeared out where correlations from the region 4-5 Å have instead moved into the region 3.3-3.7 Å. The non-local correlation differences in the functionals do not, however, result in significantly different O-O PCFs. In contrast, the very recent vdW-DF MD simulation showed that by changing the exchange in vdW-DF from revPBE to PBE, the second shell structure again became well defined.[72] However, the exchange functionals of revPBE and PBE are quite different, and the potential of the dimer is not reproduced very well using the PBE exchange with LDA and non-local correlation.
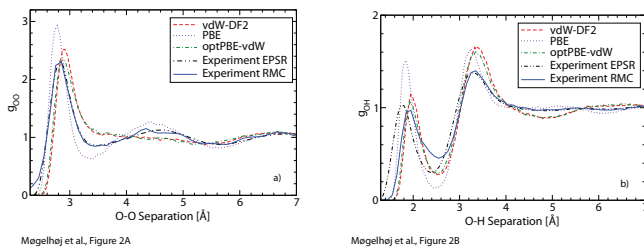

Møgelhøj et al., Figure 2A

Møgelhøj et al., Figure 2B

FIG. 2: a) Oxygen-oxygen PCFs (g_{OO}) obtained from experimental data using EPSR[44] and RMC[14] in comparison with PCFs obtained by DFT MD simulations using PBE, optPBE-vdW and vdW-DF2. b) Oxygen-hydrogen PCFs (g_{OH}) obtained from experimental data using EPSR[44] and RMC[14] in comparison with PCFs from PBE, optPBE-vdW and vdW-DF2.

Compared to the experimentally derived O-O PCFs it is clear that the PCF obtained from PBE is severely over-

structured while the simulations including vdW forces have resulted in a structure significantly less structured than what is experimentally observed for ambient liquid water. We will return to this point in the discussion section below.

Some discrepancy in the O-H PCF function for the vdW XC functionals compared to experiment is seen in Fig. 2 b), which we shall now discuss. The O-O correlations can be obtained from a Fourier transform of the x-ray diffraction data, if a large enough Q-range has been measured and the data can be properly normalized; x-ray scattering is strongly dominated by the electron-rich oxygens. Neutron diffraction data, on the other hand, contain simultaneous information on the H-H, O-H and to some extent, the O-O PCFs, making a direct Fourier transform to extract a specific PCF inapplicable. Various fitting schemes of structure models to the experimental structure factors have therefore been developed, and we show two such fits to the same experimental data using the EPSR[44] and RMC method[14], respectively.

There is a significant difference in the first peak position in the O-H PCF between the two methods compared to what is found for the O-O PCF. This can be understood from the relatively lower sensitivity of the neutron data to specifically the O-H correlation in comparison to the sensitivity of x-ray data to the O-O correlation.[14] The EPSR technique uses the assumed reference pair-potential to provide structural aspects not included in the experimental data,[14,24] while structural aspects not determined by the experimental data, or imposed constraints, will in the RMC technique simply result in a phase-space weighted sampling of structures consistent with the experimental structure factors;[95] combining the two methods thus gives additional information on the uncertainties and assumptions in the resulting fits. It is interesting to note that the RMC method gives a shift in the first peak of the O-H correlation out to nearly 2 Å,[14] which agrees well with the vdW MD simulations presented here, while the EPSR solution is closer in position to the PBE, likely reflecting the starting potential in the EPSR fitting procedure. Note, that both the RMC and EPSR fits reproduce the experimental scattering data equally well, implying that the position of the first intermolecular OH correlation is not strictly determined by the data, leaving an uncertainty in the diffraction-derived PCFs.[14,96] The first peak in the PBE O-H PCF is clearly too high and the first minimum at 2.5 Å too low, however, while all three simulations exaggerate the height of the second peak at 3.2 - 3.6 Å.

C. Angular distribution functions and hydrogen-bonding analysis

That the van der Waals functionals provide a smoother angular structure with less tetrahedral bonding can be demonstrated by considering the angular distribution functions and the average number of H-bonds per wa-

ter molecule. The cone criterion from Ref. 1 has been applied as a geometric H-bond definition: $r_{OO} < r_{OO}^{max} - 0.00044\delta_{HOO}^2$, which defines a cone around each H-bond-donating OH group, where $r_{OO}^{max} = 3.3$ Å is the maximum OO distance at zero angle δ_{HOO}, where δ_{HOO} is the H-O$\cdots$O angle quantifying the angular distortion of the H-bond. Table I shows the H-bond statistics for PBE, optPBE-vdW and vdW-DF2. PBE is seen to prefer a tetrahedral structure with a majority of the molecules having 4 H-bonds. With its relatively more repulsive exchange optPBE-vdW gives its water molecules less incentive to choose a fully H-bonded structure, resulting in a larger amount of water molecules having two or three H-bonds. The vdW-DF2 comes in between with its relatively weaker vdW interaction giving slightly higher preference to forming H-bonds. This analysis suggests that there is a competition between isotropic vdW forces and directional H-bonds, resulting in fewer or more H-bonds per water molecule depending on the applied approximations; however, between the vdW models the average number of H-bonds varies only weakly despite differences in vdW strength.
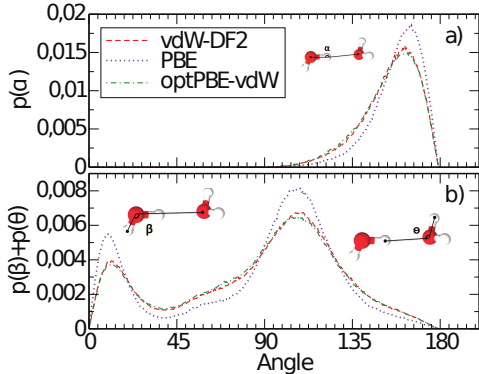
Møgelhøj et al., Figure 3

FIG. 3: Molecular angular distributions in liquid water according to MD simulations using DFT with the indicated functional. a) The angular distribution functions of the O-H$\cdots$O angle. b) the H-O$\cdots$O (first peak) and $\theta = <$H$\cdots$O-H (second peak) angles obtained using the XC functionals PBE (yellow), vdW-DF2 (red) and optPBE-vdW (green). When including vdW interactions a softening of the structure is seen from the broader distribution of angles.

We note in particular the low number of double-donor, double-acceptor tetrahedral molecules according to the cone criterion[1] for the two vdW models. In fact, the large number of broken H-bonds in the vdW simulations suggests that these models are in closer agreement with predictions from x-ray spectroscopies[1,12,15,97] compared to most other AIMD models and future calculated x-ray spectra based on optPBE-vdW and vdW-DF2 structures will provide an interesting opportunity to obtain further insight regarding the interpretation of these spectra.

No. H-bonds \ Method	PBE	optPBE-vdW	vdW-DF2
1	2	10	8
2	12	29	27
3	31	37	38
4	52	22	25
5	3	1	1

TABLE I: Percentage distribution of hydrogen bonds per water molecule calculated using the cone criterion from Ref. 1. PBE results are shown to favor more H-bonds compared to either vdW functional, which both allow for a larger number of molecules to break the tetrahedral structure with four bonds.

The angular distribution functions (ADFs) of the H-bonds are shown in Fig. 3. The ADFs of H-bond acceptor and donor give information on the orientational flexibility of the water molecules. In the ADFs only the angles between a central molecule and the molecules of the first solvation shell are considered by using a cutoff distance corresponding to the first minimum in the PBE O-O PCF; this distance was applied also to the vdW MDs where the second shell is smeared out and no minimum is visible. Fig. 3 a) displays the distributions of donor angles $\alpha = <$O-H$\cdots$O for the various simulations. The first peak in Fig. 3 b) is β, the deviation of the O-H$\cdots$O bond from being linear, which gives information on the flexibility of donor H-bonds while the second peak is the acceptor angle $\theta = <$H$\cdots$O-H. The distribution of angles has been found to depend on the choice of water model.[9] The picture of a competition between non-directional vdW interactions and directed H-bonds seems to be supported by the ADFs as illustrated by the fact that the model without vdW forces (PBE) has no incentive to deviate from a structure of strong H-bonds, thus resulting in a relatively straight H-bond angle. When including vdW forces the H-bonds become significantly more bent. In general a softening of the structure is seen from the broader ADFs obtained in case of the vdW-DFs.

D. Tetrahedrality and asphericity

Two useful measures of the local coordination of molecules in water are the tetrahedrality[98,99] and asphericity[100] parameters. The former quantifies the degree of tetrahedrality in the nearest neighbor O-O-O angles and is defined as

$$Q = 1 - \frac{3}{8}\sum_{i=1}^{3}\sum_{j>i}^{4}\left(\cos\theta_{i0j} + \frac{1}{3}\right)^2 \qquad (3)$$

where θ_{i0j} is the angle formed by two neighboring oxygen atoms i and j and the central molecule 0. Only the four nearest neighbors are taken into account which makes Q a very local measure. Perfect hexagonal ice gives $Q = 1$ for all molecules while the ensemble average over an ideal gas gives $<Q> = 0$.[99] The asphericity parameter is defined

as

$$\eta = \frac{A^3}{36\pi V^2} \qquad (4)$$

where A and V are the area and volume of the Voronoi polyhedron of the molecule in question. Contrary to Q, η is sensitive also to interstitial molecules outside the first shell and to the second coordination shell since these add surfaces to the Voronoi polyhedron, making it more spherical. The two relevant limits for water are that of hexagonal ice, which gives $\eta = 2.25$, and that of a perfect sphere which gives $\eta = 1$; larger disorder in the local coordination thus gives smaller values of η.
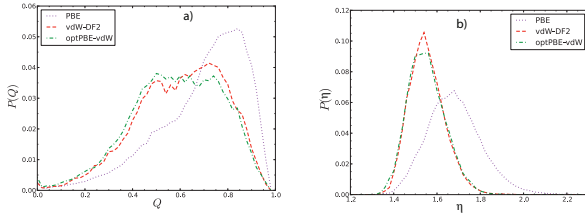
Møgelhøj et al., Figure 4A   Møgelhøj et al., Figure 4B

FIG. 4: a) Distributions of the tetrahedrality parameter Q. vdW interactions lead to significantly lower average tetrahedrality and a strong low-Q peak from interstitial molecules around $Q = 0.5$. b) Distributions of the asphericity parameter η. A large effect of vdW interactions is seen with a shift towards more spherical (less ice-like) values.

As Fig. 4 shows, the inclusion of the vdW interaction has a dramatic effect on both the tetrahedrality and asphericity distributions. The PBE simulation displays a strong peak at $Q = 0.8$, signifying a dominance of locally tetrahedral O-O-O angles, while both vdW simulations show an attenuation and shift of the high-Q peak to lower tetrahedrality along with the appearance of a strong low-Q peak associated with interstitial molecules at non-tetrahedral positions in the first coordination shell. Out of the two vdW models, optPBE-vdW is seen to be somewhat less tetrahedral, consistent with their differences in H-bond statistics and PCFs discussed above. This is clearly illustrated by the average tetrahedrality which is 0.692, 0.602 and 0.583 for PBE, vdW-DF2 and optPBE-vdW, respectively. In comparison the average tetrahedrality has been estimated to be 0.576 using the EPSR method;[101] note, however, that the tetrahedrality parameter is rather uncertain, *i.e.* the same diffraction data have been shown to support tetrahedrality values ranging from 0.488 to 0.603.[14] An even larger difference is seen in the asphericity distributions; the two vdW models show sharper peaks centered at lower asphericity values compared to PBE. This directly reveals the large disorder in second-shell correlations in the vdW models, resulting from the tendency to form more isotropic local structures when vdW forces are included. Similarly to the comparison between the PCFs of the two vdW models discussed above, it can be seen

here that despite non-local differences between vdW-DF2 and optPBE-vdW their respective liquid water structures turn out to be rather comparable in terms of both first- and second-shell correlations. The average asphericity is 1.681, 1.552 and 1.552 for PBE, vdW-DF2 and optPBE-vdW, respectively.

IV. DISCUSSION

Comparison of the results from the simulations using PBE with those including the vdW interactions shows a strong shift in the balance between directional H-bonding and more isotropic interactions; the former leads to tetrahedral H-bond coordination and low density while the latter favors a more close-packed ordering and higher density as evidenced by the loss of distinction between first and second coordination shells and the reduced number of H-bonds in that case. Having two balancing interactions that favor opposite structural properties is a prerequisite for fluctuations; it is clear that by tuning either the importance of H-bonding or the vdW interaction the preference for either structure will be affected in the simulations. If we consider the proposed model of fluctuations between HDL and LDL,[15,102] it could well be that the vdW models under the present conditions only generated an HDL-like structure while without including vdW the resulting structure is more LDL-like.

Computational resources only allow the 64 molecules to be followed for a time of up to about 10 ps. If the two proposed structures of liquid water truly coexist as endpoints of fluctuations in nanosized patches of different local density, as suggested in Ref. 15, then an AIMD with only 64 water molecules in a fixed volume may not be suitable to observe this behavior; a much larger box size or an NPT ensemble simulation allowing the box size to vary would be required. The relatively small simulation (12.42 Å box length) and short run time will only observe a local structure of water which, in this picture, is either approximating LDL- or HDL-like; LDL-like simulations can be performed with the PBE XC functional, which is known to give a local tetrahedrally coordinated H-bond structure, but to prefer a density significantly lower than for ambient water.[72] It should be noted that the simulations are run in the NVE ensemble with density fixed to correspond to ambient conditions which, under the assumption that ambient water is dominated by HDL,[1,12,15,103,104] should favor an HDL-like structure over fluctuations towards LDL, if energetically allowed, as seems to be the case with vdW interactions included.

The structure obtained with the vdW functionals is an important step towards an HDL-dominated liquid at ambient conditions as suggested should be the case by all studies of the phase diagram in the supercooled regime. The tendency towards an HDL-like liquid is seen by comparing the PCFs from MD simulations performed using the vdW-DF2 and optPBE-vdW XC functional (Fig. 5 a)), respectively, with the results of a neutron diffraction
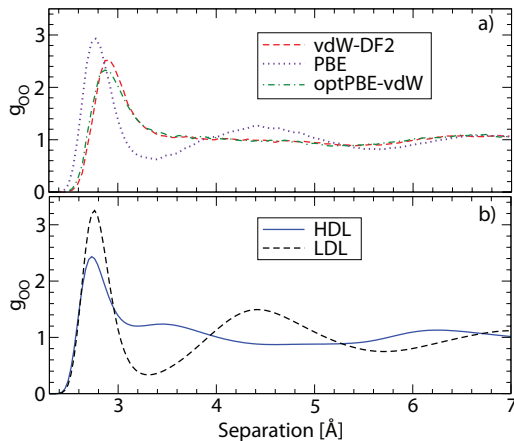
Møgelhøj et al., Figure 5

FIG. 5: a) Oxygen-oxygen PCFs (g_{OO}) obtained by MD simulations from DFT with PBE, optPBE-vdW and vdW-DF2 functionals. b) Experimental PCFs for high- and low-density water.[48]

study[48] where the LDL and HDL PCFs were extrapolated from data at different pressures; the resulting LDL and HDL PCFs are illustrated in Fig. 5 b). The EPSR derived HDL PCF is rather similar to the PCF obtained using a Fourier transform of x-ray diffraction data at high pressures[105] and furthermore seen to be very similar in terms of the second- and third-shell structure to that derived from vdW-DF2 and optPBE-vdW MD simulations; the effect of increasing pressure on the O-O PCF is that the 4.5 Å correlation disappears and moves to the 3.3 - 3.7 Å region and the third shell is shifted down to 6 Å.[105] The O-O PCFs obtained using the vdW functionals similarly show a lack of a well defined structure at 4.5 Å, an increase in correlations at 3.3-3.7 Å and show a shift towards shorter separations in comparison to PBE of the correlation at 6 - 6.5 Å, as is seen from Fig. 5. Both are clear indications towards HDL water. However, in contrast to the high pressure PCFs, a well defined peak at 3.5 Å is not present in the vdW MD simulations, but only an increase in correlations, and the first peak position is shifted outwards, which is not observed for pressurized water. It could be argued that a well-defined peak at 3.5 Å should not be expected since HDL-like water at ambient conditions should be thermally excited with a more expanded first shell and therefore further disordered in comparison to HDL water obtained under pressure.[12,15] In particular, entropy effects due to high thermal excitations leading to higher disorder can be expected to create a structure, where both the first shell and, in particular, the collapsed second shell are distributed over a range of distances, leading to what is often denoted interstitial positions and with the first O-O peak appearing at longer distance when not under pressure. In this respect a comparison with the amorphous high-density (HDA) and very high-density (VHDA) ices is of interest, where for VHDA the second shell moves inwards and a peak at

3.4 Å develops while for HDA the second peak broadens significantly which indicates that various interstitial sites may be occupied making the high-density forms less well-defined.[106–110] It should be mentioned that a peak at ~3.7 Å is present in the MD simulation performed by Wang et al.[72] using the earlier vdW-DF [71] formulation of the functional.

A minimum prerequisite for the hypothesis of fluctuations in the real liquid between HDL and LDL-like local structures is that the O-O PCF can be reproduced in such a picture while keeping in mind that reproducing the details of the O-O PCF does not guarantee a good description in other respects. However, it does provide a significant base-line that should be attained by any model of liquid water. The PCFs are, however, not directly measurable but derived from experimental data and we first need to discuss specifically the choice of O-O PCF for the comparison.

X-ray and neutron diffraction data treated in conjunction, either by the technique of empirical-potential structure refinement (EPSR)[44] or by reverse Monte Carlo (RMC) simulations,[10,14] as well as from directly Fourier transforming the latest high-quality x-ray diffraction data sets,[45,46] give a broad and slightly asymmetric first O-O peak with height 2.1-2.3 which is significantly lower than from standard MD simulations (height ~3) and from previous analyses of either only neutron diffraction data using EPSR[48] or analysis of the total x-ray scattering I(Q) in terms of comparison to computed I(Q) from MD simulations.[49]

There were, however, problems with both the latter approaches[48,49] since neutron diffraction mainly measures H-H and O-H correlations and thus contain insufficient data to modify the initial MD force-field guess in EPSR to a solution that also describes the O-O PCF, which is mainly determined by x-ray diffraction. The assumption by Hura et al.[49] was that some existing MD force-field should describe the total I(Q); the best agreement was found for the TIP4P-pol2 potential from which pair-correlation functions were subsequently extracted. However, the internal molecular scattering strongly dominates I(Q) in x-ray scattering and masks the more relevant intermolecular scattering such that small, but significant discrepancies in phase and amplitude at higher Q,[10] which determine the shape and height of the first O-O peak, were not observed and taken into account. Since the two independent studies based on, respectively, neutron and x-ray diffraction data arrived simultaneously at similar peak height and shape this was understandably taken as proof that the O-O PCF had been determined correctly; however, both studies reproduced in a sense the force-field used for the analysis and neither was strictly correct.

This state of affairs was analyzed more deeply in subsequent work by Soper, who in two seminal papers[24,44] first showed that diffraction data do not contain enough information to discriminate between structure models of strongly different H-bond topology and then that a com-

8

bination of x-ray (sensitive to O-O and O-H correlations) and neutron diffraction data (sensitive to O-H and H-H correlations) is required to obtain reliable estimates of the three PCFs. Considering the significantly reduced height of the first O-O peak it was concluded that softer MD potentials were called for;[44] similar conclusions were reached based on RMC fits to the same data sets.[10,14]
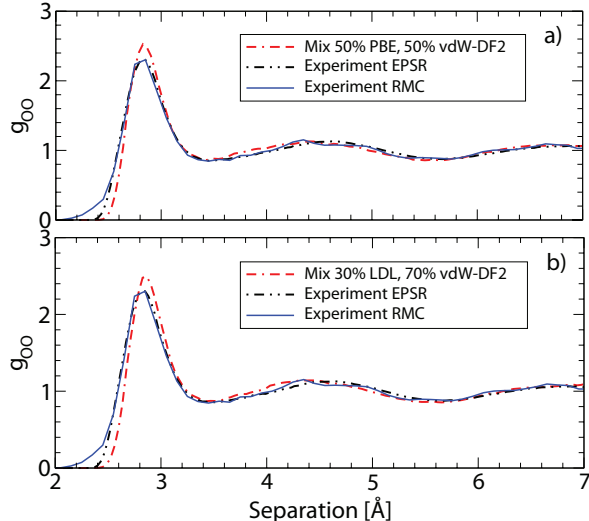
Møgelhøj et al., Figure 6

FIG. 6: a) Oxygen-oxygen PCFs based on mixing the vdW-DF2 and PBE structures. b) Mixing of experimental LDL and vdW-DF2 oxygen-oxygen PCFs in comparison with PCFs from reverse Monte Carlo (RMC) [14] and EPSR analyses (EPSR) of experimental data.[44]

We now test whether the obtained O-O PCF from the vdW models, with their low and asymmetric first peak at long distance and smeared out second shell, can be compatible with the PCF for ambient water by weighting together the vdW models with models of LDL to a combined PCF and comparing with the PCF derived from experiment using EPSR[44] and RMC.[14] We have used two approximations of the LDL contribution. Since the PBE model gives severe over-structuring we can assume that it describes the low-density tetrahedral water structure (LDL), albeit not at its preferred density.[72] In Fig. 6 a) the O-O PCF is plotted using a mixture of PBE and vdW-DF2 PCFs. This suggests that a 1:1 mixture of HDL (vdW-DF2) and LDL (PBE) could be compatible with the experimental O-O PCF. However, since the PBE simulated structure is far from its preferred density,[72] it can be assumed to have too large distortions from the "real" LDL, and we therefore also compare with the experimental LDL PCF from Soper and Ricci.[111] In fitting to the experimental O-O PCF we obtain an equivalent agreement (Fig. 6 b)) with a 70:30 mixture between vdW-DF2 HDL PCF and the experimentally derived LDL PCF.[111] This ratio is most interesting, since it is very close to the original estimate of Wernet et al.[1] and the estimation based on x-ray emission spectroscopy,[12,15]

as well as to that from interpreting infrared data in connection with analysis of a fractional Stokes-Einstein relation in water.[104] Note furthermore, that quantum effects have not been included in the simulations which would be expected to bring down and broaden the first O-O correlation additionally.[112,113]

As has been pointed out by Soper[23] when combining two separate PCFs one must also consider whether the combination introduces additional cross-terms between the two, i.e. that the contribution to the total PCF from considering pairs of atoms, one from each distribution, could change the picture. This would be expected from a combination of two highly structured PCFs with well-defined peaks occurring at different interparticle separations in the two distributions. However, considering that both the LDL and HDL local structures give a peak in the region of 2.7 - 3 Å and beyond that the HDL-like PCF is basically without structure it seems likely that in this particular case no extra features should be expected from cross contributions to a combined PCF.

The question is naturally why the vdW simulation only shows the appearance of HDL-like water and why, in order to obtain agreement with x-ray diffraction experiments, it is necessary to artificially add an LDL component. One potential explanation could be related to the fact that the simulation is performed in the NVE ensemble which keeps the volume fixed and thus does not allow fluctuations of the density of the box and that this penalizes LDL to a greater extent than HDL once the more isotropic vdW interactions are included; the NVE ensemble is equivalent to adding a pressure to maintain the box size which would disfavor fluctuations to lower density assuming that the density at ambient conditions corresponds more closely to that of HDL. The box is furthermore rather limited with only 64 molecules. In order for spatially separated fluctuations between HDL and LDL to develop fully it might be necessary to use much larger simulation boxes, in particular if the fluctuations are of a mean length scale around 1 nm as suggested in Ref. 15. There is furthermore some experimental evidence from thin water films on slightly hydrophobic surfaces that only an HDL related structure is observed even in the supercooled regime,[114] indicating that if the system size becomes very small, indeed only one class of local structure is observed and the formation of LDL-like local regions is suppressed.

V. CONCLUSIONS

The new van der Waals density functionals optPBE-vdW and vdW-DF2 show great promise in describing the basic structural constituents of liquid water, as seen from comparing calculations of water dimer and hexamers with benchmark coupled cluster CCSD(T) results.[73,79,82] A softening of the structure of liquid water at ambient conditions is observed when including vdW interactions, consistent with previous work.[67,72] This is seen

from the broader angular distributions, the more disordered tetrahedrality and asphericity distributions, and from the much lower and broader first peak of the oxygen-oxygen PCF obtained from the optPBE-vdW and vdW-DF2 models compared to PBE. The lower first peak of the O-O PCF improves the agreement with experiment significantly. However, the outer structure is washed out by the vdW forces. This has been suggested[72] to be related to non-local correlations, but our study of functionals with different non-local correlation strength did not show any significant difference in the liquid structures, while both were found to be very accurate for the water dimer. Instead we find that the inclusion of the more isotropic vdW interaction shifts the balance over from directional H-bonding towards a more close-packed system, *i.e.* a competition between directional and isotropic interactions.

The vdW simulations seem to be potentially consistent with a picture of fluctuations between two different water structures instantaneously coexisting in nanoscale patches albeit not directly observing fluctuations except in the sense of obtaining two alternative endpoints with vdW forces included (HDL) or excluded (LDL). The relatively small simulation can only give a picture of the local structure of water, and while PBE predominantly describes an approximation to low-density water, both optPBE-vdW and vdW-DF2 tend to describe an approximation to high-density water. By comparing the O-O PCFs of the vdW models with PCFs from x-ray[105] and neutron[48] diffraction of water at different pressures we note a resemblance between the vdW models and high-density water in terms of effects on the second- and third-neighbor correlations while the expansion of the first coordination sphere found in the simulations may in experiments be counteracted by the pressure applied to generate pure HDL experimentally. The comparison to HDL is further supported by the reduction of the average number of H-bonds per molecule in the vdW MD simulations, which is a result of the isotropic vdW forces competing with the directional H-bond formation. Varying the strength of the exchange interaction does not result in a significant change in number of bonds once the vdW interaction is included. A 1:1 mixture of PBE (LDL) and vdW-DF2 (HDL) structures is compatible with the latest x-ray O-O PCF, an equivalent agreement is achieved for a 70:30 mixture of vdW-DF2 and the experimentally determined LDL PCF.

The present work does not resolve the debate on water structure but it suggests for further investigation the van der Waals interaction as a physically sound mechanism which affects the balance between directional H-bonding and higher packing and may thus indicate a way to reconcile the interpretation of recent x-ray spectroscopic data with structures obtained from AIMD simulations of liquid water. It is likely that much larger and longer simulations in the NPT ensemble are needed to determine whether current vdW models support a temperature-dependent balance of fluctuations between HDL and LDL-like structures in ambient water, as suggested by recent x-ray spectroscopic and scattering results,[15] and which would be enhanced upon cooling, as they must according to all scenarios for water at supercooled temperatures. From the present work it is, however, clear that a consistent description of the vdW interaction in AIMD simulations provides the key to tuning such a balance.

VI. ACKNOWLEDGMENTS

[1] Ph. Wernet, D. Nordlund, U. Bergmann, M. Cavalleri, M. Odelius, H. Ogasawara, L.Å. Näslund, T.K. Hirsch, L. Ojamäe, P. Glatzel, L.G.M. Pettersson, and A. Nilsson. *Science*, 304:995, 2004.

[2] J.D. Smith, C.D. Cappa, K.R. Wilson, B.M. Messer, R.C. Cohen, and R.J. Saykally. Energetics of Hydrogen Bond Network Rearrangements in Liquid Water. *Science*, 306:851, 2004.

[3] A. Nilsson, Ph. Wernet, D. Nordlund, U. Bergmann, M. Cavalleri, M. Odelius, H. Ogasawara, L.-Å. Näslund, T. K. Hirsch, L. Ojamäe, P. Glatzel, and L. G. M. Pettersson. Comment on Energetics of Hydrogen Bond Network Rearrangements in Liquid Water. *Science*, 308:793a, 2005.

[4] B. Hetényi, F. De Angelis, P. Giannozzi, and R. Car. Calculation of near-edge x-ray-absorption fine structure at finite temperatures: Spectral signatures of hydrogen bond breaking in liquid water. *J. Chem. Phys.*, 120:8632, 2004.

[5] M. Cavalleri, D. Nordlund, M. Odelius, A. Nilsson, and L.G.M. Pettersson. Half or full core-hole in Density Functional Theory X-ray absorption spectrum calculations of water? *Phys. Chem. Chem. Phys.*, 7:2854, 2005.

[6] D. Kennedy and C. Norman. *Science*, 309:75, 2005.

[7] M. Odelius, M. Cavalleri, A. Nilsson, and L.G.M. Pettersson. The X-ray Absorption Spectrum of Liquid Water from Molecular Dynamics Simulations: Asymmetric Model. *Phys. Rev. B*, 73:024205, 2006.

[8] D. Prendergast and G. Galli. X-ray absorption spectra of water from first principles calculations. *Phys. Rev. Lett.*, 96:215502, 2006.

[9] H.S. Lee and M.E. Tuckerman. *J. Chem. Phys.*, 125:154507, 2006.

[10] M. Leetmaa, K. T. Wikfeldt, M. P. Ljungberg,

M. Odelius, J. Swenson, A. Nilsson, and L. G. M. Pettersson. Diffraction and IR/Raman data do not prove tetrahedral water. *J. Chem. Phys.*, 129:084502, 2008.

[11] O. Fuchs, M. Zharnikov, L. Weinhardt, M. Blum, M. Weigand, Y. Zubavichus, M. Bär, F. Maier, JD Denlinger, C. Heske, et al. Isotope and temperature effects in liquid water probed by X-ray absorption and resonant X-ray emission spectroscopy. *Phys. Rev. Lett.*, 100(2):27801, 2008.

[12] T. Tokushima, Y. Harada, O. Takahashi, Y. Senba, H. Ohashi, L. G. M. Pettersson, A. Nilsson, and S. Shin. High resolution X-ray emission spectroscopy of liquid water: The observation of two structural motifs. *Chem. Phys. Lett.*, 460(4-6):387–400, 2008.

[13] L.G.M. Pettersson, T. Tokushima, Y. Harada, O. Takahashi, S. Shin, and A. Nilsson. Comment on Isotope and Temperature Effects in Liquid Water Probed by X-ray Absorption and Resonant X-ray Emission Spectroscopy. *Phys. Rev. Letters*, 100:249801, 2008.

[14] K.T. Wikfeldt, M. Leetmaa, M.P. Ljungberg, A. Nilsson, and L.G.M. Pettersson. *J. Phys. Chem. B*, 113:6246, 2009.

[15] C. Huang, K. T. Wikfeldt, T. Tokushima, D. Nordlund, Y. Harada, U. Bergmann, M. Niebuhr, T.M. Weiss, Y. Horikawa, M. Leetmaa, M.P. Ljungberg, O. Takahashi, A. Lenz, L. Ojamäe, A.P. Lyubartsev, S. Shin, L.G.M. Pettersson, and A. Nilsson. The inhomogeneous structure of water at ambient conditions. *Proc. Natl. Acad. Sci. USA*, 106:15214, 2009.

[16] F. Mallamace, M. Broccio, C. Corsaro, A. Faraone, D. Majolino, V. Venuti, L. Liu, C.-Y. Mou, and S.-H. Chen. *Proc. Natl. Acad. Sci. USA*, 104:424–428, 2007.

[17] M. Odelius. Molecular dynamics simulations of fine structure in oxygen K-edge x-ray emission spectra of liquid water and ice. *Phys. Rev. B*, 79(14):144204, 2009.

[18] A.K. Soper, J. Teixeira, and T. Head-Gordon. Is ambient water inhomogeneous on the nanometer-length scale? *Proc. Natl. Acad. Sci. USA*, 107:E44, 2010.

[19] C. Huang, K. T. Wikfeldt, T. Tokushima, D. Nordlund, Y. Harada, U. Bergmann, M. Niebuhr, T.M. Weiss, Y. Horikawa, M. Leetmaa, M.P. Ljungberg, O. Takahashi, A. Lenz, L. Ojamäe, A.P. Lyubartsev, S. Shin, L.G.M. Pettersson, and A. Nilsson. Reply to Soper "Fluctuations in water around a bimodal distribution of local hydrogen bonded structural motifs". *Proc. Natl. Acad. Sci. USA*, 107:E45, 2010.

[20] W. Chen, X. Wu, and R. Car. X-Ray Absorption Signatures of the Molecular Environment in Water and Ice. *Phys. Rev. Lett.*, 105:017802, 2010.

[21] G.N.I. Clark, G.L. Hura, J. Teixeira, A.K. Soper, and T. Head-Gordon. Small-angle scattering and the structure of ambient liquid water. *Proc. Natl. Acad. Sci. USA*, 107(32):14002–14007, 2010.

[22] G. N. I. Clark, C. D. Cappa, J. D. Smith, R. J. Saykally, and T. Head-Gordon. The Structure of Ambient Water. *Mol. Phys.*, 108:1415, 2010.

[23] A.K. Soper. Recent Water Myths. *Pure Appl. Chem.*, 82:1855, 2010.

[24] A. K. Soper. *J. Phys. Condens. Matter*, 17:S3271–S3282, 2005.

[25] K.T. Wikfeldt, M. Leetmaa, A. Mace, A. Nilsson, and L.G.M. Pettersson. *J. Phys. Chem.*, 132:104513, 2010.

[26] S.V. Lishchuk, N.P. Malomuzh, and P.V. Makhlaichuk. Why thermodynamic properties of normal and heavy water are similar to those of argon-like liquids? *Phys. Lett.*

[27] A, 374:2084, 2010.

P.G. Debenedetti. Supercooled and glassy water. *J. Phys.: Condens. Matt.*, 15:R1669, 2003.

[28] H.E. Stanley, S.V. Buldyrev, G. Franzese, P. Kumar, F. Mallamace, M.G. Mazza, K. Stokely, and L. Xu. *J. Phys.: Condens. Matter*, 22:284101, 2010.

[29] F. Mallamace. *Proc. Natl. Acad. Sci. USA*, 106:15097, 2009.

[30] R.J. Speedy. *J. Phys. Chem.*, 86:3002, 1982.

[31] H.E. Stanley and J. Teixeira. *J. Chem. Phys.*, 73:3404, 1980.

[32] P.H. Poole, F. Sciortino, U. Essmann, and H.E. Stanley. *Nature*, 360:324–328, 1992.

[33] K. Stokely, M.G. Mazza, H.E. Stanley, and G. Franzese. Effect of hydrogen bond cooperativity on the behavior of water. *Proc. Natl. Acad. Sci. USA*, 107(4):1301, 2010.

[34] R.J. Speedy and C.A. Angell. Isothermal compressibility of supercooled water and evidence for a thermodynamic singularity at -45 C. *J. Chem. Phys.*, 65:851, 1976.

[35] O. Mishima and H. E. Stanley. *Nature*, 396:329, 1998.

[36] P.H. Poole, F. Sciortino, T. Grande, H.E. Stanley, and C.A. Angell. *Phys. Rev. Lett.*, 73:1632, 1994.

[37] S.S. Borick, P.G. Debenedetti, and S. Sastry. *J. Phys. Chem.*, 99:3781, 1995.

[38] I. Brovchenko and A. Oleinikova. *J. Chem. Phys.*, 124:164505, 2006.

[39] S. Sastry, P. G. Debenedetti, F. Sciortino, and H. E. Stanley. Singularity-Free Interpretation of the Thermodynamics of Supercooled Water. *Phys. Rev. E*, 53:6144, 1996.

[40] C. A. Angell. Insights into Phases of Liquid Water from Study of Its Unusual Glass-Forming Properties. *Science*, 319:582, 2008.

[41] R. J. Speedy. Stability-limit conjecture. An interpretation of the properties of water. *J. Phys. Chem.*, 86:982, 1982.

[42] R. Car and M. Parrinello. *Phys. Rev. Lett.*, 55:2471, 1985.

[43] V. Molinero and E.B. Moore. Water Modeled As an Intermediate Element between Carbon and Silicon. *J. Phys. Chem. B*, 113(13):4008–4016, 2008.

[44] A.K. Soper. *J. Phys. Condens. Matter*, 19:335206, 2007.

[45] L. Fu, A. Bienenstock, and S. Brennan. *J. Chem. Phys.*, 131:234702, 2009.

[46] J. Neuefeind, C.J. Benmore, J.K.R. Weber, and D. Paschek. More accurate X-ray scattering data of deeply supercooled bulk liquid water. *Mol. Phys.*, XX:XX, 2010.

[47] E.B. Moore and V. Molinero. Growing correlation length in supercooled water. *J. Chem. Phys.*, 130:244505, 2009.

[48] A.K. Soper. *Chem. Phys.*, 258:121, 2000.

[49] G. Hura, J.M. Sorenson, R.M. Glaeser, and T. Head-Gordon. *J. Chem. Phys.*, 113:9140, 2000.

[50] D. Paschek, A. Rüppert, and A. Geiger. Thermodynamic and Structural Characterization of the Transformation from a Metastable Low-Density to a Very High-Density Form of Supercooled TIP4P- Ew Model Water. *ChemPhysChem*, 9(18):2737–2741, 2008.

[51] I. Brovchenko, A. Geiger, and A. Oleinikova. Liquid-liquid phase transitions in supercooled water studied by computer simulations of various water models. *J. Chem. Phys.*, 123:044515, 2005.

[52] C.T. Lee, W.T. Yang, and R.G. Parr. *Phys. Rev. B*, 37(2):785, 1988.

[53] J.P. Perdew, K. Burke, and M. Ernzerhof. *Phys. Rev. Lett.*, 77:3865, 1996.

[54] J.C. Grossman, E. Schwegler, E.W. Draeger, F. Gygi, and

G. Galli. *J. Chem. Phys.*, 120:300, 2004.

[55] I.F.W. Kuo, C.J. Mundy, M.J. McGrath, J.I. Siepmann, J. VandeVondele, M. Sprik, J. Hutter, B. Chen, M.L. Klein, F. Mohamed, M. Krack, and M. Parrinello. *J. Phys. Chem. B*, 108:12990, 2004.

[56] P.H.L. Sit and N. Marzari. *J. Chem. Phys.*, 122:204510, 2005.

[57] J. VandeVondele, F. Mohamed, M. Krack, J. Hutter, M. Sprik, and M. Parrinello. *J. Chem. Phys.*, 122:014515, 2005.

[58] T. Todorova, A.P. Seitsonen, J. Hutter, I.F.W. Kuo, and C.J. Mundy. *J. Phys. Chem. B*, 110:3685, 2006.

[59] S. Yoo, X. C. Zeng, and S. S. Xantheas. On the phase diagram of water with density functional theory potentials: The melting temperature of ice i$_h$ with the perdew–burke–ernzerhof and becke–lee–yang–parr functionals. *J. Chem. Phys.*, 130(22):221102, 2009.

[60] J. Ireta, J. Neugebauer, and M. Scheffler. *J. Phys. Chem. A*, 108:5692, 2004.

[61] B. Santra, A. Michaelides, M. Fuchs, A. Tkatchenko, C. Filippi, and M. Scheffler. *J. Chem. Phys.*, 129:194111, 2008.

[62] C.H. Cho, S. Singh, and G.W. Robinson. *J. Chem. Phys.*, 107:7979, 1997.

[63] R. Schmid. *Monatsh. Chem.*, 132:1295, 2001.

[64] A. Michaelides. Private communication.

[65] S. Kristyan and P. Pulay. *Chem. Phys. Lett.*, 229:175, 1994.

[66] R.M. Lynden-Bell and P.G. Debenedetti. *J. Phys. Chem. B*, 109:6527, 2005.

[67] I.C. Lin, A.P. Seitsonen, M.D. Coutinho-Neto, I. Tavernelli, and U. Rothlisberger. *J. Phys. Chem. B*, 113:1127, 2009.

[68] F.A. Gianturco, F. Paesani, M.F. Laranjeira, V. Vassilenko, and M.A. Cunha. Intermolecular forces from density functional theory. III. A multiproperty analysis for the Ar(^{1}S)-CO($^1\Sigma$) interaction. *J. Chem. Phys.*, 110:7832, 1999.

[69] S. Grimme. *J. Comput. Chem.*, 25:1463, 2004.

[70] R.W. Williams and D. Malhotra. *Chem. Phys.*, 327:54, 2006.

[71] M. Dion, H. Rydberg, E. Schröder, D.C. Langreth, and B.I. Lundqvist. *Phys. Rev. Lett.*, 92:246401, 2004.

[72] J. Wang, G. Roman-Perez, J. M. Soler, E. Artacho, and M. V. Fernandez-Serra. Density, structure, and dynamics of water: The effect of van der Waals interactions. *J. Chem. Phys.*, 134:024516, 2011.

[73] A.K. Kelkkanen, B.I. Lundqvist, and J.K. Norskov. *J. Chem. Phys.*, 131:046102, 2009.

[74] A. Gulans, M.J. Puska, and R.M. Nieminen. *Phys. Rev. B*, 79(20):201105, 2009.

[75] D.C. Langreth, B.I. Lundqvist, S.D. Chakarova-Kack, V.R. Cooper, M. Dion, P. Hyldgaard, A. Kelkkanen, J. Kleis, L.Z. Kong, S. Li, P.G. Moses, E. Murray, A. Puzder, H. Rydberg, E. Schröder, and T. Thonhauser. *J. Phys.: Condens. Matter*, 21:084203, 2009.

[76] A. Puzder, M. Dion, and D.C. Langreth. *J. Chem. Phys.*, 124, 2006.

[77] E.D. Murray, K. Lee, and D.C. Langreth. *J. Chem. Theory Compt.*, 5:2754, 2009.

[78] J.P. Perdew and W. Yue. *Phys. Rev. B*, 33:8800, 1986.

[79] J. Klimes, D.R. Bowler, and A. Michaelides. *J. Phys. Conden. Matter*, 22:022201, 2010.

[80] V.R. Cooper. *Phys. Rev. B*, 81:161104, 2010.

[81] J. Wellendorff, A. Møgelhøj, V. Petzvold, T. Bligaard, K.W. Jacobsen and J.K. Nørskov. to be submitted.

[82] K. Lee, E.D. Murray, L. Kong, B.I. Lundqvist, and D.C. Langreth. *Phys. Rev. B*, 82:081101, 2010.

[83] G. Roman-Perez and J.M. Soler. *Phys. Rev. Lett.*, 103:096102, 2009.

[84] Y.K. Zhang and W.T. Yang. *Phys. Rev. Lett.*, 80:890, 1998.

[85] P. Jurecka, J. Sponer, J. Cerny, and P. Hobza. *Phys. Chem. Chem. Phys.*, 8:1985, 2006.

[86] Y. Wang and J. Perdew. *Phys. Rev. B: Condens. Matter*, 33:8800(R), 1986.

[87] L.F. Molnar, X. He, B. Wang, and K.M. Merz. *J. Chem. Phys.*, 131:065102, 2009.

[88] T. Takatani, E.G. Hohenstein, M. Malagoli, M.S. Marshall, and C.D. Sherrill. Basis set consistent revision of the S22 test set of noncovalent interaction energies. *J. Chem. Phys.*, 132:144104, 2010.

[89] J. Enkovaara, C. Rostgaard, J. J. Mortensen, J. Chen, M. Dulak, L. Ferrighi, J. Gavnholt, C. Glinsvad, V. Haikola, H. A. Hansen, H. H. Kristoffersen, M. Kuisma, A. H. Larsen, L. Lehtovaara, M. Ljungberg, O. Lopez-Acevedo, P. G. Moses, J. Ojanen, T. Olsen, V. Petzold, N. A. Romero, J. Stausholm-Moller, M. Strange, G. A. Tritsaris, M. Vanin, M. Walter, B. Hammer, H. Hakkinen, G. K. H. Madsen, R. M. Nieminen, J. K. Norskov, M. Puska, T. T. Rantala, J. Schiotz, K. S. Thygesen, and K. W. Jacobsen. Electronic structure calculations with GPAW: a real-space implementation of the projector augmented-wave method. *J. Phys.: Cond. Mat.*, 22:253202, 2010.

[90] L. B. Hansen J. J. Mortensen and K. W. Jacobsen. *Phys. Rev. B*, 71:035109, 2005.

[91] L.A. Curtiss, K. Raghavachari, P.C. Redfern, and J.A. Pople. *J. Chem. Phys.*, 106:1063, 1997.

[92] J.M. Sorenson, G. Hura, R.M. Glaeser, and T. Head-Gordon. *J. Chem. Phys.*, 113:9149, 2000.

[93] T. Head-Gordon and G. Hura. *Chem. Rev.*, 102:2651, 2002.

[94] R. L. McGreevy and L. Pusztai. *Mol. Simul.*, 1:359, 1988.

[95] P. Jedlovszky, I. Bako, G. Palinkas, T. Radnai, and A.K. Soper. RMC giving maximally disordered structures. *J. Chem. Phys.*, 105:245, 1996.

[96] L. Pusztai. Partial pair correlation functions of liquid water. *Phys. Rev. B*, 60(17):11851–11854, 1999.

[97] S. Myneni, Y. Luo, L.Å. Näslund, M. Cavalleri, L. Ojamäe, H. Ogasawara, A. Pelmenschikov, Ph. Wernet, P. Väterlein, C. Heske, Z. Hussain, L.G.M. Pettersson, and A. Nilsson. Spectroscopic probing of local hydrogen bonding structures in liquid water. *J. Phys.: Condens. Mat.*, 14:L213, 2002.

[98] P. -L. Chau and A. J. Hardwick. *Mol. Phys.*, 93:511, 1998.

[99] J.R. Errington and P.G. Debenedetti. Relationship Between Structural Order and the Anomalies of Liquid Water. *Nature*, 409:318, 2001.

[100] G. Ruocco, M. Sampoli, and R. Vallauri. Analysis of the network topology in liquid water and hydrogen sulphide by computer simulation. *J. Chem. Phys.*, 96:6167, 1992.

[101] A. Soper and C.J. Benmore. *Phys. Rev. Lett.*, 101:065502, 2008.

[102] C. Huang, T. M. Weiss, D. Nordlund, K. T. Wikfeldt, L. G. M. Pettersson, and A. Nilsson. Increasing correlation length in bulk supercooled H$_2$O, D$_2$O, and NaCl solution determined from small angle x-ray scattering. *J. Chem.*

Phys., 133:134504, 2010.

[103] P. Kumar. Breakdown of the StokesEinstein relation in supercooled water. *Proc. Natl. Acad. Sci. USA*, 103:12955–12956, 2006.

[104] L. Xu, F. Mallamace, Z. Yan, F. W. Starr, S. V. Buldyrev, and H. E. Stanley. Appearance of a Fractional Stokes-Einstein Relation in Water and a Structural Interpretation of Its Onset. *Nature Physics*, 5:565–569, 2009.

[105] A.V. Okhulkov, Y.N. Demianets, and Y. E. Gorbaty. *J. Chem. Phys.*, 100:1578, 1994.

[106] J. L. Finney, D. T. Bowron, A. K. Soper, T. Loerting, E. Mayer, and A. Hallbrucker. Structure of a New Dense Amorphous Ice. *Phys. Rev. Lett.*, 89:20553, 2002.

[107] M.M. Koza, B. Geil, K. Winkel, C. Kähler, F. Czeschka, M. Scheuermann, H. Schober, and T. Hansen. Nature of Amorphous Polymorphism of Water. *Phys. Rev. Lett.*, 94:125506, 2005.

[108] M.M. Koza, T. Hansen, R.P. May, and H. Schober. *J. Non-Cryst. Solids*, 352:4988, 2006.

[109] H. Schober, M. Koza, A. Tölle, F. Fujara, C.A. Angell, and R. Böhmer. *Physica B*, 241:897, 1998.

[110] C.A. Tulk, C.J. Benmore, J. Utquidi, D.D. Klug, J. Neuefeind, B. Tomberli, and P.A. Egelstaff. *Science*, 297:1320, 2002.

[111] A. K. Soper and M. A. Ricci. *Phys. Rev. Lett.*, 84:2881, 2000.

[112] F. Paesani, S. Iuchi, and G.A. Voth. *J. Chem. Phys.*, 127:074506, 2007.

[113] F. Paesani and G.A. Voth. *J. Phys. Chem. B*, 113:5702, 2009.

[114] S. Kaya, S. Yamamoto, N. Huang, J. T. Newberg, H. Bluhm, L. G. M. Pettersson, H. Ogasawara, and A. Nilsson. . *unpublished*.

Paper 8

A. K. Kelkkanen and B. I. Lundqvist,
Nature of van der Waals-Distorted Hydrogen Bond as Revealed by Water Dimer and Hexamer Calculations,
manuscript

Nature of van der Waals-Distorted Hydrogen Bond as Revealed by Water Dimer and Hexamer Calculations

A. K. Kelkkanen [a] and B. I. Lundqvist [a,b]

[a] Center for Atomic-scale Materials Design, Department of Physics, Technical University of Denmark, DK-2800 Kongens Lyngby, Denmark,
[b] Department of Applied Physics, Chalmers University of Technology, SE-41296 Göteborg, Sweden.

Manuscript February 2, 2011

Abstract

While it is well established that hydrogen bonds give the major contributing factor to the dynamics and structure of water, van der Waals (vdW) interactions have also been suggested to be important. Bond lengths in hydrogen bonds are shorter than those for typical vdW bonds, making both adsorption and water call for improved exchange functionals in density-functional theory (DFT). Results of DFT calculations for water dimer and hexamer, and liquid water are here described. For the four low-energetic isomers of the water hexamer we have earlier shown that the vdW-DF accurately determines the energetic trend on these small clusters, however, with too small dissociation-energy values. The exchange approximation used is judged too repulsive. With the vdW-DF and other functionals that account for vdW forces, the total isomer energies are minimized in molecular configurations, which are compact, and in which many hydrogen bonds (HBs) can be described as distorted, even as broken, with a common definition. The hexamer experience of such criteria and effects of vdW forces can be used in interpretation of results of molecular dynamics (MD) simulations of ambient water, where vdW forces qualitatively result in liquid water with fewer pure but more distorted HBs. This is interesting in regards to the ongoing debate in the on the level of HB distortion in ambient water, and where MD simulations without first principles vdW forces have played an important role to suggest that liquid water is almost tetrahedral, with few distorted HBs. Simulations with improved vdW-DF functionals, the so-called vdW-DF2 and optPBE-vdW ones, result in a structure similar to the HDL phase (high-density liquid) under proper conditions, and thus shows that vdW forces may be vital in the two-liquid model suggested in http://www.sciencemag.org/content/304/5673/995.abstract. By tying fundamental features of the exchange and vdW parts of the density functional in electron theory to experimental observations on liquid water, via calculated vdW effects on water hexamers, including compactness and distorted hydrogen bonds, vdW interactions are shown to be important for water structure. This supports the two-liquid model and contributes to the understanding of anomalies in liquid water, for example, the fact that solid ice is formed on top of liquid water, unlike the situation in simple liquids.

I. INTRODUCTION

A hydrogen bond (HB) is the attractive interaction of a hydrogen atom with an electronegative atom, like nitrogen, oxygen or fluorine [1,2]. It must not be confused with a pure covalent bond to hydrogen, as the hydrogen atom must be covalently bonded to another electronegative atom to create the HB. It can be inter- or intramolecular and is stronger (5 - 30 kJ/mole, 50 – 300 meV) than a van der Waals (vdW) or dispersion interaction but weaker than typical covalent or ionic bonds. While it is well established that HBs give the major contributing factor to the dynamics and structure of water, vdW interactions have also been suggested to be important [3,4] The bond type occurs in both inorganic (*e.g.,* water) and organic molecules (*e.g.,* DNA) and is, for instance, behind the high boiling point of water and and contributes to the secondary, tertiary, and quaternary structures of proteins and nucleic acids.
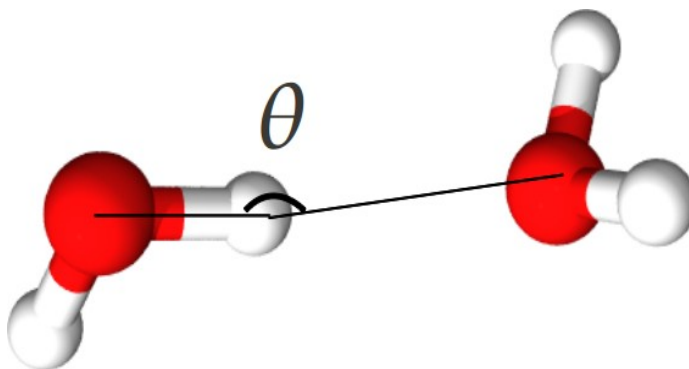

Figure 1. Schematics of the water dimer.

The HB is at times mentioned as stiff and at other times flexible, and this ambiguous nature is addressed here. The directionality of the HB is commonly taken as the angle θ between the intermolecular bond of the H atom on the donor molecule and its intermolecular HB with the acceptor molecule (Fig. 1). Studies of various HB dimers suggest that decreasing θ (from 180°) follows an increase in vdW interactions [5-9]. A study of a large database on molecular structures [10] implies that weak HB's can be distinguished from vdW interactions via angular distributions [5]. HB's are inherently directional, with inherently directional geometries favored energetically over distorted HB's. In contrast, vdW contacts are isotropic, with interaction energies independent of the contact angle θ. The density-functional theory (DFT) [11] is useful to describe materials and molecules, but has here to account also for vdW forces. One such, the vdW-DF functional [12] gives a promising description of a variety of systems [13,14], incl. pure vdW systems but also, *e.g.,* HB'ed nucleobase pairs [9].

With the vdW-DF [12,15], vdW-DF2 [16], and similar methods, we study HB's, in particular, the angular dependencies of hydrogen- and vdW-bonded molecules, including the water dimer and hexamer and H_2S and H_2Se. The purpose is to understand, how and when vdW forces make the bond less directional, *i.e.* more isotropic. The water hexamer is used for benchmarking, but the deduced principle should be general. As for the energetically low-lying isomers of the hexamer. it permits more distorted HB's, to benefit stabilization, as demonstrated for the four lowest water-hexamer isomers [17,18]. The hexamer set is also used to study criteria for HB's [19] and understand their nature.

This paper treats effects of vdW forces on water di- and hexamers, as well as effects of approximations in descriptions of exchange and nonlocal correlation, the latter including vdW forces. The analysis aims at isolating vdW effects on bond directionality and definition, and on structural stability. In conceptual pictures of water systems, and liquid water in particular, HB's play key roles and the number of various kinds of HB's are of interest. Several criteria for the number of various kinds of HB's are proposed in the literature, and we study how two of them work on water hexamers and thereby learn about the nature of HB's. The experience is then used for studies of liquid water.

II. WATER DIMER, VAN DER WAALS FORCES, AND THEORETICAL METHODS

In a parallel study of liquid water [20], together with coworkers, we seek the mechanism behind the formation of a high-density liquid (HDL) of water, provide evidence for DFT's that account for vdW forces to provide an HDL

phase, and anticipate that a qualitative picture emanating from HB properties is applicable [19]. Pure, deformed and broken HB's are important concepts in discussions of liquid water, as is the degree of tetrahedrality in the nearest-neighbor θ = O-H· · · O angles and sets focus on the angular dependence of bond properties. The water dimer $(H_2O)_2$ is a natural reference system to study. However, it appears that no weaken angular variation of the interaction potential appears on this molecule.. It is the smallest system that exhibits a HB. Its smallness allows accurate wave-function calculations to be carried out on it. Yet it is a member of the S22 benchmark set [21-25].

The potential-energy surface (PES) of the water dimer is calculated with the vdW-DF [12] and vdW-DF2 [16] functionals, results agreeing with earlier ones [13,16]. Potential-energy curves (PEC's) calculated with DFT in a number of approximations for the DFT functional are compared with accurate wave-function results [22] in Fig. 2. The PEC expresses, how the interaction energy varies with the separation between the two water molecules. The GGA-PBE functional describes HB's with chemical accuracy (1 kcal/mole = 0.04 eV) [26]. The
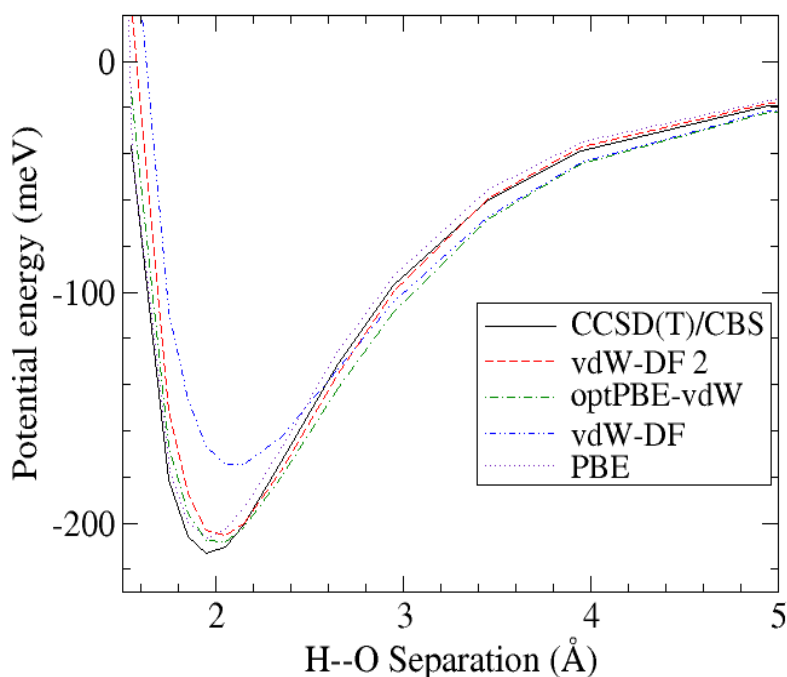

Figure 2. Interaction energy (PEC) for the water dimer. The DFT results with PBE, vdW-DF, optPBE-vdW, and vdW-DF2 are compared with those of an accurate wave-function method (CCSD(T)/CBS) [22].

vdW-DF functional underbinds the dimer and gives too long an equilibrium bond [27]. The optPBE-vdW [28] and vdW-DF2 [16] functionals give PEC's rather close to each other and to the wave-function result [22], restoring chemical accuracy for the HB of the water dimer. However, they are doing so for different reasons, the optPBE-vdW being based on the same nonlocal correlation functional as the vdW-DF, while the vdW-DF2 is based on the PW86 exchange functional [29] and a nonlocal-correlation functional with a new internal function, which gives a slightly softer and less attractive vdW approximation [16]. The difference can be seen for larger separations, as the vdW-DF2 PEC follows the shape of the CCSD(T)/CBS curve [22], while both the vdW-DF and the optPBE-vdW slightly overestimate the nonlocal-correlation attraction. While this difference might be small and irrelevant for the dimer, it might make a statistical difference in liquid water, as seen below.
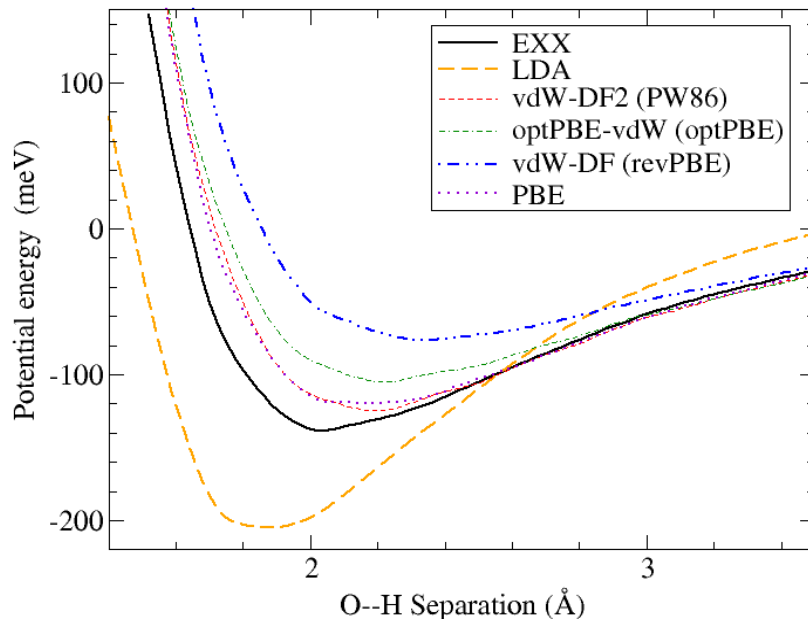
Figure 3. Interaction energy of the water dimer, with only exchange included, illustrates that the revPBE exchange is too repulsive around 2 Å, where PBE is closer to exact exchange (EXX) [30]. This is the reason for the underbinding given by the vdW-DF [31,27,28,32,33,16].

A source for differences in PEC results, like equilibrium-bond-length values, with respect to exchange functionals [33] are explained in a plot of the water-dimer exchange energy as a function of the separation r_{O-H} (Fig. 2). In this figure, dimer results for several exchange-energy functionals are compared with those for exact exchange (EXX) [30] which mimics the Hartree-Fock (HF) approximation. It shows that revPBE exchange is much too repulsive at separations relevant to describe the HB's, that at these small separations the PBE is a better approximation for HF of this HB systems [27], and that LDA overestimates exchange for this system. Analysis of the exchange functionals in terms of the reduced density gradient s shows that these functionals are often rather close to each other, in particular in the small-s limit. However, the source for differences should be searched for in $F_x(s)$.
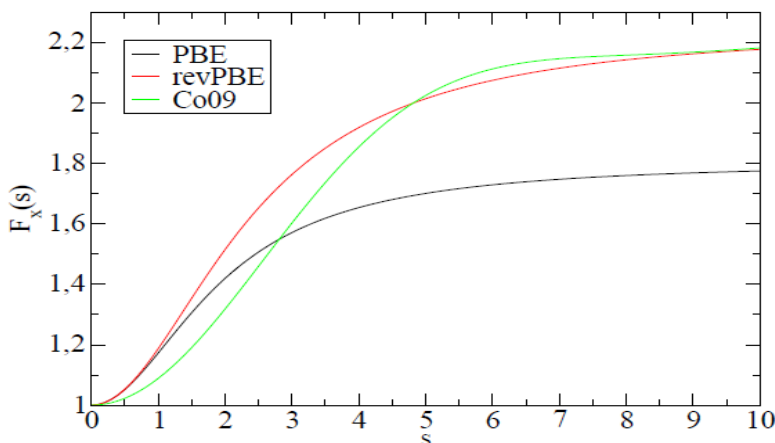

Figure 4. Exchange enhancement factor $F_x(s)$ for some exchange approximations [29,34,35,28,33].

The exchange functional used in the original vdW-DF is meant for typical vdW separations[12]. At other separations, *e.g.*, those for HB's, other exchange functionals are called for [31,27,32,28,33,16]. Current studies [36] attempt to assess improvements obtained with, *e.g.*, the optPBE [28], Co09 [33], and PW86R [29,32,16]

exchange functionals. The vdW-DF method restores chemical accuracy for the water hexamers and the S22 dataset [28,16], when the revPBE exchange functional is replaced by the optPBE one [28] and vdW-DF by the vdW-DF2 functional [16].

For the water dimer, there are thus vdW-improved density functionals that perform for the HB at least as well as the PBE exchange-correlation functional. The vdW-DF method in improved versions can can thus be used to study the role of vdW forces with confidence. Below results from such an approach are given for the angular dependence of the water-dimer PEC, but before that an earlier study is reviewed. Both studies analyze trends with respect to the relative strength of vdW forces in relation to other forces.

Extensive reviews of HB's are available [37], and the HB is regarded as a complex interaction composed of several constituents that have different origins [7]. There is still an active debate about the degree of covalency in the water HB [38]. For ordinary solid ice Ih the covalency of the HB, direct X-ray measurements, a fully quantum-mechanical bonding model for ice Ih, and the disagreement with a purely electrostatic (classical) bonding model support an interpretation with evidence for a substantial covalent nature of this HB [39]. For the present discussion, the question about the relative contributions to the HB in water dimer, hexamer, and fluid can be held open,

In Ref. [5], large amounts of empirical structural data [10] are used with focus on the distinction between weak HB and vdW interaction. The strength of the former is varied according to well known trends within groups of radicals. For instance, the angular distributions of C-H---O interactions for different types of C-H groups show that the directionality decreases with decreasing C-H polarization, but that it is still clearly recognizable for methyl groups [5]. In contrast, the pure vdW contact in the C-H---H-C dimer has an isotropic angular characteristics. C-H groups are weak HB donors, and C-H donor strength obeys the inequalities $C(sp)-H > C(sp^2)-H > C(sp^3)-H$. HB's are inherently directional, linear or close to linear, while vdW contacts are isotropic. Differences in directionality behavior between any kind of C-H---O HB and the vdW interaction are observed and described as consequences of the fundamental differences in distance and angle fall-off characteristics of these interactions [5].

As an indication that data empirism and calculations give the same trend information, we have undertaken vdW-DF calculations on the angular dependencies of bonds in the dimers of H_2O, H_2S, and H_2Se and looked for trends in directionality of the dimer bond related to electronegativity. While the data-set study uses C-H groups as hydrogen bond donors and a structural database to distinguish between the weak HB and the vdW interactions and thereby study the directionality of weak bonds, we generate the necessary variation in relative HB and vdW strength by going down a column in the periodic system, with H_2O, H_2S, and H_2Se dimers. The dissociation-energy values vary with the angle to the HB (Fig. 5), θ, where $\theta = 180$ degrees means that O-H--O is completely linear (Fig. 1), and the steepness of the variation is higher, the higher the electronegativity of the group VI element. It is close to isotropic for $(H_2Se)_2$, while having a distinct directionality for $(H_2Se)_2$, with a variation in the meV range. The covalent and ionic parts of the interaction are expected to give a stronger angular dependence than the vdW part. The calculated binding-energy values of the two fragments vary according to the same trend, being 18, 38, and 164 meV for $(H_2Se)_2$, $(H_2S)_2$, and $(H_2O)_2$ (Fig. 5), respectively. Energy trends follow the electronegativity trend, just telling that the vdW forces are the weaker ones. The separation between the fragments of the different dimers varies rather much. In the water dimer it (the HB H--O) is 2.1 Å, while it in $(H_2S)_2$ is 3.2 Å and in $(H_2Se)_2$ 3.3 Å, all calculated by the vdW-DF method [12]. In short, the bonds in $(H_2S)_2$ and $(H_2Se)_2$ have weaker directional dependence and are almost only of vdW type, while it for the H_2O dimer depends on both electrostatic/covalent and vdW forces, where the first one is directionally dependent and the latter one is not. Figure 5, and, in particular, Table 1 show that the vdW contributions are about equally large in all cases. So the message is about the same as that given in Ref. [5]. We have found three simple systems that illustrate the variation in non-vdW forces. Percentage-wise the angular dependence is smaller, when vdW forces are accounted for. However, the revPBE result does not have a particularly strong angular dependence either. The mere fact that vdW secures an attractive interaction is important, as is the possibility to affect atoms to be in the attractive well, securing attractive energy and thus contributing to the stabilization of distorted HB's.
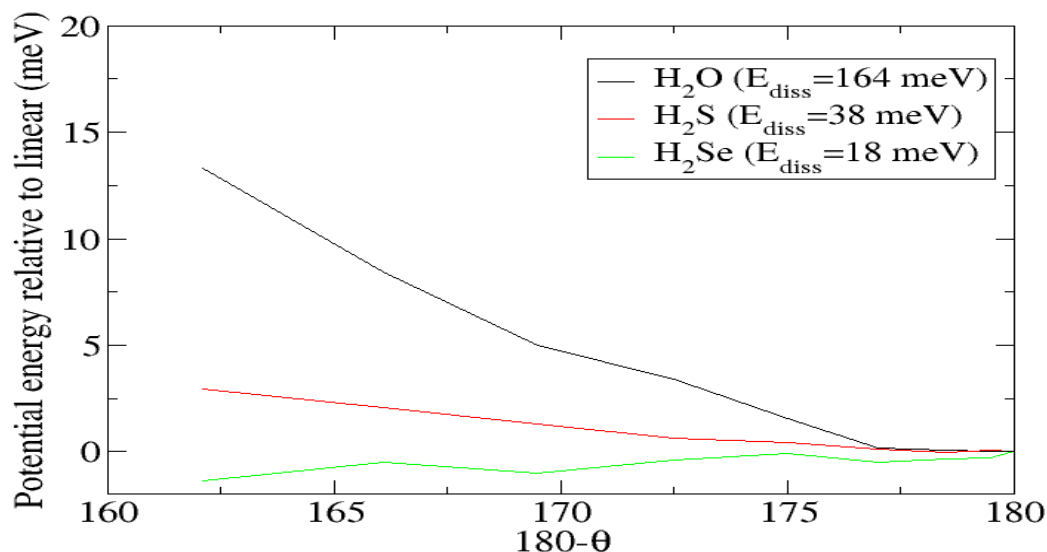
Figure 5: Calculated interaction-energy values energy values of $(H_2O)_2$, $(H_2S)_2$, and $(H_2Se)_2$ dimers, as functions of the bond angle (180 degrees meaning the linear bond), calculated with the vdW-DF functional [12].

(meV)	H2O Dimer		H2S Dimer		H2Se Dimer	
Angle O-H—O	revPBE	VdW-DF	revPBE	VdW-DF	revPBE	VdW-DF
180.0	-128	-164	-5	-38	20	-18
179.5	-128	-164	-5	-38	20	-18
178.5	-128	-164	-5	-38	20	-18
177.0	-128	-164	-5	-38	20	-18
175.0	-126	-162	-5	-38	20	-18
172.5	-124	-161	-5	-37	20	-18
169.5	-122	-159	-5	-37	19	-19
166.1	-119	-155	-4	-36	19	-18
162.1	-114	-151	-4	-35	18	-19

Table 1. Calculated interaction-energy values energy values of $(H_2O)_2$, $(H_2S)_2$, and $(H_2Se)_2$, as functions of the bond angle (180 degrees meaning the linear bond), calculated with the vdW-DF functional [12].

III. WATER HEXAMER AND CRITERIA FOR THE HYDROGEN BOND

Water molecules cluster in various forms. Six H_2O molecules make a hexamer, which appears in many structural forms. Of such isomers several have low energy values, and the four most stable ones form an excellent set for a sensitive benchmarking, as their relative stabilities and structures are well known. Traditional DFT, *i.e.* with LDA or GGA exchange-correlation functionals, fails to identify the correct internal trend of stability for these four [17]. However, this problem can be corrected by including vdW forces [17]. To calculate this, several methods have been used [17,40,41,12,28,16]. The vdW-DF [12] is shown to correctly account for this trend, but with a significant underestimation of the adsorption energy [18]. This is a general issue for HB's [17,27,32,16].
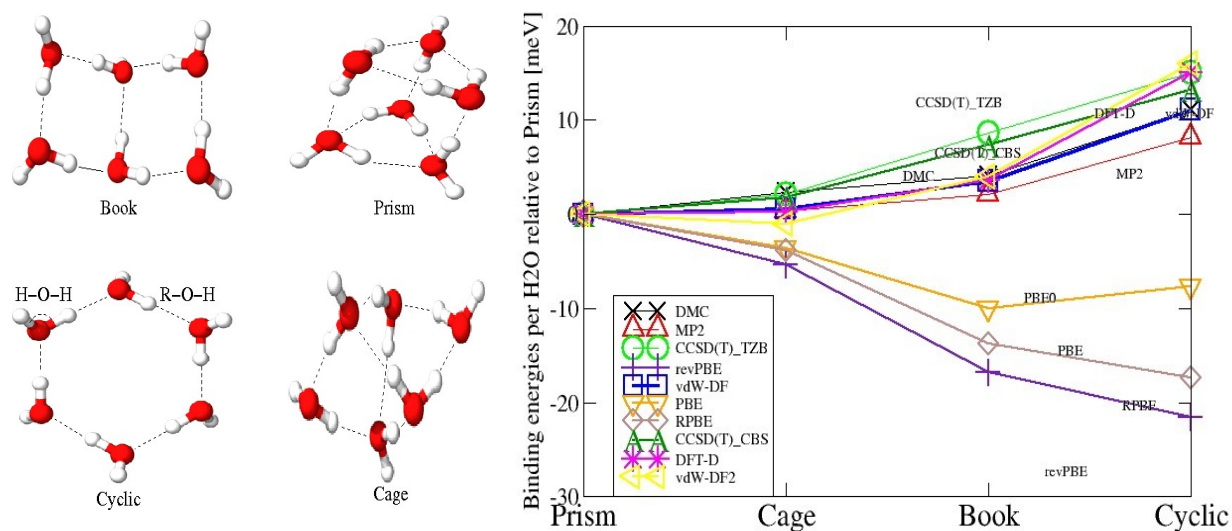
Figure 6: Binding energy per H$_2$O molecule of the water hexamer in the low-lying isomer structures shown (left; the dashed lines indicates available HB locations, 6 for cyclic, 7 for book, 8 for cage, and 9 for prism), calculated with wave-function methods (MP2$_{augccpVTZ}$ [17], DMC [17], and CCSD(T)$_{CBS}$ [42] and DFT methods (with XC functionals in the PBE0 [43], DFT-D [17], PBE, RPBE and revPBE flavors of GGA and in vdW-DF [18], relative to the energy of the prism isomer.

Paper [18] shows results for the water-hexamer interaction energy for the indicated isomer structures that are calculated with a variety of methods. With the vdW-DF functional the energy trends agree with those from more accurate wave-function methods, however, with a consistent underbinding of around 18%. The likely error derives from the too repulsive exchange given by the revPBE exchange functional at small separations (around 2 Å). The revPBE exchange functional is by construction included in vdW-DF, as it is close to Hartree-Fock exchange at typical vdW separations, around 3 - 5 Å. Tests of various exchange functionals on, *e.g.*, the water dimer show that PBE exchange is better at these small separations, and should be so also for the hexamers [18]. The underestimate can be reduced by using a less repulsive exchange functional in the vdW-DF functional, like the PBE [31,27,32] and other exchange functionals [32,28,33,16], used in the vdW-DF method [31,32,28,33,16]. One can get a hint towards an optimal exchange functional from the optPBE [28], Co09 [33], and PW86R [29,32,16] functionals. It has also been shown that the exchange in the vdW-DF method can be optimized to work well for certain systems, like the S22 [21,24] datasets [28,16]. Such optimization has been shown to restore chemical accuracy for the water hexamers. Current studies, like [36], attempt to assess improvements by functionals like these.

Compared to traditional DFT, functionals that account for vdW forces give a reversed stability trend for the low-lying isomers. This can be related to the nonlocal dependence of the vdW interaction on the density [17,18]. While semilocal GGA's give a relatively stiff HB, this stabilizing aspect is represented either by average atomic distances [40], or by the density- and distance-dependent interaction kernel Φ in vdW-DF [12]. Compared with the tetrahedral HB's that are energetically favored by traditional LDA and GGA functionals, this nonlocal correlations provide extra attraction that can help stabilizing distorted HB's.

Cyclic		Book		Cage		Prism	
ROO	O-H-O	ROO	O-H-O	ROO	O-H-O	ROO	O-H-O
2.75	2.60	2.74	10.3	2.8	17.4	2.86	20.6
2.75	2.70	2.86	11.2	2.79	15.4	3.07	33.3
2.75	2	2.84	10.6	3.03	20.7	3.09	44.8
2.75	2.5	2.86	10.5	3.13	31.8	2.85	25
2.75	2.70	2.73	9.2	2.72	11.3	3	29
2.75	2	2.73	9.6	2.8	17.2	3.14	45.5
		3	21.7	3.06	29.7	3.03	18.9
				3.13	31.8	2.72	10
						2.83	12

Table II: The values for the oxygen-oxygen separation R_{OO} and of the angular deviation θ = O-H---O for "available HB's" (Cf. Fig. 6) of the hexamer isomers.

Further consequences of vdW forces are shown in Fig. 7, where distortions of the HB's of the four low-lying isomers are marked in a plot with O-O separations R_{O-O} and O-H-O angular distortion from linearity, θ, on the axes, respectively. At first glance, vdW forces seem to stabilize hexamer structures with most HB's. However, this clearly depends on the definition of the HB, as is seen in Fig. 7. Two geometric HB definitions are used. In the first, rectangular condition, requirements are set on the distance r_{o-o} < 3.5 Å and the angle HO ¤ O > 135° for the HB to be intact (the dashed rectangle in Fig. 7). By this definition, only one HB is broken, and the prism and cage configurations both end up with 8 HB's per hexamer, while the book and cyclic isomers get 7 and 6 HB's, respectively.
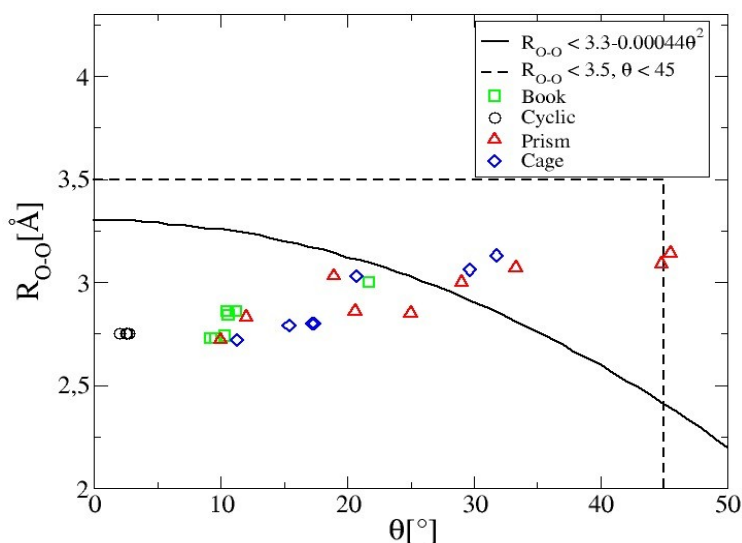

Figure 7. Hydrogen-bond distortion for the four hexamer isomers, calculated with the vdW-DF functional. The figure illustrates, how O-O separations and O-H---O angular distortions θ from linearity are distributed for them. The dashed rectangle and the full-drawn curve illustrate two criteria for HB's., pure HB's being inside each contour and distorted HB's outside. The two hexamers with highest stability, thanks to vdW forces, the prism and cage isomers, are the ones with most distorted HB's. By one definition, almost one half of the HB's are distorted in the prism configuration.

As an alternative criterion we apply the cone criterion from Ref. [19]: r_{o-o} < r_{o-o}^{max} - 0.00044 δ_{HOO}^2, which defines a cone around each HB-donating OH group, where
r_{o-o}^{max} = 3.3 Å is the maximum O-O distance at zero angle δ_{HOO}, where δ_{HOO} is the HO ¤ O angle quantifying the

angular distortion of the HB. This tighter definition (full-drawn curve in Fig. 7) suggests that many HB's are distorted on the two denser hexamers, resulting in 5 pure HB's for prism and cage, compared with 7 for the book and 6 for the cyclic hexamer isomers. So with this definition, stability follows a decrease in the number of undistorted HB's, or grows with the number of distorted bonds. The incentive for this second definition of HB's is the molecular arrangement in the first coordination shell of liquid water [19]. The local structure is characterized by comparison with bulk and surface of ordinary hexagonal ice Ih and with calculated spectra. For liquid water, the views differ about amounts of molecules in two-HB'ed configurations (with one strong donor and one strong acceptor HB) or in four-HB'ed tetrahedral structures. Upon heating, some of the molecules change from tetrahedral environments to two-HB'ed configurations. Findings are consistent with neutron and X-ray diffraction data, and combining the results sets a strong limit for possible local structure distributions in liquid water. Serious discrepancies with structures based on MD simulations based on traditional DFT are observed, however. For liquid water there is an ambiguity in the correlation between the O-H stretching frequency and HB length, often used to get structural information from IR spectroscopies [19].
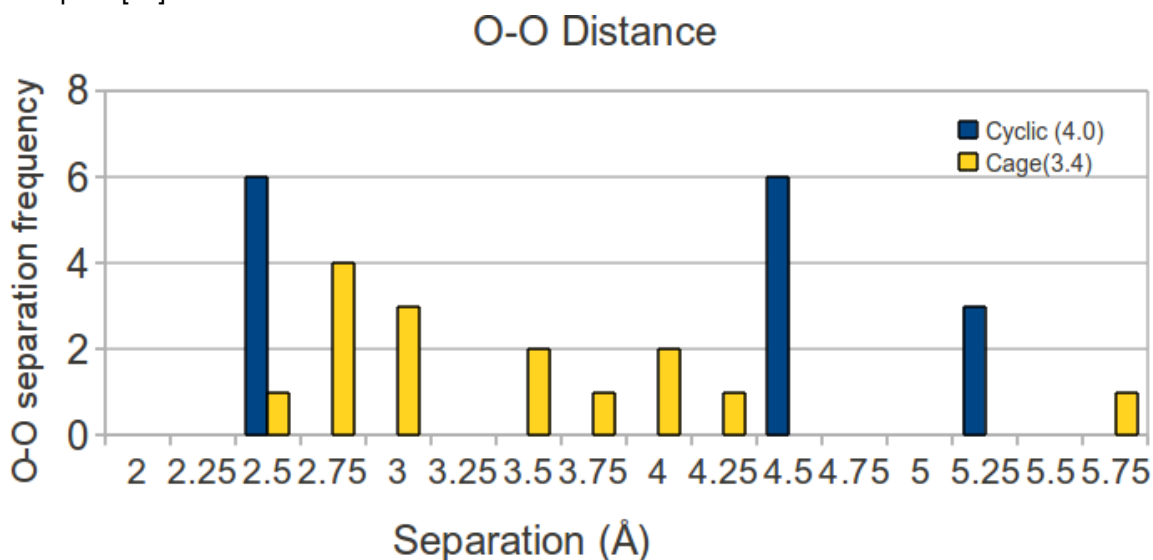

Figure 8. Oxygen-oxygen separation for the hexamers. The histogram illustrates a measure of compactness for each hexamer, where the average O-O separation (in Å) is shown in the legend. The prism and cage configurations have the shortest average separation, which increases stability, when also accounting for vdW forces.

A third way to compare the structures is by measuring the distances between each O atom and the other ones. All in all, this results in 15 distances that are plotted in a histogram (Fig. 8). This illustrates nicely that the cyclic structure, favored by GGA, has a high number of close-distance neighbors, as well as a high number of long-distance neighbors. The prism isomer, on the other hand, favored by vdW, has most of its neighbors at intermediate separations. The average O-O separation is smallest for prism and cage (3.4 Å) and largest for the cyclic isomer (4.0 Å). As prism and cage are the most stable isomers, this illustrates how vdW interactions favor the stability of hexamer isomers with many "available HB positions", which are then also most compact, as pointed out in Ref.~\onlinecite{Santra2008}. So, vdW forces favor stability for the more compact structures. This is done by the more compact structures having the constituting atoms closer to each other, thereby having more atoms benefiting from the attractive well of the vdW potential. In addition to favoring the compact isomer structures, the inclusion of vdW interaction distorts the internal HB. With the more restrictive definition of the HB, vdW forces can be interpreted as favoring distorted or broken HB's, a kind of quantity that is easier to observe in experiments and simulations of liquid water. Thus the vdW attraction gives a link between distorted HB's and stabilization: the more distorted or broken HB's, the more stable a structure.

IV. LIQUID WATER IMPLICATIONS

The HB governs the overall structure and the dynamics of water [44]. The reduced directionality of the water hexamer might be a key factor in this [18], and it should impact the radial distribution function (RDF) and the diffusion coefficient. By the cone criterion for the HB, the amount of distorted or broken HB's can be identified. Diffusion should be weak with pure HB's, a stiffness that results from traditional density-functional-theory (DFT) calculations, without vdW account (other suggestions for the too small diffusion coefficient exist, however [45]. DFT with an account of vdW forces help HB's to distort. This might have great implications, including increased diffusivity and changed radial distribution function (RDF). The HB's in liquid water have been found to be perturbed similarly to those in the most stable hexamer configurations.

Molecular-dynamics (MD) simulations with such DFT's have been made to calculate RDF's with the original vdW-DF functional [46], the optPBE-vdW [28], and the vdW-DF2 [16] functionals [47]. Exchange-repulsion considerations [32] make functionals like optPBE [28], Co09 [33], and vdW-DF2 [16] interesting, in particular in view of mproved performance on S22 benchmarks [21,24], *e.g.*, the vdW-DF2 [16] binding-energy deviations being less than 8 per cent from the latest CC benchmark [24].
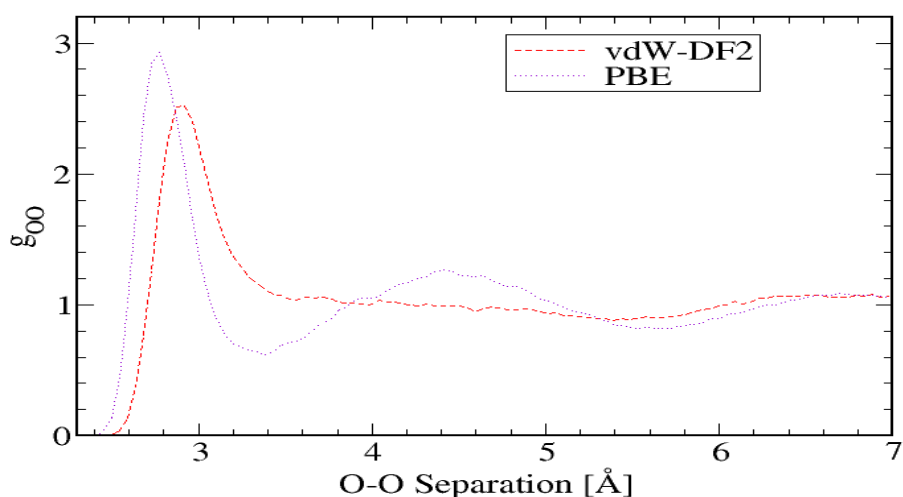

Figure 9. Oxygen-oxygen pair correlation function of liquid water, $g_{OO}(r)$, where r is separation between two water molecules, measured and calculated in the indicated approximations.

By comparing the average O-O separation in each $g_{OO}(r)$ curve of Fig. 9 to Fig. 8, one sees the same trend. The separations imply that the vdW-DF2-derived structure is more compact and the PBE-derived structure is more open. This is in agreement with the identification of HDL- and LDL-liquids in [47], which might be an gportant step in the understanding of the structure of liquid water. Angular distribution functions and HB analyss are important tools to demonstrate the fact that the vdW functionals provide a more smooth angular structure with less tetrahedral bonding. Using the two geometric HB definitions, the square-box and cone [19] criteria (Fig. 7), a clear message is given by the HB statistics for MD simulations with PBE, optPBE-vdW and vdW-DF2 functionals [47]:

Calculations with the PBE functional seem to favor a tetrahedral structure, with 4 HB's for a majority of the molecules, according to both HB definitions (64 and 52 %, respectively). The relatively more repulsive exchange with optPBE-vdW gives the water molecules less incentive to fully H-bonded structure (51 and 22 %), making many of them having two (5 or 29 %) or three (29 and 37 %) HB's. The inbetween vdW-DF2 functional, with its relatively weaker vdW attraction giving a slightly higher preference to forming HB's (54 and 25 % for 4, 26 and 38 % for 3, and 6 and 25 % for 2). This analysis [47] suggests that there is a competition between isotropic vdW forces and directional HB's, resulting in fewer or more HB's per water molecule, depending on the applied approximations.

In particular, the two vdW models pointed out by the cone criterion give low numbers of double-donor, double-

acceptor tetrahedral molecules. In fact, the large number of distorted HB's in the vdW simulations suggests that these models are in closer agreement with certain predictions from x-ray spectroscopies [19,48,49}, compared to most other AIMD models.

Angular distribution functions (ADF's) of the HB's give information on the orientational flexibility of the water molecules [47]. The distribution of angles depends on the choice of water model [50]. The picture of a competition between vdW interactions and HB's seems to be supported by the ADF's. In fact, the model without vdW forces (PBE) has no incentive to deviate from a structure of strong HB's, thus resulting in a relatively straight HB angle. When including vdW forces, the angles of the HB's become significantly more distorted. In general a softening of the structure is seen from the broader ADF's obtained in case of the vdW-DF's

The inclusion of the vdW interaction has a dramatic effect on both the tetrahedrality and asphericity distributions [47], the PBE simulation telling that locally tetrahedral O-H-O angles dominate, and the vdW simulations signaling non-tetrahedral positions in the first coordination shell [47].

So, there is a striking resemblance between the hexamer results and those of liquid water regarding the straining and breaking of HB's. In the hexamer case the cause for this was increased compactness, equivalent to higher electronic density, could this also be the driving force why vdW forces favor the high density liquid? When comparing the O-O histogram of the prism structure in Fig. 8 with the vdW-DF2 PCF in Fig. 9, they do have some common features. Both have its first peak shifted outwards, compared with the cyclic histogram and the PBE PCF. After the first peak at around 3 Å, both distributions gradually decline, without a clear minimum or void that cyclic and the PBE PCF share. The structural heterogeneities in water has been reported to be on the 1 nm scale [49], just slightly larger than the cross section of the prism and cage structures, which measure 0.5 - 0.7 nm. If the reported fluctuations exist, perhaps they share similarities with the prism and cage structure, rather than to the cyclic structure.

V. CONCLUSIONS

The new van der Waals density functionals optPBE-vdW and vdW-DF2 show great promise in describing the basic structural constituents of liquid water, as seen from comparing calculations of water dimer and hexamers with coupled cluster results [28,16]. A softening of the structure of liquid water at ambient conditions is observed, when including vdW interactions, consistent with previous work [51,52]. This is seen from the broader angular distributions, the more disordered tetrahedrality and asphericity distributions, and from the much lower and broader first peak of the oxygen-oxygen PCF obtained from the optPBE-vdW and vdW-DF2 models compared to PBE. The lower first peak of the O-O PCF improves the agreement with experiment significantly. However, the outer structure is washed out by the vdW forces. This has been suggested [52] to be related to nonlocal correlations. Our study of functionals with different nonlocal correlation strengths confirms this but do not show any significant difference in the liquid structures, while both were found to be very accurate for the water dimer.

As written in Ref. [47], the vdW simulations seem to be consistent with the picture of fluctuations between two different water structures instantaneously coexisting in nanoscaled patches. The relatively small simulation can only give a picture of the local structure of water, and while PBE predominantly describes low density water, both optPBE-vdW and vdW-DF2 tend to describe high density water. By comparing the O-O PCF's of the vdW models with PCF's from x-ray [54] and neutron [38] diffraction of water at different pressures, the resemblance between the vdW models and high-density water is clear. This is further supported by the reduction of the average number of HB's per molecule in the vdW MD simulations, which is a result of the isotropic vdW forces competing with the directional HB formation. Varying the strength of the exchange interaction does not result in a significant change in number of bonds. A 1:1 mixture of PBE (LDL) and vdW-DF2 (HDL) structures gives a good fit to an x-ray O-O PCF, but an even better agreement is achieved for a 70:30 mixture of vdW-DF2 and an experimentally determined LDL PCF [47].

A consistent picture should include the consequence that the vdW-DF2 and optPBE-vdW functionals should predict a LDL at lower pressure. In Fig.10 results of simulations with PBE and vdW-DF2, done with a 15 per cent larger cell size which represents a water density of 0.8 g/cm$_3$. When running the simulation for 8 ps with PBE, the resulting PCF is merely a shifted
version of the original simulation. When redoing the simulation with vdW-DF2, some qualitative

differences with the original PCF becomes apparent as the PCF marginally restores the second peak in the PCF, indicating more tetrahedrality than in the denser simulation. It would be very interesting to follow this trend over a larger span of densities to see if the vdW-DF2 simulation can also be transformed into a structure similar to LDL .
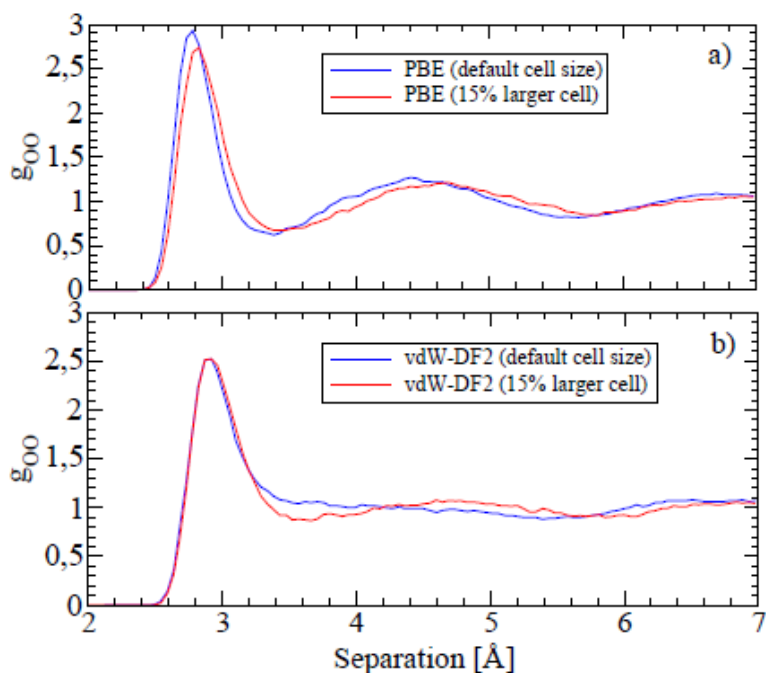

Figure 10: Preliminary results on the effects of the size of simulation cell, equivalent to the effects of altered pressure. With reduced pressure the vdW-DF2 PCF restore its second peak, indicative for tetrahedrality. With this sort of simulation it may be possible to sample the effect of pressure.

By calculations on four water hexamers it is shown that the vdW-DF accurately determines the energetic trend on these small clusters, but that the exchange approximation is too repulsive for accurate dissociation energies. By analysis of the hydrogen bonds (HB's) in the hexamers it is suggested that vdW forces generally distorts HBs in water molecules, a direct consequence of favoring compact molecules with short average separations. This effect prevails in molecular dynamics (MD) simulations of ambient water where vdW forces qualitatively result in liquid water with fewer and more distorted HB's. This is interesting as there is currently a heated debate in the water community on the level of HB distortion in ambient water, and where MD simulations without first principles vdW forces have played an important role to suggest that liquid water is almost tetrahedral, with few distorted HB's.

References:

[1]   Wikipedia

[2]   [IUPAC] International Union of Pure and Applied Chemistry. "hydrogen bond". *Compendium of Chemical Terminology* Internet edition.

[3]   C.H. Cho, S. Singh, and G.W. Robinson. J. Chem. Phys., **107**:7979, 1997.

[4]   ~\cite{63}.

[5]   T. Steiner and G.R Desiraju, Chem. Commun **891** (1998)

[6]   ~\cite{NoLaMo98}

[7]   Steiner02] Thomas Steiner Angew. Chem. Int. Ed. 2002, 41, 48.

[8]   J. Ireta, J. Neugebauer, and M. Scheffler. J. Phys. Chem. A, 108:5692, 2004.

[9]   Cooper V C, Thonhauser T and Langreth D C 2008 J. Chem. Phys. 128 204102

[10]   Cambridge Structural Database (CSD)

[11]   Kohn W and Sham L J 1965 Phys. Rev. 140 A1133

[12]   M. Dion, H. Rydberg, E. Schroder, D.C. Langreth, and B.I. Lundqvist. Phys. Rev. Lett., 92:246401, 2004.

[13]   ~D C Langreth, B I Lundqvist, S D Chakarova-Kˇck, V R Cooper, M Dion, P Hyldgaard, A Kelkkanen, J Kleis, Lingzhu Kong, Shen Li, P G Moses, E Murray,
        A Puzder, H Rydberg, E Schr̈der, and T Thonhauser. Journal of Physics: Condensed Matter, 21(8):084203, 2009.

[14]   J. Björk, F. Hanke, C.-A. Palma, P. Samori, M. Cecchini, and M. Persson, J. Phys. Chem. Lett. **2010**, 1, 3407.

[15]   Thonhauser T, Cooper V R, Shen Li, Puzder A, Hyldgaard P and Langreth D C 2007 Phys. Rev. B 76 125112

[16]   K. Lee, et al., Phys. Rev. B 82, 081101 (2010)

[17]   B. Santra and et al. J. Chem. Phys., 129:194111, 2008

[18]   A.K. Kelkkanen, B.I. Lundqvist, and J.K. Norskov. J. Chem. Phys., 131:046102, 2009.

[19]   Ph. Wernet, D. Nordlund, U. Bergmann, and et al. Science, 304:995, 2004.

[20]   ~A. Møgelhøj, A.K. Kelkkanen, K.T. Wikfeldt, J. Schiøtz, J. J. Mortensen, L.G.M. Pettersson, B.I. Lundqvist, K.W. Jacobsen, A. Nilsson and J.K. Nørskov, subm to J. Phys. Chem., http://arxiv.org/abs/1101.5666.

[21]   P. Jurecka, J. Sponer, J. Cerny, and P. Hobza. Phys. Chem. Chem. Phys. 8, 1985 (2006).

[22]   L. F. Molnar, X. He, B.Wang, and K. M. Merz, J. Chem. Phys. 131, 065102 (2009).

[23]   C.D. Sherrill, T. Takatani, and E. G. Hohenstein, J. Phys.Chem. A 113, 10146 (2009).

[24]   Tait Takatani, Edward G. Hohenstein, Massimo Malagoli, Michael S. Marshall, and C. David Sherrill. The Journal of Chemical Physics , 132(14):144104, 2010.

[25]   R. Podeszwa, K. Patkowski, and K. Szalewicz, Phys. Chem. Chem. Phys. 12, 5974 (2010).

[26]   J. Ireta *et al.*, J. Phys.Chem. B 107, 1432 (2004).

[27]   A. Gulans, M.J. Puska, and R.M. Nieminen. Phys. Rev. B, 79(20):201105, 2009.

[28]   J. Klimes, D.R. Bowler, and A. Michaelides. J. Phys.Conden. Matter, 22:022201, 2010.

[29]   J. P. Perdew and Y. Wang, Phys. Rev. B 33, 8800(R)

[30]   Städele, M. and Moukara, M. and Majewski, J. A. and Vogl, P. and Görling, A. , Phys. Rev. B **59** 15 10031 1999

[31]   A Puzder, et al., J. Chem. Phys. 126, (2006) 164105

[32]   M. D. Murray, et al., J. Chem. Theor. Comput. 5 (2009) 2754

[33]   V. R. Cooper, Phys. Rev. B 81 (2010) 161104

[34]   J.P. Perdew, K. Burke, and M. Ernzerhof. Phys. Rev. Lett., 77:3865, 1996.

[35]   Y.K. Zhang and W.T. Yang. Phys. Rev. Lett., 80:890, 1998.

[36]   I. Hamada and M. Otani, Phys. Rev. B 82, 153412 (2010)

[37]   See, *e.g.*, G. A. Jeffrey, An Introduction to Hydrogen Bonding, Oxford University Press, Oxford, 1997.

[38]   A K Soper 2005 J. Phys.: Condens. Matter **17** S3273

[39]   Isaacs E D, Shulka A, Platzman P M, Hamann D R, Bariellini B and Tulk C A Phys. Rev. Lett. **82**, 600 (1999)

[40]   S. Grimme. J. Comput. Chem., 25:1463, 2004.

[41]   Alexandre Tkatchenko and Matthias Scheffler. 102(7):073005, 2009.

[42]   Bates,D.M and Tschumper, G.S, J. Phys. Chem. A, 2009, 113, 3555

[43]   C Adamo and V Barone. J. Chem. Phys., 110(13):6158–6170, 1999.

[44]   F. Mallamace. Proc. Natl. Acad. Sci. USA, 106:15097, 2009.

[45]   ~\cite{REF})

[46]   ~\cite{Spaniards} [Samma som Wang? [52]?

[47]   A. Møgelhøj, A. K. Kelkkanen, K. T. Wikfeldt, J. Schøtz, J. J. Mortensen,
         L. G. M. Pettersson, B. I. Lundqvist, K. W. Jacobsen, A. Nilsson and J. K. Nørskov, Density functional van der Waals forces provide room
         for density fluctuations in simulated water, Arxiv: http://arxiv.org/abs/1101.5666

[48]   Tokushima08high, T. Tokushima, Y. Harada, O. Takahashi, Y. Senba, H. Ohashi, L. G. M. Pettersson, A. Nilsson, and S. Shin. High resolution X-ray emission spectroscopy of liquid   water: The observation of two structural motifs. Chem. Phys. Lett., 460(4-6):387–400, 2008.

[49]   C. Huang, K. T. Wikfeldt, T. Tokushima, D. Nordlund, Y. Harada, U. Bergmann, M. Niebuhr, T.M. Weiss, Y. Horikawa, M. Leetmaa, M.P. Ljungberg, O. Takahashi, A. Lenz,   L. Ojam̈e, A.P. Lyubartsev, S. Shin, L.G.M. Pettersson, and A. Nilsson. The inhomogeneous structure of water at ambient conditions. Proc. Natl. Acad. Sci. USA, 106:15214, 2009.

[50]   Lee06 H.S. Lee and M.E. Tuckerman. J. Chem. Phys., 125:154507, 2006.

[51]   Lin2009 I.-C. Lin, A. P. Seitsonen, M. D. Coutinho-Neto, I. Tavernelli, and U. Rothlisberger, J. Phys. Chem. B 113, 1127 (2009).

[52]   J. Wang, G. Roman-Perez, J. M. Soler, E. Artacho, and M. V. Fernandez-Serra. Density, structure, and dynamics of water: The effect of van der Waals interactions. J.   Chem. Phys., 134:024516, 2011.

[53]   A.V. Okhulkov, Y.N. Demianets, and Y. E. Gorbaty. J. Chem. Phys., 100:1578, 1994.

[54]

[55]